

Investigations on regulatory mechanisms of the central
carbon metabolism in *Synechocystis* sp. PCC 6803

Untersuchungen zu regulatorischen Mechanismen des zentralen
Kohlenstoffmetabolismus in *Synechocystis* sp. PCC 6803

Kumulative Dissertation

zur Erlangung des Grades

doctor rerum naturalium (Dr. rer. nat.)

am Institut für Biowissenschaften

der Mathematisch-Naturwissenschaftlichen Fakultät

der Universität Rostock

vorgelegt von

Stefan Lucius

geb. am 02.03.1995 in Köthen (Anhalt)

Rostock, 2023

Reviewers: Prof. Dr. Martin Hagemann, University of Rostock
Prof. Dr. Wolfgang R. Hess, University of Freiburg

Date of submission: 30.11.2023
Date of defense: 03.05.2024

*“ What do you see inside your mind?
Is it your dreams or just the torment of life?
Break away from your anxieties today
Don't ever let them drag you down. “*

“Road of Kings”

Mark Shelton, Manilla Road, 1985

Contents

1	LIST OF ABBREVIATIONS	6
2	LIST OF FIGURES	8
3	LIST OF TABLES	8
4	SUMMARY	9
5	ZUSAMMENFASSUNG	10
6	INTRODUCTION	11
6.1	CYANOBACTERIA	11
6.2	MODEL STRAIN <i>SYNECHOCYSTIS</i> SP. PCC 6803	11
6.3	OVERVIEW OF THE CENTRAL CARBON METABOLISM OF <i>SYNECHOCYSTIS</i>	13
6.3.1	<i>Photosynthetic energy supply for carbon fixation</i>	13
6.3.2	<i>Inorganic carbon uptake and the cyanobacterial carbon-concentrating mechanism</i>	13
6.3.3	<i>Organic carbon uptake</i>	14
6.3.4	<i>Significance of central carbon metabolic routes</i>	15
6.3.5	<i>Anabolic carbon routes and glycogen formation</i>	17
6.3.6	<i>Catabolic carbon routes and glycogen breakdown</i>	17
6.3.7	<i>Glycolytic routes as anaplerotic shunts</i>	19
6.4	IMPORTANCE OF REGULATION OF THE CENTRAL CARBON METABOLISM IN <i>SYNECHOCYSTIS</i>	20
6.4.1	<i>Regulating the switch between photoautotrophic and heterotrophic modes of lifestyle</i> 20	
6.4.2	<i>The triosephosphate hub around key enzymes GapDH and Pgam</i>	22
6.4.3	<i>Cp12 protein as regulator of the Calvin-Benson-Bassham cycle</i>	23
6.5	CONNECTION OF CARBON AND NITROGEN METABOLISM IN <i>SYNECHOCYSTIS</i>	26
6.5.1	<i>Nitrogen assimilation in Synechocystis</i>	26
6.5.2	<i>Significance of C/N homeostasis in Synechocystis</i>	26
6.5.3	<i>Regulation of nitrogen metabolism by the PII protein in Synechocystis</i>	27
6.5.4	<i>PirC as novel interactor with PII in Synechocystis</i>	28
7	AIMS OF THIS INVESTIGATION	29
8	GENERAL DISCUSSION	30
8.1	REGULATION OF THE CENTRAL CARBON METABOLISM DURING CHANGING CO ₂ CONDITIONS	30
8.1.1	<i>General overview</i>	30
8.1.2	<i>Glycolytic routes in changing CO₂ conditions</i>	32
8.1.3	<i>Cp12-dependent regulation in changing CO₂ conditions</i>	37
8.1.4	<i>Connection between PirC and CO₂ availability</i>	38
8.2	REGULATION OF THE CENTRAL CARBON METABOLISM DURING SUPPLY WITH EXTERNAL GLUCOSE .	39
8.2.1	<i>General overview</i>	39
8.2.2	<i>Glycolytic routes in heterotrophic and mixotrophic growth conditions</i>	39
8.2.3	<i>Cp12 regulation during glucose supply</i>	40
8.3	REGULATION OF THE CENTRAL CARBON METABOLISM DURING NITROGEN LIMITATION	44
8.3.1	<i>General overview</i>	44

8.3.2	<i>Role of glycolytic routes for resuscitation from chlorosis</i>	45
8.3.3	<i>Regulation of the triosephosphate hub in nitrogen limitation</i>	45
9	CONCLUDING REMARKS AND OUTLOOK	49
10	REFERENCES	50
11	PUBLICATIONS	61
11.1	PUBLICATION I: THE ENTNER-DOUDOROFF PATHWAY CONTRIBUTES TO GLYCOGEN BREAKDOWN DURING HIGH TO LOW CO ₂ SHIFTS IN THE CYANOBACTERIUM <i>SYNECHOCYSTIS</i> SP. PCC 6803	61
11.2	PUBLICATION II: CP12 FINE-TUNES THE CALVIN-BENSON CYCLE AND CARBOHYDRATE METABOLISM IN CYANOBACTERIA	79
11.3	PUBLICATION III: THE NOVEL P _{II} -INTERACTOR PIRC IDENTIFIES PHOSPHOGLYCERATE MUTASE AS KEY CONTROL POINT OF CARBON STORAGE METABOLISM IN CYANOBACTERIA	105
12	APPENDIX	135
12.1	CONTRIBUTION TO MANUSCRIPTS	135
12.2	WISSENSCHAFTLICHER LEBENSLAUF	137
12.3	SELBSTÄNDIGKEITSERKLÄRUNG	140
12.4	ACKNOWLEDGEMENTS	141

1 List of Abbreviations

Abbreviation	Meaning
2OG	2-oxoglutarate
2PG	2-phosphoglycolate
2PGA	2-phosphoglycerate
3PGA	3-phosphoglycerate
6PG	6-phosphogluconate
ABC	ATP-binding cassette
ADP	Adenosine diphosphate
AgrE	Arginine dihydrolase
ATP	Adenosine triphosphate
BCT1	ABC-type HCO ₃ ⁻ transporter
BicA	HCO ₃ ⁻ transporter
C	Carbon
CA	Carbonic anhydrase
CBB (cycle)	Calvin-Benson-Bassham (cycle)
CCM	Carbon concentrating mechanism
CcmP	Minor carboxysome shell protein
CfrA	Carbon flow regulator A
Ci	Inorganic carbon
CO ₂	Carbon dioxide
CoA	Coenzyme A
CoIP	Co-immunoprecipitation
Cp12	Chloroplast protein of 12 kDa
Cys	Cysteine
DCMU	3-(3,4-dichlorophenyl)-1,1-dimethylurea
DHAP	Dihydroxyacetone phosphate
ED (pathway)	Entner-Doudoroff (pathway)
Eda	KDPG aldolase
Edd	6-phosphogluconate dehydratase
EMP (pathway)	Embden-Meyerhof-Parnas (pathway)
eYFP	Enhanced yellow fluorescent protein
F6P	Fructose 6-phosphate
FBP	Fructose 1,6-bisphosphate
FNR	Ferredoxin-NADP ⁺ reductase
G1,3BP	Glycerate 1,3-bisphosphate
G1P	Glucose 1-phosphate
G6P	Glucose 6-phosphate
GAP	Glyceraldehyde 3-phosphate
GapDH	Glyceraldehyde 3-phosphate dehydrogenase
GC-MS	Gas chromatography–mass spectrometry
Gck	Glucokinase
GlcP	Glucose transporter
GlgA	Glycogen synthase
GlgB	Glycogen branching enzyme
GlgC	Glucose 1-phosphate adenylyltransferase
GlgP1/2	Glycogen phosphorylase 1 and 2
GlgX	Glycogen debranching enzyme
Gnd	6-phosphogluconate dehydrogenase
GOGAT	Glutamine oxoglutarate aminotransferase

Abbreviation	Meaning
GS	Glutamine synthetase
HC	High carbon
HCO ₃ ⁻	Bicarbonate
kDa	Kilodalton
KDPG	2-dehydro-3-deoxy-6-phosphogluconate
K_m	Michaelis-Menten constant
LC	Low carbon
LC-MS	Liquid chromatography–mass spectrometry
Mg	Magnesium
mM	Millimolar
N/N ₂	Nitrogen
NaCl	Sodium chloride
NAD ⁺ / NADH	Nicotinamide adenine dinucleotide
NADP ⁺ / NADPH	Nicotinamide adenine dinucleotide phosphate
NAGK	N-acetyl-L-glutamate kinase
NbIA	Phycobilisome degradation protein
NDH	NAD(P)H dehydrogenase
NdhR	NDH regulator
NrtABCD	Nitrate/nitrite transport system
NtcA	Nitrogen control transcription factor
O/O ₂	Oxygen
OPP (pathway)	Oxidative pentose phosphate (pathway)
PAGE	Polyacrylamide gelelectrophoresis
PCA	Principal component analysis
PCC	Pasteur culture collection
PDH	Pyruvate dehydrogenase
PEPC	Phosphoenolpyruvate carboxylase
Pfk	Phosphofructokinase
Pgam	Phosphoglycerate mutase
Pgam1	2,3-phosphoglycerate independent phosphoglycerate mutase
Pgk	Phosphoglycerate kinase
Pgm	Phosphoglucomutase
PHB	Polyhydroxybutyrate
PipX	PII-interacting protein X
PirC	PII-interacting regulator of carbon metabolism
Prk	Phosphoribulokinase
PSI	Photosystem I
PSII	Photosystem II
R5P	Ribulose 5-phosphate
RuBisCO	Ribulose 1,5-bisphosphate carboxylase/oxygenase
RuBP	Ribulose 1,5-bisphosphate
SbtA	Sodium-dependent bicarbonate transporter
SbtB	PII-like regulatory protein
SDS	Sodium dodecyl sulfate
TCA (cycle)	Tricarboxylic acid (cycle)
UrtABCD	Urea transporter system
V_{max}	Maximum velocity
WT	Wild type
Zwf	Glucose 6-phosphate dehydrogenase

2 List of Figures

Figure 1: Schematic detailing the ultrastructure of <i>Synechocystis</i> sp. PCC 6803 showing various subcellular components (Mills et al., 2020).	12
Figure 2: Overview of the central carbon metabolism in <i>Synechocystis</i> . Adapted from Koch et al. (2019).	16
Figure 3: Model of structural changes for redox-dependent complex formation mediated by Cp12 in <i>T. elongatus</i> (McFarlane et al. 2019).	25
Figure 4: Central carbon metabolism of <i>Synechocystis</i> with indication of affected enzymes in the studied mutant strains. Adapted from Lucius et al. (2021).	33
Figure 5: Steady states of selected metabolites in the context of entire carbon metabolism (Lucius et al., 2021).	35
Figure 6: Model of regulation of central carbon metabolism by PirC, PII, and Pgam1 interactions (Orthwein et al., 2021)..	47

3 List of Tables

Table 1: Details of mutant strains used in CO ₂ shift experiments for Publication 1 (Lucius et al., 2021).....	32
Table 2: Details of mutant strains with $\Delta cp12$ background used in Publication 2 (Lucius et al., 2022).....	41

4 Summary

Cyanobacteria are the only prokaryotes capable of performing oxygenic photosynthesis. Their ability to engage in different trophic modes, ranging from photoautotrophy and heterotrophy to mixotrophic growth, in response to environmental fluctuations and nutrient availability, emphasizes the immense influence of this ancient bacterial phylum on the global carbon and nitrogen cycles. However, the regulatory mechanisms allowing a flexible switch between these lifestyles are poorly understood, especially for unicellular cyanobacteria without major subcellular compartmentation. As anabolic fixation of CO₂ in the Calvin-Benson-Bassham cycle and catabolic glycolytic pathways share intermediates and enzymatic capacity, a tight regulatory network is required to enable simultaneous opposed metabolic fluxes. The discovery of novel mechanisms regulating carbon allocation at crucial branching points could identify ways for targeted redirection of metabolic routes towards desired compounds, and thus help to further establish cyanobacteria as green cell factories for biotechnological applications with concurrent utilisation of CO₂. This dissertation presents new insights on regulations of the central carbon metabolism of *Synechocystis* sp. PCC 6803, and therein highlights the importance of specific key enzymes of anabolic and catabolic pathways.

The Entner-Doudoroff pathway around the enzyme Eda was found to be a crucial glycolytic route for glycogen breakdown in changing CO₂ levels, in addition to the Embden-Meyerhof-Parnas pathway and the oxidative pentose phosphate pathway. Metabolite analyses on *Synechocystis* mutants deficient in either of these main glycolytic routes revealed a distinct metabolic phenotype for strain Δ eda during acclimation to CO₂ shifts.

Cp12 is a widespread small protein known to downregulate the Calvin-Benson-Bassham cycle in darkness by inhibiting photosynthetic phosphoribulokinase and glyceraldehyde 3-phosphate dehydrogenase. The formation of such inhibitory complex could be visualized *in vivo* via fluorescence-tagged mutants. New results of metabolomics and redox level analyses on mutant Cp12 strains extend the known role of Cp12 regulation and reveal an importance for acclimation to external glucose supply in dark phases as well as to shifts in CO₂ levels in constant light.

Carbon and nitrogen metabolism are closely linked as *Synechocystis* maintains an essential C/N homeostasis. The small protein regulator PirC was characterized as interactor with the nitrogen-signal transduction protein PII and identifies phosphoglycerate mutase (Pgam) as central branching point for carbon allocation. In nitrogen depletion, PirC is released from PII and inhibits Pgam, thus promoting glycogen storage metabolism. Altered metabolite levels in the central carbon metabolism of Δ pirC during nitrogen starvation experiments confirm this regulatory mechanism.

5 Zusammenfassung

Cyanobakterien sind die einzigen Prokaryoten mit der Fähigkeit zur Durchführung oxygener Photosynthese. Als Reaktion auf Umweltfluktuationen können sie sowohl photoautotroph, heterotroph als auch mixotroph wachsen, was den enormen Einfluss dieses bakteriellen Phylums auf globale Kohlenstoff- und Stickstoffkreisläufe unterstreicht. Die regulatorischen Mechanismen für einen flexiblen Wechsel zwischen diesen Lebensweisen sind jedoch unzureichend verstanden, insbesondere für einzellige Cyanobakterien ohne wesentliche subzelluläre Kompartimentierung. Da anabole CO₂-Fixierung im Calvin-Benson-Bassham-(CBB)-Zyklus und katabole glykolytische Wege überlappen, ist ein enges regulatorisches Netzwerk erforderlich, um derart gegenläufige Stoffwechselwege gleichzeitig zu ermöglichen. Neuentdeckte Regulationen für die Kohlenstoffverteilung an entscheidenden Verzweigungen könnten eine gezielte Umleitung von Stoffwechselwegen ermöglichen, und dadurch Cyanobakterien als grüne Zellfabriken für biotechnologische Anwendungen unter Nutzung von CO₂ verstärkt etablieren. Diese Dissertation präsentiert neue Einblicke in die Regulation des zentralen Kohlenstoffstoffwechsels von *Synechocystis* sp. PCC 6803 und hebt die Bedeutung spezifischer Schlüsselenzyme anaboler und kataboler Wege hervor.

Der Entner-Doudoroff-Weg um das Enzym Eda wurde neben dem Embden-Meyerhof-Parnas-Weg und dem oxidativen Pentosephosphatweg als entscheidender glykolytischer Weg für den Glykogenabbau bei wechselnden CO₂-Leveln identifiziert. Metabolitanalysen an *Synechocystis*-Mutanten, die je einen dieser Glykolysewege nicht besitzen, zeigten einen distinkten Stoffwechselphänotyp für Δeda während der Antwort auf CO₂-Shifts.

Cp12 ist ein weit verbreitetes kleines Protein, das den CBB-Zyklus im Dunkeln durch Inhibition der photosynthetischen Phosphoribulokinase und der Glyceraldehyd-3-phosphat-Dehydrogenase herunterreguliert. Die Bildung von inhibitorischen Komplexen konnte *in vivo* mithilfe von fluoreszenzmarkierten Mutanten visualisiert werden. Metabolomics und Redox-Level-Analysen an Cp12-Mutanten erweiterten die bisher bekannte Rolle der Cp12-Regulation und zeigten eine Bedeutung für die Anpassung an externe Glukose in Dunkelphasen, sowie an CO₂-Schwankungen im Dauerlicht.

Kohlenstoff- und Stickstoffstoffwechsel sind eng miteinander verbunden, da *Synechocystis* eine essentielle C/N-Homöostase aufrechterhält. Das kleine Protein PirC interagiert mit dem Stickstoffsignaltransduktionsprotein PII und identifiziert Phosphoglyceratmutase (Pgam) als zentralen Verzweigungspunkt für die Kohlenstoffverteilung. Bei Stickstoffmangel wird PirC von PII freigesetzt und inhibiert Pgam, wodurch der Glykogenaufbau gesteigert wird. Veränderte Metabolitenlevel im zentralen Kohlenstoffstoffwechsel der Mutante $\Delta pirC$ während Stickstoffmangel-Experimenten bestätigten diesen Regulationsmechanismus.

6 INTRODUCTION

6.1 Cyanobacteria

Cyanobacteria are a phylum of Gram-negative prokaryotes from the domain of bacteria. They are the only prokaryotes known to perform oxygenic photosynthesis. Thereby, they are able to use light energy for water splitting to generate electrons and protons for the photosynthetic electron transport chain combined with the release of molecular oxygen (O_2) as a byproduct (e.g., Sánchez-Baracaldo & Cardona, 2020). Cyanobacteria evolved this process at least 2.7 billion years ago, leading to a drastic increase of O_2 in Earth's atmosphere, thus tremendously impacting biogeochemical processes and evolution of life (Hohmann-Marriott & Blankenship, 2011; Schirmer et al., 2016). The long-term evolution of cyanobacteria allowed adaptation to numerous abiotic stresses, resource limitations and growth conditions. Ranging from terrestrial growth in microbial mats to life in freshwater and marine ecosystems, cyanobacterial habitats show a strong diversity including extreme locations like salt lakes (Alvarenga et al., 2018) or desert soil crusts (Oren et al., 2019). Cyanobacteria are important prokaryotic biomass producers, with genera *Synechococcus* and *Prochlorococcus* alone accounting for up to 25% of all marine primary production (Flombaum et al., 2013). Several filamentous cyanobacterial strains are also able to fixate atmospheric nitrogen (N_2) in specialized cells called heterocysts (Flores et al., 2018) and contribute to the global N-cycle.

The photosynthetic fixation of carbon dioxide (CO_2) to form organic carbon was transferred from early cyanobacteria to eukaryotes by endosymbiosis, which essentially initiated the development of plastids in plants and algae approximately 1.5 billion years ago (Hedges et al., 2004). Therefore, numerous cyanobacterial biochemical pathways and physiological traits remain conserved in higher plants. This makes cyanobacterial metabolism an attractive subject of fundamental research for plant photosynthesis and energy metabolism. Moreover, the natural production and accumulation of biopolymers such as glycogen, cyanophycin or polyhydroxybutyrate (PHB) highlights cyanobacteria as suitable green cell factories for application in biotechnology (Santos-Merino et al., 2019).

6.2 Model strain *Synechocystis* sp. PCC 6803

The paraphyletic genus *Synechocystis* comprises several unicellular coccoid non-diazotrophic (unable to perform N_2 fixation) cyanobacterial species, including the widely studied strain *Synechocystis* sp. PCC 6803 (hereafter *Synechocystis*). *Synechocystis* was originally isolated from a freshwater lake in California in 1968 (Stanier et al., 1971). Despite its original isolation site, it is also able to survive in terrestrial and marine habitats, and displays a salt tolerance of up to 7% NaCl, equivalent to twofold sea salt concentrations

(Reed & Stewart, 1985). Following multiple lab mutations, several sub-genotypes derived from the original strain, including glucose-tolerant lines. This added to the popularity of *Synechocystis* as a model strain for fundamental research on physiology of photosynthesis due to its different modes of lifestyle: The ability of photoautotrophic growth during light periods as well as growing mixotrophically and heterotrophically via glycolytic pathways utilising stored glycogen or exogenously provided glucose (Rippka et al., 1979). Furthermore, *Synechocystis* is a naturally transformable organism capable of efficient homologous recombination which allows easy genetic manipulation and generation of targeted knock-out mutants for physiological studies. In 1996, *Synechocystis* became the first phototrophic organism to have its genome completely sequenced (Kaneko et al., 1996), which enabled further profound research to be performed on genomic, transcriptomic and proteomic levels over decades to follow. A schematic illustration of this model organism is given in Figure 1.

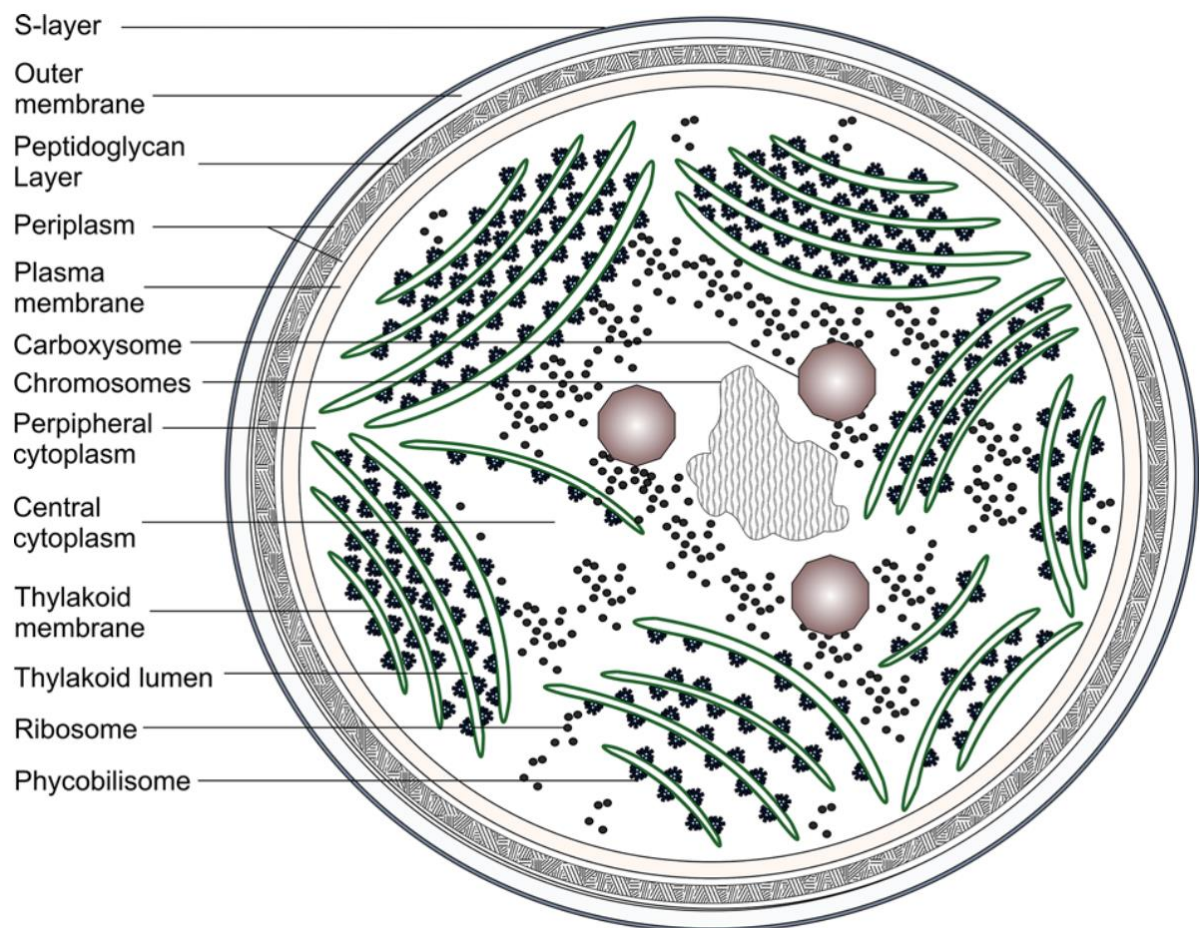


Figure 1: Schematic detailing the ultrastructure of *Synechocystis* sp. PCC 6803 showing various subcellular components (Mills et al., 2020).

6.3 Overview of the central carbon metabolism of *Synechocystis*

6.3.1 *Photosynthetic energy supply for carbon fixation*

Synechocystis mainly produces nicotinamide adenine dinucleotide phosphate (NADPH) and adenosine triphosphate (ATP) in the light-dependent reaction of oxygenic photosynthesis. The light-dependent reaction takes place in the thylakoid membrane and converts light energy to chemical energy (Vermaas, 2001). In brief, chlorophyll *a* in the photosystem II (PSII) reaction center is excited by light energy. It transfers one electron to plastoquinone, thus starting the photosynthetic electron transport chain along the thylakoid membrane. Subsequently reduced electron acceptors are the cytochrome *b6f* complex and plastocyanin, with the latter then donating one electron to photosystem I (PSI). Excited chlorophyll *a* from PSI then reduces ferredoxin which in turn can transfer an electron to ferredoxin-NADP⁺ reductase (FNR) in a linear electron transport, thus producing the reducing equivalent NADPH (Lea-Smith et al., 2016). The water-splitting complex and the proton pump activity of cytochrome *b6f* generate a proton gradient between the thylakoid lumen and the cytoplasm which is utilised by the ATP synthase to convert adenosine diphosphate (ADP) to ATP. To adjust the physiological NADPH/ATP ratio, ferredoxin can also transfer electrons back to plastoquinone, generating only ATP, thus creating a cyclic electron transport (Bendall & Manasse, 1995). This is especially important during stress when the demand for ATP is increased or when NADP⁺ levels are decreased in conditions such as low CO₂ availability. Most of the produced NADPH and ATP is then used to fix atmospheric CO₂ in the Calvin-Benson-Bassham (CBB) cycle.

6.3.2 *Inorganic carbon uptake and the cyanobacterial carbon-concentrating mechanism*

Dissolved CO₂ and bicarbonate (HCO₃⁻) are the two relevant inorganic carbon (Ci) sources that can be used by cyanobacteria to autotrophically produce organic carbon compounds (Badger et al., 2006). *Synechocystis* possesses five well-described Ci uptake systems to concentrate bicarbonate in the cytoplasm: Three HCO₃⁻ transporters BCT1 (Omata et al., 1999), SbtA (Shibata et al., 2002) and BicA (Price et al., 2004), which are located in the plasma membrane, and the two CO₂-uptake complexes NDH-1₃ and NDH-1₄ that are thylakoid-bound and convert CO₂ to HCO₃⁻ (Rae et al., 2013). After Ci import, HCO₃⁻ then diffuses into cyanobacterial microcompartments called carboxysomes, which harbour the enzymes carbonic anhydrase (CA) and RuBisCO, short for ribulose-1,5-bisphosphate carboxylase-oxygenase. Here, HCO₃⁻ is converted back to CO₂ by CA while the proteinaceous carboxysome shell prevents the loss of CO₂ as basis of the carbon concentrating mechanism (CCM), and thus increases its concentration around RuBisCO (Turmo et al., 2017).

Cyanobacteria evolved their CCM in response to evolutionary pressure caused by the increase of O₂ and decrease of CO₂ concentration in their environment that followed the rise of oxygenic photosynthesis (Raven et al., 2017). The requirement for such a mechanism lies in the biochemical properties of RuBisCO. The carboxylation reaction of RuBisCO enables fixation of C_i in the form of CO₂ to ribulose 1,5-bisphosphate (RuBP) to generate two molecules of 3-phosphoglycerate (3PGA) as part of the CBB cycle. However, RuBisCO has a low affinity and specificity for CO₂, because it can also incorporate O₂ into RuBP via its oxygenase activity, resulting in the production of one molecule each of 3PGA and 2-phosphoglycolate (2PG) (Kaplan & Reinhold, 1999). The metabolite 2PG is toxic for oxygenic photosynthetic organisms and is known to inhibit CBB cycle enzymes such as triosephosphate isomerase and seduheptulose 1,7-bisphosphatase in *Arabidopsis thaliana* (Anderson et al., 1971; Flügel et al., 2017). Therefore, 2PG needs to be metabolized by the photorespiratory salvage pathway. The CCM of *Synechocystis* reduces the oxygenase reaction of RuBisCO to a flux below 1% (Young et al., 2011), because CO₂ is enriched into carboxysomes and O₂ diffusion is hampered by the proteinaceous carboxysome shell. However, despite having an active CCM, the metabolization of 2PG is also essential for *Synechocystis* (Eisenhut et al., 2008a), adding metabolic flexibility and supporting synthesis of amino acids serine and glycine. During photorespiration, 2PG is reconverted to 3PGA at the expense of ATP, and CO₂ and ammonia are released from previously assimilated C_i and combined nitrogen sources. Therefore, the development of the cyanobacterial CCM mediating localized carbon fixation in a high CO₂ / low O₂ compartment reduced these photorespiratory losses to a large extent (Badger & Price, 2003).

6.3.3 Organic carbon uptake

Some *Synechocystis* strains including *Synechocystis* sp. PCC 6803 are also able to take up external organic carbon in the form of sugars. This includes the utilisation of glucose which can be imported into the cell via the GlcP transporter (Schmetterer, 1990). The imported glucose is phosphorylated by the hexokinase Hk as it enters the central carbon metabolism. From there, it can be metabolized and oxidized by following glycolytic routes. Fructose can also pass GlcP but is toxic for *Synechocystis* (Joset et al., 1988). The ability to take up external glucose is significant for *Synechocystis*, as it enables the cells to grow heterotrophically in conditions where photosynthetic CO₂ fixation is not feasible, like dark phases. Glucosylglycerol is another organic carbon source that is not efficiently used for growth but used as osmoprotective compatible solute in salt acclimation. It can be synthesized by *Synechocystis* but is also reimported into the cell via an ATP-binding cassette (ABC) transporter to counter leakage (Mikkat & Hagemann, 2000). Other sugars that use the

same transport complex are sucrose and trehalose which also function as compatible solutes in salt stress conditions (Hagemann, 2011).

6.3.4 Significance of central carbon metabolic routes

The central carbon metabolism of *Synechocystis* comprises several biochemical pathways that allow the organism to live photoautotrophically, heterotrophically and mixotrophically (Pelroy et al., 1972). These different modes of lifestyle are fundamentally defined by the direction of enzymatic reactions in the respective central metabolic routes. In that way, a complex metabolic network is created to intertwine anabolic reactions of the CBB cycle with gluconeogenesis for C_4 reduction and storage, and catabolic reactions of glycolytic pathways which oxidize organic carbon sources like stored glycogen and imported glucose (Xiong et al., 2017). For a unicellular organism like *Synechocystis*, which does not possess organelles or major cellular compartments, a tight regulation of metabolic routes and overlapping central carbon pathways is essential to react and adjust to rapid environmental changes like fluctuations of light or CO_2 availability (Jablonsky et al., 2016). Figure 2 gives an overview of the main routes in the central carbon metabolism of *Synechocystis*.

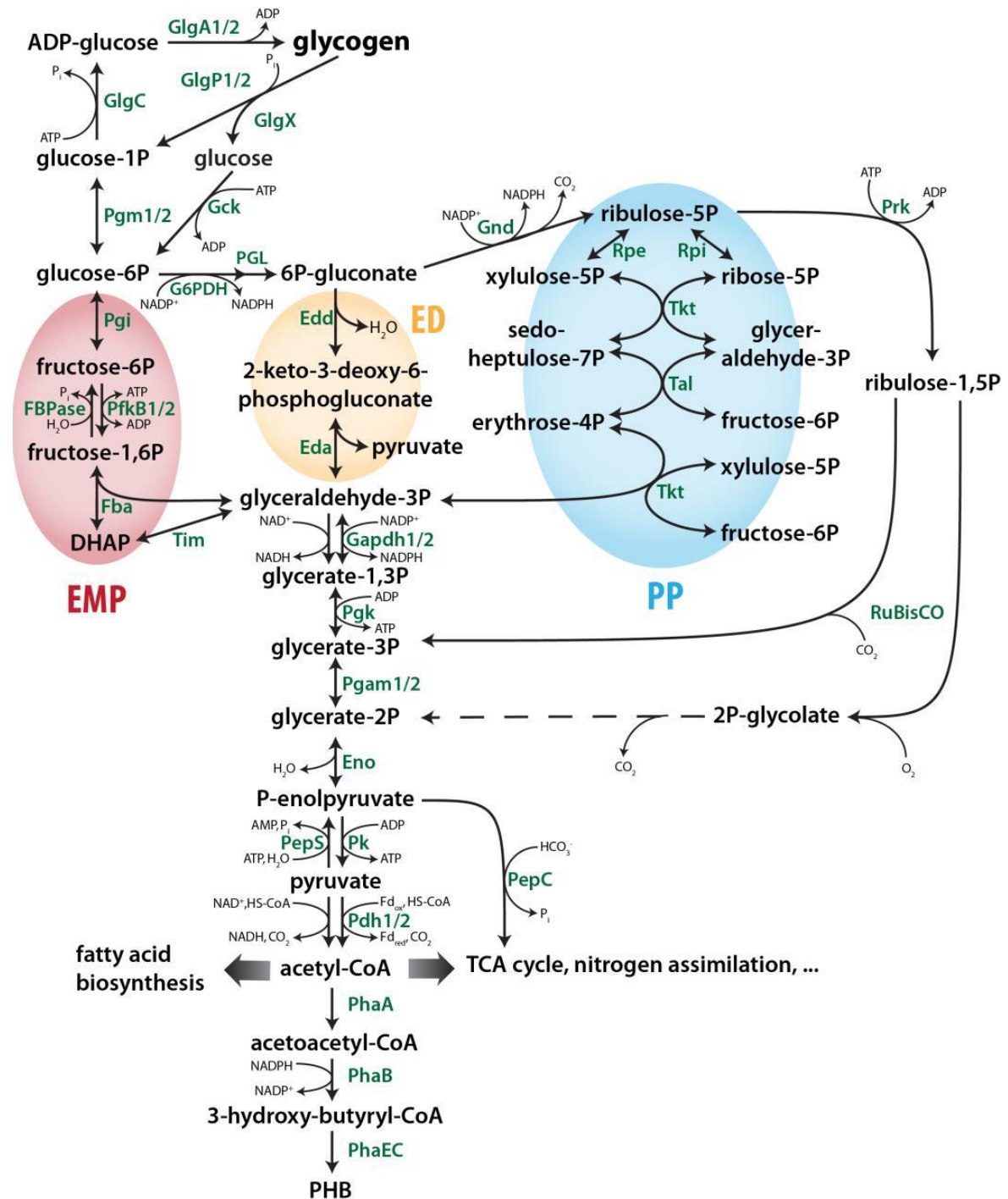


Figure 2: Overview of the central carbon metabolism in *Synechocystis*. Adapted from Koch et al. (2019). Dotted lines represent several enzymatic reactions. The EMP, ED and OPP pathways are highlighted in green, blue and yellow, respectively. **Eda** – KDPG aldolase, **Edd** – Phosphogluconate dehydratase, **Eno** – Enolase, **Fba** – Fructose bisphosphate aldolase, **FBpase** – Fructose 1,6-bisphosphatase, **G6PDH** – Glucose 6-phosphate dehydrogenase, **Gapdh** – Glyceraldehyde 3-phosphate dehydrogenase, **Gck** – Hexokinase, **GlgA** – Glycogen synthase, **GlgC** – Glucose 1-phosphate adenylyltransferase, **GlgP** – Glycogen phosphorylase, **GlgX** – Glycogen debranching enzyme, **Gnd** – 6-phosphogluconate dehydrogenase, **Pdh** – Pyruvate 16lycol16genase, **PepC** – Phosphoenolpyruvate carboxylase, **PepS** – Phosphoenolpyruvate synthase, **PfkB** – Phosphofructokinase, **Pgam** – Phosphoglycerate mutase, **Pgi** – Glucose 6-phosphate isomerase, **Pgk** – Phosphoglycerate kinase, **PGL** – 6-Phosphogluconolactonase, **Pgm** – Phosphoglucomutase, **PhaA** – Acetyl-CoA acetyltransferase, **PhaB** – Acetoacetyl-CoA reductase, **PhaEC** – PHB synthase, **PHB** – Polyhydroxybutyrate, **Pk** – Pyruvate kinase, **Prk** – Phosphoribulokinase, **Rpe** – Ribulose 5-phosphate 3-epimerase, **Rpi** – Ribose 5-phosphate isomerase, **RuBisCO** – Ribulose 1,5-bisphosphate carboxylase/oxygenase, **Tal** – Transaldolase, **Tim** – Triosephosphate isomerase, **Tkt** – Transketolase

6.3.5 *Anabolic carbon routes and glycogen formation*

The anabolic pathways of the central carbon metabolism are based on the reduction of C_i to organic sugars and metabolic intermediates in the CBB cycle (Durall & Lindblad, 2015). Here, CO_2 is photosynthetically fixed by RuBisCO to RuBP in the carboxysome, leading to the production of two molecules of 3PGA. Then, 3PGA is mainly metabolized for the regeneration of the precursor molecule RuBP to conclude the CBB cycle. In this process, the key enzyme glyceraldehyde 3-phosphate dehydrogenase 2 (GapDH2, Sll1342 in *Synechocystis*, Koksharova et al., 1998) requires NADPH from the photosynthetic light reaction to convert glycerate 1,3-bisphosphate (G1,3BP) to glyceraldehyde 3-phosphate (GAP). Likewise, photosynthetic ATP is used in the CBB cycle at the steps of phosphoglycerate kinase (P_{gk}) and phosphoribulokinase (P_{rk}). Excess of fixed carbon can also be redirected to gluconeogenic pathways that lead to the formation of carbon storage compounds like glycogen (Gründel et al., 2012). During gluconeogenesis, the precursor metabolite 3PGA is enzymatically converted to glucose 1-phosphate (G1P), which includes a key reaction by fructose 1,6-bisphosphatase (FBPase) to convert fructose 1,6-bisphosphate (FBP) to fructose 6-phosphate (F6P), a metabolite that is shared with the CBB cycle. Glycogen is a glucose polymer and serves as a storage compound in cyanobacteria (Ball & Morell, 2003; Zilliges, 2014). It is synthesized starting with the formation of ADP-glucose from G1P and ATP by a glucose 1-phosphate adenylyltransferase (GlgC). Then, the glycogen synthase GlgA transfers the glycosyl group from ADP-glucose to an existing glycogen chain by an α -1,4 glycosidic bond. Further branching is then possible through insertion of α -1,6 glycosidic bonds by the glycogen branching enzyme GlgB to create a granule structure (Preiss & Romeo, 1994).

6.3.6 *Catabolic carbon routes and glycogen breakdown*

Glycogen can be broken down and metabolized by glycolytic routes to provide organic carbon and energy in conditions when photosynthesis is insufficient for energetic and metabolic needs (Preiss & Romeo, 1994). First, glycogen chains are enzymatically debranched and split by debranching enzyme GlgX and glycogen phosphorylases GlgP1 and GlgP2 to release glucose and G1P, which are then converted to glucose 6-phosphate (G6P) by hexokinase Hk and phosphoglucomutase Pgm, respectively (Doello et al., 2018). G6P is the key metabolite for catabolic carbon metabolism as it is the shared entry point of three main glycolytic routes: The Embden-Meyerhof-Parnas (EMP) pathway, the oxidative pentose phosphate (OPP) pathway and the Entner-Doudoroff (ED) pathway (Chen et al., 2016). Along these pathways, C₆ sugars like glucose are stepwise oxidized to the C₃ intermediate GAP that can then enter lower glycolysis. The substrate glucose can originate from glycogen

degradation or extracellular uptake. The enzymatic reactions of the lower glycolysis are shared between the three glycolytic routes and describe the conversion of GAP to pyruvate. The oxidative reactions of these catabolic pathways are coupled to the production of energy as ATP and different ratios of reduction equivalents in the form of nicotinamide adenine dinucleotide (NADH) and/or NADPH (Vermaas, 2001).

The EMP pathway, also called “classical” glycolysis, is the energetically most efficient route producing two molecules of ATP per molecule glucose. The key enzyme phosphofructokinase (Pfk) catalyses the conversion of F6P to FBP and is encoded by two gene copies in the *Synechocystis* genome (Knowles & Plaxton, 2003).

The OPP pathway, the main route for glucose catabolism in *Synechocystis*, mainly runs in the opposite direction of the regenerative phase of the CBB cycle thus producing C5 sugars essential for biosynthesis of nucleic acids (Ueda et al., 2018). It is the most efficient way for NADPH production in the dark and requires lower enzymatic resource cost due to shared enzymes with the CBB cycle (Yang et al., 2002). The OPP pathway key enzymes are the glucose 6-phosphate dehydrogenase (Zwf, G6PDH) and the 6-phosphogluconate dehydrogenase (Gnd), which catalyse the conversion of G6P to 6-phosphogluconate (6PG) and then to ribulose 5-phosphate (R5P), respectively. In this route, glucose can be completely oxidized stepwise to CO₂ that is released by the Gnd reaction (Jansén et al., 2010). The intermediate F6P is shared with the CBB cycle and the EMP pathway and thus allows the OPP pathway to be either cyclic or non-cyclic. In the cyclic mode, F6P from the OPP pathway is converted back to G6P to re-enter the cycle, whereas the non-cyclic mode has F6P metabolized by Pfk to enter glycolysis.

The ED pathway is the latest discovered glycolytic route in cyanobacteria (Chen et al., 2016). It branches off the OPP pathway with a 6-phosphogluconate dehydratase (Edd) producing the intermediate 2-dehydro-3-deoxy-6-phosphogluconate (KDPG) from 6PG. The key enzyme Eda, an KDPG aldolase, directly converts KDPG to GAP and pyruvate. This route does not share intermediates with the CBB cycle and was thus proposed as the preferential glycolytic route in conditions of photosynthetic CO₂ assimilation (Chen et al., 2016). However, its contribution to the overall glucose degradation has recently been debated (Bachhar & Jablonsky, 2022; Schulze et al., 2022).

Apart from the entry intermediate G6P, these three pathways also overlap in the lower glycolysis reactions, in which glyceraldehyde 3-phosphate (GAP) is stepwise converted to pyruvate. In addition to the glucose degradation, organic carbon can be directly imported into lower glycolysis from the CBB cycle via the conversion of 3PGA to 2PGA by phosphoglucomutase (Pgam), especially under low C/N ratios. Pyruvate is mainly converted to acetyl-CoA and channelled into the tricarboxylic acid (TCA) cycle or fatty acid biosynthesis pathways to create carbon skeletons as cellular building blocks (Zhang & Bryant, 2011).

Another main sink of acetyl-CoA is the biosynthesis of PHB (Hauf et al., 2013), which is the second cyanobacterial carbon and energy storage compound and accumulates highest in nitrogen or phosphate starvation conditions (Koch et al., 2020).

6.3.7 *Glycolytic routes as anaplerotic shunts*

In photoautotrophic conditions, the central carbon metabolism of *Synechocystis* is mainly associated with the fixation of CO₂ in the CBB cycle for generation of carbon skeletons, and rerouting fixed carbon excess towards glycogen formation. During the last years, the image of the CBB cycle as an autonomous self-sufficient cycle has been rated an oversimplified view. Instead, the CBB cycle is embedded into a network of replenishing and consuming reactions to ensure continuous operation, similar to the TCA cycle. Makowka et al. (2020) discovered these replenishing properties of the ED, EMP and OPP pathways in *Synechocystis*. These glycolytic routes can mobilize stored glycogen at their full length at night, but also function as shortened anaplerotic shunts for the CBB cycle in light. This was initially indicated by a decreased photoautotrophic growth and impaired glycogen catabolism in light for *Synechocystis* mutant strains deficient in the KDPG aldolase Eda. Follow-up research confirmed the importance of these glycolytic shunts especially to restart an arrested CBB cycle after dark to light transitions (Makowka et al., 2020). These catabolic routes thereby fine-tune CO₂ fixation and carbon allocation in *Synechocystis* under photoautotrophic conditions.

6.4 Importance of regulation of the central carbon metabolism in *Synechocystis*

6.4.1 *Regulating the switch between photoautotrophic and heterotrophic modes of lifestyle*

Carbon allocation describes the process of directing organic carbon products into specific anabolic or catabolic routes of the central carbon metabolism. The defined routing of intermediates requires a complex decision process based on internal cellular factors like growth stage, metabolite steady state values and glycogen disposability, and external factors like relative concentrations of C_i and nitrogen sources (Ciebiada et al., 2020). However, the exact mechanisms how cyanobacterial cells regulate their primary metabolism and carbon allocation in response to external and internal triggers remain mostly unknown. Additionally, habitat types ranging between terrestrial locations and open waters can highly influence intensity and availability of light, as well as occurrence of competing organisms. For planktonic *Synechocystis*, the ever-changing location in the waterbody influences population density and solubility of CO_2 in water, thus causing fluctuations in C_i supply and light intensity, respectively (Badger et al., 2006). These constant and rapid fluctuations require a flexible and equally rapid switch between heterotrophy and photoautotrophy for *Synechocystis* to adjust its metabolism according to resource availability, as heterotrophic and photoautotrophic metabolic routes share intermediates and enzymes of the central carbon metabolism (Makowka et al., 2020).

The metabolism of *Synechocystis* mainly reacts to intracellular changes of energy and/or metabolic levels as results of environmental changes (Galperin, 2005). Especially for carbon allocation in fluctuating C_i availability, *Synechocystis* requires a flexible and reversible switch within the central carbon metabolism and relies on a decision-making process on several regulatory layers. In shared pathways, especially bidirectional enzymes or reactions that can be catalysed by more than one enzyme, so-called isoenzymes, constitute specific metabolic branching points. Thereby, the directions of enzymatic catalysis can be regulated by various cellular mechanisms and thus, the allocating flux of intermediates is adjusted towards either carbon catabolism or anabolism without causing futile cycles. Here, it is important to note that the protein levels for key enzymes stay widely unchanged to retain the catalytic capacities needed for both heterotrophic and photoautotrophic modes. In contrast, regulating the gene expression for central enzymes by transcriptional mechanisms changes protein abundance and takes comparably longer (Jablonsky et al., 2016). Generally, the abundances of key enzymes of C metabolism and their corresponding mRNA amounts do not change under different C_i conditions (Klähn et al., 2015; Spät et al., 2021; Barske et al., 2023), which, however, have a profound influence on carbon allocation (Eisenhut et al., 2008b). Therefore, regulation of transcription levels can be largely ruled out in this context, and has

instead been described mostly for nitrogen assimilation (Ohashi et al., 2011) and the CCM (Burnap et al., 2015). Instead, rather post-transcriptional strategies that enable comparatively quick adaptations are needed to adjust metabolic fluxes for carbon allocation. These strategies include protein-protein interaction, protein phosphorylation, redox regulation, signalling cascades or effector molecule binding. These mechanisms can inhibit or enhance enzymatic activity at branching points temporarily without affecting the respective protein abundance (Jablonsky et al., 2016). In biotechnological application, the knowledge of such metabolic regulatory points would be beneficial for product yield if a flux can be directed towards a specific carbon-based compound like alcohols, diols, fatty acids and organic acids (Knoot et al., 2018).

The switch between heterotrophy and photoautotrophy is neither exclusively dependent on day-night cycles, nor is it only caused by fluctuations in light availability that directly influence photosynthesis efficiency. It is rather a steady process that also occurs in constant light conditions, as an adaptation to changes in nutrient supply that alter the energetic and metabolic state of the cell. For example, a sudden shift from high to low CO₂ levels causes a similar metabolic profile as a switch from autotrophic to heterotrophic modes after light-to-dark changes (Burnap et al., 2015). The flexibility of *Synechocystis* to alternate between modes of lifestyles appears to be improved by a kind of metabolic memory that is so far hardly understood. Alterations in extracellular conditions can cause specific modifications within metabolic pathways that serve as a transient storage of information. This includes accumulation of signal metabolites characteristic for nitrogen or carbon limitation like 2OG and 2PG, respectively (Muro-Pastor et al., 2001; Eisenhut et al., 2008b; Zhang et al.; 2018). Their changing levels can cause signalling cascades to reroute metabolic fluxes of carbon or nitrogen assimilation. Similarly, a characteristic accumulation of storage compound glycogen in nitrogen starvation stores information about environmental conditions until glycogen is swiftly mobilized upon nitrogen resuscitation (Doello et al., 2018). This might help to make coherent decisions during the switch from photoautotrophy to heterotrophy to avoid futile cycles and metabolic stress.

6.4.2 The triosephosphate hub around key enzymes GapDH and Pgam

In *Synechocystis*, CO₂ is mainly fixed in the CBB cycle leading to the production of triosephosphate 3PGA as the first stable organic carbon intermediate. Then, 3PGA is subject to carbon allocation and can be metabolized in two opposing directions. One way is its conversion by Pgk and GapDH to GAP to then refuel the CBB cycle or to initiate gluconeogenesis. The second way includes conversion of 3PGA by Pgam to 2-phosphoglycerate (2PGA) to follow the lower glycolysis towards the TCA cycle (Mills et al., 2020). This process requires coherent decision-making and precise regulation of metabolic fluxes for two reasons. First, fluxes need to be directed depending on the environmental conditions like light intensity and extracellular Ci concentrations. In high CO₂ conditions, gluconeogenesis can be enhanced to accumulate glycogen as storage compound (Gründel et al., 2012). In low light and Ci limitation, the CBB cycle provides fewer triosephosphates, and anaplerotic reactions in catabolic direction are preferred. Secondly, cyanobacterial GapDH and Pgam are bidirectional enzymes (Koksharova et al., 1998; Jablonsky et al., 2013). Without regulatory mechanisms, these enzymes would cause futile reactions halting the directed carbon allocation, and wasting energy in the process.

Hence, the enzymatic reactions and intermediates ranging from the stepwise conversion of GAP to 2PGA and vice versa in the lower glycolysis have been identified as a central carbon distribution hub that can be referred to as the so-called “triosephosphate hub”. This hub contains key enzymes GapDH and Pgam as major branching points for organic carbon allocation. Therefore, it serves as an important target for metabolic regulation of the heterotrophy-autotrophy switch in *Synechocystis*.

There are two different GapDH isoenzymes in *Synechocystis* with distinct functions (Koksharova et al., 1998). GapDH1 is a protein of 354 amino acids (37.8 kDa) encoded by the gene *slr0884*. GapDH2, encoded by *slr1342*, contains 337 amino acids (36.4 kDa). Both are bidirectional enzymes that catalyse the interconversion of GAP and G1,3BP in the triosephosphate hub. However, they diverge in the use of coenzymes. While GapDH2 can utilise both NAD(H) and NADP(H), GapDH1 is only able to use NAD(H). Therefore, GapDH2 is also part of the CBB cycle, where it oxidizes NADPH from the photosynthetic electron transport chain to NADP⁺ during regeneration of RuBP for Ci fixation (Koksharova et al., 1998). The catabolic reactions of both GapDH variants are crucial for heterotrophic growth and mixotrophic growth using stored glycogen or external glucose, respectively.

Two different phosphoglycerate mutases are annotated for *Synechocystis*. Protein Slr1945 (Pgam1) is a 2,3-bisphosphoglycerate-independent phosphoglycerate mutase, while putative Pgam2 Slr1124 has an additional annotation as phosphoserine phosphatase. In this context, this dissertation elaborates on the function of candidate regulatory proteins in the

triosephosphate hub and their role for the switch between hetero- and photoautotrophic modes of lifestyle.

6.4.3 Cp12 protein as regulator of the Calvin-Benson-Bassham cycle

One exemplary regulatory protein discussed in this dissertation is Cp12. This small protein is conserved in almost all oxygenic photoautotrophic organisms, present from cyanobacteria to algae and land plants. Cp12 was first identified in leaves of pea, spinach and tobacco (Pohlmeyer et al., 1996). Due to its aberrated behaviour in SDS-PAGE experiments, it was then named “chloroplast protein of 12 kDa”, or “Cp12” in short. However, the actual molecular mass of the protein at around 8.5 kDa is lower than assumed, because of its properties as a conditionally disordered protein. The disordered state is considered the inactive reduced form of Cp12 while under certain oxidizing conditions, it takes structure mediated by conserved cysteine pairs (Graciet et al., 2003a). Canonical Cp12 proteins among photoautotrophic organisms possess two cysteine pairs close to the N-terminus and C-terminus, respectively, that can form redox-dependent disulfide bridges (Groben et al., 2010). These conformational changes then allow the initially disordered Cp12 protein to restructure and subsequently interact with its main binding partners phosphoribulokinase Prk and glyceraldehyde 3-phosphate dehydrogenase GapDH. In the CBB cycle, Prk produces RuBP, the direct substrate for CO₂ fixation by RuBisCO, while GapDH activity is an essential branching point for the regeneration path of RuBP. Thereby, Prk and GapDH use ATP and NADPH, respectively, which are both products of photosynthesis. Upon reducing conditions, the complex dissociates again by disulfide reduction allowing GapDH and Prk to be reactivated along with the CBB cycle. Cp12 is an important downregulator of the CBB cycle in darkness, as its oxidized form is able to bind Prk and GapDH in a supramolecular ternary complex, thus inhibiting both enzymes. This major impact on the central carbon metabolism makes Cp12 an excellent candidate for investigations on carbon-related regulatory mechanisms in *Synechocystis*.

The work of McFarlane et al. (2019) solved the crystal structure of the ternary complex between Cp12, Prk and GapDH of *Thermosynechococcus elongatus*. This study in the field of cyanobacteria confirmed the sequential order of complex formation *in vitro* that had already been described for *Chlamydomonas reinhardtii* (Graciet et al., 2003b). A cyanobacterial GapDH tetramer is first bound by two oxidized copies of Cp12 to form a GapDH-Cp12 subcomplex. Subsequently, Cp12 forms an ordered disulfide-locked helical hairpin that allows interaction with Prk (McFarlane et al., 2019). Two GapDH-Cp12 subcomplexes in turn can then bind two Prk dimers, thus forming a ternary supramolecular complex consisting of two GapDH tetramers, two Prk dimers and four ordered Cp12 (Figure 3). The canonical consensus sequence AWD_VEEL of Cp12 interacts with the Ru5P-binding

site of Prk (Yu et al., 2020). This way, Cp12 molecules bridge the active sites of GapDH and Prk, thereby locking this inhibitory complex (McFarlane et al., 2019).

Until recently, physiological studies on Cp12 in unicellular photosynthetic species had mostly been conducted on green algae *C. reinhardtii* (Gerárd et al., 2022), while studies on cyanobacterial physiology mainly included *Synechococcus elongatus* PCC 7942 (hereafter *Synechococcus* 7942) and *T. elongatus* (McFarlane et al., 2019; Matsumura et al., 2011; Tamoi et al., 2005). However, *C. reinhardtii* possesses chloroplast structures that mediate spatial separation of the CBB cycle and other routes of the central carbon metabolism, and the Cp12 sequence in *Synechococcus* 7942 lacks the N-terminal pair of cysteine residues (Tamoi et al., 2005), in contrast to *Synechocystis*. In higher plants, Prk and GapDH are additionally directly redox-regulated by thioredoxins, while most cyanobacterial CBB cycle enzymes are not (Marri et al., 2009; Tamoi et al., 2005). Instead, the cyanobacterial mechanism is an indirect redox-regulation of the CBB cycle by oxidized Cp12.

In cyanobacteria, Cp12 complex formation is mediated in response to the intracellular NAD(H)/NADP(H) ratio (Tamoi et al., 2005). In *Synechococcus* 7942, increasing the NAD⁺/NADPH ratio led to complex formation while a decreased ratio following a higher NADPH concentration caused the complex to dissociate *in vitro*. Furthermore, Cp12 was found to act as competitive inhibitor for NADP⁺ in GapDH in *T. elongatus* (McFarlane et al., 2019). For *Synechocystis*, only *in vitro* complex formation studies with recombinant proteins had been conducted (Wedel & Soll, 1998).

Apart from serving as a dark-light redox switch of the CBB cycle, Cp12 is an intriguing protein regulator with further potential functions. Its role might span additional environmental conditions that require a redox regulation of the CBB cycle, such as fluctuating CO₂ levels or the supply of external carbon sources impacting the cellular redox status. For example, Cp12 is involved in high light protection in *Synechococcus* 7942 (Tamoi & Shigeoka, 2021). Additionally, Cp12 might have regulatory interactions with other proteins besides GapDH and Prk. In *C. reinhardtii*, Cp12 can bind aldolase as another interactor protein (Erales et al., 2008a). Furthermore, the impact of other structural properties of Cp12, apart from the essential cysteine residues, might harbour yet unknown regulatory capacities. For example, a mutated aspartate in the canonical Cp12 core sequence AWD_VEEL impairs the binding of Cp12 to GapDH in *C. reinhardtii* (Lebreton et al., 2006). Furthermore, Cp12 in *Synechocystis* has been identified as phosphoprotein under different CO₂ conditions, which might offer additional regulatory possibilities (Spät et al., 2021).

In *Synechocystis*, the gene *ssl3364* of 225 bp encodes a Cp12 protein of 74 amino acids (8.3 kDa). It possesses both canonical cysteine pairs at the N terminus (Cys19, Cys29) and C terminus (Cys60, Cys69), and contains the canonical core sequence AWD_VEEL. Prk in *Synechocystis* is encoded by *sl1525* for a protein size of 332 amino acids. Both

Synechocystis glyceraldehyde 3-phosphate dehydrogenases, GapDH1 and GapDH2, are active in the triosephosphate hub while GapDH2 (Sll1342) is additionally essential for a functioning CBB cycle as it can utilise photosynthetic NADPH (Koksharova et al., 1998).

Synechocystis is capable of taking up external organic carbon sources which allows heterotrophic and mixotrophic growth. Because carbon allocation requires a flexible switch in reaction to such environmental and therefore intracellular changes, the importance of CBB cycle regulation by Cp12 is discussed in this dissertation.

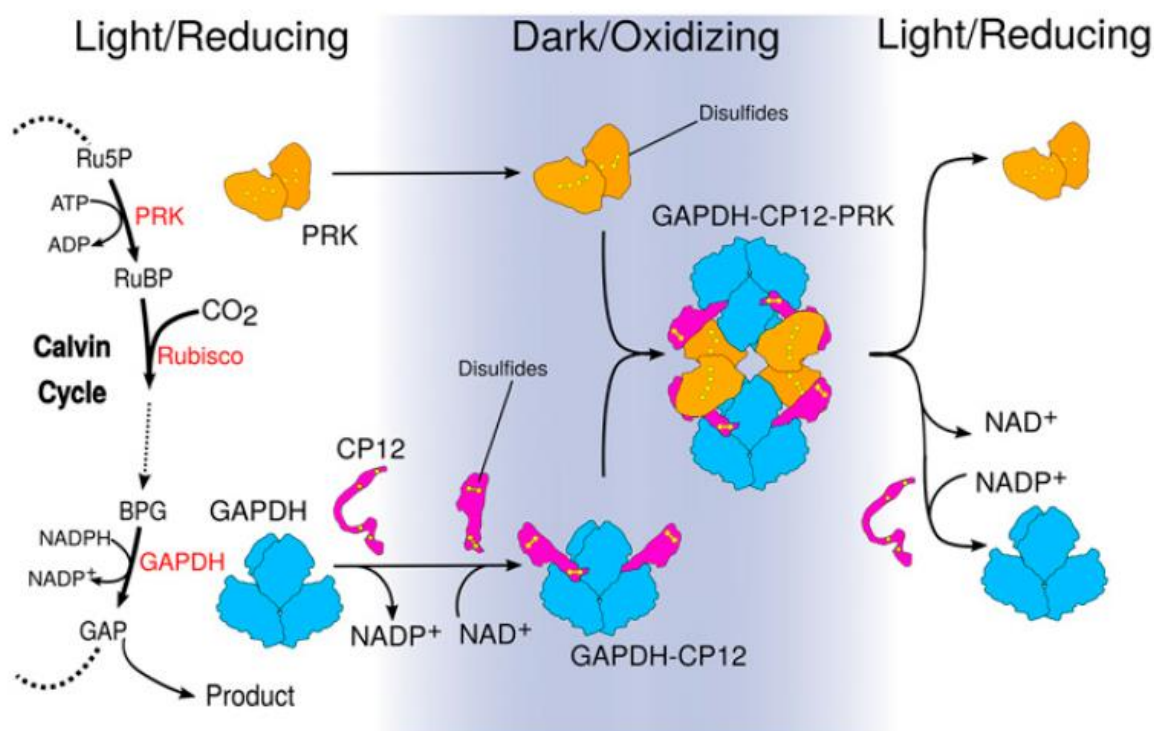


Figure 3: Model of structural changes for redox-dependent complex formation mediated by Cp12 in *T. elongatus* (McFarlane et al. 2019). **BPG** – Glycerate 1,3-bisphosphate, **GAP** – Glyceraldehyde 3-phosphate, **GAPDH** – Glyceraldehyde 3-phosphate dehydrogenase, **PRK** – Phosphoribulokinase, **Ru5P** – Ribulose 5-phosphate, **Rubisco** – Ribulose 1,5-bisphosphate carboxylase/oxygenase, **RuBP** – Ribulose 1,5-bisphosphate

6.5 Connection of carbon and nitrogen metabolism in *Synechocystis*

6.5.1 Nitrogen assimilation in *Synechocystis*

Apart from carbon, nitrogen (N) is a second key nutrient for cyanobacterial growth and is incorporated into essential cellular building blocks like amino acids for protein biosynthesis (Esteves-Ferreira et al., 2018). Cyanobacteria developed different N assimilation strategies depending on habitat and cell differentiation. Diazotrophic cyanobacteria can fix atmospheric nitrogen (N_2) through the nitrogenase reaction. However, N_2 fixation and oxygenic photosynthesis are incompatible, because the nitrogenase complex is oxygen-sensitive (Berman-Frank et al., 2003). Therefore, either spatial separation by fixing N_2 in specialized cells called heterocysts is realized in filamentous cyanobacteria, or temporal separation enables fixation of N_2 during the night in non-heterocystous strains. In contrast, *Synechocystis* is a non-diazotrophic strain and relies on combined nitrogen sources like ammonium (NH_4^+), nitrate (NO_3^-) or urea. Nitrite (NO_2^-) and NO_3^- are the most common N sources in habitats of *Synechocystis*. Both are taken up by the transporter system NrtABCD (Luque et al., 1994; Aichi et al., 2001), while urea is transported via UrtABCD (Valladares et al., 2002). Both import complexes are ABC transporters and are followed by respective enzymatic conversions via nitrate reductase and/or nitrite reductase to NH_4^+ inside the cell. Direct uptake of NH_4^+ is achieved via ammonium permeases under low N conditions, while in the presence of high ammonia (NH_3) availability, this nutrient can diffuse through the cytoplasmic membrane (Montesinos et al., 1998). In general, NH_4^+ is the energetically preferred combined nitrogen source, because NO_3^- and NO_2^- reduction to NH_3 is highly energy-demanding. Cellular NH_3 is incorporated into the primary metabolism via the glutamine synthetase / glutamine oxoglutarate aminotransferase (GS/GOGAT) cycle (Muro-Pastor et al., 2005). In this cycle, GS first catalyses the reaction of glutamate and NH_3 to glutamine at the expense of ATP. The amino group of glutamine is then transferred to 2-oxoglutarate (2OG) using reduced ferredoxin by GOGAT, generating two molecules of glutamate (Flores & Herrero, 2005). One glutamate molecule can thus re-enter the cycle while the second one can be directed towards further biosynthetic pathways.

6.5.2 Significance of C/N homeostasis in *Synechocystis*

In contrast to other bacteria, cyanobacteria adjust their metabolism according to their internal homeostasis, rather than directly reacting to environmental changes (Galperin, 2005). Therefore, it is essential to monitor their intracellular metabolic levels to readjust their carbon to nitrogen (C/N) balance. For vegetative growth with balanced carbon and nitrogen assimilation, a C/N ratio of 5:1 is maintained (Wolk, 1973). The carbon metabolism is directly linked to the nitrogen metabolism by 2OG. The production of this metabolite as carbon

precursor for ammonia assimilation is one of the main functions of the “incomplete” TCA cycle in cyanobacteria (Steinhauser et al., 2012). The TCA cycle is fuelled by CO₂ fixation products via lower glycolysis and from there, 2OG enters the GS/GOGAT cycle. The availability of 2OG as a carbon skeleton essentially influences the rate of nitrogen assimilation (Esteves-Ferreira et al., 2018). Changing 2OG levels signalize changes in the C/N balance. While assimilation of ammonium reduces the 2OG pool, carbon allocation towards the TCA cycle after CO₂ fixation leads to increased levels. Likewise, an accumulation of 2OG signalizes a limitation of nitrogen sources and a C/N imbalance towards carbon. These metabolic signals can be read out by the regulatory signal transduction protein PII in *Synechocystis* (Forchhammer & Selim, 2020).

6.5.3 Regulation of nitrogen metabolism by the PII protein in *Synechocystis*

PII proteins are a family of trimeric proteins that are highly conserved among plants and cyanobacteria as well as heterotrophic bacteria (Forchhammer et al., 2022). They can integrate metabolic signals by binding specific effector molecules. In general, this binding causes conformational changes in the protein structure, which enables PII proteins to interact with various targets to maintain the C/N homeostasis (Forchhammer & Lüddecke, 2016). In *Synechocystis*, ATP and ADP can bind to PII where they compete for the same binding sites. When Mg²⁺-ATP is already bound, PII can additionally bind 2OG. These interactions cause changes of conformation in the target-binding loop structures (T-loops) depending on the effector molecule (Merrick, 2015). These structural rearrangements of PII thereby reflect the integrated information about cellular levels of bound metabolites and thus enable specific interaction with a range of target proteins. A signal transduction towards these targets can then cause cascades of metabolic regulation processes to react to energy imbalances and reconstitute the C/N ratio. One primary cyanobacterial target protein is the N-acetyl-L-glutamate kinase (NAGK) which controls arginine biosynthesis (Heinrich et al., 2004). During low 2OG levels due to sufficient nitrogen sources, PII with bound ATP can form an activating complex with NAGK leading to a higher flux towards arginine (Lüddecke & Forchhammer, 2015). Arginine can then be utilised for the formation of cyanophycin, the cyanobacterial nitrogen storage compound (Stephan et al., 2000). High 2OG levels lead to the dissociation of the PII-NAGK complex (Maheswaran et al., 2004). Likewise, PII-ADP cannot bind to NAGK, making this regulation also dependent on energy sensing.

In excess nitrogen conditions, PII can bind to the small protein PipX, a coactivator of NtcA, which is a global cyanobacterial nitrogen control transcription factor (Espinosa et al., 2007). At higher 2OG levels indicating nitrogen depletion, the PII-PipX complex dissolves and PipX can bind to NtcA again to regulate expression of nitrogen assimilation related genes (Espinosa et al., 2014). An example how PII can additionally regulate the carbon metabolism

is given by its interaction with phosphoenolpyruvate carboxylase PEPC. PEPC is the second major enzyme for carbon fixation in *Synechocystis* and is activated by PII-ATP in the presence of 2OG (Scholl et al., 2020).

6.5.4 *PirC as novel interactor with PII in Synechocystis*

A second exemplary protein discussed in this dissertation regarding its possible regulatory role in the central carbon metabolism is PirC, a small protein in *Synechocystis* of 112 amino acids, that is highly conserved among cyanobacteria (Orthwein et al., 2021). It is encoded by gene *sll0944* and had initially been identified as an interactor of unknown function with the protein PII in *Synechocystis* (Watzer et al., 2019). It is part of the NtcA regulon (Giner-Lamia et al., 2017) and was shown to be upregulated and highly abundant in nitrogen starvation conditions (Spät et al., 2018), and repressed under low CO₂ conditions (Spät et al., 2021). The *pirC* gene is located upstream of the gene for the glycogen synthase GlgA1 required for glycogen synthesis that is highly activated during the acclimation to nitrogen deprivation. However, co-immunoprecipitation (CoIP) studies identified Pgam1 (Slr1945) as second strong interaction partner with PirC in presence of 2OG and ATP. As Pgam1 is a key enzyme of the triosephosphate hub, this finding suggested PirC as an important regulatory link between central carbon and nitrogen metabolism in *Synechocystis*. The significance of PirC for Pgam1 regulation and its eponymous role as “PII-interacting regulator of carbon metabolism” have been investigated in this dissertation and are discussed in more detail below.

7 AIMS OF THIS INVESTIGATION

The scientific aims of this dissertation all concern the regulatory diversity and flexibility of the central metabolism of the cyanobacterium *Synechocystis* sp. PCC 6803. Fluctuating environmental conditions as well as varying intracellular metabolite and energy levels require a quick acclimation and respective regulatory mechanisms. This ensures that metabolic fluxes during alternations of photoautotrophic and heterotrophic lifestyle modes remains efficient. In this regard, this dissertation focuses on carbon allocation regulation as well as synthesis and glycolytic mobilization of storage metabolite glycogen. The investigational approach and the presentation of results in the respective scientific context fall into three categories.

First, changing CO₂ conditions require regulations of the central carbon routes. The preference for specific glycolytic pathways and the underlying mechanisms are largely unknown. By physiological analysis of mutant strains deficient in different key enzymes of the EMP, ED and OPP pathways, the importance of each of these catabolic routes was investigated. In CO₂ shift experiments, we aimed to identify the roles of these pathways during acclimation to drastic changes in availability of Ci. Therefore, glycogen and metabolic analyses were performed to study putative CO₂-dependent effects.

Second, *Synechocystis* is also exposed to changing availabilities of organic carbon sources as well as fluctuating light conditions and day-night rhythms. Light availability determines carbon assimilation in the CBB cycle by supplying reduction equivalents from photosynthesis. External sugars like glucose can be taken up and metabolized in catabolic routes that require respective regulations in light. Therefore, we aimed to investigate the role of the small protein Cp12 as regulator of the CBB cycle in reaction to different light intensities and conditions that would change the redox status of the cell. Notably, one interactor of Cp12 is GapDH, which is a central enzyme in the triosephosphate hub and therefore an important branching point for carbon allocation. Thus, the goal was to broaden the knowledge about Cp12 as a regulator of the central carbon metabolism beyond its significance in day-night regulation of the CBB cycle.

Third, nitrogen and carbon assimilation are tightly connected in cyanobacteria and a maintained C/N homeostasis is key to an efficient central metabolism. The small protein PirC had been identified as interactor with the central nitrogen regulator PII as well as with the key triosephosphate hub enzyme Pgam1. This suggested PirC as a candidate regulatory protein for nitrogen starvation with close relation to the regulation of carbon allocation. In nitrogen shift experiments with coupled analyses of metabolite levels, we aimed to elucidate the significance of these protein-protein interactions for carbon storage and during nitrogen depletion.

8 GENERAL DISCUSSION

8.1 Regulation of the central carbon metabolism during changing CO₂ conditions

8.1.1 General overview

Cyanobacteria regularly experience fluctuating levels of Ci in aquatic habitats depending on pH, temperature and salinity that influence the solubility of CO₂ and conversion to bicarbonate (Kupriyanova et al., 2023). The availability of Ci determines the carbon fixation capacity through the CBB cycle, on the assumption of continuous light conditions. Ci fixed in excess is redirected to glycogen synthesis to prepare for low photosynthetic conditions, e.g. at night, and to maintain the C/N homeostasis by adjusting the intracellular C/N ratio (Forchhammer & Selim, 2019).

To a large extent, regulation of the central carbon metabolism involves adjusting the CCM as a way to maintain CO₂ fixation efficiency in limiting conditions. In contrast to the central carbon metabolism, which is in the focus of this dissertation, the CCM activity is strongly regulated at transcriptional level (Burnap et al., 2015; Hagemann et al., 2021). The transcription factor NdhR represses the expression of genes in the largest Ci regulon in *Synechocystis* under high CO₂ conditions (Figge et al., 2001, Klähn et al., 2015). NdhR is fine-tuned by 2OG and 2PG to sense intracellular C/N ratios (Muro-Pastor et al., 2001, Jiang et al., 2018, Zhang et al., 2018). Another transcription factor, CmpR, activates the BCT1 transporter under low carbon conditions (Omata et al., 2001, Nishimura et al., 2008). Moreover, there are indications for the cyanobacterial regulator CyAbrB2 to regulate the repressor NdhR and to affect PSI subunit expression during acclimation to carbon limitation (Orf et al., 2016; Ishii & Hihara, 2008). In addition to these transcriptional regulations, the cyanobacterial CCM is also regulated by a PII-paralog, which is co-expressed with the sodium/bicarbonate symporter SbtA in the *sbtAB* operon. The protein SbtB has structural similarities to PII-signalling proteins (Selim et al., 2018). It can bind to second messenger adenyl nucleotides cAMP and c-di-AMP and is involved in low Ci acclimation in *Synechocystis* (Mantovani et al., 2022). It was recently suggested that SbtB acts a valve plug regulator for SbtA to prevent leakage of bicarbonate (Haffner et al., 2023).

Synechocystis cells grown in high CO₂ conditions accumulate high levels of glycogen, whereas they mobilize this stored glycogen when carbon supply is limited. A sudden decrease of natural Ci levels requires a rapid acclimation of the cyanobacterial metabolism for carbon assimilation and catabolic glycolytic routes. In that, carbon is drained from the CBB cycle via glycolysis and TCA cycle to maintain biosynthesis of amino acids while photorespiration is activated (Jablonsky et al., 2016). This condition can be simulated by CO₂

shift experiments in liquid culture. To this end, *Synechocystis* cultures grown with supplied 5% CO₂ (high CO₂ conditions, HC) are shifted to ambient air conditions with 0.04% CO₂ (low CO₂ conditions, LC) by manually abruptly cutting off the excess CO₂ aeration. Such CO₂ shift protocols have been established to study CO₂-dependent changes of the central metabolism, combined with metabolite and transcript analyses. Previous studies revealed that *Synechocystis* cells undergo a global metabolic reprogramming upon HC to LC shifts (Eisenhut et al., 2008b) with a distinct metabolic signature. Here, CBB cycle activity decreases while the accumulation of metabolites like 2PG, glycine and a transient increase of 3PGA point to an active photorespiration. Simultaneously, glycogen breakdown is enhanced, and most amino acid levels decline (Orf et al., 2016). Shifts from HC to LC do not cause significant changes in transcript levels for primary carbon metabolism enzymes (Klähn et al., 2015). Likewise, proteomic studies revealed that carbon fixation proteins respond more strongly to light intensity changes, but barely to different Ci availability (Jahn et al., 2018; Spät et al., 2021, Barske et al., 2023). Such findings point toward biochemical control rather than transcriptional regulation in *Synechocystis* to enable a quick acclimation without comparatively high energetic costs for proteomic responses (Jablonsky et al., 2016).

There are multiple strategies for biochemical regulation of enzymes in the central carbon metabolism of *Synechocystis* in order to adjust carbon allocation in changing Ci levels. One possibility is to influence the activity of bidirectional enzymes, often present as isoenzymes in *Synechocystis*, at crucial branching points in the triosephosphate hub like Pgam1, GapDH1, GapDH2 and Pkg. A potential regulation of these enzymes enables *Synechocystis* to adjust carbon allocation in anabolic or catabolic direction during acclimation to varying Ci conditions (Koksharova et al., 1998; Jablonsky et al., 2014). Another way is protein phosphorylation of key enzymes in the triosephosphate hub as transient modification. Previous studies revealed alterations in the *Synechocystis* phosphoproteome depending on CO₂ availability for important carbon-related proteins like Cp12 and BCT1 subunits (Spät et al., 2021). In the glycogen hub, crucial phosphorylation sites of the key enzyme Pgm1 for glycogen mobilization were discovered (Doello et al., 2022).

Redox regulation is another way of adjusting the metabolism to changing Ci conditions. In *Synechocystis*, anabolic and catabolic routes of the central carbon metabolism operate only in the cytoplasm with overlapping intermediates, thus bearing the risk of futile cycles. Reducing equivalents like NADPH are produced by the photosynthetic electron transport chain and are utilised for reductive reactions of the CBB cycle. Therefore, a strategy to adjust carbon allocation is to sense the cellular redox status (Ansong et al., 2014). While key enzymes in the CBB cycle of plants like Prk and GapDH are redox-regulated in a thioredoxin-mediated way, the majority of cyanobacterial CBB cycle enzymes are not directly redox-regulated (Lindahl & Florencio, 2003; Tamoi et al., 2005).

8.1.2 Glycolytic routes in changing CO₂ conditions

Glycogen metabolism is not bound to day-night changes. Fluctuating glycogen levels in response to changing C_i and nitrogen availability have been reported for *Synechocystis* in constant light (Doello et al., 2018) and photosynthetic fluxes via the OPP pathway into the CBB cycle have been described (Young et al., 2011). Preferred routes for glycogen breakdown in constant light had been largely unknown. The discovery of the ED pathway in cyanobacteria by Chen et al. (2016) proposed another possible route of glycogen mobilization during the day as it does not share intermediates with the CBB cycle which would risk futile cycles. The catabolic routes of OPP pathway, ED pathway and EMP pathway can function as glycolytic shunts that replenish the CBB cycle in photoautotrophic conditions (Makowka et al., 2020).

Glycogen formation and breakdown depends on C_i availability. This dissertation discusses new findings that revealed a regulation of glycogen mobilization in light during changing CO₂ conditions. Results by Lucius et al. (2021) indicate a major contribution of the ED shunt for rapid acclimation to fluctuating C_i levels. This was concluded from physiological and metabolomic studies for a set of defined mutants in a CO₂ shift.

Synechocystis deletion mutants described in Chen et al. (2016) were used that are deficient in genes encoding respective key enzymes of the glycolytic ED, OPP and EMP routes (Table 1). By knocking out the gene for the *Synechocystis* glucose 6-phosphate dehydrogenase Zw_f, the mutant Δzw_f has both OPP and ED pathways blocked. Only the OPP pathway is blocked in Δgnd after deletion of the gene for the 6-phosphogluconate dehydrogenase Gnd. The mutant Δp_{fk} has the genes for both isoforms of the phosphofructokinases P_{fk}B1 and P_{fk}B2 deleted, thus interrupting the EMP pathway. In the mutant Δeda, the gene for the 2-dehydro-3-deoxy-6-phosphogluconate (KDPG) aldolase Eda is knocked out to specifically disrupt the ED pathway (Figure 4).

Table 1: Details of mutant strains used in CO₂ shift experiments for **Publication 1** (Lucius et al., 2021)

Strain	Deleted gene	Deleted enzyme	Pathway blocked
Δeda	<i>sll0107 (eda)</i>	2-dehydro-3-deoxy-6-phosphogluconate aldolase (Eda)	Entner-Doudoroff pathway
Δgnd	<i>sll0329 (gnd)</i>	6-phosphogluconate dehydrogenase (Gnd)	Oxidative pentose phosphate pathway
Δp _{fk}	<i>sll1196 (p_{fk}B1)</i> <i>sll0745 (p_{fk}B2)</i>	Phosphofructokinase (P _{fk} B1) Phosphofructokinase (P _{fk} B2)	Embden-Meyerhof-Parnas pathway
Δzw _f	<i>slr1843 (zw_f)</i>	Glucose 6-phosphate dehydrogenase (Zw _f)	Oxidative pentose phosphate pathway, Entner-Doudoroff pathway

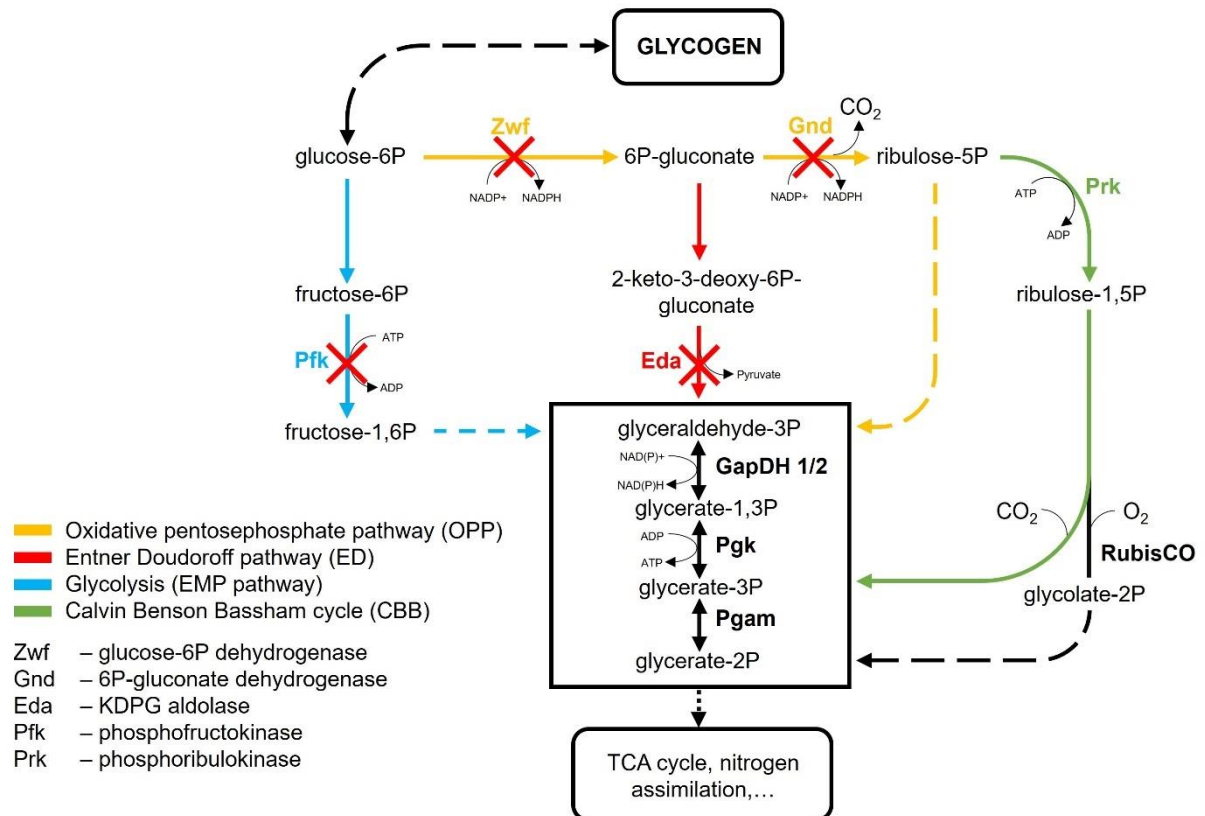


Figure 4: Central carbon metabolism of *Synechocystis* with indication of affected enzymes in the studied mutant strains. Adapted from Lucius et al. (2021). **GapDH** – Glyceraldehyde 3-phosphate dehydrogenase, **Pgam** – Phosphoglycerate mutase, **Pgk** – Phosphoglycerate kinase, **RubisCO** – Ribulose 1,5-bisphosphate carboxylase/oxygenase

The experimental strategy chosen by Lucius et al. (2021) for the analysis of CO₂-dependent glycogen mobilization is a HC-LC-HC shift experiment in continuous light (HC – High CO₂ of 5%; LC – Low CO₂ of 0.04% at ambient level). This setup enabled the investigation of both the metabolic acclimation to a sudden decrease in C_i supply, as well as a re-acclimation to saturating CO₂ conditions. The results from glycogen analysis and metabolic analysis by LC-MS were compared between the defined mutants considering the importance of the respective deleted glycolytic routes.

Cells of *Synechocystis* WT, Δzwf , Δgnd , Δpfk and Δeda were first cultivated in liquid cultures under HC conditions for CO₂ acclimation (Lucius et al., 2021). As expected, the WT showed high glycogen levels in HC conditions in preparation for future C_i limitations and to adjust the cellular C/N ratio. Glycogen rapidly decreased in the WT within 24 hours after the shift to LC conditions, representing a quick mobilization to rebalance carbon fluxes in the central carbon metabolism towards the TCA cycle and downstream cellular biosynthesis pathways. This was accompanied by a simultaneous growth delay. After the subsequent shift back to HC levels, WT cells rapidly accumulated glycogen again as increased CO₂ fixation promotes gluconeogenesis. Cells resumed growth within 24 hours after this second shift.

Similar behaviours during the HC-LC-HC shifts were observed for Δzwf , Δgnd and Δpfk regarding growth and glycogen metabolism. This suggests that an ED pathway with an intact Eda enzyme in these mutants is sufficient to utilise stored glycogen in constant light and rebalance the metabolism in a WT-like manner in acclimation to changing CO₂ conditions. Comparable absolute levels in cellular glycogen contents between this set of three single deletion mutants and the WT over the course of the two shifts also indicate that the EMP and OPP pathways play only a minor role in glycogen utilisation in constant light. This was expected as the OPP pathway is the preferred glycolytic route in darkness (Yang et al., 2002).

In contrast, Δeda showed a significantly different pattern in cellular glycogen levels (Lucius et al., 2021). Initial levels were around two times higher compared to all other examined *Synechocystis* strains. Therefore, the synthesis of glycogen in HC conditions is not impaired when the ED pathway is interrupted. After the HC-LC shift, glycogen is consumed comparatively slow. However, most notably, glycogen levels did not increase again in reaction to the LC-HC shift but stayed stable for at least three hours afterwards. Furthermore, after 24 h under resupplied HC conditions, Δeda showed a significant growth delay compared to WT and the other mutants. Apparently, *Synechocystis* relies on the glycolytic ED shunt or Eda activity to replenish and thus reactivate the CBB cycle after Ci limitation periods, as discovered by Makowka et al. (2020). Thus, EMP and OPP pathways cannot compensate the dysfunctional ED shunt in light. This enhances the knowledge about glycogen metabolism in constant light beyond its role for heterotrophic carbon supply in night phases of a diurnal cycle.

Although no apparent differences were detected for growth and glycogen metabolism between WT, Δzwf , Δgnd and Δpfk , distinct physiological differences of each affected pathway exist on a metabolic level (Lucius et al., 2021). All cultures included in the HC-LC-HC shift were sampled at specific time points to check for gradual metabolic effects in regard to acclimation to the two contrary CO₂ shifts. The first three hours after each shift document a gradual acclimation and progressing in glycogen metabolism, while samples taken after 24 hours revealed steady state metabolite data after responding to the CO₂ shifts. Steady state metabolite levels in the context of the entire carbon metabolism are illustrated in Figure 5 (**Publication 1, Figure 9**). Unfortunately, 2OG could only be quantified in few samples, which did not permit to include it in the final comparison of the different mutants. However, it should be mentioned that expected rapid changes in 2OG levels after HC or LC shifts were not detected by Lucius et al. (2021) as reported before (e.g., Eisenhut et al., 2008b), whereas 2PG levels changed as expected. Hence, the regulatory role of 2OG as a signal for different Ci conditions needs more investigations.

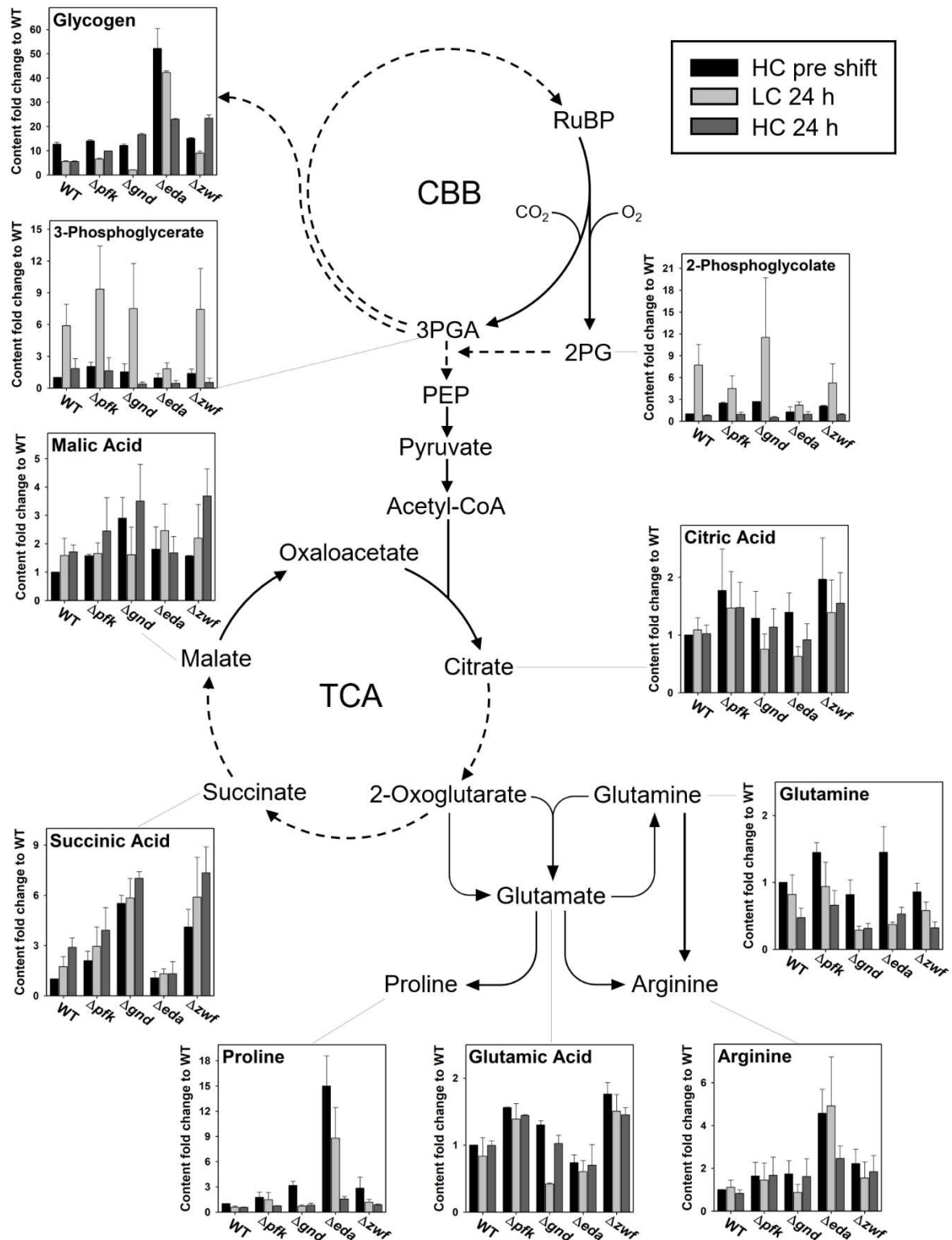


Figure 5: Steady states of selected metabolites in the context of entire carbon metabolism (Lucius et al., 2021). Dashed arrows indicate that more than one enzymatic reaction is required to catalyse this step. **2PG** – 2-Phosphoglycolate, **3PGA** – 3-Phosphoglycerate, **CBB** – Calvin-Benson-Bassham cycle, **HC** – High CO₂ conditions (5%), **LC** – Low CO₂ conditions (0.04%), **PEP** – Phosphoenolpyruvate, **RuBP** – Ribulose 1,5-bisphosphate, **TCA** – Tricarboxylic acid cycle. For denomination of mutant strains, see Table 1.

A principal component analysis (PCA) identified certain metabolites that lead to a distinction of the mutant strains from each other and from the WT during Ci acclimation (**Publication 1, Figures 4 and 5**). Among this selection are the RuBisCO products 3PGA and 2PG. In the WT, these two metabolites accumulate in LC acclimation because of increased oxygenation reaction of RuBisCO (2PG) and a decreased metabolization during readjustment of the CBB cycle (3PGA). Mutant strains Δzwf , Δgnd and Δpfk accumulated 3PGA amounts comparable to WT or at slightly increased levels. The same is true for 2PG levels upon the HC-LC shift. An ED pathway, that is blocked at the Eda step, suggests a preference for the OPP shunt as a replacement. Here, release of CO₂ at the Gnd decarboxylation step might reduce photorespiration in low Ci conditions. Such a blockage would also prevent replenishment of the CBB cycle with triosephosphates as Eda also plays a role in glycogen breakdown in low CO₂ conditions. These implications are supported by distinctly lower accumulations of 2PG and 3PGA in Δeda after the HC-LC shift in comparison with the WT (**Publication 1, Figure 6**).

The importance of the ED pathway for Ci acclimation is further underlined by specific amino acid levels in response to the shifts. The Eda-deficient strain accumulates high amounts of proline as stress response during LC acclimation and shows increased arginine levels (**Publication 1, Figure 8**). For other organisms, proline accumulation has been reported for maintenance of a redox balance in case of elevated NADPH levels (Fichman et al., 2015; Zhang & Becker, 2015). Another possibility is a metabolite spillover from accumulated arginine in response to the first CO₂ shift, as a conversion from arginine to proline via ornithine by AgrE has been reported for cyanobacteria (Zhang & Yang, 2019). Moreover, Eda also has an annotated function as (4S)-4-hydroxy-2-oxoglutarate aldolase (database KEGG, entry SII0107), catalysing the conversion of 4-hydroxy 2-oxoglutarate in glyoxylate and pyruvate and thus participates in amino acid metabolism, which correlates with the observed strong over-accumulation of proline in the mutant Δeda .

Altogether, an intact ED shunt supports the rapid reactivation of growth by elevated Ci levels after limiting periods of LC. This confirms the growth impairment of Δeda in photoautotrophic conditions reported in previous studies (Chen et al., 2016; Makowka et al., 2020). On a first view, these results could indicate that the ED pathway represents the main glycolytic route for glycogen utilisation under LC conditions. However, the integration of all data from the study by Lucius et al. (2021) rather indicate a regulatory role of the Eda enzyme in acclimation to changing Ci conditions instead of an increased flux through the ED pathway. In Δzwf , the glycolytic ED pathway is disrupted at the G6P-dehydrogenase (Zwf) step, an enzyme acting upstream of the divergence of ED and OPP routes. Hence, the flux through ED and OPP pathways should be blocked in mutant Δzwf . However, significantly fewer physiological and metabolic differences were found between WT and Δzwf compared with

Δeda. These data rule out that the flux through the ED pathway might be the most important reason for the observed phenotypic differences, but rather the impact of Eda or its substrate on metabolic regulation is crucial. This is supported by recent bioinformatics and experimental findings that there is no detectable flux through the ED pathway in mixotrophic conditions accompanied with the absence of key intermediate KDPG in *Synechocystis* (Bachhar & Jablonsky, 2022; Schulze et al., 2022). The actual regulatory role of Eda is so far unknown.

8.1.3 *Cp12-dependent regulation in changing CO₂ conditions*

The CBB cycle activity for fixation of CO₂ depends on availability of C_i, ATP and reducing equivalents from the photosynthetic light reaction in the form of NADPH. In *Synechocystis*, NADPH is used by the anabolic reaction of glyceraldehyde 3-phosphate dehydrogenase GapDH2 (Sll1342) in the triosephosphate hub, producing GAP from G1,3BP as part of the RuBP regeneration and for gluconeogenesis. In darkness and low light conditions, the CBB cycle is downregulated in *Synechocystis* by inhibition of GapDH2 and Prk due to Cp12 association. However, according to our results, Cp12 regulation also plays a role during acclimation to changing CO₂ levels in constant light (Lucius et al., 2022). This is indicated by results from CO₂ shift experiments comparing *Synechocystis* WT and mutant *Δcp12* which is deficient in the Cp12-encoding gene *ss/3364*. Cultures of these strains were first grown at HC conditions, then shifted to LC levels. LC-MS and GC-MS analyses were performed to analyse levels of metabolites that are part of the CBB cycle and the central carbon metabolism routes in general. Among this set of metabolites, the levels of the RuBisCO substrate RuBP strongly increased in *Δcp12* in response to the HC-LC shift compared to the WT. Similarly, levels of dihydroxyacetone phosphate (DHAP), the more detectable isomer of GAP, increased in the Cp12-deficient strain upon the shift (**Publication 2, Figure 2**). This points at a more active CBB cycle with increased activities of Prk and GapDH2 due to the lack of Cp12 inhibition, whereas WT cells reduce CBB cycle activity after a HC-LC shift. The lack of Cp12 does not affect the activity and abundance of GapDH2 and Prk in *Synechocystis* (Blanc-Garin et al., 2022), in contrast to other organisms like *Arabidopsis thaliana* in which a Cp12-deficiency causes decreased Prk expression (Lopez-Calcano et al., 2017).

CO₂ fixation and the photosynthetic light reaction are tightly connected. A sudden decrease of CO₂ fixation due to low C_i levels can saturate the sink capacity of the CBB cycle for photosynthetic NADPH. An over-reduction of the photosystems by subsequent NADPH accumulation must be prevented. For example, cyclic electron flow decreases the production of reactive oxygen species that would otherwise damage the photosynthetic machinery. This

quick process protects PSI and leads to a decreased photosynthetic rate (Alvarenga-Lucius et al., 2023). The consequent oxidized cellular state could potentially initiate the Cp12-mediated inhibition of the CBB cycle by binding of GapDH2 and Prk, even in constant light. Growth experiments of $\Delta cp12$ and WT cultures grown under HC or LC conditions, respectively, show similar growth phenotypes. However, during CO₂ shifts, metabolic changes during Ci acclimation become pronounced (Lucius et al., 2022). These results show that Cp12-dependent regulation is relevant during other redox imbalances caused by environmental fluctuations apart from day-night transitions.

8.1.4 Connection between *PirC* and CO₂ availability

No direct connection between the function of *PirC* and different CO₂ availability has been described so far. However, its expression on RNA and protein levels is clearly different under HC and LC conditions (Klähn et al., 2015, Spät et al., 2021, Barske et al., 2023). Moreover, a main regulatory target of *Synechocystis* *PirC*, phosphoglycerate mutase *Pgam1*, was previously predicted as a key control point in carbon metabolism from modelling data of *Synechococcus* 7942 (Jablonsky et al., 2014). Metabolomic data from HC-LC shifts on *Synechocystis* and *Synechococcus* 7942 suggest that under LC conditions, the catabolic *Pgam1* reaction is increased to provide lower glycolysis and subsequent TCA cycle with newly fixed carbon, which sustains ammonia assimilation via the GS/GOGAT cycle, diminishing glycogen synthesis. This is indicated by LC-shift induced accumulation of the *Pgam1* reaction product 2PGA (Eisenhut et al., 2008b; Schwarz et al., 2011). Furthermore, the overexpression of *PirC* led to an increased glycogen accumulation in sufficient CO₂ availability (Muro-Pastor et al., 2020) indicating a regulatory impact of *PirC* on carbon flux redirection. Further detailed insights into the regulatory mechanism of *PirC* on *Pgam1* in *Synechocystis* are described in 8.3.3.

8.2 Regulation of the central carbon metabolism during supply with external glucose

8.2.1 General overview

Apart from C_i , aquatic habitats provide various forms of organic carbon sources. One of the most abundant organic sugars in aquatic and marine ecosystems is glucose (Skoog et al., 1999). Glucose mostly originates from dead organic matter as a component of dissolved polysaccharides (Benner et al., 1992). Blooms of phytoplankton, for example in coastal regions, may temporarily significantly increase the glucose availability for microbial growth (Ittekkot et al., 1981). Heterotrophic aquatic bacteria can use this organic carbon source, whereas external glucose supply may also facilitate mixotrophic growth for certain cyanobacteria. *Synechocystis* is a photosynthetic cyanobacterium capable of photoautotrophy and uptake of extracellular sugars like glucose via transporter GlcP (Schmetterer, 1990). Therefore, *Synechocystis* can grow heterotrophically in darkness at the expense of stored glycogen and external glucose, but also mixotrophically in light.

Mixotrophy for *Synechocystis* describes the capacity of the central carbon metabolism to have anabolic reactions of CO_2 fixation, and catabolic reactions of glycolytic routes, running simultaneously. *Synechocystis* is facultatively mixotrophic (Pelroy et al., 1972), and performs non-compartmented mixotrophy in contrast to plants which can spatially separate trophic modes. This makes the regulatory mechanisms for such simultaneous opposing fluxes especially interesting research topics.

Previous studies confirmed that CO_2 fixation in the CBB cycle is not interrupted by supply of external glucose in light (Nakajima et al., 2014). Interestingly, growth rates of *Synechocystis* are found to be higher in mixotrophic conditions than the sum of photoautotrophic and heterotrophic yield (Lopo et al., 2012; Chen et al., 2016), suggesting mixotrophy as a separate mode of lifestyle instead of just a mechanism to overcome nutrient scarcity.

8.2.2 Glycolytic routes in heterotrophic and mixotrophic growth conditions

In light, external glucose and glycogen-derived glucose are mostly entering the CBB cycle. For this, the different glycolytic routes operate as truncated shunts to replenish and fine-tune the CBB cycle in cyanobacteria (Nakajima et al., 2014; Sharkey & Weise, 2016; Makowka et al., 2020). Flux analyses in mixotrophic conditions showed that this routing mechanism aids to maximize fixation of CO_2 in *Synechocystis* (Schulze et al., 2022). Growth in darkness with supplied glucose has been simulated for metabolomics experiments by creating photoheterotrophic conditions using photosynthetic electron transport chain inhibitors like atrazine (Nakajima et al., 2014; Yoshikawa et al., 2013). If grown in complete darkness,

glucose-tolerant *Synechocystis* will only grow when given a short daily light pulse, termed as “light-activated heterotrophy” (Anderson & McIntosh, 1991).

Glycogen breakdown with concomitant CO₂ fixation in light resembles mixotrophic growth conditions (Doello et al., 2018). As Eda-deficient *Synechocystis* mutants show delayed mixotrophic growth (Chen et al., 2016), the influence of the ED route on glycogen metabolization in continuous light is underlined again. However, in mixotrophic conditions, no flux through the ED pathway towards KDPG could be detected using GC-MS-based ¹³C-based metabolic flux analyses (Schulze et al., 2022). This indicates that Eda might operate on another regulatory layer apart from different metabolic activity. Therefore, its exact role is still controversial and needs further investigation. Additionally, the absence of Eda leads to impairment of growth in day-night cycles, as well as fluctuating light (Schulze et al., 2022). Thus far, no insights on the role of the ED pathway in heterotrophic conditions have been published for *Synechocystis*.

The OPP pathway is the dominating glucose metabolic route for *Synechocystis* in light-activated heterotrophic conditions, because strains deficient in Zwf and Gnd showed a strong growth impairment in darkness with glucose supplied (Yang et al., 2002; Jansén et al., 2010; Wan et al., 2017). Furthermore, *in vivo* Zwf activity is increased under heterotrophic conditions (Kurian et al., 2006). The EMP pathway as glycolytic route shares the intermediate F6P with the CBB cycle which is produced by phosphoglucose isomerase (PGI). The metabolic shunt was therefore termed “PGI shunt” for refuelling the CBB cycle at the step of F6P (Makowka et al., 2020). G6P is the entry point for the OPP, PGI and ED shunts. Carbon flux analysis at this node in mixotrophic growth revealed that glucose flux divides mainly into the PGI shunt as shortened EMP pathway and the OPP shunt, with a small remainder allocated to glycogen synthesis (Schulze et al., 2022).

8.2.3 *Cp12 regulation during glucose supply*

In previous studies, physiological investigations on cyanobacterial Cp12 had mostly been conducted on *Synechococcus* 7942 cultures. However, this strain cannot utilise externally supplied glucose, in contrast to *Synechocystis* (Zhang et al., 1998). Therefore, these studies had not taken into account the potential role of Cp12-dependent regulation for the adjustment of the cyanobacterial metabolism in the presence of external glucose.

In this dissertation, the connection between redox regulation of Cp12 complex formation and external glucose supply was investigated. For this, a set of *Synechocystis* strains expressing mutated Cp12 versions that are deficient in binding to GapDH2 and/or Prk were used. Denominations of these mutants along with a brief description are listed in Table 2.

The WT variant of Cp12 expressed by gene *ss/3364* in *Synechocystis* harbours two cysteine pairs and thus belongs to the group of Cp12-N/C according to Stanley et al. (2013). In

oxidizing conditions, these cysteines form two respective disulfide bridges to partially structure the Cp12 protein near to its GapDH-binding domain at the C-terminus and the Prk-binding domain in proximity to the N-terminus. This structural order by redox regulation basically enables Cp12 to function as inhibitor of the two target CBB cycle enzymes. Thus, complementation mutant strains were generated in the *Synechocystis* $\Delta cp12$ background, expressing different variants of Cp12, lacking either the N-terminal cysteines Cys19 and Cys29, or the C-terminal pair by Cys60 and Cys69, along with a strain expressing a Cp12 variant lacking all four cysteines (Lucius et al., 2022). These strains permit the analysis of the relative importance of Cp12-mediated inhibition of either GapDH2 or Prk. However, cyanobacterial Prk also possesses cysteine residues that allow direct redox regulation of this enzyme independent from the Cp12-mediated mechanism (Fukui et al., 2022).

Table 2: Details of mutant strains with $\Delta cp12$ background used in **Publication 2** (Lucius et al., 2022).

Strain	Deleted cysteines	Affected binding domain
$\Delta cp12::cp12\text{-}\Delta\text{CysN}$	N-terminal Cys19 and Cys29	Prk
$\Delta cp12::cp12\text{-}\Delta\text{CysC}$	C-terminal Cys60 and Cys69	GapDH2
$\Delta cp12::cp12\text{-}\Delta\text{CysNC}$	Cys19, Cys29, Cys60, Cys69	GapDH2 and Prk
$\Delta cp12$	Entire gene <i>ss/3364</i> deleted	GapDH2 and Prk

So far, no apparent role was suggested for Cp12 in *Synechocystis* during mixotrophic growth in standard experimental light conditions of 50 to 100 $\mu\text{mol photons m}^{-2} \text{s}^{-1}$. In constant light, cells are mainly in a reduced state due to high NADPH levels from the photosynthetic light reaction and thus Cp12 is in its conditionally disordered state.

External glucose can be utilised for glycogen formation or channelled into glycolytic routes, hence, it should theoretically further support cellular growth. However, in lower light intensities of 12.5 $\mu\text{mol photons m}^{-2} \text{s}^{-1}$, mutant $\Delta cp12$ shows a clearly diminished growth when grown in liquid medium supplied with glucose (Blanc-Garin et al., 2022). This necessity for Cp12 in decreasing light under glucose influence is further confirmed by the inability of $\Delta cp12$ to grow heterotrophically in darkness on glucose (Lucius et al., 2022). Thus, Cp12 appears crucial for glucose catabolism in low photosynthetic activity. Further, the lack of Cp12 leads to growth inhibition under photoheterotrophic conditions in constant light with added DCMU (3-(3,4-dichlorophenyl)-1,1-dimethylurea) (Lucius et al., 2022; Blanc-Garin et al., 2022). DCMU is a photosynthetic electron chain inhibitor blocking the electron transfer from PSII to plastoquinone, thereby preventing photosynthetic NADPH production (Häder, 1975). Thus, in the presence of DCMU, the cell mainly relies on reducing power generated from glucose oxidation that is sufficient for the *Synechocystis* WT but does not work for $\Delta cp12$ cells, most likely caused by a cellular redox imbalance.

In diurnal growth of alternating 12-hour phases of light and darkness without external glucose supply, $\Delta cp12$ displays a WT-like growth and thus, Cp12 regulation appears dispensable under this condition in *Synechocystis* (Lucius et al., 2022; Blanc-Garin et al., 2022). For other cyanobacterial strains such as *Synechococcus* 7942, a Cp12-deficient strain even shows impaired growth after long-term acclimation to diurnal growth (Tamoi et al., 2005). However, when diurnal growth experiments are performed with the *Synechocystis* WT and the Cp12-deficient strain in the presence of glucose, the $\Delta cp12$ mutant is unable to grow in alternating 12-hour dark/light phases whereas the WT was not affected (Lucius et al., 2022; Blanc-Garin et al., 2022). Growth experiments in 12-hour diurnal conditions in glucose-containing medium (**Publication 2, Figure 4**) revealed a WT-like growth for $\Delta cp12::cp12-\Delta CysN$. In contrast, strains $\Delta cp12::cp12-\Delta CysC$ and $\Delta cp12::cp12-\Delta CysNC$ with affected GapDH2 binding show a strong growth impairment comparable to $\Delta cp12$ with a rather late acclimation to such light and glucose conditions. Binding of GapDH2 by Cp12 mediates an improved glucose utilisation from the medium and enables the proper breakdown of glycogen reserves. This was concluded from a strong delay in all $\Delta cp12$ strains with deleted GapDH2 binding domain cysteines during assays for determination of glucose and glycogen. Glucose might cause a redox imbalance for the cell in situations where GapDH2 should be inactive. Catabolic production of NADPH from glucose oxidation then could be opposed by anabolic NADPH consumption by GapDH2 in *Synechocystis* leading to futile wasteful cycles. In darkness, Zwf and Gnd of the OPP pathway are the only enzymes that produce NADPH from oxidation of glucose. Therefore, the NADPH pool is limited and should only be available for metabolic enzymes that require this exact reducing equivalent and cannot accept NADH. In low photosynthetic activity in darkness or low light, GapDH1 is the active GapDH isoenzyme which only utilises NADH, while GapDH2 is inhibited by Cp12. This inhibition prevents GapDH2 from depleting the NADPH pool in such conditions and could explain the $\Delta cp12$ phenotypes in dark phases with supplied glucose. Inhibition of GapDH2 by Cp12 seems to be of higher relevance than binding of Prk for proper acclimation to glucose supply in dark phases (Lucius et al., 2022). However, the exact regulatory mechanisms how the glucose import and immediate metabolization is affected requires further research.

In vivo experiments can elucidate details about true functions of regulatory mechanisms and provide another dimension of cellular response analyses to actual environmental changes. In case of Cp12, for the first time, *in vivo* dynamics of Cp12-mediated binding of Prk and GapDH2 could be visualized in dark/light changes in *Synechocystis* (Lucius et al., 2022). *Synechocystis* strains expressing eYFP-tagged versions of GapDH2 or Prk, respectively, were used to determine the chronology of Cp12-GapDH-Prk complex formation by fluorescence microscopy imaging. Clear aggregates visible as fluorescent spots formed in cells of the eYFP strains upon darkness. Signals became first visible in the eYFP-GapDH

cells and appeared time-displaced in eYFP-Prk cells (**Publication 2, Figure 1**). The temporal sequence of this spot formation thus confirms the primary binding of GapDH2 by Cp12 in dark/oxidizing conditions and the subsequent incorporation of Cp12-bound Prk into the Cp12-GapDH-Prk complex. Upon re-illumination, the fluorescent spots dispersed first in the eYFP-Prk strain and then in cells with eYFP-tagged GapDH2. This dissociation resembles the reverse sequence of complex formation. As negative control, no fluorescent spots formed in the Cp12-deficient strain $\Delta cp12$. The fluorescent signals appeared as roughly five to ten bright circular spots per cell in the eYFP-tagged strains. The reasons for this pattern and potential influence of other cellular mechanisms on the complex localization remains unknown thus far. According to the number of spots formed in darkness, an association of complex formation close to carboxysomes might be reasonable. However, fluorescent Cp12 spots do not overlay signals of fluorescence-tagged carboxysome-related proteins in a respective *Synechocystis* mutant (unpublished results, Kirstin Gutekunst group). Also, an aggregation of supramolecular Cp12 complexes by interacting eYFP fluorescence protein tags cannot be excluded yet.

In vivo analysis of the intracellular redox status was chosen to assess the lethal phenotype of $\Delta cp12$ in dark phases combined with supplied external glucose. Measurements of the *in vivo* oxidation level of NAD(P)H revealed an importance of Cp12 during redox state regulation dependent on light intensity (Lucius et al., 2022). This was assessed by monitoring the NAD(P)H fluorescence for WT, $\Delta cp12$, $\Delta cp12::cp12-\Delta CysN$, $\Delta cp12::cp12-\Delta CysC$ and $\Delta cp12::cp12-\Delta CysNC$ during acclimation to different light intensities and during a subsequent high light pulse followed by an immediate shift to darkness. The high light pulse reduces the major part of the photo-reducible NAD(P)⁺ pool to NAD(P)H. The rate of re-oxidation of NADPH to NADP⁺ after the dark shift thus depends on the level of CBB cycle regulation during the light acclimation before the light pulse, because uninhibited GapDH2 would quickly oxidize NADPH in darkness via its respective anabolic reaction.

In fact, the experimental results suggest a gradually increased association of Cp12 with GapDH2 in decreasing light intensities (**Publication 2, Figure 6**). Therefore, the CBB cycle is not only downregulated by Cp12 in dark/light phases but also fine-tuned in lower light intensities and fluctuations thereof. This is indicated by a faster NAD(P)H oxidation rate in darkness for the WT the higher the pre-acclimation light intensity was set. During acclimation to lower light, the CBB cycle is gradually downregulated by partial Cp12-mediated binding of GapDH2 and thus the re-oxidation rate is lower in WT cells. The crucial role of Cp12 for this re-oxidation is confirmed by redox measurements on the Cp12-deficient mutant. There, $\Delta cp12$ displays consistently high oxidation rates after the dark shift, independent of previous light settings. Due to the lack of Cp12, the GapDH2 pool is permanently unbound and greatly contributes to NADPH oxidation in darkness. Intermediate re-oxidation rates for mutants

$\Delta cp12::cp12-\Delta CysC$ and $\Delta cp12::cp12-\Delta CysNC$ again support the superordinate role of binding of GapDH2 by Cp12 instead of Prk for this regulatory mechanism. These *in vivo* NAD(P)H measurements suggest a strong redox imbalance during low light acclimation by lack of Cp12 that is potentially increased during addition of external glucose, leading to a lethal phenotype.

8.3 Regulation of the central carbon metabolism during nitrogen limitation

8.3.1 General overview

Nitrogen limitation causes deficiencies in synthesis of nitrogen-containing macromolecules like pigments, proteins and nucleic acids in *Synechocystis*. Therefore, limiting nitrogen conditions require adjustments to the metabolism for acclimation and cell survival (Yoshihara & Kobayashi, 2022). Because 2OG connects carbon and nitrogen metabolism in *Synechocystis*, regulations of nitrogen assimilation in limiting conditions are ultimately accompanied by regulations of carbon catabolism and anabolism (Forchhammer & Selim, 2019). Nitrogen/carbon signal transduction by specific 2OG-binding proteins like PII and NtcA trigger regulatory cascades for metabolic adjustment and maintenance of the C/N homeostasis.

In prolonged absence of combined nitrogen sources, *Synechocystis* transitions into a dormant state called chlorosis (Neumann et al., 2021). A visible response is the bleaching reaction, in which photosynthetic pigments, initially phycobilisomes as the cyanobacterial light-harvesting antennae and later chlorophyll, are degraded under nitrogen shortage. Phycobilisome degradation is mainly initiated by the protein NblA that is transcriptionally activated by NtcA at high 2OG levels (Luque et al., 2001). The disassembly of phycobiliproteins and the pigments therein leads to a yellow phenotype of *Synechocystis* cells. If the absence of nitrogen sources persists, cell growth is arrested and metabolic activity is gradually minimized as cells enter a dormant state for long-term survival in nutrient limitation (Klotz & Forchhammer, 2017; Hauf et al., 2015).

When combined nitrogen sources are limited, products of photosynthetic CO₂ fixation are redirected towards synthesis of glycogen (Klotz et al., 2016). In late stage chlorosis, PHB slowly accumulates in granular structures promoted by glycogen turnover (Klotz et al., 2019). The enhanced synthesis of glycogen reserves also serves as a preparation for recovery from chlorosis when nitrogen availability induces recovery of growth. The mobilization of stored glycogen during awakening from chlorosis supports the metabolism with energy and carbon skeletons (Doello et al., 2018). This is an essential process, as *Synechocystis* mutants deficient in glycogen synthesis do not enter chlorosis and die by nitrogen starvation (Gründel et al., 2012).

8.3.2 Role of glycolytic routes for resuscitation from chlorosis

The awakening of dormant cyanobacteria from chlorosis after nitrate addition requires an early phase of glycogen breakdown (Klotz et al., 2016). Under these conditions, glycogen degradation relies on the catabolic activity of GlgP2, the main glycogen phosphorylase in *Synechocystis* (Doello et al., 2018). The released sugar phosphates can be used in different glycolytic routes whereas the ED pathway and especially the OPP pathway are the crucial routes upon new availability of nitrogen after chlorosis. Nitrogen recovery studies on *Synechocystis* mutant strains deficient in key enzymes Eda, Zwf and Gnd of ED and OPP pathways, respectively, showed a lack of glycogen degradation along with a poor resuscitation ability (Doello et al., 2018). In Δzwf , 6-phosphogluconate accumulation leads to delayed resumption of CO₂ fixation by inhibition of RuBisCO, which emphasizes the respective importance of the OPP pathway (Doello et al., 2018). Furthermore, *Synechocystis* can anticipate a necessary glycogen mobilization in response to resupplied nitrogen (Klotz et al., 2016). This is indicated by increased expression of *zwf* and *gnd* during nitrogen starvation and chlorosis (Doello et al., 2018; Spät et al., 2018).

8.3.3 Regulation of the triosephosphate hub in nitrogen limitation

The triosephosphate hub in the central carbon metabolism of *Synechocystis* takes part in the acclimation to limiting nitrogen conditions. Here, phosphoglycerate mutase Pgam1 is blocked and the isoenzymes GapDH1 and GapDH2 participate in the reallocation of fixed carbon towards glycogen storage. The increase of glycogen is a direct response to low nitrogen levels (Klotz et al., 2015).

3PGA represents the first stable intermediate after CO₂ fixation by RuBisCO cycle and most of 3PGA remains in the CBB cycle. However, part of 3PGA can be taken out by the conversion into 2PGA via Pgam in catabolic direction. Therefore, Pgam is a crucial branching point for carbon allocation in the triosephosphate hub and new findings providing evidences for its role in nitrogen starvation are further elucidated in this dissertation. Orthwein et al. (2021, **Publication 3**) discovered that the activity of Pgam1, the product of gene *slr1945*, is regulated by the small protein PirC via competitive inhibition.

PII binds PirC in low 2OG levels and releases it in high 2OG levels, which reflect nitrogen-sufficient and nitrogen-limiting conditions, respectively. Released PirC can then bind to Pgam1 and inhibits its activity at high cellular C/N ratios. The Pgam1 inhibition redirects carbon flux towards formation of glycogen storage. This facilitates adjustment of the C/N homeostasis and also prepares the cell for potential long-term nitrogen starvation. When cells are replenished with nitrogen again, PirC is bound again to PII, and amounts of PirC decrease gradually (Doello et al., 2018). A model of this regulation is shown in Figure 6 (**Publication 3, Figure 5**).

PirC was first characterized via affinity tests *in vitro* in which it co-eluted with ATP or ADP-bound PII, but not with ATP and 2OG (Orthwein et al., 2021), which is a common characteristic of PII-interacting partners (Zeth et al., 2014). Bio-layer interferometry (BLI) analysis revealed that presence of effectors ATP or ADP significantly amplified binding properties. Also, an inhibitory effect of 2OG on PII-PirC interaction was first observed. This concludes that occupancy of all three effector binding sites of PII by 2OG prevents complex formation with PirC. The effect of high 2OG levels, together with the identification of an NtcA-binding domain of PirC thus suggested a nitrogen-related function of the small protein. The significance of PirC for acclimation to nitrogen depletion was then detected by physiological analyses. After one month of nitrogen starvation in continuous light, a deletion mutant $\Delta pirC$ showed slightly slower pigment degradation and delayed growth compared to WT, and, strikingly, exhibited reduced glycogen accumulation compared to WT and the native complementation strain $\Delta pirC::pirC$. Conversely, $\Delta pirC$ accumulated a significantly higher PHB content during nitrogen depletion. These findings first showed the importance of PirC for redirection of carbon fluxes towards glycogen and PHB during acclimation to decreasing nitrogen availability.

In an independent study by Muro-Pastor et al. (2020), increased levels of PirC (alternatively named “CfrA”) by overexpression revealed a proportional glycogen accumulation. During resuscitation from nitrogen depletion, a PirC-deficient mutant displayed faster glycogen consumption and a more rapid re-greening compared to WT. This indicated that in nitrogen resuscitation, a gradual degradation of PirC might be required to decrease a potential inhibiting behaviour of this small protein.

Further coimmunoprecipitation experiments were carried out to potentially identify other targets of PirC in carbon metabolism. Upon addition of 2OG/ATP, the 2,3-bisphosphoglycerate-independent phosphoglycerate mutase Pgam1 (Slr1945) emerged as the main PirC interactor. These results suggested a regulatory switch to modulate Pgam1 activity in nitrogen starvation by binding or release of PirC by PII. A negative regulation of Pgam1 by PirC would explain observed altered glycogen and increased PHB levels in $\Delta pirC$, as Pgam1 directs fixed carbon from the CBB cycle towards lower glycolysis, producing acetyl-CoA as precursor metabolite of PHB. In enzymatic assays, PirC inhibited recombinant Pgam1 in a competitive manner by raising the K_m value for the substrate 3PGA, rather than decreasing the V_{max} . Addition of PirC in excess caused a more than tenfold reduction of Pgam1 catalytic activity. In these assays, PII was found to counteract inhibition of Pgam1 by PirC in absence of 2OG. High 2OG levels re-enabled PirC to inhibit Pgam1, as when PII was absent.

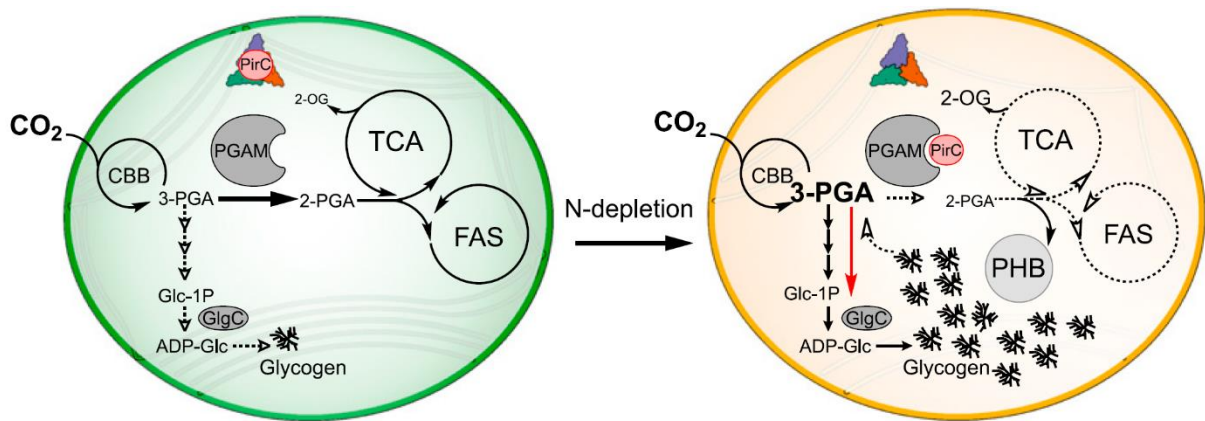


Figure 6: Model of regulation of central carbon metabolism by PirC, PII, and Pgam1 interactions (Orthwein et al., 2021). **2-OG** – 2-Oxoglutarate, **2-PGA** – 2-Phosphoglycerate, **3-PGA** – 3-Phosphoglycerate, **ADP-Glc** – ADP-Glucose, **CBB** – Calvin-Benson-Bassham cycle, **FAS** – Fatty acid synthesis, **Glc-1P** – Glucose 1-phosphate, **GlgC** – Glucose 1-phosphate adenylyltransferase, **PGAM** – Phosphoglycerate mutase, **PHB** – Polyhydroxybutyrate, **TCA** – Tricarboxylic acid cycle.

Physiological analysis by Muro-Pastor et al. (2020) revealed that overexpression of PirC in a PII-deficient mutant leads to a lower total protein content. This indicates that excess PirC, unbound by PII, constantly inhibits Pgam1 activity, thus blocking the metabolic flux in lower glycolysis towards TCA cycle and amino acid biosynthesis.

To further assess the role of PirC regulation on a metabolic level, a nitrogen shift experiment coupled with metabolome analysis was performed on short-term (48 h) nitrogen-depleted cells of WT and $\Delta pirC$ (Orthwein et al., 2021). Similar to CO₂ shift experiments, such abrupt change of nutrient availability requires an immediate reaction to adjust metabolic flow and maintain the C/N homeostasis. Specific differences in metabolite steady-state levels between both strains were detected upon nitrogen depletion (**Publication 3, Figure 4**). Notably, 2OG levels rose immediately in $\Delta pirC$ after the nitrogen shift and remained elevated, while levels gradually decreased in WT. This result shows that the inhibition feedback of a functioning Pgam-PirC regulation causes a reduced metabolic flux towards the TCA cycle in nitrogen depletion, by which the initial responsive accumulation of 2OG is slowly wearing off. 3PGA levels remained low for $\Delta pirC$, whereas increasing levels for the WT indicate inhibition of Pgam by PirC. This observation confirms that in nitrogen depletion, regulation via PirC causes 3PGA accumulation which is redirected to glycogen formation. Furthermore, rising 3PGA levels activate GlgC, which catalyses the conversion of G1P to ADP-glucose in the glycogen hub (Preiss, 1984). This mechanism enables PirC-mediated stimulation of glycogen synthesis while lower glycolysis is simultaneously restricted. High pyruvate levels in $\Delta pirC$ indicate an increased conversion of 3PGA to 2PGA by flux through Pgam, aligning with increased PHB levels derived from acetyl-CoA. Overall, our metabolic investigations deliver evidence that in nitrogen depletion, the Pgam downstream reaction is normally curbed by PirC as not enough nitrogen is available for subsequent amino acid biosynthesis.

So far, no fully segregated Pgam1 (Slr1945) mutant could be obtained for *Synechocystis*, preventing significant physiological studies on strains lacking this enzymatic function. However, these difficulties suggest that Pgam1 is essential for the central carbon metabolism of *Synechocystis*, and cannot be substituted by any other enzyme, thus enhancing the significance of Pgam1 as a key control point for carbon allocation. Equally, this finding makes the existence of other functional Pgam isoenzymes in *Synechocystis* unlikely.

A potential for biotechnological applications after characterization of PirC regulation could already be demonstrated (Koch et al., 2020). In nitrogen starvation, there is a constant turnover of glycogen during progressing chlorosis and dormancy (Koch et al., 2019). This residual flux creates acetyl-CoA as precursor for PHB. In a PirC-deficient strain, this flux is increased because Pgam1 is uninhibited in low nitrogen conditions leading to a significant increase in PHB storage (Orthwein et al., 2021). There, these properties of $\Delta pirC$ to redirect carbon metabolism towards synthesis of PHB were used in part to engineer a *Synechocystis* strain that showed the highest accumulation of PHB under nitrogen limitation so far, reaching over 80% PHB per cell dry weight (Koch et al., 2020). Beyond that, first results using PirC-deficient *Synechocystis* mutants could demonstrate a conditional increase of ethanol production (Böhm et al., 2023).

Kinetic and binding studies revealed competitive inhibition of Pgam1 by PirC. In the future, a structural analysis of the complex formation could elucidate further details of the regulation. Other potential interaction partners of PirC have been identified by coimmunoprecipitation experiments. Among candidates are dihydrolipoamide dehydrogenase, dihydrolipoamide acetyltransferase, and pyruvate dehydrogenase E1 beta as three components of the pyruvate dehydrogenase (PDH) complex in *Synechocystis* (Muro-Pastor et al., 2020), as well as an ortholog of CcmP encoded by the gene *slr0169* (Orthwein et al., 2021). In *Synechococcus*, CcmP is a carboxysome shell protein with a central pore potentially functioning in metabolite transport (Larsson et al., 2017). Identification of other regulatory properties of PirC for metabolite flux in the central carbon metabolism is therefore an interesting goal for future research.

9 CONCLUDING REMARKS AND OUTLOOK

The results of this dissertation help to broaden the knowledge about how *Synechocystis* regulates its central carbon metabolism based on certain environmental conditions, like changing availabilities of inorganic and organic carbon, as well as acclimation to and resuscitation from nitrogen limitation.

We discovered that the Entner-Doudoroff pathway somehow contributes to glycogen breakdown during high to low CO₂ shifts in *Synechocystis*. Future research on the postulated regulatory function of key enzyme Eda would increase understanding of cyanobacterial glycogen metabolism during light phases. Other regulatory layers that determine the preference for a specific glycolytic route in dependence of certain environmental fluctuations could be targets for future experiments.

Further, our results show that Cp12 contributes to redox regulation in conditions with supplied external glucose and can fine-tune the CBB cycle and carbohydrate metabolism in *Synechocystis*. This extends the role of Cp12 beyond dark-night regulation and also reveals contribution to acclimation to changing CO₂ conditions. This dissertation presents one of the first sets of results from *in vivo* analyses on Cp12 complex formation in *Synechocystis*. If further potential targets or interactors of Cp12 can be identified, this could unravel an extended regulatory network of this versatile conditionally disordered protein. In this regard, another auspicious layer of regulation that requires further research efforts is the influence of phosphorylation of Cp12 itself and related effects on the CBB cycle.

Lastly, the novel PII-interactor PirC identifies phosphoglycerate mutase Pgam1 as a key control point of carbon storage metabolism in *Synechocystis*. The characterization of the PirC-mediated regulation of such a crucial branching point for carbon allocation harbours great potential for biotechnological applications as it implies new ways to redirect fluxes towards target metabolites or biopolymers such as PHB. Also, structural analysis of enzymatic complexes could help to further elucidate the inhibitory mechanism of PirC on Pgam1.

In conclusion, the cyanobacterial central metabolism is elusively complex where hidden regulatory layers and unknown protein interactions involved in the switch between photoautotrophy and heterotrophy will offer research topics for decades to come.

10 References

- Aichi, M., Takatani, N., & Omata, T. (2001). Role of NtcB in Activation of Nitrate Assimilation Genes in the Cyanobacterium *Synechocystis* sp. Strain PCC 6803. *Journal of Bacteriology*, 183(20), 5840–5847.
- Alvarenga, L., Vieira Vaz, M. G. M., Genuário, D. B., Esteves-Ferreira, A. A., Almeida, A. V. M., de Castro, N. V., Lizieri, C., Souza, J. J. L. L., Schaefer, C. E. G. R., Nunes-Nesi, A., & Araújo, W. L. (2018). Extending the ecological distribution of *Desmonostoc* genus: Proposal of *Desmonostoc salinum* sp. Nov., a novel Cyanobacteria from a saline–alkaline lake. *International Journal of Systematic and Evolutionary Microbiology*, 68(9), 2770–2782.
- Alvarenga-Lucius, L., Linhartová, M., Schubert, H., Maaß, S., Becher, D., Hess, W. R., Sobotka, R., & Hagemann, M. (2023). The high-light-induced protein *SliP4* binds to *NDH1* and photosystems facilitating cyclic electron transport and state transition in *Synechocystis* sp. PCC 6803. *New Phytologist*, 239(3), 1083–1097.
- Anderson, L. E. (1971). Chloroplast and cytoplasmic enzymes II. Pea leaf triose phosphate isomerases. *Biochimica et Biophysica Acta (BBA) – Enzymology*, 235(1), 237–244.
- Anderson, S. L., & McIntosh, L. (1991). Light-activated heterotrophic growth of the cyanobacterium *Synechocystis* sp. Strain PCC 6803: a blue-light-requiring process. *Journal of Bacteriology*, 173(9), 2761–2767.
- Ansong, C., Sadler, N. C., Hill, E. A., Lewis, M. P., Zink, E. M., Smith, R. D., Beliaev, A. S., Konopka, A. E., & Wright, A. T. (2014). Characterization of protein redox dynamics induced during light-to-dark transitions and nutrient limitation in cyanobacteria. *Frontiers in Microbiology*, 5.
- Bachhar, A., & Jablonsky, J. (2022). Entner-Doudoroff pathway in *Synechocystis* PCC 6803: Proposed regulatory roles and enzyme multifunctionalities. *Frontiers in Microbiology*, 13.
- Badger, M. R., Price, G. D., Long, B. M., & Woodger, F. J. (2006). The environmental plasticity and ecological genomics of the cyanobacterial CO₂ concentrating mechanism. *Journal of Experimental Botany*, 57(2 SPEC. ISS.), 249–265.
- Ball, S. G., & Morell, M. K. (2003). From Bacterial Glycogen to Starch: Understanding the Biogenesis of the Plant Starch Granule. *Annual Review of Plant Biology*, 54(1), 207–233.
- Barske, T., Spät, P., Schubert, H., Walke, P., Maček, B., & Hagemann, M. (2023). The Role of Serine/Threonine-Specific Protein Kinases in Cyanobacteria – SpkB Is Involved in Acclimation to Fluctuating Conditions in *Synechocystis* sp. PCC 6803. *Molecular & Cellular Proteomics*, 22(11), 100656.
- Bendall, D. S., & Manasse, R. S. (1995). Cyclic photophosphorylation and electron transport. *Biochimica et Biophysica Acta (BBA) – Bioenergetics*, 1229(1), 23–38.
- Benner, R., Pakulski, J. D., McCarthy, M., Hedges, J. I., & Hatcher, P. G. (1992). Bulk Chemical Characteristics of Dissolved Organic Matter in the Ocean. *Science*, 255(5051), 1561–1564.
- Berman-Frank, I., Lundgren, P., & Falkowski, P. (2003). Nitrogen fixation and photosynthetic oxygen evolution in cyanobacteria. *Research in Microbiology*, 154(3), 157–164.

- Blanc-Garin, V., Veaudor, T., Sétif, P., Gontero, B., Lemaire, S. D., Chauvat, F., & Cassier-Chauvat, C. (2022).** First in vivo analysis of the regulatory protein CP12 of the model cyanobacterium *Synechocystis* PCC 6803: Biotechnological implications. *Frontiers in Plant Science*, 13.
- Böhm, J., Kauss, K., Michl, K., Engelhardt, L., Brouwer, E. M., & Hagemann, M. (2023).** Impact of the carbon flux regulator protein pirC on ethanol production in engineered cyanobacteria. *Frontiers in Microbiology*, 14.
- Burnap, R., Hagemann, M., & Kaplan, A. (2015).** Regulation of CO₂ Concentrating Mechanism in Cyanobacteria. *Life*, 5(1), 348–371.
- Chen, X., Schreiber, K., Appel, J., Makowka, A., Fähnrich, B., Roettger, M., Hajirezaei, M. R., Sönnichsen, F. D., Schönheit, P., Martin, W. F., & Gutekunst, K. (2016).** The Entner-Doudoroff pathway is an overlooked glycolytic route in cyanobacteria and plants. *Proceedings of the National Academy of Sciences of the United States of America*, 113(19), 5441–5446.
- Ciebiada, M., Kubiak, K., & Daroch, M. (2020).** Modifying the cyanobacterial metabolism as a key to efficient biopolymer production in photosynthetic microorganisms. *International Journal of Molecular Sciences*, 21(19), 1–24.
- Doello, S., Klotz, A., Makowka, A., Gutekunst, K., & Forchhammer, K. (2018).** A specific glycogen mobilization strategy enables rapid awakening of dormant cyanobacteria from chlorosis. *Plant Physiology*, 177(2), 594–603.
- Doello, S., Neumann, N., & Forchhammer, K. (2022).** Regulatory phosphorylation event of phosphoglucomutase 1 tunes its activity to regulate glycogen metabolism. *FEBS Journal*, 289(19), 6005–6020.
- Durall, C., & Lindblad, P. (2015).** Mechanisms of carbon fixation and engineering for increased carbon fixation in cyanobacteria. *Algal Research*, 11, 263–270.
- Eisenhut, M., Ruth, W., Haimovich, M., Bauwe, H., Kaplan, A., & Hagemann, M. (2008a).** The photorespiratory glycolate metabolism is essential for cyanobacteria and might have been conveyed endosymbiotically to plants. *Proceedings of the National Academy of Sciences*, 105(44), 17199–17204.
- Eisenhut, M., Huege, J., Schwarz, D., Bauwe, H., Kopka, J., & Hagemann, M. (2008b).** Metabolome phenotyping of inorganic carbon limitation in cells of the wild type and photorespiratory mutants of the cyanobacterium *Synechocystis* sp. Strain PCC 6803. *Plant Physiology*, 148(4), 2109–2120.
- Erales, J., Avilan, L., Lebreton, S., & Gontero, B. (2008).** Exploring CP12 binding proteins revealed aldolase as a new partner for the phosphoribulokinase/glyceraldehyde 3-phosphate dehydrogenase/CP12 complex – Purification and kinetic characterization of this enzyme from *Chlamydomonas reinhardtii*. *FEBS Journal*, 275(6), 1248–1259.
- Espinosa, J., Forchhammer, K., & Contreras, A. (2007).** Role of the *Synechococcus* PCC 7942 nitrogen regulator protein PipX in NtcA-controlled processes. *Microbiology*, 153(3), 711–718.
- Espinosa, J., Rodríguez-Mateos, F., Salinas, P., Lanza, V. F., Dixon, R., de La Cruz, F., & Contreras, A. (2014).** PipX, the coactivator of NtcA, is a global regulator in cyanobacteria. *Proceedings of the National Academy of Sciences of the United States of America*, 111(23).
- Esteves-Ferreira, A. A., Inaba, M., Fort, A., Araújo, W. L., & Sulpice, R. (2018).** Nitrogen metabolism in cyanobacteria: metabolic and molecular control, growth consequences and biotechnological applications. *Critical Reviews in Microbiology*, 44(5), 541–560.

- Fichman, Y., Gerdes, S. Y., Kovács, H., Szabados, L., Zilberstein, A., & Csonka, L. N. (2015).** Evolution of proline biosynthesis: enzymology, bioinformatics, genetics, and transcriptional regulation. *Biological Reviews*, 90(4), 1065–1099.
- Figge, R. M., Cassier-Chauvat, C., Chauvat, F., & Cerff, R. (2001).** Characterization and analysis of an NAD(P)H dehydrogenase transcriptional regulator critical for the survival of cyanobacteria facing inorganic carbon starvation and osmotic stress. *Molecular Microbiology*, 39(2), 455–469.
- Flombaum, P., Gallegos, J. L., Gordillo, R. A., Rincón, J., Zabala, L. L., Jiao, N., Karl, D. M., Li, W. K. W., Lomas, M. W., Veneziano, D., Vera, C. S., Vrugt, J. A., & Martiny, A. C. (2013).** Present and future global distributions of the marine Cyanobacteria *Prochlorococcus* and *Synechococcus*. *Proceedings of the National Academy of Sciences of the United States of America*, 110(24), 9824–9829.
- Flores, E., Nieves-Mori6n, M., & Mullineaux, C. (2018).** Cyanobacterial Septal Junctions: Properties and Regulation. *Life*, 9(1), 1.
- Flores, E., & Herrero, A. (2005).** Nitrogen assimilation and nitrogen control in cyanobacteria. *Biochemical Society Transactions*, 33(1), 164–167.
- Flügel, F., Timm, S., Arrivault, S., Florian, A., Stitt, M., Fernie, A. R., & Bauwe, H. (2017).** The photorespiratory metabolite 2-phosphoglycolate regulates photosynthesis and starch accumulation in *Arabidopsis*. *Plant Cell*, 29(10), 2537–2551.
- Forchhammer, K., Selim, K. A., & Huergo, L. F. (2022).** New views on PII signaling: from nitrogen sensing to global metabolic control. *Trends in Microbiology*, 30(8), 722–735.
- Forchhammer, K., & Lüddecke, J. (2016).** Sensory properties of the PII signalling protein family. *FEBS Journal*, 283(3), 425–437.
- Forchhammer, K., & Selim, K. A. (2020).** Carbon/nitrogen homeostasis control in cyanobacteria. *FEMS Microbiology Reviews*, 44(1), 33–53.
- Fukui, K., Yoshida, K., Yokochi, Y., Sekiguchi, T., Wakabayashi, K., Hisabori, T., & Mihara, S. (2022).** The Importance of the C-Terminal Cys Pair of Phosphoribulokinase in Phototrophs in Thioredoxin-Dependent Regulation. *Plant and Cell Physiology*, 63(6), 855–868.
- Galperin, M. Y. (2005).** A census of membrane-bound and intracellular signal transduction proteins in bacteria: Bacterial IQ, extroverts and introverts. *BMC Microbiology*, 5(1), 35.
- Gérard, C., Carrière, F., Receveur-Bréchet, V., Launay, H., & Gontero, B. (2022).** A Trajectory of Discovery: Metabolic Regulation by the Conditionally Disordered Chloroplast Protein, CP12. *Biomolecules*, 12(8), 1047.
- Giner-Lamia, J., Robles-Rengel, R., Hernández-Prieto, M. A., Muro-Pastor, M. I., Florencio, F. J., & Futschik, M. E. (2017).** Identification of the direct regulon of NtcA during early acclimation to nitrogen starvation in the cyanobacterium *Synechocystis* sp. PCC 6803. *Nucleic Acids Research*, 45(20), 11800–11820.
- Graciet, E., Gans, P., Wedel, N., Lebreton, S., Camadro, J. M., & Gontero, B. (2003a).** The small protein CP12: A protein linker for supramolecular complex assembly. *Biochemistry*, 42(27), 8163–8170.
- Graciet, E., Lebreton, S., Camadro, J. M., & Gontero, B. (2003b).** Characterization of native and recombinant A4 glyceraldehyde 3-phosphate dehydrogenase: Kinetic evidence for conformation changes upon association with the small protein CP12. *European Journal of Biochemistry*, 270(1), 129–136.

- Groben, R., Kaloudas, D., Raines, C. A., Offmann, B., Maberly, S. C., & Gontero, B. (2010). Comparative sequence analysis of CP12, a small protein involved in the formation of a Calvin cycle complex in photosynthetic organisms. *Photosynthesis Research*, 103(3), 183–194.
- Gründel, M., Scheunemann, R., Lockau, W., & Zilliges, Y. (2012). Impaired glycogen synthesis causes metabolic overflow reactions and affects stress responses in the cyanobacterium *Synechocystis* sp. PCC 6803. *Microbiology (United Kingdom)*, 158(12), 3032–3043.
- Häder, D.-P. (1975). The effect of inhibitors on the electron flow triggering photo-phobic reactions in cyanophyceae. *Archives of Microbiology*, 103(1), 169–174.
- Haffner, M., Hou, W.-T., Mantovani, O., Walke, P. R., Hauf, K., Borisova, M., Hagemann, M., Zhou, C.-Z., Forchhammer, K., & Selim, K. A. (2023). PII signal transduction superfamily acts as a valve plug to control bicarbonate and ammonia homeostasis among different bacterial phyla. *BioRxiv*, 2023.08.10.552651.
- Hagemann, M. (2011). Molecular biology of cyanobacterial salt acclimation. *FEMS Microbiology Reviews*, 35(1), 87–123.
- Hauf, W., Schlebusch, M., Hüge, J., Kopka, J., Hagemann, M., & Forchhammer, K. (2013). Metabolic changes in *Synechocystis* PCC6803 upon nitrogen-starvation: Excess NADPH sustains polyhydroxybutyrate accumulation. *Metabolites*, 3(1), 101–118.
- Hauf, W., Watzer, B., Roos, N., Klotz, A., & Forchhammer, K. (2015). Photoautotrophic Polyhydroxybutyrate Granule Formation Is Regulated by Cyanobacterial Phasin PhaP in *Synechocystis* sp. Strain PCC 6803. *Applied and Environmental Microbiology*, 81(13), 4411–4422.
- Hedges, S., Blair, J. E., Venturi, M. L., & Shoe, J. L. (2004). A molecular timescale of eukaryote evolution and the rise of complex multicellular life. *BMC Evolutionary Biology*, 4(1), 2.
- Heinrich, A., Maheswaran, M., Ruppert, U., & Forchhammer, K. (2004). The *Synechococcus elongatus* PII signal transduction protein controls arginine synthesis by complex formation with N-acetyl-L-glutamate kinase. *Molecular Microbiology*, 52(5), 1303–1314.
- Hohmann-Marriott, M. F., & Blankenship, R. E. (2011). Evolution of photosynthesis. *Annual Review of Plant Biology*, 62, 515–548.
- Ishii, A., & Hihara, Y. (2008). An AbrB-Like Transcriptional Regulator, SII0822, Is Essential for the Activation of Nitrogen-Regulated Genes in *Synechocystis* sp. PCC 6803. *Plant Physiology*, 148(1), 660–670.
- Ittekkot, V., Brockmann, U., Michaelis, W., & Degens, E. (1981). Dissolved Free and Combined Carbohydrates During a Phytoplankton Bloom in the Northern North Sea. *Marine Ecology Progress Series*, 4, 299–305.
- Jablonsky, J., Hagemann, M., Schwarz, D., & Wolkenhauer, O. (2013). Phosphoglycerate Mutases Function as Reverse Regulated Isoenzymes in *Synechococcus elongatus* PCC 7942. *PLoS ONE*, 8(3), e58281.
- Jablonsky, J., Schwarz, D., & Hagemann, M. (2014). Multi-Level Kinetic Model Explaining Diverse Roles of Isozymes in Prokaryotes. *PLoS ONE*, 9(8), e105292.
- Jablonsky, J., Papacek, S., & Hagemann, M. (2016). Different strategies of metabolic regulation in cyanobacteria: from transcriptional to biochemical control. *Scientific Reports*, 6(1), 33024.

- Jahn, M., Vialas, V., Karlsen, J., Maddalo, G., Edfors, F., Forsström, B., Uhlén, M., Käll, L., & Hudson, E. P. (2018). Growth of Cyanobacteria Is Constrained by the Abundance of Light and Carbon Assimilation Proteins. *Cell Reports*, 25(2), 478–486.e8.
- Jansén, T., Kurian, D., Raksajit, W., York, S., Summers, M. L., & Mäenpää, P. (2010). Characterization of trophic changes and a functional oxidative pentose phosphate pathway in *Synechocystis* sp. PCC 6803. *Acta Physiologiae Plantarum*, 32(3), 511–518.
- Jiang, Y.-L., Wang, X.-P., Sun, H., Han, S.-J., Li, W.-F., Cui, N., Lin, G.-M., Zhang, J.-Y., Cheng, W., Cao, D.-D., Zhang, Z.-Y., Zhang, C.-C., Chen, Y., & Zhou, C.-Z. (2018). Coordinating carbon and nitrogen metabolic signaling through the cyanobacterial global repressor NdhR. *Proceedings of the National Academy of Sciences*, 115(2), 403–408.
- Joset, F., Buchou, T., Zhang, C.-C., & Jeanjean, R. (1988). Physiological and genetic analysis of the glucose-fructose permeation system in two *Synechocystis* species. *Archives of Microbiology*, 149(5), 417–421.
- Kaneko, T., Sato, S., Kotani, H., Tanaka, A., Asamizu, E., Nakamura, Y., Miyajima, N., Hirose, M., Sugiyama, M., Sasamoto, S., Kimura, T., Hosouchi, T., Matsuno, A., Muraki, A., Nakazaki, N., Naruo, K., Okumura, S., Shimpo, S., Takeuchi, C., Tabata, S. (1996). Sequence Analysis of the Genome of the Unicellular Cyanobacterium *Synechocystis* sp. Strain PCC6803. II. Sequence Determination of the Entire Genome and Assignment of Potential Protein-coding Regions. *DNA Research*, 3(3), 109–136.
- Kaplan, A., & Reinhold, L. (1999). CO₂ Concentrating Mechanisms in Photosynthetic Microorganisms. *Annual Review of Plant Physiology and Plant Molecular Biology*, 50(1), 539–570.
- Klähn, S., Orf, I., Schwarz, D., Matthiessen, J. K. F., Kopka, J., Hess, W. R., & Hagemann, M. (2015). Integrated Transcriptomic and Metabolomic Characterization of the Low-Carbon Response Using an *ndhR* Mutant of *Synechocystis* sp. PCC 6803. *Plant Physiology*, 169(3), 1540–1556.
- Klotz, A., Reinhold, E., Doello, S., & Forchhammer, K. (2015). Nitrogen Starvation Acclimation in *Synechococcus elongatus*: Redox-Control and the Role of Nitrate Reduction as an Electron Sink. *Life*, 5(1), 888–904.
- Klotz, A., Georg, J., Bučinská, L., Watanabe, S., Reimann, V., Januszewski, W., Sobotka, R., Jendrossek, D., Hess, W. R., & Forchhammer, K. (2016). Awakening of a Dormant Cyanobacterium from Nitrogen Chlorosis Reveals a Genetically Determined Program. *Current Biology*, 26(21), 2862–2872.
- Klotz, A., & Forchhammer, K. (2017). Glycogen, a major player for bacterial survival and awakening from dormancy. *Future Microbiology*, 12(2), 101–104.
- Knoot, C. J., Ungerer, J., Wangikar, P. P., & Pakrasi, H. B. (2018). Cyanobacteria: Promising biocatalysts for sustainable chemical production. *Journal of Biological Chemistry*, 293(14), 5044–5052.
- Knowles, V. L., & Plaxton, W. C. (2003). From Genome to Enzyme: Analysis of Key Glycolytic and Oxidative Pentose-Phosphate Pathway Enzymes in the Cyanobacterium *Synechocystis* sp. PCC 6803. *Plant and Cell Physiology*, 44(7), 758–763.
- Koch, M., Doello, S., Gutekunst, K., & Forchhammer, K. (2019). PHB is produced from Glycogen turn-over during nitrogen starvation in *Synechocystis* sp. PCC 6803. *International Journal of Molecular Sciences*, 20(8).
- Koch, M., Bruckmoser, J., Scholl, J., Hauf, W., Rieger, B., & Forchhammer, K. (2020). Maximizing PHB content in *Synechocystis* sp. PCC 6803: a new metabolic engineering strategy based on the regulator PirC. *Microbial Cell Factories*, 19(1).

- Koksharova, O., Schubert, M., Shestakov, S., & Cerff, R. (1998).** Genetic and biochemical evidence for distinct key functions of two highly divergent GAPDH genes in catabolic and anabolic carbon flow of the cyanobacterium *Synechocystis* sp. PCC 6803. In *Plant Molecular Biology*, Jan;36(1):183-94.
- Kupriyanova, E. v., Pronina, N. A., & Los, D. A. (2023).** Adapting from Low to High: An Update to CO₂-Concentrating Mechanisms of Cyanobacteria and Microalgae. *Plants*, 12(7), 1569.
- Kurian, D., Jansèn, T., & Mäenpää, P. (2006).** Proteomic analysis of heterotrophy in *Synechocystis* sp. PCC 6803. *PROTEOMICS*, 6(5), 1483–1494.
- Larsson, A. M., Hasse, D., Vålegård, K., & Andersson, I. (2017).** Crystal structures of β -carboxysome shell protein CcmP: ligand binding correlates with the closed or open central pore. *Journal of Experimental Botany*, 68(14), 3857–3867.
- Lea-Smith, D. J., Bombelli, P., Vasudevan, R., & Howe, C. J. (2016).** Photosynthetic, respiratory and extracellular electron transport pathways in cyanobacteria. *Biochimica et Biophysica Acta – Bioenergetics*, 1857(3), 247–255.
- Lebreton, S., Andreescu, S., Graciet, E., & Gontero, B. (2006).** Mapping of the interaction site of CP12 with glyceraldehyde-3-phosphate dehydrogenase from *Chlamydomonas reinhardtii*: Functional consequences for glyceraldehyde-3-phosphate dehydrogenase. *FEBS Journal*, 273(14), 3358–3369.
- Lindahl, M., & Florencio, F. J. (2003).** Thioredoxin-linked processes in cyanobacteria are as numerous as in chloroplasts, but targets are different. *Proceedings of the National Academy of Sciences*, 100(26), 16107–16112.
- López-Calcano, P. E., Abuzaid, A. O., Lawson, T., & Raines, C. A. (2017).** *Arabidopsis* CP12 mutants have reduced levels of phosphoribulokinase and impaired function of the Calvin-Benson cycle. *Journal of Experimental Botany*, 68(9), 2285–2298.
- Lopo, M., Montagud, A., Navarro, E., Cunha, I., Zille, A., de Crdoba, P. F., Moradas-Ferreira, P., Tamagnini, P., & Urchuegua, J. F. (2012).** Experimental and modelling analysis of *Synechocystis* sp. PCC 6803 growth. *Journal of Molecular Microbiology and Biotechnology*, 22(2), 71–82.
- Lucius, S., Theune, M., Arrivault, S., Hildebrandt, S., Mullineaux, C. W., Gutekunst, K., & Hagemann, M. (2022).** CP12 fine-tunes the Calvin-Benson cycle and carbohydrate metabolism in cyanobacteria. *Frontiers in Plant Science*, 13.
- Lucius, S., Makowka, A., Michl, K., Gutekunst, K., & Hagemann, M. (2021).** The Entner-Doudoroff Pathway Contributes to Glycogen Breakdown During High to Low CO₂ Shifts in the Cyanobacterium *Synechocystis* sp. PCC 6803. *Frontiers in Plant Science*, 12.
- Lüddecke, J., & Forchhammer, K. (2015).** Energy Sensing versus 2-Oxoglutarate Dependent ATPase Switch in the Control of *Synechococcus* PII Interaction with Its Targets NAGK and PipX. *PLOS ONE*, 10(8), e0137114.
- Luque, I., Flores, E., & Herrero, A. (1994).** Molecular mechanism for the operation of nitrogen control in cyanobacteria. *The EMBO Journal*, 13(12), 2862–2869.
- Luque, I., Zabulon, G., Contreras, A., & Houmard, J. (2001).** Convergence of two global transcriptional regulators on nitrogen induction of the stress-acclimation gene *nblA* in the cyanobacterium *Synechococcus* sp. PCC 7942. *Molecular Microbiology*, 41(4), 937–947.
- Maheswaran, M., Urbanke, C., & Forchhammer, K. (2004).** Complex formation and catalytic activation by the PII signaling protein of N-acetyl-L-glutamate kinase from *Synechococcus elongatus* strain PCC 7942. *Journal of Biological Chemistry*, 279(53), 55202–55210.

- Makowka, A., Nichelmann, L., Schulze, D., Spengler, K., Wittmann, C., Forchhammer, K., & Gutekunst, K. (2020).** Glycolytic Shunts Replenish the Calvin–Benson–Bassham Cycle as Anaplerotic Reactions in Cyanobacteria. *Molecular Plant*, 13(3), 471–482.
- Mantovani, O., Reimann, V., Haffner, M., Herrmann, F. P., Selim, K. A., Forchhammer, K., Hess, W. R., & Hagemann, M. (2022).** The impact of the cyanobacterial carbon-regulator protein SbtB and of the second messengers cAMP and c-di-AMP on CO₂-dependent gene expression. *New Phytologist*, 234(5), 1801–1816.
- Marri, L., Zaffagnini, M., Collin, V., Issakidis-Bourguet, E., Lemaire, S. D., Pupillo, P., Sparla, F., Miginiac-Maslow, M., & Trost, P. (2009).** Prompt and Easy Activation by Specific Thioredoxins of Calvin Cycle Enzymes of *Arabidopsis thaliana* Associated in the GAPDH/CP12/PRK Supramolecular Complex. *Molecular Plant*, 2(2), 259–269.
- Matsumura, H., Kai, A., Maeda, T., Tamoi, M., Satoh, A., Tamura, H., Hirose, M., Ogawa, T., Kizu, N., Wadano, A., Inoue, T., & Shigeoka, S. (2011).** Structure Basis for the Regulation of Glyceraldehyde-3-Phosphate Dehydrogenase Activity via the Intrinsically Disordered Protein CP12. *Structure*, 19(12), 1846–1854.
- McFarlane, C. R., Shah, N. R., Kabasakal, B. v., Echeverria, B., Cotton, C. A. R., Bubeck, D., & Murray, J. W. (2019).** Structural basis of light-induced redox regulation in the Calvin–Benson cycle in cyanobacteria. *Proceedings of the National Academy of Sciences of the United States of America*, 116(42), 20984–20990.
- Merrick, M. (2015).** Post-translational modification of PII signal transduction proteins. *Frontiers in Microbiology*, 5(JAN).
- Mikkat, S., & Hagemann, M. (2000).** Molecular analysis of the ggtBCD gene cluster of *Synechocystis* sp. strain PCC6803 encoding subunits of an ABC transporter for osmoprotective compounds. *Archives of Microbiology*, 174(4), 273–282.
- Mills, L. A., McCormick, A. J., & Lea-Smith, D. J. (2020).** Current knowledge and recent advances in understanding metabolism of the model cyanobacterium *Synechocystis* sp. PCC 6803. *Bioscience Reports*, 40(4).
- Montesinos, M. L., Muro-Pastor, A. M., Herrero, A., & Flores, E. (1998).** Ammonium/methylammonium permeases of a Cyanobacterium: Identification and Analysis of three nitrogen-regulated *amt* Genes in *Synechocystis* sp. PCC 6803. *Journal of Biological Chemistry*, 273(47), 31463–31470.
- Muro-Pastor, M. I., Reyes, J. C., & Florencio, F. J. (2001).** Cyanobacteria Perceive Nitrogen Status by Sensing Intracellular 2-Oxoglutarate Levels. *Journal of Biological Chemistry*, 276(41), 38320–38328.
- Muro-Pastor, M. I., Reyes, J. C., & Florencio, F. J. (2005).** Ammonium assimilation in cyanobacteria. *Photosynthesis Research*, 83(2), 135–150.
- Muro-Pastor, M. I., Cutillas-Farray, Á., Pérez-Rodríguez, L., Pérez-Saavedra, J., Vega-De Armas, A., Paredes, A., Robles-Rengel, R., & Florencio, F. J. (2020).** CfrA, a novel carbon flow regulator, adapts carbon metabolism to nitrogen deficiency in cyanobacteria. *Plant Physiology*, 184(4), 1792–1810.
- Nakajima, T., Kajihata, S., Yoshikawa, K., Matsuda, F., Furusawa, C., Hirasawa, T., & Shimizu, H. (2014).** Integrated metabolic flux and omics analysis of *Synechocystis* sp. PCC 6803 under mixotrophic and photoheterotrophic conditions. *Plant and Cell Physiology*, 55(9), 1606–1612.
- Neumann, N., Doello, S., & Forchhammer, K. (2021).** Recovery of Unicellular Cyanobacteria from Nitrogen Chlorosis: A Model for Resuscitation of Dormant Bacteria. *Microbial Physiology*, 31(2), 78–87.

- Nishimura, T., Takahashi, Y., Yamaguchi, O., Suzuki, H., Maeda, S. I., & Omata, T. (2008). Mechanism of low CO₂-induced activation of the *cmp* bicarbonate transporter operon by a LysR family protein in the cyanobacterium *Synechococcus elongatus* strain PCC 7942. *Molecular Microbiology*, 68(1), 98–109.
- Ohashi, Y., Shi, W., Takatani, N., Aichi, M., Maeda, S., Watanabe, S., Yoshikawa, H., & Omata, T. (2011). Regulation of nitrate assimilation in cyanobacteria. *Journal of Experimental Botany*, 62(4), 1411–1424.
- Omata, T., Price, G. D., Badger, M. R., Okamura, M., Gohta, S., & Ogawa, T. (1999). Identification of an ATP-binding cassette transporter involved in bicarbonate uptake in the cyanobacterium *Synechococcus* sp. strain PCC 7942. *Proceedings of the National Academy of Sciences*, 96(23), 13571–13576.
- Omata, T., Gohta, S., Takahashi, Y., Harano, Y., & Maeda, S. I. (2001). Involvement of a CbbR homolog in low CO₂-induced activation of the bicarbonate transporter operon in cyanobacteria. *Journal of Bacteriology*, 183(6), 1891–1898.
- Oren, N., Raanan, H., Kedem, I., Turjeman, A., Bronstein, M., Kaplan, A., & Murik, O. (2019). Desert cyanobacteria prepare in advance for dehydration and rewetting: The role of light and temperature sensing. *Molecular Ecology*, 28(9), 2305–2320.
- Orf, I., Schwarz, D., Kaplan, A., Kopka, J., Hess, W. R., Hagemann, M., & Klähn, S. (2016). CyAbrB2 contributes to the transcriptional Regulation of low CO₂ Acclimation in *Synechocystis* sp. PCC 6803. *Plant and Cell Physiology*, 57(10), 2232–2243.
- Orthwein, T., Scholl, J., Spät, P., Lucius, S., Koch, M., Macek, B., Hagemann, M., & Forchhammer, K. (2021). The novel P_{II}-interactor PirC identifies phosphoglycerate mutase as key control point of carbon storage metabolism in cyanobacteria. *Proceedings of the National Academy of Sciences*, 118(6), 2019988118.
- Pelroy, R. A., Rippka, R., & Stanier, R. Y. (1972). Metabolism of glucose by unicellular blue-green algae. *Archiv Für Mikrobiologie*, 87(4), 303–322.
- Pohlmeyer, K., Paap, B. K., Soll, J., & Wedel, N. (1996). CP12: a small nuclear-encoded chloroplast protein provides novel insights into higher-plant GAPDH evolution. *Plant Molecular Biology*, 32(5), 969–978.
- Preiss, J. (1984). Bacterial Glycogen Synthesis and its Regulation. *Annual Review of Microbiology*, 38(1), 419–458.
- Preiss, J., & Romeo, T. (1994). Molecular Biology and Regulatory Aspects of Glycogen Biosynthesis in Bacteria. *Progress in Nucleic Acid Research and Molecular Biology*, 47:299–329.
- Price, G. D., Woodger, F. J., Badger, M. R., Howitt, S. M., & Tucker, L. (2004). Identification of a SulP-type bicarbonate transporter in marine cyanobacteria. *Proceedings of the National Academy of Sciences*, 101(52), 18228–18233.
- Rae, B. D., Long, B. M., Badger, M. R., & Price, G. D. (2013). Functions, Compositions, and Evolution of the Two Types of Carboxysomes: Polyhedral Microcompartments That Facilitate CO₂ Fixation in Cyanobacteria and Some Proteobacteria. *Microbiology and Molecular Biology Reviews*, 77(3), 357–379.
- Raven, J. A., Beardall, J., & Sánchez-Baracaldo, P. (2017). The possible evolution and future of CO₂-concentrating mechanisms. *Journal of Experimental Botany*, 68(14), 3701–3716.
- Reed, R. H., & Stewart, W. D. P. (1985). Osmotic adjustment and organic solute accumulation in unicellular cyanobacteria from freshwater and marine habitats. *Marine Biology*, 88(1), 1–9.

- Rippka, R., Deruelles, J., Waterbury, J. B., Herdman, M. & Stanier, R. Y. (1979).** Generic Assignments, Strain Histories and Properties of Pure Cultures of Cyanobacteria. *Microbiology* 111, 1–61.
- Sánchez-Baracaldo, P., & Cardona, T. (2020).** On the origin of oxygenic photosynthesis and Cyanobacteria. *New Phytologist*, 225(4), 1440–1446.
- Santos-Merino, M., Singh, A. K., & Ducat, D. C. (2019).** New Applications of Synthetic Biology Tools for Cyanobacterial Metabolic Engineering. *Frontiers in Bioengineering and Biotechnology*, 7(FEB).
- Schirrmeister, B. E., Sanchez-Baracaldo, P., & Wacey, D. (2016).** Cyanobacterial evolution during the Precambrian. *International Journal of Astrobiology*, 15(3), 187–204.
- Schmetterer, G. R. (1990).** Sequence conservation among the glucose transporter from the cyanobacterium *Synechocystis* sp. PCC 6803 and mammalian glucose transporters. *Plant Molecular Biology*, 14(5), 697–706.
- Scholl, J., Dengler, L., Bader, L., & Forchhammer, K. (2020).** Phosphoenolpyruvate carboxylase from the cyanobacterium *Synechocystis* sp. PCC 6803 is under global metabolic control by PII signaling. *Molecular Microbiology*, 114(2), 292–307.
- Schulze, D., Kohlstedt, M., Becker, J., Cahoreau, E., Peyriga, L., Makowka, A., Hildebrandt, S., Gutekunst, K., Portais, J.-C., & Wittmann, C. (2022).** GC/MS-based ¹³C metabolic flux analysis resolves the parallel and cyclic photomixotrophic metabolism of *Synechocystis* sp. PCC 6803 and selected deletion mutants including the Entner-Doudoroff and phosphoketolase pathways. *Microbial Cell Factories*, 21(1), 69.
- Schwarz, D., Nodop, A., Hüge, J., Purfürst, S., Forchhammer, K., Michel, K. P., Bauwe, H., Kopka, J., & Hagemann, M. (2011).** Metabolic and transcriptomic phenotyping of inorganic carbon acclimation in the cyanobacterium *Synechococcus elongatus* PCC 7942. *Plant Physiology*, 155(4), 1640–1655.
- Selim, K. A., Haase, F., Hartmann, M. D., Hagemann, M., & Forchhammer, K. (2018).** PII-like signaling protein SbtB links cAMP sensing with cyanobacterial inorganic carbon response. *Proceedings of the National Academy of Sciences of the United States of America*, 115(21), E4861–E4869.
- Sharkey, T. D., & Weise, S. E. (2016).** The glucose 6-phosphate shunt around the Calvin–Benson cycle. *Journal of Experimental Botany*, 67(14), 4067–4077.
- Shibata, M., Katoh, H., Sonoda, M., Ohkawa, H., Shimoyama, M., Fukuzawa, H., Kaplan, A., & Ogawa, T. (2002).** Genes Essential to Sodium-dependent Bicarbonate Transport in Cyanobacteria. *Journal of Biological Chemistry*, 277(21), 18658–18664.
- Skoog, A., Biddanda, B., & Benner, R. (1999).** Bacterial utilisation of dissolved glucose in the upper water column of the Gulf of Mexico. *Limnology and Oceanography*, 44(7), 1625–1633.
- Spät, P., Klotz, A., Rexroth, S., Maček, B., & Forchhammer, K. (2018).** Chlorosis as a Developmental Program in Cyanobacteria: The Proteomic Fundament for Survival and Awakening. *Molecular & Cellular Proteomics*, 17(9), 1650–1669.
- Spät, P., Barske, T., Maček, B., & Hagemann, M. (2021).** Alterations in the CO₂ availability induce alterations in the phosphoproteome of the cyanobacterium *Synechocystis* sp. PCC 6803. *New Phytologist*, 231(3), 1123–1137.
- Stanier, R. Y., Kunisawa, R., Mandel, M., & Cohen-Bazire, G. (1971).** Purification and properties of unicellular blue-green algae (order Chroococcales). *Bacteriological Reviews*, 35(2), 171–205.

- Stanley, D. N., Raines, C. A., & Kerfeld, C. A. (2013).** Comparative analysis of 126 cyanobacterial genomes reveals evidence of functional diversity among homologs of the redox-regulated CP12 protein. *Plant Physiology*, 161(2), 824–835.
- Steinhauser, D., Fernie, A. R., & Araújo, W. L. (2012).** Unusual cyanobacterial TCA cycles: not broken just different. *Trends in Plant Science*, 17(9), 503–509.
- Stephan, D. P., Ruppel, H. G., & Pistorius, E. K. (2000).** Interrelation between Cyanophycin Synthesis, L-Arginine Catabolism and Photosynthesis in the Cyanobacterium *Synechocystis* Sp. Strain PCC 6803. *Zeitschrift Für Naturforschung C*, 55(11–12), 927–942.
- Tamoi, M., Miyazaki, T., Fukamizo, T., & Shigeoka, S. (2005).** The Calvin cycle in cyanobacteria is regulated by CP12 via the NAD(H)/NADP(H) ratio under light/dark conditions. *Plant Journal*, 42(4), 504–513.
- Tamoi, M., & Shigeoka, S. (2021).** Cp12 is involved in protection against high light intensity by suppressing the *ros* generation in *Synechococcus elongatus* PCC7942. *Plants*, 10(7).
- Turmo, A., Gonzalez-Esquer, C. R., & Kerfeld, C. A. (2017).** Carboxysomes: metabolic modules for CO₂ fixation. *FEMS Microbiology Letters*, 364(18).
- Ueda, K., Nakajima, T., Yoshikawa, K., Toya, Y., Matsuda, F., & Shimizu, H. (2018).** Metabolic flux of the oxidative pentose phosphate pathway under low light conditions in *Synechocystis* sp. PCC 6803. *Journal of Bioscience and Bioengineering*, 126(1), 38–43.
- Valladares, A., Montesinos, M. L., Herrero, A., & Flores, E. (2002).** An ABC-type, high-affinity urea permease identified in cyanobacteria. *Molecular Microbiology*, 43(3), 703–715.
- Vermaas, W. F. (2001).** Photosynthesis and Respiration in Cyanobacteria. eLS. Wiley.
- Wan, N., DeLorenzo, D. M., He, L., You, L., Immethun, C. M., Wang, G., Baidoo, E. E. K., Hollinshead, W., Keasling, J. D., Moon, T. S., & Tang, Y. J. (2017).** Cyanobacterial carbon metabolism: Fluxome plasticity and oxygen dependence. *Biotechnology and Bioengineering*, 114(7), 1593–1602.
- Watzer, B., Spät, P., Neumann, N., Koch, M., Sobotka, R., Macek, B., Hennrich, O., & Forchhammer, K. (2019).** The signal transduction protein PII controls ammonium, nitrate and urea uptake in cyanobacteria. *Frontiers in Microbiology*, 10(JUN).
- Wedel, N., & Soll, J. (1998).** Evolutionary conserved light regulation of Calvin cycle activity by NADPH-mediated reversible phosphoribulokinase/CP12/ glyceraldehyde-3-phosphate dehydrogenase complex dissociation. *Proceedings of the National Academy of Sciences*, 95(16), 9699–9704.
- Wolk, C. P. (1973).** Physiology and cytological chemistry blue-green algae. *Bacteriological Reviews*, 37(1), 32–101.
- Xiong, W., Cano, M., Wang, B., Douchi, D., & Yu, J. (2017).** The plasticity of cyanobacterial carbon metabolism. *Current Opinion in Chemical Biology*, 41, 12–19.
- Yang, C., Hua, Q., & Shimizu, K. (2002).** Metabolic flux analysis in *Synechocystis* using isotope distribution from ¹³C-labeled glucose. *Metabolic Engineering*, 4(3), 202–216.
- Yoshihara, A., & Kobayashi, K. (2022).** Photosynthesis and Cell Growth Trigger Degradation of Phycobilisomes during Nitrogen Limitation. *Plant and Cell Physiology*, 63(2), 189–199.
- Yoshikawa, K., Hirasawa, T., Ogawa, K., Hidaka, Y., Nakajima, T., Furusawa, C., & Shimizu, H. (2013).** Integrated transcriptomic and metabolomic analysis of the central metabolism of *Synechocystis* sp. PCC 6803 under different trophic conditions. *Biotechnology Journal*, 8(5), 506–507.

- Young, J. D., Shastri, A. A., Stephanopoulos, G., & Morgan, J. A. (2011).** Mapping photoautotrophic metabolism with isotopically nonstationary ^{13}C flux analysis. *Metabolic Engineering*, 13(6), 656–665.
- Yu, A., Xie, Y., Pan, X., Zhang, H., Cao, P., Su, X., Chang, W., & Li, M. (2020).** Photosynthetic phosphoribulokinase structures: Enzymatic mechanisms and the redox regulation of the Calvin-Benson-Bassham cycle. *Plant Cell*, 32(5), 1556–1573.
- Zeth, K., Fokina, O., & Forchhammer, K. (2014).** Structural Basis and Target-specific Modulation of ADP Sensing by the *Synechococcus elongatus* PII Signaling Protein. *Journal of Biological Chemistry*, 289(13), 8960–8972.
- Zhang, C.-C., Jeanjean, R., & Joset, F. (1998).** Obligate phototrophy in cyanobacteria: more than a lack of sugar transport. *FEMS Microbiology Letters*, 161(2), 285–292.
- Zhang, C.-C., Zhou, C.-Z., Burnap, R. L., & Peng, L. (2018).** Carbon/Nitrogen Metabolic Balance: Lessons from Cyanobacteria. *Trends in Plant Science*, 23(12), 1116–1130.
- Zhang, H., & Yang, C. (2019).** Arginine and nitrogen mobilization in cyanobacteria. *Molecular Microbiology*, 111(4), 863–867.
- Zhang, L., & Becker, D. F. (2015).** Connecting proline metabolism and signaling pathways in plant senescence. *Frontiers in Plant Science*, 6.
- Zhang, S., & Bryant, D. A. (2011).** The tricarboxylic acid cycle in cyanobacteria. *Science*, 334(6062), 1551–1553.
- Zilliges, Y. (2014).** Glycogen, a dynamic cellular sink and reservoir for carbon. in Cell Biology of Cyanobacteria (ed. Flores, E.). *The Cell Biology of Cyanobacteria*, Caister Academic Press.

11 Publications

11.1 Publication I: The Entner-Doudoroff Pathway Contributes to Glycogen Breakdown During High to Low CO₂ Shifts in the Cyanobacterium *Synechocystis* sp. PCC 6803

Lucius, S., Makowka, A., Michl, K., Gutekunst, K., & Hagemann, M. (2021). *Frontiers in Plant Science*, 12:787943.



The Entner-Doudoroff Pathway Contributes to Glycogen Breakdown During High to Low CO₂ Shifts in the Cyanobacterium *Synechocystis* sp. PCC 6803

Stefan Lucius¹, Alexander Makowka², Klaudia Michl¹, Kirstin Gutekunst^{2,3} and Martin Hagemann^{1,4*}

¹ Department of Plant Physiology, Institute of Biosciences, University of Rostock, Rostock, Germany, ² Department of Biology, Botanical Institute, Christian-Albrechts-University, Kiel, Germany, ³ Department of Molecular Plant Physiology, Bioenergetics in Photoautotrophs, University of Kassel, Kassel, Germany, ⁴ Interdisciplinary Faculty, Department Life, Light and Matter, University of Rostock, Rostock, Germany

OPEN ACCESS

Edited by:

Cornelia Spetea,
University of Gothenburg, Sweden

Reviewed by:

Dorota Muth-Pawlak,
University of Turku, Finland
Peter Lindblad,
Uppsala University, Sweden

*Correspondence:

Martin Hagemann
martin.hagemann@uni-rostock.de

Specialty section:

This article was submitted to
Plant Physiology,
a section of the journal
Frontiers in Plant Science

Received: 01 October 2021

Accepted: 12 November 2021

Published: 09 December 2021

Citation:

Lucius S, Makowka A, Michl K,
Gutekunst K and Hagemann M (2021)
The Entner-Doudoroff Pathway
Contributes to Glycogen Breakdown
During High to Low CO₂ Shifts
in the Cyanobacterium *Synechocystis*
sp. PCC 6803.
Front. Plant Sci. 12:787943.
doi: 10.3389/fpls.2021.787943

Cyanobacteria perform plant-like oxygenic photosynthesis to convert inorganic carbon into organic compounds and can also use internal carbohydrate reserves under specific conditions. A mutant collection with defects in different routes for sugar catabolism was studied to analyze which of them is preferentially used to degrade glycogen reserves in light-exposed cells of *Synechocystis* sp. PCC 6803 shifted from high to low CO₂ conditions. Mutants defective in the glycolytic Embden–Meyerhof–Parnas pathway or in the oxidative pentose-phosphate (OPP) pathway showed glycogen levels similar to wild type under high CO₂ (HC) conditions and were able to degrade it similarly after shifts to low CO₂ (LC) conditions. In contrast, the mutant Δeda , which is defective in the glycolytic Entner-Doudoroff (ED) pathway, accumulated elevated glycogen levels under HC that were more slowly consumed during the LC shift. In consequence, the mutant Δeda showed a lowered ability to respond to the inorganic carbon shifts, displayed a pronounced lack in the reactivation of growth when brought back to HC, and differed significantly in its metabolite composition. Particularly, Δeda accumulated enhanced levels of proline, which is a well-known metabolite to maintain redox balances via NADPH levels in many organisms under stress conditions. We suggest that deletion of *eda* might promote the utilization of the OPP shunt that dramatically enhance NADPH levels. Collectively, the results point at a major regulatory contribution of the ED pathway for the mobilization of glycogen reserves during rapid acclimation to fluctuating CO₂ conditions.

Keywords: CO₂ acclimation, glycolytic pathways, metabolome, mutant, sugar catabolism

INTRODUCTION

Cyanobacteria evolved oxygenic photosynthesis approximately 2.7 billion years ago (Hohmann-Marriott and Blankenship, 2011). By this process, they can efficiently convert inorganic carbon (Ci), either as CO₂ or bicarbonate into organic material at the expense of light energy. This capability makes cyanobacteria an interesting chassis for the CO₂-neutral production of organic fuels or feedstock (e.g., Hagemann and Hess, 2018). The Calvin-Benson-Bassham (CBB) cycle is the main Ci incorporating route with ribulose 1,5-bisphosphate carboxylase/oxygenase (RubisCO) as key enzyme, which incorporates either CO₂ into ribulose 1,5-bisphosphate (RuBP) leading to two molecules 3-phosphoglycerate (3PGA) or O₂ into RuBP resulting in the appearance of 3PGA and 2-phosphoglycolate (2PG). The latter intermediate turned out to be toxic for the CBB cycle and associated metabolic pathways (e.g., Flügel et al., 2017) and must be efficiently recycled via the photorespiratory 2PG metabolism, which likely evolved in parallel with oxygenic photosynthesis in ancient cyanobacteria (Eisenhut et al., 2008a).

The available amount of Ci for photosynthesis changed in different time scales in the environment of cyanobacteria. In the long term, it dramatically decreased to the present low CO₂ content of about 0.04% in the Earth's atmosphere mainly due to the photosynthetic activities of cyanobacteria, algae and plants. In parallel, the amount of O₂ rose to 21%. This gas ratio appeared to be problematic for RubisCO, because it has a rather low affinity and specificity for CO₂ (Tcherkez et al., 2006). Especially in aquatic habitats, the Ci levels are also fluctuating in short time scales depending on the pH, salinity and temperature influencing the solubility of CO₂ and its conversion into bicarbonate. To respond to limiting Ci conditions, cyanobacteria evolved an inorganic carbon-concentrating mechanism (CCM), which enables them to accumulate CO₂ in the vicinity of RubisCO, permitting the enzyme to work under saturated CO₂ conditions thereby suppressing the oxygenase reaction (Kaplan et al., 2008). The CCM activity in model strains such as *Synechocystis* sp. PCC 6803 (hereafter *Synechocystis*) is mainly regulated at the transcriptional level due to the action of several regulatory proteins such as NdhR, CmpR, CyAbrB2, and SbtB (reviewed in Hagemann et al., 2021).

In addition to the transcriptional changes, the shift from high to low Ci conditions had pronounced effects on the metabolic composition of cyanobacteria (Eisenhut et al., 2008b; Schwarz et al., 2011). In the case of *Synechocystis*, these alterations seem to be mainly regulated on the biochemical level (Jablonsky et al., 2016), because the abundances of transcripts and proteins for almost all enzymes involved in primary carbon metabolism remained unchanged under different Ci conditions (Klähn et al., 2015; Spät et al., 2021). A defined metabolic signature was observed in *Synechocystis* cells shifted from high Ci (HC, 5% CO₂) to low Ci (LC, ambient air of 0.04% CO₂), which is at least partly conserved in Arabidopsis plants (Orf et al., 2016). This metabolic change indicates that the carbon export from the CBB cycle into lower glycolysis is stimulated under LC conditions, which might involve the newly identified regulator protein of phosphoglycerate mutase PirC (Orthwein et al., 2021).

Furthermore, HC-grown *Synechocystis* cells accumulate high glycogen levels. Upon shifts to LC conditions glycogen becomes degraded and long-term LC-acclimated cells are virtually free of glycogen reserves (Eisenhut et al., 2007).

Hence, different Ci conditions do not only affect carbon anabolism via the CCM and the CBB cycle but have marked influences on carbon partitioning and glycogen accumulation or degradation. Basically, four different routes have been identified, which are involved in the metabolism of glucose released from glycogen breakdown in *Synechocystis* and other cyanobacteria. In darkened cells, the oxidative pentose-phosphate (OPP) pathway has been shown to be mainly responsible for the utilization of accumulated glycogen reserves (Pelroy et al., 1972; Makowka et al., 2020). Two different glycolytic routes, the Embden-Meyerhof-Parnas (EMP) and the Entner-Doudoroff (ED) pathway are also active in cyanobacteria (Chen et al., 2016). Recently it has been shown that the ED pathway, which shows the lowest overlap with the CBB cycle, plays the main role for carbon catabolism in the light during recovery from long-term nitrogen limitation (Doello et al., 2018). Furthermore, these pathways also support the reactivation of the CBB cycle during transition from darkness into light, however, under this condition they transiently do not operate at their full length but instead probably form short shunts (Makowka et al., 2020). As fourth route, the phosphoketolase pathway can also contribute to glucose catabolism under specific conditions in *Synechocystis* (Bachhar and Jablonsky, 2020; Chuang and Liao, 2021).

In the present study, exclusively the roles of three routes, the OPP, EMP and ED pathways were characterized. We analyzed which of these glucose catabolic routes is mainly involved in the mobilization of glycogen reserves during HC to LC shifts. For this purpose, the response to fluctuating Ci conditions was compared between the *Synechocystis* wild type (WT) and a set of mutants defective in the OPP, the glycolytic EMP or ED pathways (Figure 1). Our results indicate a major regulatory impact of the glycolytic ED pathway on glycogen accumulation in the light and its mobilization during HC to LC shifts, which is crucial for a rapid acclimation to fluctuating CO₂ conditions.

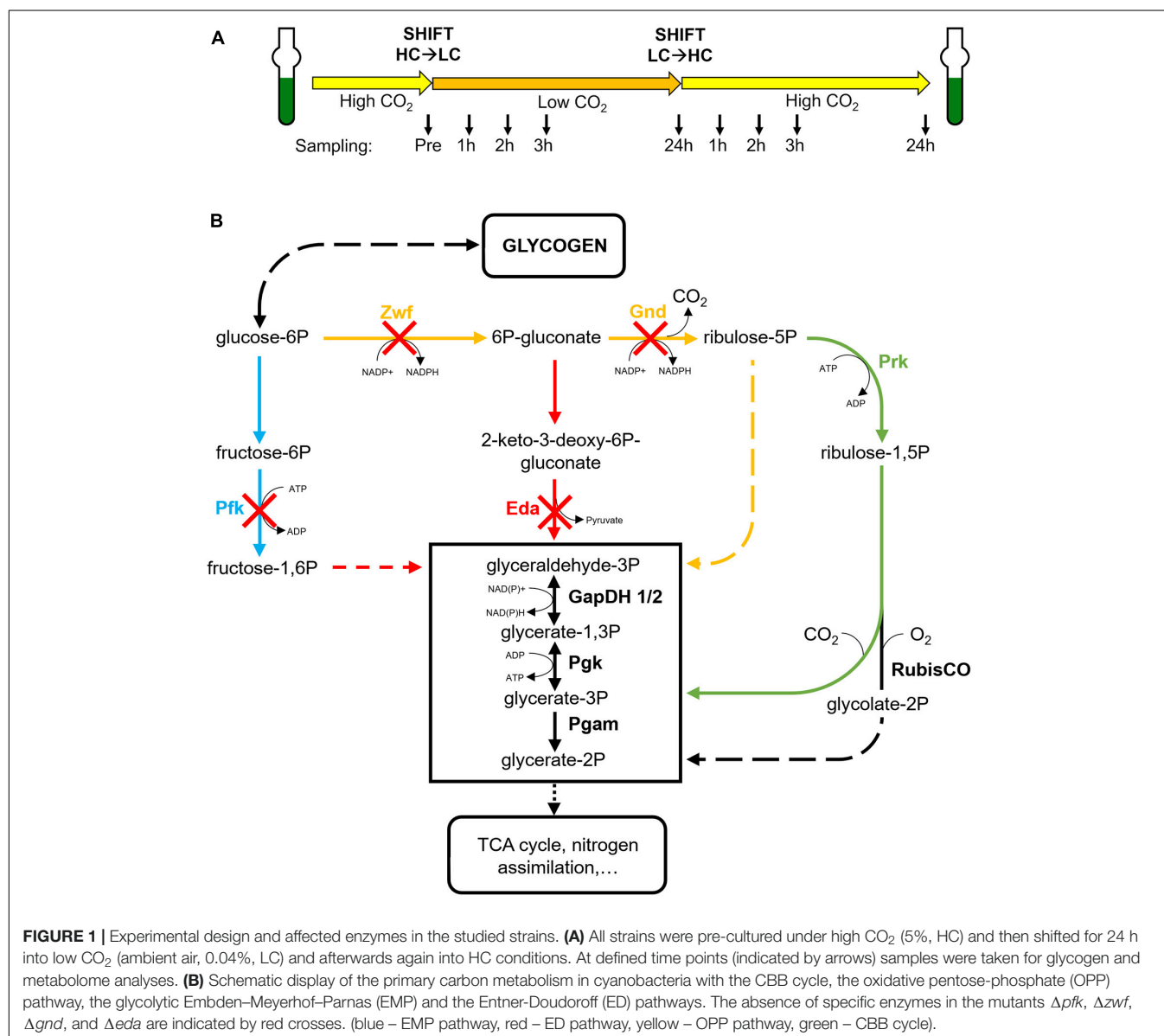
MATERIALS AND METHODS

Strains and *Synechocystis* Mutants

All analyzed wild-type and mutant strains of *Synechocystis* sp. PCC 6803 used in this study are described by Chen et al. (2016).

Shift Experiments

Cells of the *Synechocystis* WT and the mutants were pre-cultivated in batch cultures under high Ci-conditions (5% CO₂, HC) in buffered BG-11 medium (Rippka et al., 1979; TES pH 8.0) containing the respective antibiotics at 30°C and 100 μmol photons m⁻² s⁻¹ in glass tubes until the cell suspension reached the desired OD at 750 nm (OD₇₅₀) of 0.8 to 1.0. After 24 h of acclimation the *Synechocystis* cultures were diluted to OD₇₅₀ = 0.8 with fresh BG-11 (pH 8.0). After cultivation for another hour, samples for LC-MS and glycogen analysis were harvested and OD₇₅₀ was determined. To shift cultures from HC to low CO₂



(LC, 0.04% CO₂ in ambient air) conditions, cells were then centrifuged and resuspended in identical volume of BG-11 (pH 7.0) before continuing bubbling cultivation with ambient air. After 24 h, cultures were shifted back from LC to HC conditions by changing the aeration supply back to air containing 5% CO₂. Samples were taken one, two, three and 24 h after each CO₂ shift and OD₇₅₀ was measured as proxy for growth and biomass (see Figure 1A).

Glycogen Quantification

Cellular glycogen content determination was modified after Gründel et al. (2012), as described in Makowka et al. (2020). During the CO₂ shift experiments, 5 mL of cells were harvested in duplicates and pelleted by centrifugation. The pellet was resuspended in 300 μ L 30% (w/v) KOH and cells were incubated at 95°C for 2 h. After addition of 900 μ L ethanol, samples were

incubated at –20°C over night. Samples were then centrifuged (10 min, 10000 g, 4°C) for glycogen precipitation. Pellets were washed with 1 mL absolute and 1 mL 70% ethanol and then dried at 50°C. These pellets were resuspended in 200 μ L sodium acetate buffer (100 mM, pH 4.5) containing 21 U amyloglucosidase and incubated at 60°C for 90 min. After centrifugation (10 min, 10000 g, RT), the released glucose was determined in the supernatants using o-toluidine reagent. Glucose contents were calculated using a glucose calibration curve.

Metabolite Analysis

During the CO₂ shift experiments cells were harvested in duplicates of 5 mL at each respective time point on nitrocellulose filters (25 mm, Porafil, Macherey-Nagel) and resuspended in 1 mL ethanol (80%, HPLC grade, Roth, Germany). The metabolites were later normalized according to their respective

OD750nm and sample volumes. Low molecular mass compounds were extracted from the cells with ethanol at 65°C for 2 h. One microgram of carnitine was added per sample as an internal standard. After centrifugation, the supernatants were collected and freeze-dried. The dry extracts were dissolved in 800 μ l MS-grade water and filtered through 0.2 μ m filters (Omnifix®-F, Braun, Germany). The cleared supernatants were analysed using the high-performance liquid chromatograph mass spectrometer system (LCMS-8050, Shimadzu, Japan). In brief, 1 μ l of each extract was separated on a pentafluorophenylpropyl (PFPP) column (Supelco Discovery HS FS, 3 μ m, 150 x 2.1 mm) with a mobile phase containing 0.1% formic acid. The compounds were eluted at a rate of 0.25 ml min⁻¹ using the following gradient: 1 min 0.1% formic acid, 95% distilled water, 5% acetonitrile, within 15 min linear gradient to 0.1% formic acid, 5% distilled water, 95% acetonitrile, 10 min 0.1% formic acid, 5% distilled water, 95% acetonitrile. Aliquots were continuously injected in the MS/MS part and ionized via electrospray ionization (ESI). The compounds were identified and quantified using the multiple reaction monitoring (MRM) values given in the LC-MS/MS method package and the LabSolutions software package (Shimadzu, Japan). The metabolites were determined as relative metabolite abundances, which were calculated by normalization of signal intensity to that of the internal standard carnitine and optical density per sampling volume.

Data Evaluation and Statistical Analysis

The experiments were repeated at least three times with independent cultivations. Data evaluation for LC-MS was done by first calculating the averages of absolute metabolite contents per sampling point within each biological replicate and then calculating the fold change to the respective WT HC pre-shift (set to 1) data. Final metabolite values were obtained by then calculating the average of all three biological replicates' fold change data. The growth and glycogen datasets are representative of three biological replicates. A Student's *t*-test with significance level of 5% ($p \leq 0.05$) was performed. A significant deviation of every single data point of a mutant strain compared to respective WT data is marked by an asterisk. Heat map data were calculated for each metabolite as fold changes (log₁₀) to HC pre-shift values (set to 1) in WT cells. Heat maps were created in program MultiExperiment Viewer (TM4 MeV). Principal component analyses (PCAs) were performed using the program Minitab® (version 17.1.0., Minitab Inc.) with metabolite fold change values compared to the respective WT HC pre-shift data (set to 1). The first two principal components cover 52.5% of the total variance of the dataset data set, as calculated by the software during data analysis.

RESULTS

To analyze which glucose catabolic route is mainly responsible for the mobilization of glycogen reserves during HC to LC shifts, cells of the *Synechocystis* WT and a set of mutants defective in specific key enzymes of the OPP, the glycolytic EMP or ED pathways were compared under different CO₂ availability. Specifically,

the previously described mutants Δpfk [EMP pathway blocked due to the absence of two isoforms of phosphofructokinase (Pfk)], Δzwf [OPP and ED pathways blocked due to the absence of glucose 6-phosphate dehydrogenase (Zwf)], Δgnd [OPP pathway blocked due to the absence of 6-phosphogluconate dehydrogenase (Gnd)], and Δeda [ED pathway blocked due to the absence of 2-dehydro-3-deoxyphosphogluconate aldolase (Eda)] were used (Chen et al., 2016) (**Figure 1B**). All strains were first acclimated for at least one week to HC conditions (5% CO₂), then shifted to LC (ambient air with 0.04% CO₂) for 24 h and subsequently brought back to HC for 24 h (HC to LC to HC shifts; **Figure 1A**). At different time points samples were taken for glycogen and metabolome analysis, while the growth of the cultures was monitored via measurements of optical densities at 750 nm (OD₇₅₀).

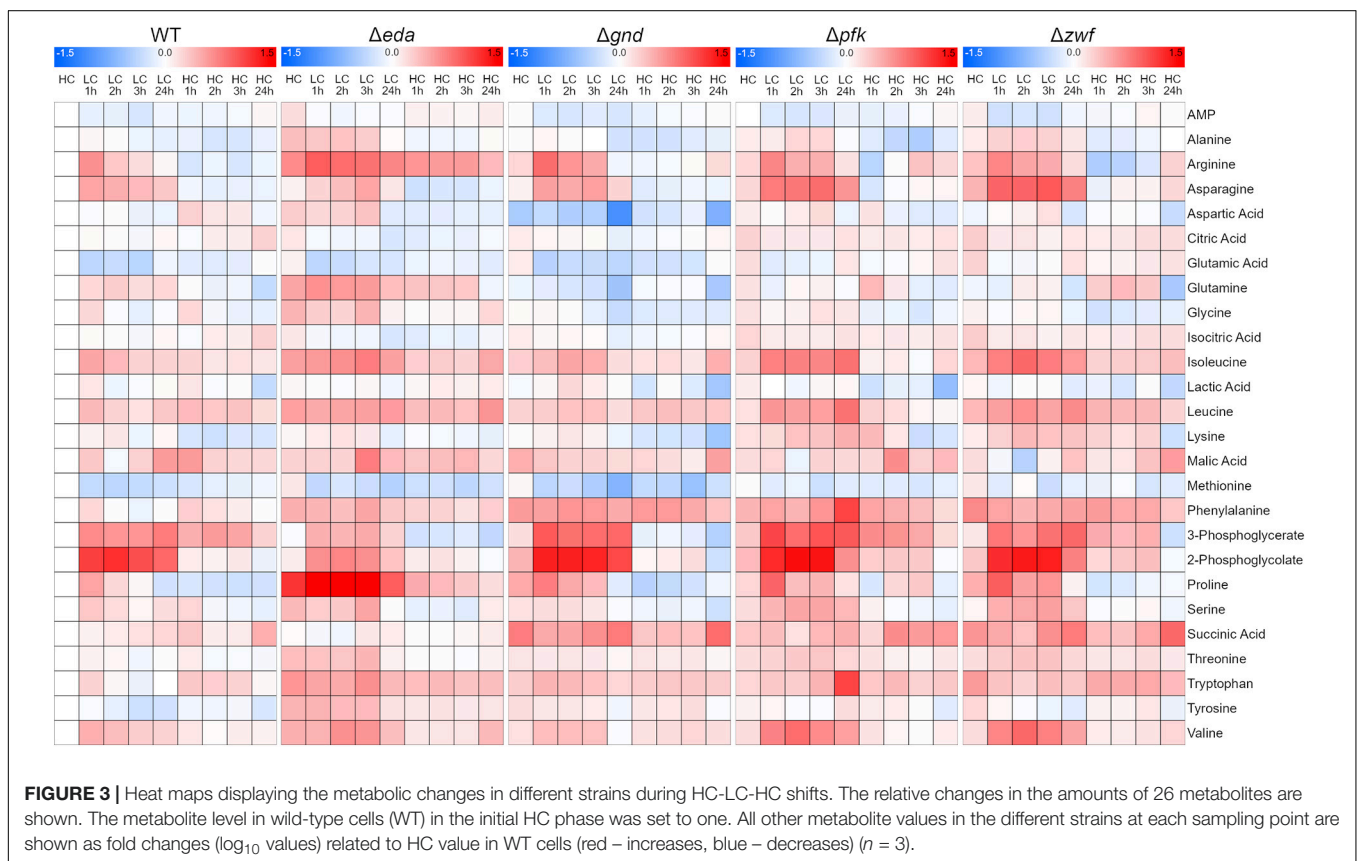
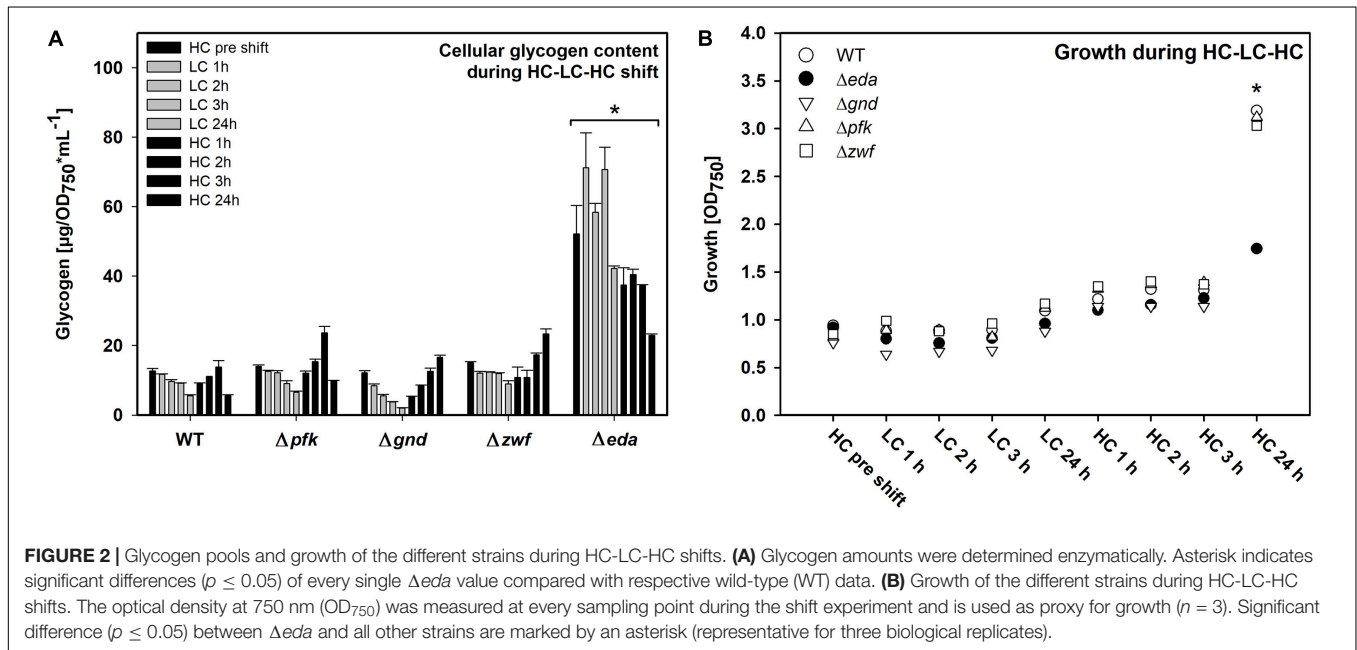
Alterations of Glycogen Levels in Strains During HC-LC-HC Shifts

Different patterns of changes in the glycogen pool were observed. As expected, the WT cells reduced the initial HC level of glycogen during the 24 h LC period and restored it in the following HC period (**Figure 2A**). This glycogen level pattern was principally also found in the mutants Δpfk , Δzwf and Δgnd . However, the Δeda mutant showed marked differences. Cells of this strain accumulated significantly higher glycogen levels under HC conditions, which were not mobilized to a significant extent during the first hours of the LC period (**Figure 2A**). Only at the end of the LC period the glycogen level decreased. Furthermore, the somehow reduced glycogen pool was not recovered in the mutant Δeda during the next HC period as in the other strains.

All mutants decreased growth to almost zero during the 24 h LC period (**Figure 2B**). Growth resumed stepwise during the following HC period for WT and mutants Δpfk , Δzwf and Δgnd . However, the mutant Δeda showed a pronounced lack in the reactivation of growth under the HC conditions. These results clearly show that absence of Eda has a strong impact on glycogen accumulation and remobilization in *Synechocystis* during HC to LC shift, and that this capability is essential for a rapid acclimation to fluctuating CO₂ conditions.

Global Changes of the Metabolome in Strains During HC-LC-HC Shifts

Next, we aimed to analyze whether the mutation of different glucose metabolizing pathways is also impacting the general carbon and nitrogen metabolism. A targeted metabolome approach was used that permitted to quantify 26 metabolites in three independent experiments. The quantified compounds include mostly amino and organic acids, whereas the phosphorylated intermediates up- and downstream of the mutations could not be detected by this method. The metabolic analysis shows that many metabolites responded to the HC-LC-HC shift conditions in these strains (the entire dataset is displayed in the **Supplementary Table 1**). These changes are illustrated in the corresponding heat map showing that selected metabolites respond differentially to the HC-LC-HC shifts in the different strains, while many metabolites show similar



patterns in the mutants and the WT (**Figure 3**). For example, the RubisCO oxygenase reaction product 2-phosphoglycolate (2PG) showed the expected rapid accumulation in the WT and all mutants after LC shift. As expected, 2PG levels resumed in the subsequent HC period, whereas the RubisCO carboxylation

product 3-phosphoglycerate (3PGA) showed lower increases after the LC shift. Glutamate and some other amino acids such as methionine showed an opposite behavior (**Figure 3**).

The global metabolic changes in the different strains under changing Ci conditions were further analyzed using principal

component analysis (PCA). This analytical tool projects a high-dimensional dataset into a low-dimensional space. Multiple measurement parameters of an analysis are transformed into few principal components in a new orthogonal coordinate system. The thus obtained PCA score plot displays similarities regarding all quantified metabolites at each sampling time point during the HC-LC-HC shift in the respective genotypes (Figure 4). The multidimensional dataset in which every measured metabolite represents one dimension per sample has therefore been reduced to a two-dimensional score plot with only two principal components. These two components are the most important for data interpretation as they explain 52.5% of the total measured variance between all data, which can be considered as the most significant contribution to their separation. Every data point in the score plot thus represents one experimental sample defined by genotype, CO₂ treatment and sampling time that is plotted according to its specific metabolic composition measured in the LC-MS analysis. As observed before for the glycogen accumulation patterns, the metabolic changes in the mutant Δeda showed clear differences compared to the WT and the other mutants. The metabolite composition in Δeda is always above all other strains in the second dimension (Figure 4). It shows higher first component values regarding the metabolite composition in the initial HC state and the first LC samples. This separation indicates that the increased glycogen level and its slow consumption in cells of mutant Δeda induces a general different metabolic composition and a delayed acclimation to LC conditions, respectively. Among the other genotypes, a clear separation of metabolic composition is found under HC versus LC conditions, mainly defined by the second component. Apart from Δeda , HC metabolic compositions in the mutants scatter together with WT in the first component and are generally shifted to lower second component values for all LC samples. Among these LC metabolic compositions, WT and mutant Δgnd are very close to each other, while it differs slightly more between WT and mutants Δpfk and Δzwf (Figure 4). Generally, the first principal component is mostly sufficient to distinguish HC and LC treatments while the second component mainly reveals the difference of Δeda and all other strains.

Next, we aimed to analyze how far specific metabolites are determining the separation of genotypes and CO₂ treatments in the PCA shown in Figure 4. The accompanying PCA loading plot (Figure 5) displays, which of the measured metabolites has the highest influence on defining the two principal components. The loading plot points out that the metabolites 3PGA and 2PG show the highest contribution to the first component and thus might be mainly responsible for the clear separation of most HC from LC samples in the score plot. The low angles between the respective vectors indicate a high positive correlation of these metabolites in the dataset. Vectors for proline, arginine, and glutamine point at the direction of the observed Δeda LC cluster in the score plot and therefore might represent metabolites responsible for the separation of these data. Their almost 180° angles toward glutamic acid and succinic acid vectors suggest a strong negative correlation between their metabolic behavior during the HC-LC-HC shift (Figure 5). Hence, these metabolites deserved closer inspections, since their changes could be related

to alterations in carbon flux or nitrogen assimilation due to the different mutations.

Specific Changes of the Metabolome in Strains During HC-LC-HC Shifts

The previous PCA indicates that specific metabolites show significant differences in their response to different Ci conditions in the mutants compared to WT. Marked changes were observed for the RubisCO reaction products 3PGA and 2PG (Figure 6). 3PGA increased approximately 4-fold after the shift of HC-acclimated cells to LC, while the 3PGA contents returned to lowered levels during the subsequent HC period. The 3PGA increase under lowered CO₂ availability rather points at a diminished metabolism of this compound in the CBB cycle than at an increased RubisCO carboxylation activity. Obviously, readjusting the CBB cycle activity needs more time during LC acclimation. Basically, similar patterns were observed in the different mutant strains, especially in the mutant Δzwf . However, the extent of changes differed in the other mutants. 3PGA became more strongly accumulated in the mutants Δpfk and Δgnd . In the mutant Δgnd it declined immediately to the initial HC levels when cells were again shifted to HC (Figure 6). Compared to all other strains, the mutant Δeda showed the smallest increase of 3PGA in LC-shifted cells. Similar observations were made of the oxygenase reaction product 2PG, which, however, showed a higher stimulation in LC-shifted cells compared to the initial HC level that indicates the expected higher stimulation of the oxygenation than the carboxylation activity of RubisCO under this condition. Again, the mutant Δeda showed a significantly smaller increase than WT, while all other mutants have the tendency to increase 2PG to a higher extent than WT. In all strains, the 2PG level returned immediately to the low, initial HC level after the retransfer into HC (Figure 6).

Some organic acids, especially intermediates of the TCA cycle showed a different response in the mutants compared to WT as well under different Ci conditions. Citric acid is almost without changes in WT and mutants Δpfk and Δzwf . However, its content decreased 24 h after LC shift in the mutants Δgnd and Δeda , thereafter it returned stepwise to the initial level in the subsequent HC period (Figure 7). Succinate was stepwise accumulated in the WT after LC shift, but it remained unchanged under different Ci regimes in mutant Δeda . The mutants Δzwf and Δgnd accumulated more succinate under HC conditions and do not show the increase under LC conditions (Figure 7). In contrast to succinate, no large deviations were seen in the pattern of malate. Its level declined in most strains 2–3 h after LC shift, but this drop was not observed for the mutant Δgnd (Figure 7).

Finally, some amino acids showed marked deviations between WT and mutants under the different Ci conditions. In this regard it is remarkable to see the very pronounced accumulation of proline in the mutant Δeda (Figure 8). Its content is about 10 times higher in HC-cultivated cells of this mutant cells compared to all other strains and increased to 40-fold higher levels in LC-shifted cells. The LC-stimulated accumulation of proline was also seen in the other strains, however, to a much smaller extent. Proline is a well-known regulatory metabolite that maintains

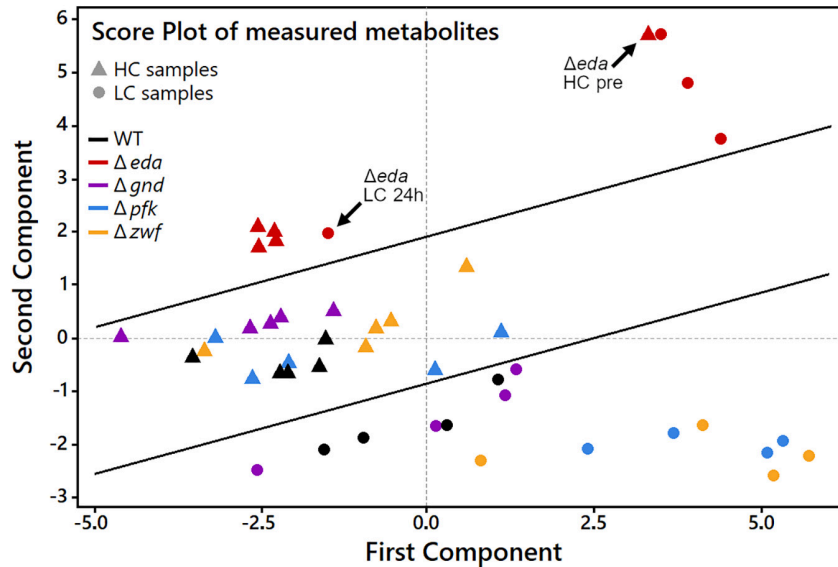


FIGURE 4 | Principal component analysis (PCA) score plot to analyze patterns in samples by genotype and CO₂ treatment during HC-LC-HC shifts. Every data point represents one sample as a combination of genotype and one of the nine sampling time points during the HC-LC-HC shift experiment. HC and LC samples, regardless of sampling time, are represented only by the same respective genotype symbol for clarity reasons. Inserted black lines mark the separation of LC, HC and Δeda samples, respectively.

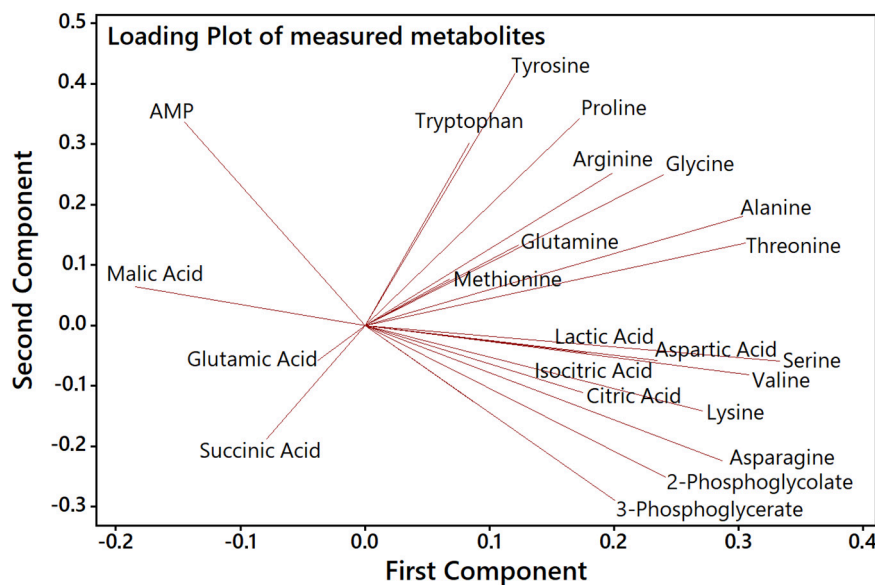
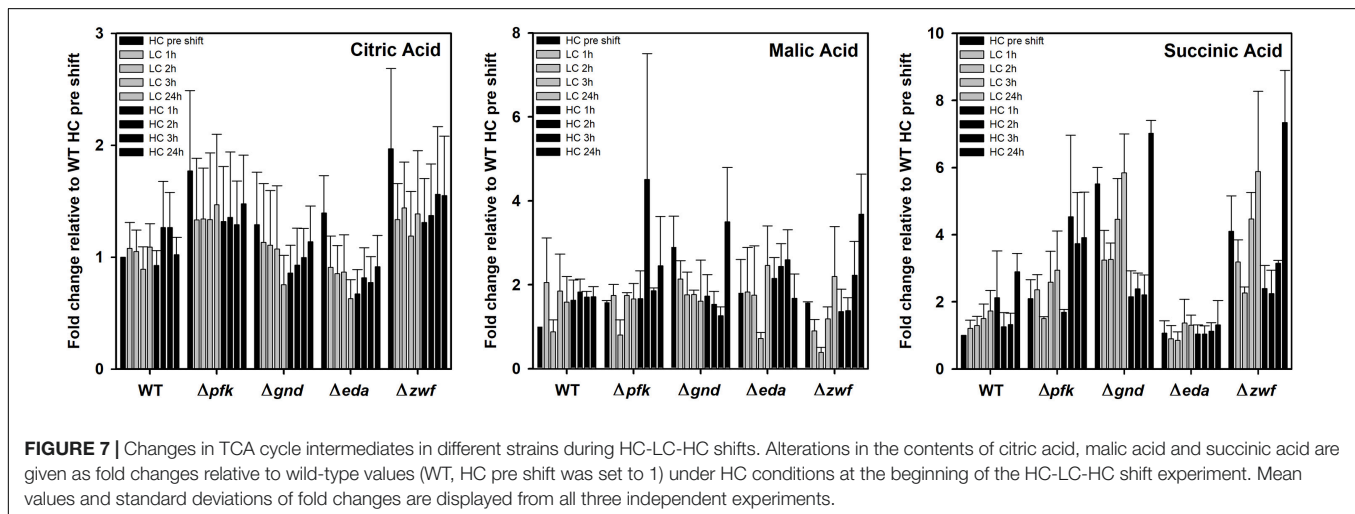
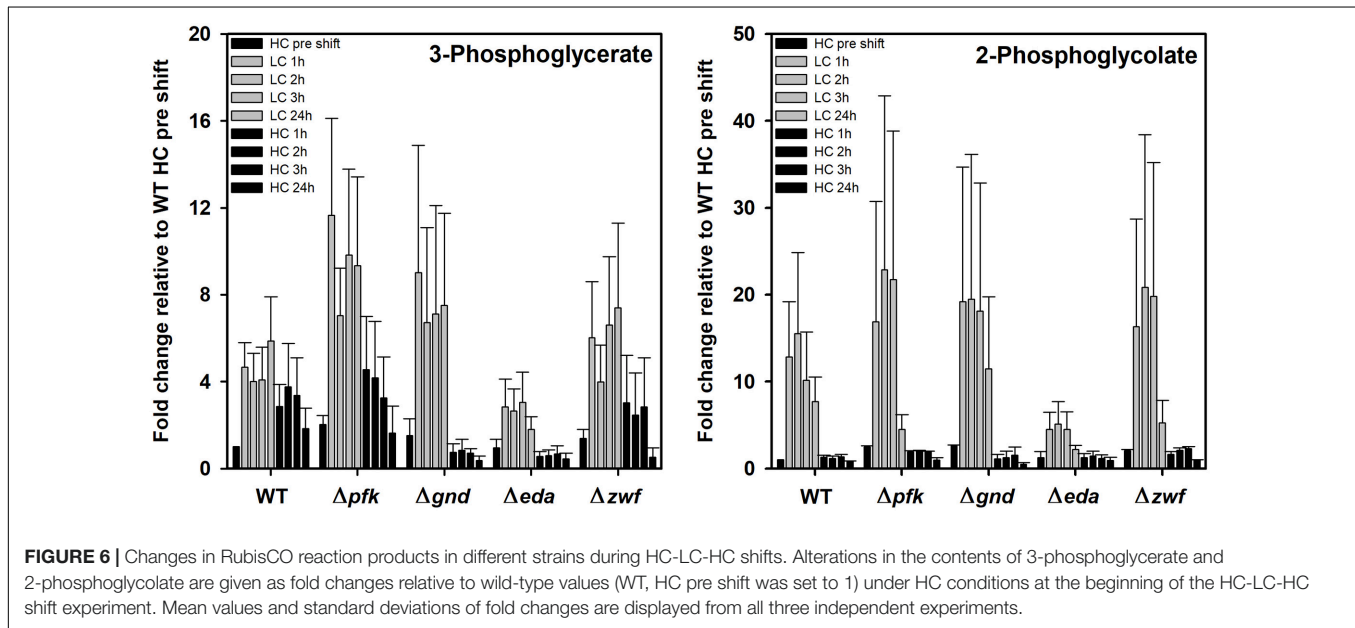


FIGURE 5 | PCA loading plot to analyze the influence of specific metabolites on the first and second component. Each quantified metabolite is represented by a vector, whereby length, angle and direction indicate the contribution of that metabolite to the first and second component.

redox balances via the modulation of NADPH levels in bacteria, animals and plants during many stress conditions (Fichman et al., 2015; Zhang and Becker, 2015). Its reversible biosynthesis from glutamate requires two NADPH. Hence, proline synthesis and oxidation can either protect cells from redox stress due to the overproduction of reactive oxygen species (ROS) or alternatively support ROS formation to induce programmed cell death. The accumulation of proline in Δeda thus points at much larger

perturbations in NADPH levels in this mutant when shifted from HC into LC conditions. After the subsequent HC shift, proline returned to the initial levels in all strains.

In addition to proline, arginine accumulates also to 4-fold higher levels in mutant Δeda compared to WT. Arginine increased in all strains after the LC shift, where the second highest stimulation was observed in mutant Δgnd that reached almost the levels of Δeda (Figure 8). Glutamate represents by far the



most abundant amino acid in *Synechocystis* and serves as amino donor in most transaminase reactions. Together with glutamine, it is part of the GS/GOGAT cycle for ammonia assimilation in cyanobacteria as in plants. Higher glutamate amounts than in WT were observed in the mutants Δpfk , Δgnd , and Δzwf , but not in Δeda in the HC-acclimated cells prior to the shifts (**Figure 8**). Its amount decreased in all cases during the first hours in LC-shifted cells, but returned to the initial level after 24 h LC with the exception of mutant Δgnd . In the latter mutant the initial glutamate level became only restored after 24 h growth under HC conditions. Again, only in the case of Δgnd stronger deviations were found for glutamine compared to WT (**Figure 8**). This mutant accumulated less glutamine and showed the strongest decline in its content after the LC shift. It is also interesting to note that glutamine became strongly re-accumulated in cells of the mutants Δpfk and Δzwf after the subsequent HC shift. To support the understanding of the

metabolic changes, selected metabolites are displayed in the context of entire carbon metabolism for the initial HC and end of the subsequent LC or HC periods in **Figure 9**.

DISCUSSION

Glycogen is the main carbon storage in cyanobacteria, which is synthesized via photosynthesis and gluconeogenesis under Ci excess conditions during the day and becomes consumed via the OPP pathway and respiration to produce carbon precursors and energy at night. In addition to the diurnal glycogen cycle, it has been shown that glycogen levels are also fluctuating in *Synechocystis* in constant light, when carbon or nitrogen availability is changing (e.g., Eisenhut et al., 2007; Doello et al., 2018). In contrast to other glycolytic routes, intermediates of the ED pathway are not overlapping with the CBB cycle and pyruvate

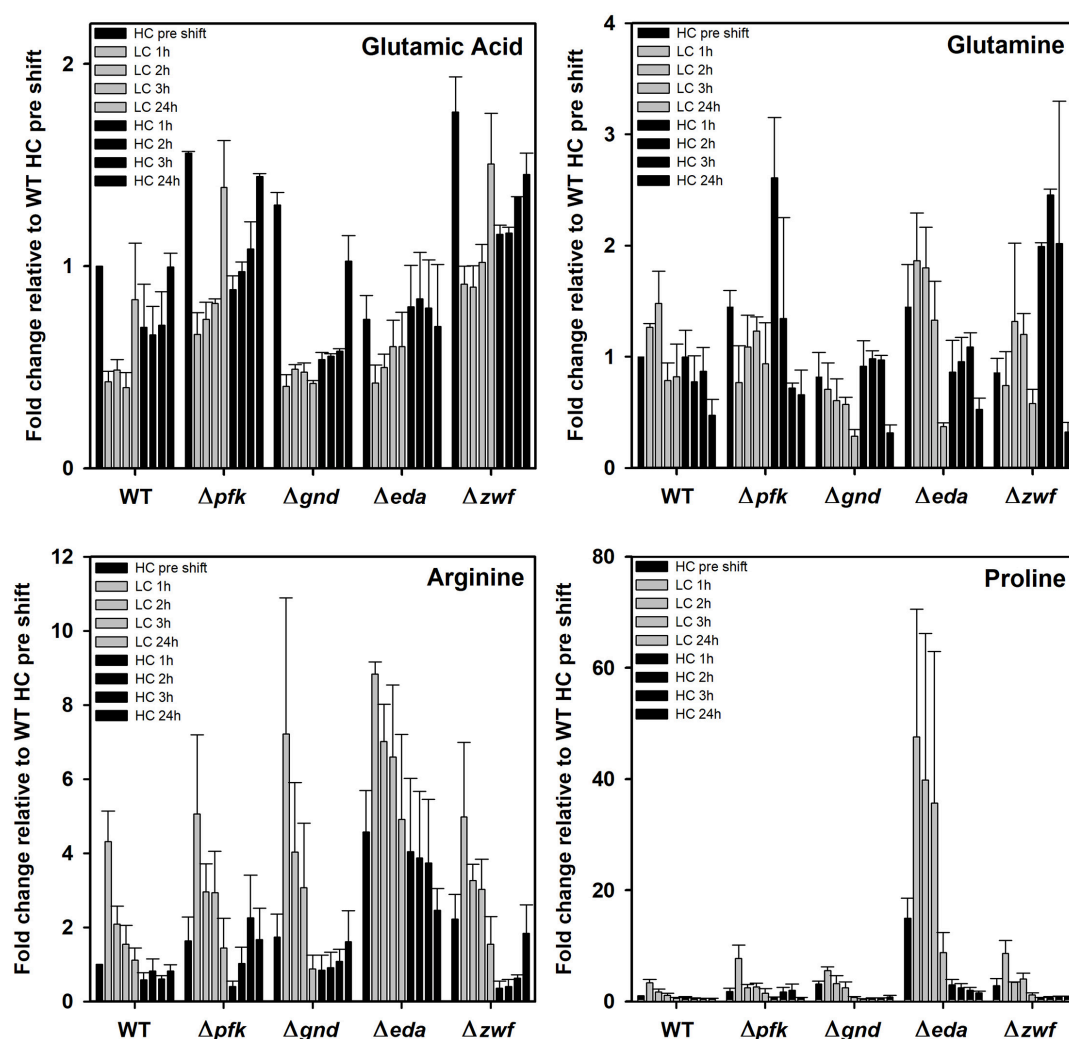


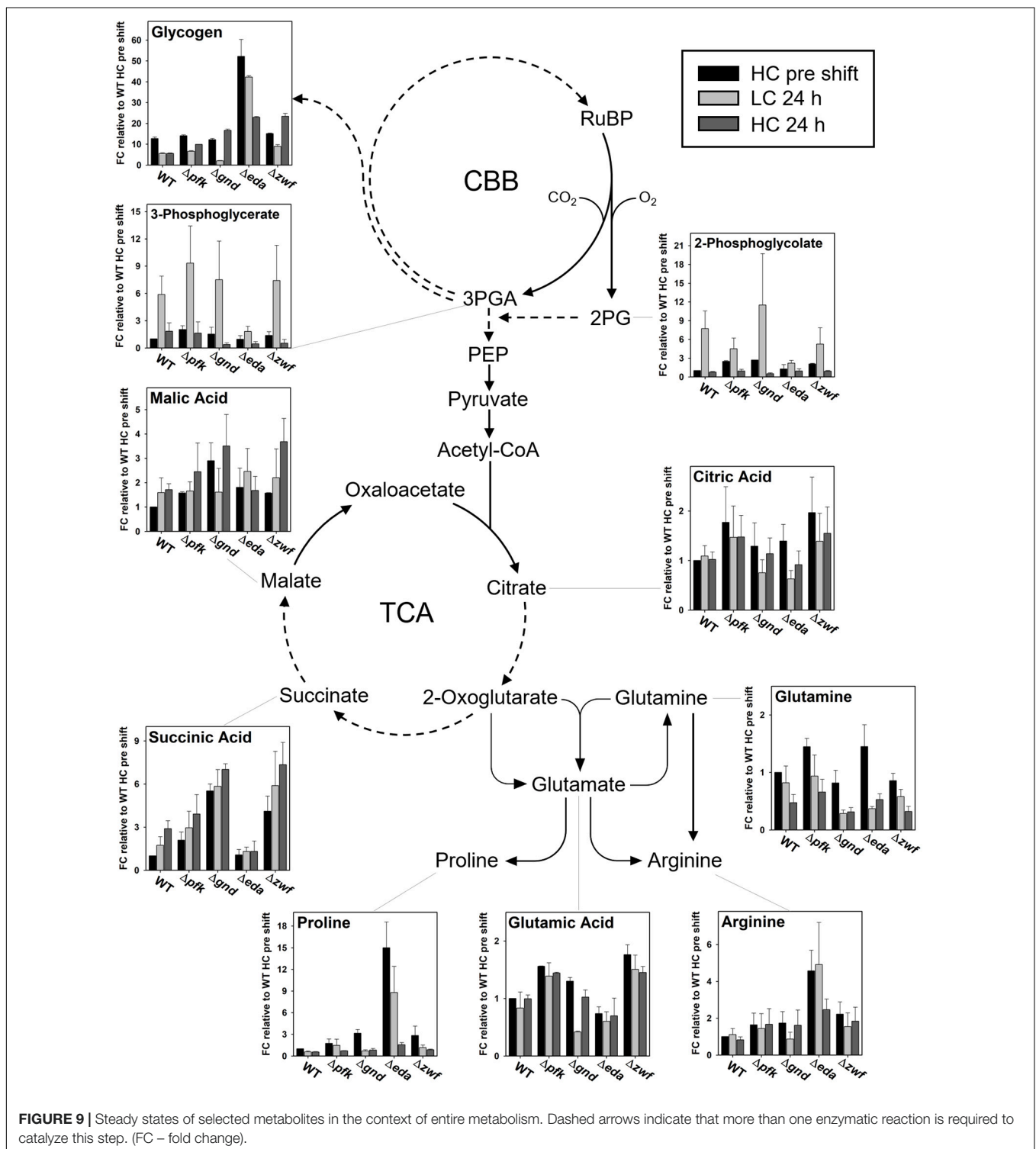
FIGURE 8 | Changes in selected amino acids in different strains during HC-LC-HC shifts. Alterations in the contents of glutamic acid, glutamine, arginine, and proline are given as fold changes relative to wild-type values (WT, HC pre shift was set to 1) under HC conditions at the beginning of the HC-LC-HC shift experiment. Mean values and standard deviations of fold changes are displayed from all three independent experiments.

can be provided directly without the need for lower glycolysis (Chen et al., 2016). This makes the ED pathway particularly suitable for carbon catabolism in the light without interfering with photosynthetic CO_2 fixation. The results from the present study point at a major, but most likely regulatory contribution of the ED shunt for the mobilization of glycogen reserves in the light, which contributes to the rapid acclimation to fluctuating CO_2 conditions. This main conclusion is based on the clearly elevated glycogen pool and its delayed mobilization upon shift to LC in combination with dramatically elevated levels of proline in the Δeda mutant. Similar observations, i.e., a decelerated glycogen consumption in the presence of an active CBB cycle were made, when the *Synechocystis* mutant Δeda was grown at constant LC conditions in the light (Makowka et al., 2020).

Obviously, the presence of Eda has a great impact on the entire carbon and associated nitrogen metabolism and supports a rapid reactivation of growth after periods of LC when HC

became newly available. This finding was not expected, because the strong decrease in glycogen pools after long-term shifts into LC conditions has been interpreted such that in the presence of limited C_i and thereby lowered CBB cycle activity, the breakdown of the organic carbon reserve glycogen is used to replenish the metabolism of *Synechocystis* at least in the transient phase before the CCM is fully activated (Eisenhut et al., 2007). However, the view that CBB cycle and glucose catabolic routes operate separately in light-exposed cyanobacteria has been modified during the last years.

Flux analyses and physiological studies in *Synechocystis* under photomixotrophic and photoautotrophic conditions revealed that external glucose or glycogen-derived glucose are metabolized in the light by entering the CBB cycle. For this purpose, glucose catabolic pathways do not operate at their full length as in darkness but instead form glycolytic shunts that enter and fine-tune the CBB cycle (Young et al., 2011; Nakajima et al., 2014;



Sharkey and Weise, 2015; Matsuda et al., 2017; Shinde et al., 2019; Makowka et al., 2020). High fluxes under photomixotrophic steady state conditions were reported for the OPP shunt, whereas fluxes via the ED shunt were either not analyzed or minor (Nakajima et al., 2014; Wan et al., 2017). It has recently been shown that the OPP and the ED shunts contribute to the

pools of the CBB cycle, when cells are shifted from darkness to light and glycogen is utilized to replenish the CBB cycle for a quick start of photosynthesis (Makowka et al., 2020). Similar observations were made in the cyanobacterium *Synechococcus elongatus* 7942 during dark-light shifts. Glycogen catabolism via the OPP shunt was shown to replenish intermediates of the CBB

cycle and to activate CBB cycle enzymes, probably by modulation of NADPH levels (Shinde et al., 2019). Shifts between darkness and light or HC and LC conditions are alike in that sense that redox pools and the CBB cycle get perturbed and require fine-tuning. One advantage of possessing several glycolytic pathways is the potential to modulate NADPH and ATP levels distinctly dependent on the route chosen (discussed in more detail by Makowka et al., 2020).

Basically, carbon from glycogen breakdown can enter the CBB cycle either via the OPP or glycolytic shunts. By deletion of the ED shunt, replenishment of the CBB cycle via the OPP shunt is likely promoted. As a consequence, CO₂ which is released by Gnd in the OPP shunt might reach elevated levels in Δeda . Thus, this elevated decarboxylation activity should reduce photorespiration and is consistent with the reduced amount of 2PG that was observed in Δeda (see **Figure 6**). In addition, NADPH levels could increase in Δeda , because 6 NADPH are formed in the case of the OPP shunt, if three molecules of glucose 6-phosphate regenerate three molecules of ribose 5-phosphate. The dramatically enhanced level of proline (and to a lesser extent also arginine, see **Figure 8**) in Δeda might be a response to these elevated amounts of NADPH. Proline synthesis from glutamate requires two NADPH whereas synthesis of arginine from glutamate requires one NADPH. Proline is produced as response to stress in several organisms to maintain osmotic equilibrium and particularly redox balance, thereby mitigating the effects of ROS by the modulation of NADPH levels (Fichman et al., 2015; Zhang and Becker, 2015). Along this line, we propose that the over-accumulation of proline, a substance compatible with cellular metabolism in high concentrations, might function to consume excess amounts of NADPH accumulating in Δeda under LC conditions. An earlier metabolome study that quantified several sugar phosphates during acclimation from HC to LC conditions found elevated levels of 6-phosphogluconate in the WT, which points to the involvement of OPP and/or ED shunt for LC acclimation (Eisenhut et al., 2008b). Shifts from HC to LC were furthermore accompanied by increased 2PGA/3PGA ratios, which was assumed to result from increased export of 3PGA from the CBB cycle into lower glycolysis at the phosphoglycerate mutase step (Eisenhut et al., 2008b; Huege et al., 2011; Jablonsky et al., 2016; Orf et al., 2016). This finding is again well in line with the view that glucose from glycogen supports the replenishment of the CBB cycle during HC to LC shifts that allows for an increased export of 3PGA from the CBB cycle in the direction of the TCA cycle.

The notion that the observed metabolic alterations of Δeda are rather based on regulatory aspects instead of missing fluxes is further supported by the fact that we observed much fewer alterations between *Synechocystis* WT and the mutant Δzwf than with Δeda under the different Ci conditions. The defect of Δzwf is upstream of the divergence of the OPP pathway and the ED glycolytic route. In the previous metabolic scenario presented by Chen et al. (2016) a second route from glucose to 6-phosphogluconate was indicated, which circumvents glucose 6-phosphate and thus Zwf. Preliminary attempts to verify this route failed, therefore, from these observations we can rule out that a such route exists in *Synechocystis* (unpublished results of team

Gutekunst). In the absence of such a bypass, the entire carbon flux from glycogen into the OPP and the ED pathways needs to include Zwf. Because we observed comparable changes in the mutant Δzwf and the mutant Δgnd , the latter being specifically blocked in the OPP pathway but not in the glycolytic ED route, we conclude that the observed changes in the mutant Δeda are rather based on regulatory effects than changed carbon flux due to the absence of Eda. It has been also shown that in Δzwf the replenishment of the CBB cycle via glycogen involves another glycolytic shunt than the ED pathway, namely the PGI shunt (for details see Makowka et al., 2020).

Collectively, our data show that deletion of *eda* deteriorates acclimation to fluctuating Ci conditions and furthermore has dramatic effects on metabolic profiles. The most prominent changes in Δeda in comparison to the WT are enhanced glycogen levels under HC conditions, slowed glycogen consumption under LC conditions, retarded reactivation of growth upon shift to HC, and a dramatic accumulation of proline. Because proline is a well-known metabolite that accumulates under several stress conditions, we assume that the absence of Eda results in imbalances of redox homeostasis. In line with earlier observations (Doello et al., 2018; Makowka et al., 2020) our study provides new evidence that Eda is of importance under fluctuating conditions rather than at metabolic steady states by fine-tuning the central carbon metabolism on a regulatory level.

DATA AVAILABILITY STATEMENT

The original contributions presented in the study are included in the article/**Supplementary Material**, further inquiries can be directed to the corresponding author.

AUTHOR CONTRIBUTIONS

MH and KG designed the work and wrote the manuscript with input from all co-authors. SL, AM, and KM carried out most of the experiments and evaluated the data together with MH and KG. All authors contributed to the article and approved the submitted version.

FUNDING

This study was performed in the research consortium SCyCode (FOR2816), which is supported by grants of the German Research Foundation (DFG; Gu1522/2-1, Gu1522/5-1, and HA2002/23-1). The open access publication costs were covered by funds of the University of Rostock.

SUPPLEMENTARY MATERIAL

The Supplementary Material for this article can be found online at: <https://www.frontiersin.org/articles/10.3389/fpls.2021.787943/full#supplementary-material>

REFERENCES

- Bachhar, A., and Jablonsky, J. (2020). A new insight into role of phosphoketolase pathway in *Synechocystis* sp. PCC 6803. *Sci. Rep.* 10:22018. doi: 10.1038/s41598-020-78475-z
- Chen, X., Schreiber, K., Appel, J., Makowka, A., Fähnrich, B., Roettger, M., et al. (2016). The Entner-Doudoroff pathway is an overlooked glycolytic route in cyanobacteria and plants. *Proc. Natl. Acad. Sci. U.S.A.* 113, 5441–5446. doi: 10.1073/pnas.1521916113
- Chuang, D. S., and Liao, J. C. (2021). Role of cyanobacterial phosphoketolase in energy regulation and glucose secretion under dark anaerobic and osmotic stress conditions. *Metab. Eng.* 65, 255–262. doi: 10.1016/j.ymben.2020.12.004
- Doello, S., Klotz, A., Makowka, A., Gutekunst, K., and Forchhammer, K. (2018). A specific glycogen mobilization strategy enables awakening of dormant cyanobacteria from chlorosis. *Plant Physiol.* 177, 594–603. doi: 10.1104/pp.18.00297
- Eisenhut, M., Ruth, W., Haimovich, M., Bauwe, H., Kaplan, A., and Hagemann, M. (2008a). The photorespiratory glycolate metabolism is essential for cyanobacteria and might have been conveyed endosymbiotically to plants. *Proc. Natl. Acad. Sci. U.S.A.* 105, 17199–17204. doi: 10.1073/pnas.0807043105
- Eisenhut, M., Huege, J., Schwarz, D., Bauwe, H., Kopka, J., and Hagemann, M. (2008b). Metabolome phenotyping of inorganic carbon limitation in cells of the wild type and photorespiratory mutants of the cyanobacterium *Synechocystis* sp. strain PCC 6803. *Plant Physiol.* 148, 2109–2120. doi: 10.1104/pp.108.129403
- Eisenhut, M., von Wobeser, E. A., Jonas, L., Schubert, H., Ibelings, B. W., Bauwe, H., et al. (2007). Long-term response towards inorganic carbon limitation in wild type and glycolate turnover mutants of the cyanobacterium *Synechocystis* sp. strain PCC 6803. *Plant Physiol.* 144, 1946–1959. doi: 10.1104/pp.107.103341
- Fichman, Y., Gerdes, S. Y., Kovacs, H., Szabados, L., Zilberstein, A., and Csonka, L. N. (2015). Evolution of proline biosynthesis: enzymology, bioinformatics, genetics, and transcriptional regulation. *Biol. Rev.* 90, 1065–1099. doi: 10.1111/brv.12146
- Flügel, F., Timm, S., Arrivault, S., Florian, A., Stitt, M., Fernie, A. R., et al. (2017). The photorespiratory metabolite 2-phosphoglycolate regulates photosynthesis and starch accumulation in *Arabidopsis*. *Plant Cell* 29, 2537–2551. doi: 10.1105/tpc.17.00256
- Gründel, M., Scheunemann, R., Lockau, W., and Zilliges, Y. (2012). Impaired glycogen synthesis causes metabolic overflow reactions and affects stress responses in the cyanobacterium *Synechocystis* sp. PCC 6803. *Microbiology* 158, 3032–3043. doi: 10.1099/mic.0.062950-0
- Hagemann, M., and Hess, W. R. (2018). Systems and synthetic biology for the biotechnological application of cyanobacteria. *Curr. Opin. Biotechnol.* 49, 94–99. doi: 10.1016/j.copbio.2017.07.008
- Hagemann, M., Song, S., and Brouwer, E. M. (2021). “Chapter 1-Inorganic carbon assimilation in cyanobacteria: mechanisms, regulation, and engineering,” in *Cyanobacteria Biotechnology, Wiley-Blackwell Biotechnology Series*, eds P. Hudson, S. Y. Lee, and J. Nielsen (Hoboken, NJ: Wiley-Blackwell), 1–31. doi: 10.1002/9783527824908.ch1
- Hohmann-Marriott, M. F., and Blankenship, R. E. (2011). Evolution of photosynthesis. *Ann. Rev. Plant Biol.* 62, 515–548. doi: 10.1146/annurev-arplant-042110-103811
- Huege, J., Goetze, J., Schwarz, D., Bauwe, H., Hagemann, M., and Kopka, J. (2011). Modulation of the major paths of carbon in photorespiratory mutants of *Synechocystis*. *PLoS One* 6:e16278. doi: 10.1371/journal.pone.0016278
- Jablonsky, J., Papacek, S., and Hagemann, M. (2016). Different strategies of metabolic regulation in cyanobacteria: from transcriptional to biochemical control. *Sci. Rep.* 6:33024. doi: 10.1038/srep33024
- Kaplan, A., Hagemann, M., Bauwe, H., Kahlon, S., and Ogawa, T. (2008). “Carbon acquisition by cyanobacteria: mechanisms, comparative genomics and evolution,” in *The Cyanobacteria Molecular Biology, Genomics and Evolution*, eds A. Herrero and E. Flores (Bodmin: Caister Academic Press), 305–334.
- Klähn, S., Orf, I., Schwarz, D., Matthiessen, J. K. F., Kopka, J., Hess, W. R., et al. (2015). Integrated transcriptomic and metabolomic characterization of the low-carbon response using an ndhR mutant of *Synechocystis* sp. PCC 6803. *Plant Physiol.* 169, 1540–1556. doi: 10.1104/pp.114.254045
- Makowka, A., Nichelmann, L., Schulze, D., Spengler, K., Wittmann, C., Forchhammer, K., et al. (2020). Glycolytic shunts replenish the Calvin–Benson–Bassham cycle as anaplerotic reactions in cyanobacteria. *Mol. Plant* 13, 471–482. doi: 10.1016/j.molp.2020.02.002
- Matsuda, F., Yoshikawa, K., Nakajima, T., Toya, Y., and Shimizu, H. (2017). Metabolic flux analysis of the *Synechocystis* sp. PCC 6803 Δ nrtABCD mutant reveals a mechanism for metabolic adaptation to nitrogen-limited conditions. *Plant Cell Physiol.* 58, 537–545. doi: 10.1093/pcp/pcx047
- Nakajima, T., Kajihata, S., Yoshikawa, K., Matsuda, F., Furusawa, C., Hirasawa, T., et al. (2014). Integrated metabolic flux and omics analysis of *Synechocystis* sp. PCC 6803 under mixotrophic and photoheterotrophic conditions. *Plant Cell Physiol.* 55, 1605–1612. doi: 10.1093/pcp/pcu091
- Orf, I., Timm, S., Bauwe, H., Fernie, A. R., Hagemann, M., Kopka, J., et al. (2016). Can cyanobacteria serve as a model of plant photorespiration?—A comparative analysis of metabolite profiles. *J. Exp. Bot.* 67, 2941–2952. doi: 10.1093/jxb/erw068
- Orthwein, T., Scholl, J., Spät, P., Lucius, S., Koch, M., Macek, B., et al. (2021). The novel PII-interactor PirC identifies phosphoglycerate mutase as key control point of carbon storage metabolism in cyanobacteria. *Proc. Natl. Acad. Sci. U.S.A.* 118:e2019988118. doi: 10.1073/pnas.2019988118
- Pelroy, R. A., Rippka, R., and Stanier, R. Y. (1972). The metabolism of glucose by unicellular blue-green algae. *Arch. Mikrobiol.* 87, 303–322. doi: 10.1007/BF00409131
- Rippka, R., Deruelles, J., Waterbury, J. B., Herdman, M., and Stanier, R. Y. (1979). Generic assignments, strain histories and properties of pure cultures of cyanobacteria. *J. Gen. Microbiol.* 111, 1–16. doi: 10.1099/00221287-111-1-1
- Schwarz, D., Nodop, A., Hüge, J., Purfürst, S., Forchhammer, K., Michel, K.-P., et al. (2011). Metabolic and transcriptomic phenotyping of inorganic carbon acclimation in the cyanobacterium *Synechococcus elongatus* PCC 7942. *Plant Physiol.* 155, 1640–1655. doi: 10.1104/pp.110.170225
- Sharkey, T. D., and Weise, S. E. (2015). The glucose 6-phosphate shunt around the Calvin–Benson cycle. *J. Exp. Bot.* 67, 4067–4077. doi: 10.1093/jxb/erv484
- Shinde, S., Zhang, X., Singapuri, S. P., Kalra, I., Liu, X., Morgan-Kiss, R. M., et al. (2019). Glycogen metabolism supports photosynthesis start through the oxidative pentose phosphate pathway in cyanobacteria. *Plant Phys.* 182, 507–517. doi: 10.1104/pp.19.01184
- Spät, P., Barske, T., Mašek, B., and Hagemann, M. (2021). Alterations in the CO₂ availability induce alterations in the phospho-proteome of the cyanobacterium *Synechocystis* sp. PCC 6803. *New Phytol.* 231, 1123–1137. doi: 10.1111/nph.17423
- Tcherkez, G. G. B., Farquhar, G. D., and Andrews, T. J. (2006). Despite slow catalysis and confused substrate specificity, all ribulose biphosphate carboxylases may be nearly perfectly optimized. *Proc. Natl. Acad. Sci. U.S.A.* 103, 7246–7251. doi: 10.1073/pnas.060605103
- Wan, N., DeLorenzo, D. M., He, L., You, L., Immethun, C. M., Wang, G., et al. (2017). Cyanobacterial carbon metabolism: fluxome plasticity and oxygen dependence. *Biotech. Bioeng.* 114, 1593–1602. doi: 10.1002/bit.26287
- Young, J. D., Shastri, A. A., Stephanopoulos, G., and Morgan, J. A. (2011). Mapping photoautotrophic metabolism with isotopically nonstationary ¹³C flux analysis. *Met. Engin.* 13, 656–665. doi: 10.1016/j.ymben.2011.08.002
- Zhang, L., and Becker, D. F. (2015). Connecting proline metabolism and signaling pathways in plant senescence. *Front. Plant Sci.* 6:552. doi: 10.3389/fpls.2015.00552

Conflict of Interest: The authors declare that the research was conducted in the absence of any commercial or financial relationships that could be construed as a potential conflict of interest.

Publisher’s Note: All claims expressed in this article are solely those of the authors and do not necessarily represent those of their affiliated organizations, or those of the publisher, the editors and the reviewers. Any product that may be evaluated in this article, or claim that may be made by its manufacturer, is not guaranteed or endorsed by the publisher.

Copyright © 2021 Lucius, Makowka, Michl, Gutekunst and Hagemann. This is an open-access article distributed under the terms of the Creative Commons Attribution License (CC BY). The use, distribution or reproduction in other forums is permitted, provided the original author(s) and the copyright owner(s) are credited and that the original publication in this journal is cited, in accordance with accepted academic practice. No use, distribution or reproduction is permitted which does not comply with these terms.

Supplementary data, Table S1 for the manuscript

The Entner-Doudoroff pathway contributes to glycogen breakdown during high to low CO₂ shifts in the cyanobacterium *Synechocystis* sp. PCC 6803

Stefan Lucius¹, Alexander Makowka², Klaudia Michl¹, Kirstin Gutekunst^{2,3}, Martin Hagemann^{1,4}

1 - Institute of Biosciences, Department of Plant Physiology, University of Rostock, D-18059 Rostock, Germany

2 – Department of Biology, Botanical Institute, Christian-Albrechts-University, D-24118 Kiel, Germany

3 – Department of Molecular Plant Physiology, Bioenergetics in Photoautotrophs, University of Kassel, D-34132 Kassel, Germany

4 – Interdisciplinary Faculty, Department Life, Light and Matter, University of Rostock, D-18059 Rostock, Germany

Supplementary Table S1: Metabolite LC-MS data as fold changes related to respective WT HC pre-shift (set to 1) data (n = 3). Significant differences (Student's t test $p \leq 0.05$) of mutant data relative to WT data of the respective sampling points are marked in red.

metabolite	strain	HC pre	Std Err	LC 1h	Std Err	LC 2h	Std Err	LC 3h	Std Err	LC 24h	Std Err	HC 1h	Std Err	HC 2h	Std Err	HC 3h	Std Err	HC 24h	Std Err
AMP	WT	1.000	0.000	0.756	0.021	0.751	0.045	0.605	0.080	0.862	0.110	0.821	0.173	0.838	0.095	0.916	0.156	1.128	0.190
	Δprk	1.008	0.725	0.652	0.433	0.614	0.404	0.636	0.457	0.781	0.520	0.751	0.519	0.786	0.613	0.944	0.655	1.124	0.727
	Δgnd	1.016	0.698	0.651	0.470	0.601	0.402	0.696	0.545	0.608	0.421	0.759	0.564	0.901	0.683	0.941	0.649	1.028	0.486
	Δeda	1.562	0.441	0.950	0.374	0.870	0.284	0.947	0.515	0.986	0.297	1.242	0.487	1.169	0.474	1.111	0.392	1.261	0.506
	Δzwf	1.276	0.985	0.542	0.305	0.591	0.380	0.537	0.383	0.867	0.631	0.894	0.696	0.925	0.737	1.156	0.874	1.039	0.651
	WT	1.000	0.000	1.123	0.141	0.990	0.152	0.808	0.163	0.757	0.115	0.764	0.156	0.589	0.100	0.620	0.112	0.771	0.222
Alanine	Δprk	1.254	0.234	1.320	0.211	1.741	0.546	1.728	0.556	0.949	0.015	0.663	0.195	0.449	0.013	0.361	0.156	0.675	0.259
	Δgnd	1.026	0.300	1.136	0.013	1.036	0.018	1.013	0.022	0.571	0.105	0.570	0.012	0.573	0.023	0.668	0.070	0.751	0.056
	Δeda	2.377	0.629	2.151	0.539	2.202	0.642	1.969	0.405	1.056	0.364	0.849	0.407	0.831	0.395	0.830	0.377	1.070	0.470
	Δzwf	1.301	0.317	1.838	0.518	1.865	0.515	1.855	0.518	1.376	0.114	0.684	0.147	0.712	0.124	0.836	0.190	1.006	0.227
	WT	1.000	0.000	4.313	0.822	2.082	0.486	1.538	0.512	1.108	0.337	0.585	0.185	0.817	0.335	0.607	0.092	0.822	0.168
	Δprk	1.639	0.638	5.055	2.144	2.957	0.759	2.934	1.118	1.445	0.804	0.399	0.151	1.028	0.442	2.250	1.163	1.673	0.848
Arginine	Δgnd	1.735	0.626	7.213	3.677	4.025	1.880	3.067	1.746	0.872	0.375	0.838	0.410	0.915	0.418	1.081	0.323	1.617	0.829
	Δeda	4.569	1.120	8.838	0.318	7.013	1.010	6.601	1.942	4.911	2.296	4.043	1.979	3.869	1.798	3.739	1.712	2.463	0.584
	Δzwf	2.219	0.674	4.977	2.011	3.259	0.441	3.030	0.810	1.541	0.754	0.361	0.188	0.408	0.184	0.633	0.089	1.835	0.770
	WT	1.000	0.000	3.294	0.348	2.958	0.663	2.454	0.461	2.119	0.605	0.873	0.231	0.755	0.114	0.763	0.057	0.797	0.148
	Δprk	1.688	0.031	5.850	0.744	5.916	0.116	7.154	0.317	4.114	0.880	0.592	0.148	0.949	0.125	1.091	0.080	1.153	0.134
	Δgnd	1.191	0.159	3.481	0.652	3.115	0.597	3.596	0.577	1.756	0.114	0.668	0.075	0.751	0.085	0.846	0.011	0.823	0.141
Asparagine	Δeda	1.214	0.258	1.754	0.581	2.346	0.998	3.316	0.993	1.415	0.447	0.534	0.093	0.624	0.065	0.615	0.068	0.813	0.097
	Δzwf	2.726	0.486	7.790	0.025	7.826	0.870	9.098	0.515	5.238	0.072	0.774	0.451	1.192	0.092	1.167	0.258	1.667	0.073
	WT	1.000	0.000	0.970	0.210	1.021	0.232	0.776	0.171	0.800	0.252	0.638	0.186	0.677	0.261	0.805	0.275	0.849	0.230
	Δprk	1.259	0.095	1.030	0.203	1.301	0.053	1.621	0.042	0.803	0.185	1.451	0.299	0.790	0.351	0.664	0.178	0.677	0.131
	Δgnd	0.327	0.013	0.466	0.004	0.360	0.073	0.373	0.102	0.089	0.015	0.550	0.181	0.620	0.050	0.794	0.153	0.183	0.091
	Δeda	1.008	0.417	0.757	0.014	0.928	0.104	1.054	0.275	0.446	0.072	0.469	0.048	0.564	0.029	0.635	0.071	0.523	0.065
Aspartic Acid	Δzwf	0.828	0.179	1.056	0.018	1.239	0.258	1.521	0.026	0.606	0.001	0.979	0.166	1.031	0.019	0.936	0.359	0.500	0.144
	WT	1.000	0.000	1.079	0.232	1.048	0.193	0.892	0.200	1.089	0.210	0.926	0.134	1.264	0.412	1.265	0.314	1.022	0.154
	Δprk	1.771	0.719	1.332	0.552	1.341	0.456	1.335	0.595	1.467	0.633	1.320	0.490	1.357	0.584	1.289	0.390	1.477	0.436
	Δgnd	1.289	0.469	1.131	0.527	1.105	0.490	1.072	0.566	0.752	0.263	0.857	0.250	0.928	0.331	0.997	0.260	1.137	0.320
	Δeda	1.395	0.334	0.908	0.280	0.852	0.252	0.867	0.335	0.629	0.170	0.672	0.217	0.814	0.270	0.772	0.232	0.915	0.278
	Δzwf	1.967	0.718	1.334	0.323	1.440	0.409	1.189	0.398	1.387	0.565	1.310	0.393	1.373	0.461	1.561	0.605	1.550	0.532

metabolite	strain	HC pre	Std Err	LC 1h	Std Err	LC 2h	Std Err	LC 3h	Std Err	LC 24h	Std Err	HC 1h	Std Err	HC 2h	Std Err	HC 3h	Std Err	HC 24h	Std Err
Glutamic Acid	WT	1.000	0.000	0.428	0.052	0.486	0.053	0.399	0.075	0.835	0.280	0.697	0.214	0.659	0.143	0.709	0.165	0.996	0.067
	Δpfk	1.560	0.009	0.662	0.087	0.736	0.109	0.815	0.023	1.389	0.233	0.884	0.068	0.973	0.048	1.086	0.133	1.444	0.014
	Δgnd	1.302	0.063	0.405	0.024	0.490	0.059	0.476	0.045	0.420	0.015	0.538	0.035	0.556	0.013	0.578	0.014	1.026	0.124
	Δeda	0.736	0.119	0.422	0.066	0.499	0.089	0.601	0.132	0.603	0.169	0.799	0.205	0.838	0.230	0.792	0.240	0.701	0.307
	Δzwf	1.763	0.173	0.911	0.107	0.896	0.090	1.019	0.089	1.506	0.249	1.156	0.047	1.163	0.029	1.343	0.001	1.453	0.106
	WT	1.000	0.000	1.265	0.287	1.481	0.031	0.787	0.159	0.819	0.296	0.996	0.242	0.777	0.232	0.868	0.216	0.474	0.144
Glutamine	Δpfk	1.448	0.148	0.767	0.289	1.086	0.332	1.232	0.128	0.938	0.367	2.609	0.543	1.345	0.905	0.718	0.048	0.659	0.222
	Δgnd	0.818	0.221	0.705	0.195	0.607	0.240	0.570	0.066	0.286	0.061	0.912	0.230	0.981	0.074	0.970	0.043	0.314	0.075
	Δeda	1.450	0.381	1.864	0.364	1.799	0.428	1.328	0.353	0.372	0.035	0.863	0.286	0.955	0.219	1.088	0.126	0.528	0.100
	Δzwf	0.859	0.128	0.739	0.706	1.316	0.308	1.198	0.192	0.579	0.128	1.993	0.033	2.456	0.053	2.018	1.279	0.322	0.089
	WT	1.000	0.000	1.015	0.134	0.955	0.140	0.727	0.200	0.940	0.221	0.663	0.195	0.890	0.182	0.769	0.132	0.758	0.146
	Δpfk	1.495	0.039	1.109	0.148	1.228	0.135	1.504	0.332	1.412	0.807	0.779	0.084	0.818	0.169	0.623	0.060	0.856	0.042
Glycine	Δgnd	1.075	0.148	1.106	0.327	1.017	0.323	0.726	0.178	0.482	0.076	0.652	0.040	0.659	0.100	0.683	0.010	0.682	0.113
	Δeda	1.811	0.376	1.532	0.402	1.743	0.202	1.369	0.198	1.173	0.167	1.028	0.272	1.111	0.283	1.123	0.272	1.028	0.203
	Δzwf	1.182	0.036	0.968	0.125	1.092	0.009	1.143	0.070	0.808	0.188	0.563	0.038	0.654	0.064	0.706	0.071	0.734	0.035
	WT	1.000	0.000	1.075	0.195	1.036	0.238	0.893	0.205	1.094	0.220	0.924	0.144	1.279	0.430	1.261	0.323	1.021	0.168
	Δpfk	1.737	0.733	1.312	0.490	1.323	0.578	1.321	0.612	1.453	0.665	1.304	0.516	1.337	0.609	1.265	0.418	1.458	0.485
	Δgnd	1.287	0.498	1.108	0.513	1.095	0.535	1.056	0.577	0.739	0.272	0.843	0.268	0.920	0.356	0.981	0.284	1.130	0.358
Isocitric Acid	Δeda	1.364	0.336	0.896	0.262	0.830	0.285	0.849	0.328	0.612	0.175	0.662	0.217	0.804	0.282	0.761	0.239	0.890	0.279
	Δzwf	1.970	0.780	1.326	0.447	1.434	0.358	1.176	0.436	1.363	0.593	1.285	0.416	1.346	0.487	1.555	0.647	1.551	0.592
	WT	1.000	0.000	1.391	0.096	0.820	0.183	0.942	0.119	1.079	0.134	1.403	0.425	0.938	0.178	1.042	0.126	0.474	0.131
	Δpfk	1.271	0.961	1.001	0.384	0.863	0.460	1.116	0.602	1.092	0.621	0.534	0.218	0.745	0.606	0.720	0.502	0.243	0.072
	Δgnd	0.919	0.345	1.125	0.934	1.673	0.426	1.259	0.749	1.040	0.528	0.576	0.252	1.032	0.709	0.650	0.345	0.295	0.212
	Δeda	1.100	0.151	1.032	0.217	0.972	0.272	1.127	0.481	0.853	0.135	0.644	0.209	0.622	0.197	0.522	0.154	0.475	0.187
Lactic Acid	Δzwf	1.140	0.742	0.837	0.618	1.015	0.496	1.038	0.593	0.698	0.420	0.784	0.510	0.595	0.406	1.015	0.796	0.454	0.385
	WT	1.000	0.000	1.205	0.324	1.377	0.132	0.819	0.221	1.092	0.312	0.592	0.070	0.523	0.098	0.632	0.173	0.620	0.166
	Δpfk	1.510	0.109	1.614	0.878	2.274	0.496	2.179	0.792	2.838	1.489	2.508	0.682	1.400	0.860	0.503	0.174	0.610	0.269
	Δgnd	1.054	0.004	1.217	0.618	1.435	0.229	1.201	0.555	0.807	0.446	0.604	0.097	0.580	0.341	0.565	0.367	0.288	0.100
	Δeda	1.122	0.124	1.287	0.424	1.470	0.234	1.346	0.487	0.762	0.323	0.972	0.196	0.881	0.225	0.846	0.231	0.748	0.223
	Δzwf	1.254	0.268	1.850	0.546	2.574	0.800	2.194	0.787	2.173	1.448	1.805	0.252	1.509	1.046	1.779	1.548	0.535	0.089
Malic Acid	WT	1.000	0.000	2.051	0.279	0.883	1.065	1.852	0.885	1.588	0.610	1.634	0.483	1.826	0.314	1.711	0.131	1.712	0.244
	Δpfk	1.581	0.046	1.741	0.360	0.802	0.266	1.745	0.068	1.660	0.373	1.671	0.665	4.512	2.994	1.861	0.067	2.451	1.176
	Δgnd	2.898	0.739	2.138	0.538	1.763	0.438	1.768	0.107	1.612	0.980	1.731	0.509	1.537	0.308	1.265	0.208	3.504	1.296
	Δeda	1.807	0.796	1.827	1.170	1.756	1.066	0.721	0.145	2.460	0.945	2.154	0.493	2.436	0.548	2.593	0.716	1.680	0.579
	Δzwf	1.575	0.016	0.897	0.123	0.390	0.277	1.183	0.289	2.198	1.192	1.361	0.537	1.386	0.306	2.225	0.808	3.681	0.960
	WT	1.000	0.000	0.897	0.123	0.390	0.277	1.183	0.289	2.198	1.192	1.361	0.537	1.386	0.306	2.225	0.808	3.681	0.960

metabolite	strain	HC pre	Std Err	LC 1h	Std Err	LC 2h	Std Err	LC 3h	Std Err	LC 24h	Std Err	HC 1h	Std Err	HC 2h	Std Err	HC 3h	Std Err	HC 24h	Std Err
Methionine	WT	1.000	0.000	0.468	0.090	0.419	0.128	0.474	0.306	0.534	0.325	0.601	0.216	0.713	0.201	0.742	0.246	0.859	0.284
	Δpfk	1.029	0.189	0.687	0.043	0.804	0.309	0.512	0.075	0.681	0.579	0.673	0.020	0.696	0.025	0.612	0.519	0.720	0.401
	Δgnd	1.105	0.044	0.412	0.129	0.502	0.049	0.348	0.103	0.197	0.121	0.467	0.038	0.434	0.011	0.260	0.185	0.525	0.366
	Δda	1.369	0.456	0.449	0.123	0.621	0.201	0.507	0.093	0.386	0.099	0.514	0.164	0.540	0.163	0.440	0.165	0.543	0.211
	Δzwf	1.370	0.113	0.678	0.074	1.066	0.081	0.506	0.134	0.730	0.537	0.777	0.074	0.923	0.009	0.589	0.487	0.669	0.543
	WT	1.000	0.000	0.668	1.118	4.009	1.302	4.079	1.513	5.876	2.026	2.849	1.026	3.749	2.000	3.367	1.733	1.830	0.948
3-Phospho- glycerate	Δpfk	2.027	0.420	11.649	4.461	7.041	2.180	9.830	3.956	9.334	4.090	4.546	2.452	4.170	2.598	3.242	1.896	1.625	1.248
	Δgnd	1.529	0.752	9.025	5.841	6.717	4.381	7.123	4.987	7.504	4.254	0.749	0.388	0.835	0.518	0.711	0.209	0.371	0.203
	Δda	0.963	0.397	2.845	1.281	2.646	1.018	3.039	1.409	1.810	0.582	0.553	0.228	0.592	0.269	0.676	0.367	0.452	0.256
	Δzwf	1.381	0.415	6.024	2.570	3.983	1.705	6.598	3.160	7.404	3.892	3.027	2.186	2.458	1.948	2.836	2.257	0.524	0.422
	WT	1.000	0.000	12.852	6.329	15.519	9.308	10.170	5.556	7.721	2.828	1.295	0.222	1.184	0.283	1.349	0.272	0.779	0.107
	Δpfk	2.477	0.124	16.894	13.856	22.863	20.010	21.737	17.101	4.484	1.735	1.925	0.122	2.036	0.086	2.002	0.009	0.951	0.281
2-Phospho- glycolate	Δgnd	2.681	0.018	19.220	15.443	19.493	16.672	18.130	14.736	11.491	8.246	1.143	0.482	1.256	0.756	1.552	0.935	0.519	0.146
	Δda	1.272	0.713	4.482	2.002	5.105	2.614	4.489	2.047	2.199	0.451	1.262	0.448	1.442	0.571	1.169	0.416	0.929	0.371
	Δzwf	2.073	0.104	16.318	12.411	20.864	17.562	19.796	15.396	5.249	2.618	1.633	0.349	2.129	0.275	2.299	0.199	0.918	0.101
	WT	1.000	0.000	3.399	0.555	1.719	0.473	1.103	0.389	0.571	0.132	0.616	0.251	0.545	0.130	0.524	0.026	0.552	0.057
	Δpfk	1.741	0.625	7.760	2.407	2.429	0.653	2.620	0.663	1.466	0.857	0.626	0.144	1.702	0.814	2.050	1.105	0.721	0.042
	Δgnd	3.146	0.522	5.558	0.656	3.221	1.387	2.468	1.014	0.700	0.179	0.395	0.101	0.462	0.164	0.567	0.065	0.832	0.231
Proline	Δda	14.984	3.577	47.585	22.992	39.858	26.350	35.662	27.309	8.794	3.638	3.009	0.951	2.456	0.733	2.011	0.529	1.559	0.303
	Δzwf	2.835	1.319	8.608	2.405	3.466	0.067	4.076	1.041	1.176	0.352	0.574	0.181	0.656	0.216	0.842	0.100	0.878	0.078
	WT	1.000	0.000	2.104	0.749	1.601	0.389	1.149	0.236	1.534	0.421	1.738	0.983	0.886	0.123	0.856	0.141	0.753	0.221
	Δpfk	1.561	0.091	2.626	0.062	3.250	0.731	3.292	0.482	2.600	0.644	1.204	0.310	0.953	0.008	0.846	0.228	0.739	0.125
	Δgnd	1.478	0.180	1.544	0.041	1.538	0.086	1.359	0.057	0.962	0.051	0.836	0.123	0.779	0.026	0.852	0.137	0.526	0.124
	Δda	2.578	0.842	1.920	0.530	2.039	0.590	3.345	1.244	1.040	0.226	0.742	0.148	0.791	0.153	0.671	0.020	1.307	0.651
Serine	Δzwf	1.154	0.213	2.825	0.511	3.212	0.268	3.533	0.593	2.141	0.041	0.959	0.226	1.017	0.139	1.087	0.053	0.833	0.019
	WT	1.000	0.000	1.211	0.241	1.299	0.271	1.502	0.433	1.730	0.610	2.125	1.391	1.263	0.419	1.328	0.335	2.896	0.552
	Δpfk	2.095	0.563	2.361	0.451	1.502	0.056	2.590	0.918	2.949	1.158	1.696	0.083	4.535	2.436	3.737	1.527	3.910	1.358
	Δgnd	5.519	0.489	3.246	0.888	3.263	0.495	4.459	1.214	5.842	1.161	2.154	0.769	2.387	0.476	2.206	0.593	7.019	0.388
	Δda	1.067	0.373	0.895	0.402	0.852	0.253	1.377	0.705	1.307	0.297	1.041	0.279	1.045	0.240	1.125	0.253	1.314	0.724
	Δzwf	4.105	1.053	3.188	0.662	2.266	0.181	4.473	0.788	5.883	2.392	2.394	0.693	2.247	0.692	3.149	0.084	7.344	1.553
Succinic Acid	WT	1.000	0.000	1.179	0.145	1.088	0.128	0.868	0.119	1.023	0.154	1.280	0.435	0.900	0.072	0.928	0.094	0.896	0.087
	Δpfk	1.543	0.044	1.786	0.060	2.007	0.190	2.139	0.109	1.727	0.329	1.447	0.147	1.229	0.046	1.118	0.281	1.358	0.149
	Δgnd	1.433	0.069	1.330	0.091	1.412	0.239	1.336	0.215	1.087	0.093	1.433	0.221	1.321	0.050	1.366	0.010	1.127	0.100
	Δda	2.411	0.494	2.194	0.321	2.152	0.292	2.626	0.566	1.226	0.221	1.030	0.124	1.053	0.101	0.977	0.126	1.177	0.080
	Δzwf	1.529	0.134	1.947	0.208	2.168	0.245	2.188	0.150	1.652	0.134	1.362	0.007	1.406	0.019	1.552	0.090	1.330	0.085
	WT	1.000	0.000	1.179	0.145	1.088	0.128	0.868	0.119	1.023	0.154	1.280	0.435	0.900	0.072	0.928	0.094	0.896	0.087
Threonine	Δpfk	1.543	0.044	1.786	0.060	2.007	0.190	2.139	0.109	1.727	0.329	1.447	0.147	1.229	0.046	1.118	0.281	1.358	0.149
	Δgnd	1.433	0.069	1.330	0.091	1.412	0.239	1.336	0.215	1.087	0.093	1.433	0.221	1.321	0.050	1.366	0.010	1.127	0.100
	Δda	2.411	0.494	2.194	0.321	2.152	0.292	2.626	0.566	1.226	0.221	1.030	0.124	1.053	0.101	0.977	0.126	1.177	0.080
	Δzwf	1.529	0.134	1.947	0.208	2.168	0.245	2.188	0.150	1.652	0.134	1.362	0.007	1.406	0.019	1.552	0.090	1.330	0.085
	WT	1.000	0.000	1.179	0.145	1.088	0.128	0.868	0.119	1.023	0.154	1.280	0.435	0.900	0.072	0.928	0.094	0.896	0.087
	Δpfk	1.543	0.044	1.786	0.060	2.007	0.190	2.139	0.109	1.727	0.329	1.447	0.147	1.229	0.046	1.118	0.281	1.358	0.149

metabolite	strain	HC pre	Std Err	LC 1h	Std Err	LC 2h	Std Err	LC 3h	Std Err	LC 24h	Std Err	HC 1h	Std Err	HC 2h	Std Err	HC 3h	Std Err	HC 24h	Std Err
Tryptophan	WT	1.000	0.000	1.785	0.357	1.105	0.152	0.779	0.057	1.007	0.192	2.070	0.479	1.873	0.280	1.827	0.159	1.117	0.241
	Δpfk	1.730	0.864	2.075	1.114	1.906	0.704	2.760	1.624	0.520	0.000	2.081	1.101	2.495	0.989	1.830	0.549	2.071	0.083
	Δgnd	1.958	0.778	2.641	1.262	2.546	1.265	2.210	1.046	1.736	1.162	1.993	0.979	2.138	0.949	2.059	0.458	1.983	0.969
	Δeda	4.014	0.886	3.364	0.565	3.106	0.632	2.623	0.746	2.529	0.584	2.400	0.531	2.523	0.515	2.184	0.487	2.329	0.606
	Δzwf	3.792	2.129	2.234	0.809	1.755	0.677	2.291	1.149	2.124	1.616	3.038	1.676	3.064	1.505	3.147	1.408	2.477	0.881
	WT	1.000	0.000	0.929	0.134	0.724	0.029	0.508	0.046	0.549	0.058	0.853	0.070	0.829	0.055	0.886	0.116	0.628	0.043
Tyrosine	Δpfk	1.211	0.386	1.159	0.298	0.945	0.233	0.946	0.379	1.563	1.190	1.324	0.466	1.282	0.387	0.989	0.152	0.700	0.001
	Δgnd	1.570	0.400	1.367	0.559	1.430	0.621	1.310	0.643	0.860	0.392	1.357	0.531	1.400	0.492	1.525	0.377	0.958	0.002
	Δeda	2.798	0.215	2.769	0.488	2.463	0.486	2.455	0.687	1.497	0.387	1.422	0.371	1.444	0.356	1.343	0.309	1.438	0.412
	Δzwf	1.730	0.713	1.137	0.229	0.951	0.267	0.808	0.274	0.686	0.279	1.192	0.506	1.174	0.380	1.384	0.334	0.783	0.013
	WT	1.000	0.000	2.800	0.468	2.427	0.413	1.892	0.286	1.805	0.329	1.388	0.462	1.063	0.204	1.260	0.251	1.212	0.332
	Δpfk	1.550	0.190	5.209	0.355	6.999	1.368	4.563	0.167	3.606	1.330	1.459	0.003	1.143	0.207	1.033	0.298	1.249	0.076
Valine	Δgnd	1.515	0.147	2.385	0.246	2.393	0.503	2.271	0.532	0.978	0.171	1.484	0.366	1.568	0.543	1.729	0.403	1.526	0.598
	Δeda	2.839	0.458	2.781	0.767	4.403	1.687	4.127	0.596	2.322	0.858	1.351	0.388	1.440	0.415	1.432	0.408	2.488	0.843
	Δzwf	1.558	0.256	4.979	0.208	7.602	0.684	5.414	0.264	3.292	0.725	1.310	0.248	1.326	0.271	1.444	0.306	1.742	0.060

11.2 Publication II: Cp12 fine-tunes the Calvin-Benson cycle and carbohydrate metabolism in cyanobacteria

Lucius, S., Theune, M., Arrivault, S., Hildebrandt, S., Mullineaux, C. W., Gutekunst, K., & Hagemann, M. (2022). *Frontiers in Plant Science*, 13.:1028794.



OPEN ACCESS

EDITED BY

Jianping Yu,
National Renewable Energy Laboratory
(DOE), United States

REVIEWED BY

Xin Wang,
Miami University, United States
Corinne Cassier-Chauvat,
UMR9198 Institut de Biologie
Intégrative de la Cellule (I2BC), France

*CORRESPONDENCE

Martin Hagemann
martin.hagemann@uni-rostock.de

SPECIALTY SECTION

This article was submitted to
Marine and Freshwater Plants,
a section of the journal
Frontiers in Plant Science

RECEIVED 26 August 2022

ACCEPTED 26 September 2022

PUBLISHED 11 October 2022

CITATION

Lucius S, Theune M, Arrivault S,
Hildebrandt S, Mullineaux CW,
Gutekunst K and Hagemann M (2022)
CP12 fine-tunes the Calvin-Benson
cycle and carbohydrate metabolism
in cyanobacteria.
Front. Plant Sci. 13:1028794.
doi: 10.3389/fpls.2022.1028794

COPYRIGHT

© 2022 Lucius, Theune, Arrivault,
Hildebrandt, Mullineaux, Gutekunst and
Hagemann. This is an open-access
article distributed under the terms of
the [Creative Commons Attribution
License \(CC BY\)](#). The use, distribution
or reproduction in other forums is
permitted, provided the original
author(s) and the copyright owner(s)
are credited and that the original
publication in this journal is cited, in
accordance with accepted academic
practice. No use, distribution or
reproduction is permitted which does
not comply with these terms.

CP12 fine-tunes the Calvin-Benson cycle and carbohydrate metabolism in cyanobacteria

Stefan Lucius¹, Marius Theune^{2,3}, Stéphanie Arrivault⁴,
Sarah Hildebrandt³, Conrad W. Mullineaux⁵,
Kirstin Gutekunst^{2,3} and Martin Hagemann^{1*}

¹Department Plant Physiology, University Rostock, Rostock, Germany, ²Molecular Plant Physiology, Bioenergetics in Photoautotrophs, University Kassel, Kassel, Germany, ³Botanical Institute, University Kiel, Kiel, Germany, ⁴Max Planck Institute of Molecular Plant Physiology, Emeritus Group System Regulation, Potsdam, Germany, ⁵School of Biological and Behavioural Sciences, Queen Mary University of London, London, United Kingdom

The regulatory protein CP12 can bind glyceraldehyde 3-phosphate dehydrogenase (GapDH) and phosphoribulokinase (PRK) in oxygenic phototrophs, thereby switching on and off the flux through the Calvin-Benson cycle (CBC) under light and dark conditions, respectively. However, it can be assumed that CP12 is also regulating CBC flux under further conditions associated with redox changes. To prove this hypothesis, the mutant $\Delta cp12$ of the model cyanobacterium *Synechocystis* sp. PCC 6803 was compared to wild type and different complementation strains. Fluorescence microscopy showed for the first time the *in vivo* kinetics of assembly and disassembly of the CP12-GapDH-PRK complex, which was absent in the mutant $\Delta cp12$. Metabolome analysis revealed differences in the contents of ribulose 1,5-bisphosphate and dihydroxyacetone phosphate, the products of the CP12-regulated enzymes GapDH and PRK, between wild type and mutant $\Delta cp12$ under changing CO₂ conditions. Growth of $\Delta cp12$ was not affected at constant light under different inorganic carbon conditions, however, the addition of glucose inhibited growth in darkness as well as under diurnal conditions. The growth defect in the presence of glucose is associated with the inability of $\Delta cp12$ to utilize external glucose. These phenotypes could be complemented by ectopic expression of the native CP12 protein, however, expression of CP12 variants with missing redox-sensitive cysteine pairs only partly restored the growth with glucose. These experiments indicated that the loss of GapDH-inhibition *via* CP12 is more critical than PRK association. Measurements of the NAD(P)H oxidation revealed an impairment of light intensity-dependent redox state regulation in $\Delta cp12$. Collectively, our results indicate that CP12-dependent regulation of the CBC is crucial for metabolic adjustment under conditions leading to redox changes such as diurnal conditions, glucose addition, and different CO₂ conditions in cyanobacteria.

KEYWORDS

diurnal cycle, fluorescence tagging, photomixotrophy, glyceraldehyde 3-phosphate dehydrogenase, phosphoribulokinase, redox regulation, *Synechocystis* 6803

Introduction

Cyanobacteria are the only prokaryotes performing oxygenic photosynthesis. This process evolved about 3 billion years ago in ancient cyanobacteria and was later conveyed *via* endosymbiosis into a eukaryotic host cell giving rise to the evolution of all eukaryotic phototrophs, i.e. algae and plants (Hohmann-Marriott and Blankenship, 2011). The light energy captured by photosynthetic complexes is first converted into NADPH and ATP, which are used to energize CO₂ conversion into organic carbon. All oxygenic phototrophs use the Calvin-Benson cycle (CBC) for CO₂ fixation. Cyanobacteria evolved an efficient inorganic carbon-concentrating mechanism, which supports CO₂ fixation *via* ribulose 1,5-bisphosphate carboxylase/oxygenase (RubisCO) under limiting and fluctuating CO₂ conditions (reviewed in Hagemann et al., 2021), which is active in the light and becomes inactivated in the dark *via* a phytochrome-sensing mechanism (Oren et al., 2021). During the past years, cyanobacteria received much attention as so-called green cell factories, which can also be used to develop sustainable CO₂-neutral biotechnology to produce energy and feedstock (e.g., Hagemann and Hess, 2018; Appel et al., 2020; Liu et al., 2022).

Photosynthetic light processes and CBC activities need to be coordinated in the diurnal light/dark cycle in all oxygenic phototrophs. This coordination is regulated at different layers and includes mainly redox-signaling to activate or inactivate specific CBC enzymes. It has been shown that CBC regulation involves the action of the small, intrinsically disordered protein CP12 in almost all cyanobacteria, algae and plants (reviewed in López-Calcano et al., 2014; Gurrieri et al., 2022). Canonical CP12 proteins are characterized by two cysteine (Cys) pairs, one near the N-terminal and another near the C-terminal part, that can form disulfide bonds, which permits CP12 to bind the two CBC enzymes glyceraldehyde 3-phosphate dehydrogenase (GapDH) and phosphoribulokinase (PRK), respectively. Biochemical and structural analyses showed that first two GapDH tetramers are bound and then two PRK dimers are recruited by four oxidized CP12 molecules (Wedel and Soll, 1998; McFarlane et al., 2019; Yu et al., 2020). The complex is formed under oxidizing conditions, particularly during the night in photosynthetic cells, leading to the inhibition of the two enzymes and the CBC in general. Under reducing conditions, i.e. in the light phase, the complex becomes unstable mainly due to the action of thioredoxin(s) or directly through elevated NADPH levels leading to the release of GapDH and PRK and activation of the CBC (Suppl. Figure S1). In addition to disulfide bond formation between the Cys pair at the N-terminal part of CP12, the conserved AWD_VEEL motif of CP12 is involved in the inactivation of PRK activity (reviewed in Gurrieri et al., 2022). Recently, it has been reported that CP12 in cyanobacteria, as well as in *Chlamydomonas*, can be phosphorylated under specific conditions (Wang et al., 2014; Spät et al., 2021), however,

how far CP12 phosphorylation contributes to or regulates ternary complex formation is not known.

CP12 proteins have been investigated in different cyanobacterial model strains, which showed that many of the basic features of CP12 function are conserved between cyanobacteria and plants (reviewed in López-Calcano et al., 2014; Gurrieri et al., 2022). It should be noted that cyanobacteria encode two different GapDH proteins. GapDH1 (in *Synechocystis* sp. PCC 6803 encoded by *slr0884*) can only use NAD(H) and is involved in glycolytic carbon catabolism, whereas GapDH2 (in *Synechocystis* sp. PCC 6803 encoded by *sll1342*) can use both, NAD(H) and NADP(H), and is specifically involved in the CBC (Koksharova et al., 1998; own non-published results). Ternary CP12-GapDH2-PRK complex formation under oxidizing conditions has been shown *in vitro* for *Synechocystis* sp. PCC 6803 (Wedel and Soll, 1998) and *Synechococcus elongatus* PCC 7942 (Tamoi et al., 2005) by biochemical measurements such as size-exclusion chromatography (SEC). In the latter strain, the CP12 encoding gene was inactivated and the corresponding mutant showed slower growth under diurnal conditions supporting the *in vivo* role of the CP12 complex formation for coordination of photosynthetic activities in light/dark cycles (Tamoi et al., 2005). Very recently, a *cp12* mutant of *Synechocystis* sp. PCC 6803 which showed severe growth changes in the presence of glucose has been analyzed. Furthermore, distinct redox changes were observed in the absence of CP12, which were used to improve the photosynthetic production of terpenes in this biotechnological chassis (Blanc-Garin et al., 2022). In addition to the canonical CP12 proteins that are conserved in structure and function between cyanobacteria and eukaryotic phototrophs, many cyanobacterial strains harbor genes encoding for CP12-like proteins (Stanley et al., 2012). The CP12-like protein from *Microcystis aeruginosa* PCC 7806 has been analyzed on structural and biochemical levels, which showed that it cannot establish the ternary complex known from canonical CP12 proteins but can inhibit PRK activity in an AMP-dependent manner (Hackenberg et al., 2018). A CP12-like protein from *Synechococcus* sp. PCC 7002 was also not able to complement the phenotypic changes of the *Synechocystis* sp. PCC 6803 *cp12* mutant (Blanc-Garin et al., 2022).

Several hints exist that CP12 also regulates CBC flux and possibly other functions under conditions associated with redox changes (e.g., López-Calcano et al., 2014). Therefore, we aimed to analyze the impact of CP12 under different growth conditions in *Synechocystis* sp. PCC 6803 (hereafter *Synechocystis*). Using mutants expressing GapDH and PRK tagged with a fluorescent protein allowed us to investigate the dynamics of CP12-dependent CBC regulation for the first time *in vivo*. Fluorescence microscopy verified that GapDH or PRK complexes do not appear in our $\Delta cp12$ mutant, which also showed distinct metabolic changes such as over-accumulation of ribulose 1,5-bisphosphate (RuBP) and dihydroxyacetone

phosphate (DHAP), the products of GapDH and PRK. The mutant had difficulties to grow in the presence of glucose under diurnal and dark conditions, because it showed strongly reduced glucose utilization compared to wild type (WT). These phenotypes could be complemented by ectopic expression of the native CP12 protein, however, expression of CP12 variants with missing redox-sensitive Cys pairs only partly restored the growth with glucose. Furthermore, measurements of the NAD (P)H oxidation kinetic in mutant $\Delta cp12$ showed an inability to regulate it properly according to the external light intensities compared to WT cells. Collectively, our results indicate that CP12-dependent regulation of the CBC is crucial for metabolic adjustment under conditions leading to redox changes such as diurnal conditions, glucose addition, and different CO₂ conditions in cyanobacteria.

Material and methods

Molecular cloning and mutant generation

For all experiments, the glucose-tolerant wild-type strain of *Synechocystis* sp. PCC 6803 was used (all strains and mutants are listed in [Suppl. Table S1](#)). The construct for complete deletion of *cp12* in *Synechocystis* was assembled in pJET1.2 (Thermo Fisher Scientific). A fragment consisting of the *cp12* gene with added *SalI* and *NdeI* restriction sites and the respective adjacent gene flanks was obtained by PCR from genomic *Synechocystis* WT DNA and ligated into the vector. The *cp12* sequence was cut out entirely *via* the added restriction sites and replaced by a kanamycin resistance cassette derived from pUC4K. The complementation constructs were assembled in pVZ322 ([Zinchenko et al., 1999](#)). The *cp12* gene variants with adjacent putative promoter sequences were synthesized (BaseGene BV, Leiden, The Netherlands; [Suppl. Figure S2](#)) and ligated into the vector *via* *PstI* and *XhoI* sites. The gentamycin resistance cassette on pVZ322 was cut out *via* *SacI* and replaced by a spectinomycin resistance derived from pUC4S. The *cp12* deletion construct was introduced into *Synechocystis* WT cells by direct transformation. The complementation constructs were transferred to $\Delta cp12$ *via* conjugation. All constructs were verified by sequencing. Schematics of plasmid constructs are provided in [Suppl. Figure S3](#).

To generate PRK-eYFP and GapDH-eYFP tagged strains, plasmids were synthesized (Genscript, New Jersey, USA) that harbored the following elements: 250 bp upstream of the C-terminal end of the gene of interest without the STOP codon, *BamHI* and *EcoRI* restriction sites, and 250 bp downstream of the site of insertion in a pUC57-Simple backbone. In a separate plasmid, the tag containing a linker region with a TEV cleavage site and a 6xHis-tag were cloned into the pRSETA-Cr_FDX1-GST-His expression vector ([Boehm et al., 2016](#)). The resulting

vector was opened with *NheI/SmaI* and the amplified eYFP was inserted *via* Gibson cloning. Subsequently, the gentamycin antibiotic resistance cassette was amplified and inserted into the *EcoRV* cut vector *via* Gibson cloning. Both plasmids were then cut with *BamHI* and *EcoRI* resulting in an opened plasmid with the target regions and a cutout fragment containing the tags. These were ligated resulting in the final plasmid transformed into *Synechocystis* to create the eYFP-tagged strains. A list of all primers that were used in this study is provided in [Suppl. Table S2](#).

Growth experiments

Cells of *Synechocystis* were pre-cultivated in shaking 250 ml Erlenmeyer flasks under ambient air conditions at 30°C in buffered BG11 medium ([Rippka et al., 1979](#); TES pH 8.0) with respective antibiotics (mutant $\Delta cp12$ with 50 µg ml⁻¹ kanamycin, complementation strains with 50 µg ml⁻¹ kanamycin and 40 µg ml⁻¹ spectinomycin, YFP-tagged strains with 5 µg ml⁻¹ gentamycin) at a light intensity of 100 µmol photons m⁻² s⁻¹ until an optical density at 750 nm (OD₇₅₀) of 0.8 to 1.0. Cells were then harvested by centrifugation and resuspended in fresh BG11 medium for an acclimation of 24 h in the light. These precultures were then diluted to the desired starting OD₇₅₀, which depended on the growth condition during the experiment. Experiment cultures were grown in 50 ml BG11 in shaking 100 ml Erlenmeyer flasks. For monitoring growth, samples of 1 ml were taken daily from the flasks to measure OD₇₅₀ using the spectrophotometer Genesys 10S UV-Vis (ThermoScientific).

Metabolite analysis

Cells of *Synechocystis* WT and $\Delta cp12$ were pre-cultivated for one week in glass tubes bubbling in either low CO₂ (ambient air with 0.04% CO₂, LC) or high CO₂ (5%, HC) conditions in buffered BG11 medium with respective antibiotics at 100 µmol photons m⁻² s⁻¹. Cells were then harvested by centrifugation and resuspended in fresh BG11 medium to OD₇₅₀ of 1.0. After 24 h of acclimation, cultures were adjusted to OD₇₅₀ of 1.0 with fresh BG11. To start the experiment, these cultures were kept growing for 3 h in their respective CO₂ condition. To shift cultures from HC to LC, cells were harvested by centrifugation and resuspended in equal volume of fresh BG11, then connected to ambient air aeration. For shifts from LC to HC, cultures were directly switched to HC bubbling. Right before, as well as 1 h and 3 h after the respective CO₂ shifts, four samples of 8 ml were harvested with glass pipettes per culture and quenched directly in 16 ml 70% methanol cooled by dry ice. Quenched cells were pelleted by centrifugation (7 min, 10000 g, 4°C), supernatants were discarded, and cell pellets were quickly frozen in liquid nitrogen and stored at -80°C until extraction. For metabolite

extraction, quenched cell pellets were resuspended in -20°C cold 47% methanol/chloroform (5:1, v/v), followed by four cycles of freezing suspensions in liquid nitrogen, 1 h storage in -80°C and thawing on ice. Extracts were lyophilized (Christ Alpha 2-4 lyophilizer, Christ, Germany), resuspended in 250 μl water and filtered (MultiScreen filter plate with Ultracel-10 membrane, Millipore). RuBP and DHAP were quantified by liquid chromatography linked to tandem mass spectrometry (LC-MS/MS) using reverse phase LC (Arrivault et al., 2009).

Glycogen and glucose quantification

Cellular glycogen was determined according to Gründel et al. (2012) with modifications described by Lucius et al. (2021). During growth experiments, two 5 ml samples of cells were harvested from the flasks and pelleted by centrifugation. The pellet was resuspended in 300 μl 30% KOH (w/v) and then incubated at 95°C for 2 h. After adding 900 μl ice-cold pure ethanol, samples were incubated over night at -20°C . For glycogen precipitation, samples were first centrifuged (10 min, 10000 g, 4°C) and pellets then washed with 1 ml absolute and 1 ml 70% ethanol. The washed pellets were then dried at 50°C . Dry pellets were resuspended in 200 μl sodium acetate buffer (100 mM, pH 4.5) containing 21 U amyloglucosidase and incubated for enzymatic digestion of glycogen at 60°C for 90 min. After centrifugation (10 min, 10000 g, RT), glucose in supernatants was determined using o-toluidine reagent. Glucose contents were calculated using a glucose calibration curve. For quantification of glucose in the medium, two 1 ml samples of culture per time point were harvested during growth experiments. After centrifugation (10 min, 5000 g), the glucose in supernatants was directly determined using o-toluidine reagent.

Glucose 6-phosphate dehydrogenase activity

Activity of glucose 6-phosphate dehydrogenase (Zwf) was determined in *Synechocystis* crude protein extracts. For light samples, cultures cultivated photoautotrophically in constant light were used, while dark samples were collected after incubation in darkness for three hours. For protein extraction, cells from 15 ml of liquid culture at an OD_{750} of 1 were harvested by centrifugation (10 min, 3000 g, 4°C) and pellets were frozen for 1 h at -20°C . The pellet was then resuspended in 400 μl Tris-HCl buffer (100 mM, pH 7.4). Cells were homogenized by sonication and the lysate was cleared by centrifugation (20 min, 3000 g, 4°C). The protein concentration in the supernatant was determined using Bradford reagent. The Zwf enzyme activity assay was carried out in 96-well plates with a total volume of 200 μl per well. Each enzymatic test was conducted in protein extraction buffer containing 10 μg

protein extract and final concentrations of 1 mM NADP^{+} and 5 mM glucose 6-phosphate as substrate at 30°C . To mimic reducing conditions, dithiothreitol (DTT, final concentration 5 mM) was added to selected assays as reducing agent, while others were not treated with DTT. The baseline at 340 nm was measured for 10 min before adding the substrate and monitoring changes in OD_{340} for 30 min. The Zwf activity was calculated from 10 min of linear increase of OD_{340} equivalent to NADPH evolution during the enzymatic reaction.

Microscopy

To prepare cells for microscopic analyses, they were usually pre-cultivated for up to 5 days in shaking flasks in BG11 medium containing respective antibiotics at 28°C and 100 $\mu\text{mol photons m}^{-2} \text{ s}^{-1}$ constant illumination. For experimental cultures, cells were transferred to glass tubes and inoculated with fresh BG11 to an OD_{750} of 0.15. Then the strains were cultivated at 28°C and 100 $\mu\text{mol photons m}^{-2} \text{ s}^{-1}$ constant illumination with ambient air bubbling for three days.

For live cell imaging, 10 μl of cell suspension were dropped on BG11-containing agar plates and incubated at 28°C in darkness for 1 h to let excess liquid evaporate. Next, a BG11 agar cylinder (\varnothing 1 cm) was cut out with a 3D-printed cutter and placed in reverse on a coverslip. This coverslip was placed in reverse on a purpose-built stainless-steel slide (26 mm x 76 mm x 10 mm stainless-steel block with a centered 20 mm hole and a glass slide as cover). The coverslip was fixed with standard petroleum jelly on the stainless-steel slide. The stainless-steel slide was engineered by the research group of Conrad W. Mullineaux (Queen Mary University of London, UK). The slide was modified and manufactured in the in-house University workshop (Christian-Albrechts-University of Kiel, Germany). All experiments were done using an LSM-880 confocal laser scanning microscope (Zeiss, Germany) equipped with a 63x oil immersion objective. Living cells were excited using the 514 nm line of an Argon laser, while fluorescence was detected from 516 – 579 nm for the eYFP channel and 650 – 695 nm for chlorophyll fluorescence (Figure 1). Pinhole size was set to 2 airy units (eYFP channel) while laser power, detector gain and scan speed were adjusted to achieve fast scan speeds and decent image quality (equal for all images taken; Metadata available at Suppl. Data 1). Fast scan speed and low laser power were essential to limit photoactive illumination. Cells were first illuminated using the bright-field lamp at 15% intensity ($\sim 100 \mu\text{mol photons m}^{-2} \text{ s}^{-1}$) for 5 min to set them into a photosynthetically-active state. Then, the image sequence was started by switching off the brightfield illumination and one image was taken every 10 s during darkness (illumination time per cell around 50 ms every 10 s). After 300 s, the brightfield illumination was switched on and a new image sequence was started, taking one picture every 0.47 s.

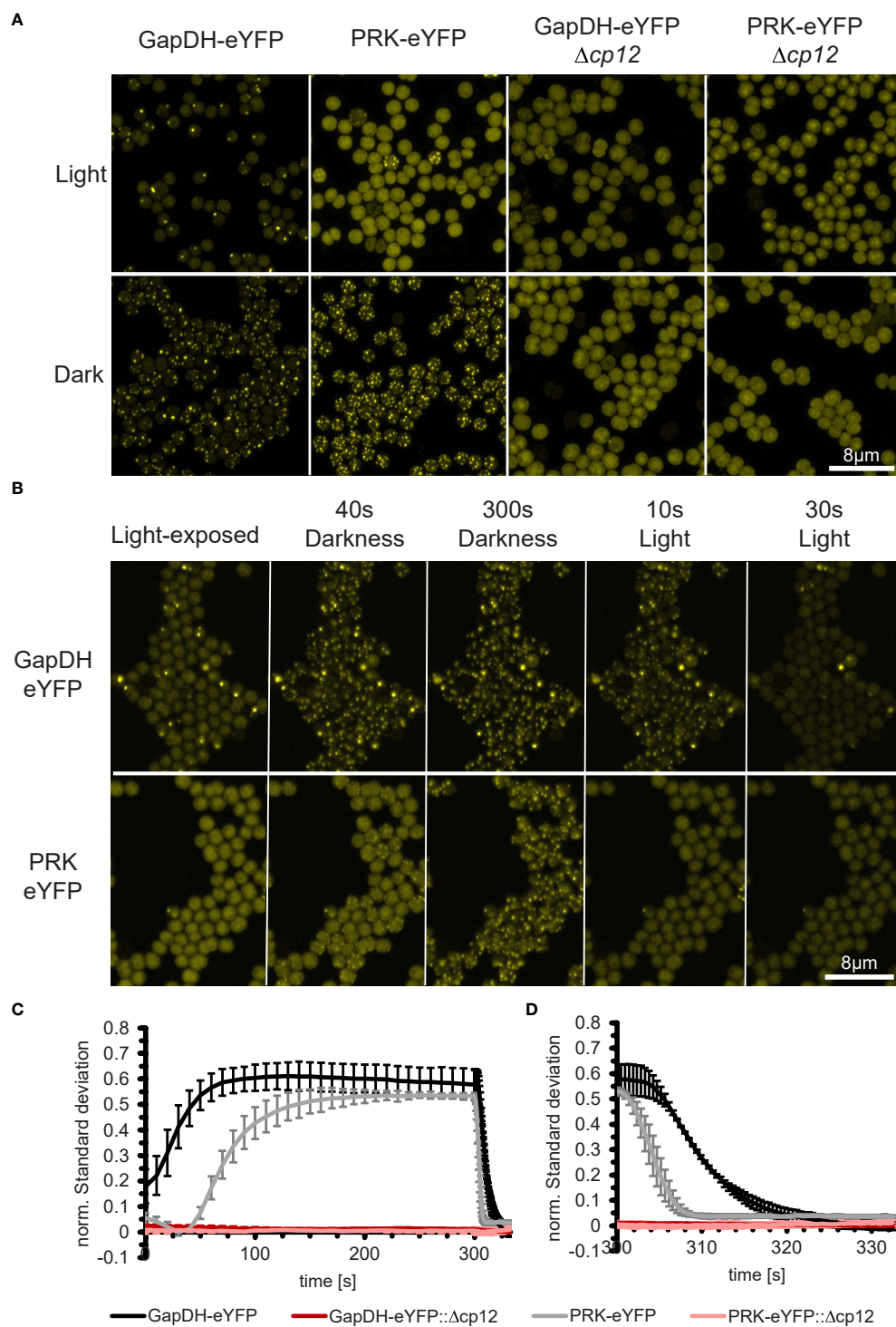


FIGURE 1

In vivo dynamics of CP12-dependent localization changes of the CBB enzymes GapDH2 and PRK in living *Synechocystis* cells during light/dark transition. **(A)** Fluorescence micrographs of *Synechocystis* cells that express GapDH2 or PRK tagged with eYFP in wild type (left two panels) or in $\Delta cp12$ mutant background (right two panels). All cells were fixed either in light or dark conditions before observation. **(B)** Light-exposed GapDH2-eYFP and PRK-eYFP strains were observed over 300 s after transferring into dark and subsequently 30 s into light conditions, respectively (selected time points are shown). **(C, D)** Kinetics of complex appearance **(C)** or disappearance **(D)** were estimated by plotting the time-dependent change in normalized standard deviations representing the heterogeneity of fluorescence signal distribution inside the cells after transfer from light into darkness **(C)** or back into light **(D)**.

For investigating PRK-eYFP and GapDH2-eYFP distribution at different illumination levels, cells were fixed at precisely defined light intensities. In these experiments, cells were cultivated as described above, harvested after 3 days from glass tubes, washed with fresh BG11, and adjusted to OD₇₅₀ of 1 using BG11. After measuring the NAD(P)H oxidation rate (see 2.8) at one defined light intensity, 25% glutaraldehyde was added to a final concentration of 2%. Illumination conditions were kept constant for 5 min until all cells had been fixed properly. Then, cells were prepared for microscopic analysis as described above. Microscope settings were also similar, but Z-stacks ranging through the single cell layer in 0.38 μm steps were taken (Metadata available at [Suppl. Data 1](#)).

For High-resolution images of PRK-eYFP and GapDH2-eYFP, cells were fixed either at constant light of 100 $\mu\text{mol photons m}^{-2} \text{s}^{-1}$ illumination or in complete darkness. For microscopy the Airy-Scan detector was used ([Figure 1](#)). To measure the eYFP channel, the 488 nm line of an Argon laser and a double band-path filter 420 - 480 nm and 495 - 550 nm was used, while the chlorophyll fluorescence was detected using a 633 nm laser-diode and a 570 - 620 nm band path + 645 nm long-path filter (Metadata available at [Suppl. Data 1](#)). Each channel was detected as a Z-stack ranging through the single cell layer in 0.15 μm steps. Finally, Airy-Scan data were processed and transformed into common Z-Stacks using Zen-Software (Zeiss, Germany).

Image analysis

Live cell images were processed by first concatenating the dark and light stacks in ImageJ ([Schindelin et al., 2012](#)) before splitting stacks into stacks of eYFP and chlorophyll fluorescence images. Next, Z-stack max projections were performed on the chlorophyll stacks, creating single-layer pictures. These images were used in an ilastik instance ([Berg et al., 2019](#)) trained to distinguish cells from the background creating probability masks used in ImageJ to create regions of interest (ROI) for each cell. These ROIs were used to measure the mean fluorescence intensity and the standard deviation of the eYFP signal in each cell on each image in a stack. The standard deviation was then divided by the mean fluorescence intensity to calculate the normalized standard deviation, representing the heterogeneity of the signal distribution ([Mahbub et al., 2020](#)). Pictures of cells fixed at different light intensities were analyzed similarly. The Z-Stacks were converted to a single two-channel image using max Z-projection tool in ImageJ prior to analysis.

NAD(P)H measurements

In vivo NAD(P)H redox dynamics were analyzed using the NAD(P)H module in combination with the Dual-KLAS-NIR system (Walz, Germany). Cultivation of cells was done as

described before for microscopic analysis (see 2.6). Cells from 50 ml culture were harvested by centrifugation (4000 g for 3 min), washed twice with BG11-0 (BG11 without nitrogen source), and finally suspended in BG11-0 to an OD₇₅₀ of 1. Cells were kept in 50 ml tubes at 28°C and 100 $\mu\text{mol photons m}^{-2} \text{s}^{-1}$ until measured for up to 3 h and then transferred into darkness 30 min before each measurement. 1.25 ml cell suspension were filled into a quartz cuvette placed into the Optical Unit ED-101US/MD connected to the Dual-KLAS-NIR system. Cells were incubated for 3 min during constant stirring at defined light intensities to let the cells acclimate to these conditions before the NAD(P)H oxidation rates were measured four times. One of the two actinic LED arrays was disabled to achieve a lower illumination level. A slow-kinetic trigger run was used containing a 1 s phase with the light intensity investigated, 600 ms high light pulse (3200 $\mu\text{mol photons m}^{-2} \text{s}^{-1}$) and 13.4 s darkness. Between each measurement, cells were incubated for 30 s at the investigated light intensity. The last three of the four measured kinetics were averaged, exported and analyzed using R in R-Studio (RStudio Boston, USA). The photo-reducible NAD(P)H level was calculated by subtracting the value at the end of the dark period from the whole measurement and dividing the maximum value between 1 s and 1.6 s by the NAD(P)H level from 0 s to 1 s. The oxidation rates were determined by fitting an exponential function to the measurement from the beginning of the dark period at 1.6 s until the slope was less than $5 \cdot 10^{-8}$.

Protein analysis and Western-blotting

Whole cell extract from *Synechocystis* strains were generated by glass bead breakage as described ([Appel et al., 2020](#)). The amount of broken cells was estimated by measuring Chlorophyll a in 2.5 μl of whole cell extract, which was dissolved in methanol to a final volume of 1 ml. Then, the absorption at 666 nm was measured to calculate the chlorophyll a content. Proteins were separated on 10% (w/v) denaturing SDS-Bis/Tris gels using an MES running buffer and Western-blotting were performed as described by [Appel et al. \(2020\)](#). Primary antibodies used in this study were Mouse anti Penta Histidine (Bio-Rad Laboratories, California, USA), Mouse anti Green Fluorescent Protein (Bio-Rad Laboratories, California, USA), and Peroxidase AffiniPure Rabbit Anti-Mouse IgG + IgM (Jackson ImmunoResearch Europe, Ely, UK).

Results

Absence of CP12 prevents *in vivo* complex formation with GapDH and PRK

To analyze the impact of CP12 on carbon metabolism in the model cyanobacterium *Synechocystis*, we generated a completely

segregated mutant $\Delta cp12$. Deletion of the native *cp12* gene (*ssl3364*) was achieved by replacing the entire coding sequence of CP12 with a kanamycin-resistance cartridge. Genotyping by PCR confirmed complete loss of the gene in $\Delta cp12$ (Suppl. Figure S4).

In the past, the appearance of the ternary CP12-GapDH-PRK complex was usually proven by biochemical measurements such as SEC, native gel electrophoresis, plasmon resonance analysis, or FRET-measurements *in vitro* (e.g., Avilan et al., 1997; Wedel and Soll, 1998; Moparthy et al., 2015). We aimed to obtain the first *in vivo* documentation of complex formation in *Synechocystis* using a fluorescence-tagging approach. To this end, the native GapDH2 (Sll1342) or PRK (Sll1525) encoding genes were replaced by constructs, in which their coding sequences were C-terminally fused with eYFP-encoding sequences and expressed from their native promoters. Genotyping revealed that in the case of PRK, the native gene could be completely replaced by the eYFP-tagged copy, while GapDH2 did not fully segregate (Suppl. Figure S5). These eYFP-tagged strains expressed the expected fusion proteins (Suppl. Figure S6). When grown under photoautotrophic conditions, they showed only minor growth difference compared to the *Synechocystis* WT, which verifies that the eYFP-tagged enzymes were functional in the CBC (Suppl. Figure S7). Fluorescence microscopy showed strong eYFP fluorescence dispersed homogeneously in cells exposed to the light, however, after transfer into darkness within 1–2 min, distinct fluorescing spots appeared in the GapDH2-eYfp-tagged as well as in the PRK-eYFP-tagged strains, which disappeared when the cells were re-exposed to light (Figures 1A, B).

Interestingly, these eYFP complexes could not be further observed when the *cp12* gene was mutated in the eYFP-tagged strains (Figure 1). Videos showing the kinetics of appearance and disappearance of fluorescent tagged complexes are shown in the supplementary data 2. These results show for the first time the CP12-dependent complex formation with GapDH2 or PRK during light/dark transitions inside living *Synechocystis* cells. Furthermore, the speed of complex formation and disappearance was quantified in the eYFP-tagged strains. The results showed that the binding of GapDH2 occurred faster than the binding of PRK (Figure 1C), whereas upon re-illumination, first PRK and then GapDH2 are released from the CP12-dependent complexes (Figure 1D). The different kinetics are consistent with the sequential order of binding/releasing the two proteins to oxidized/reduced CP12 found e.g. during crystallography (McFarlane et al., 2019).

Phenotyping of mutant $\Delta cp12$ and different complementation strains

The applied mutation strategy permitted the use of the *cp12* flanking regions in attempts for the expression of CP12 variants

under control of the native *cp12* promoter. To this end, the native *cp12* gene was reintegrated and the entire construct was cloned into the self-replicating plasmid pVZ322 to achieve the complementation strain $\Delta cp12::cp12$ -WT. Furthermore, *cp12* gene variants were synthesized, in which the codons for the N-terminal Cys pair (Cys19 and Cys29, docking site for PRK), the C-terminal Cys pair (Cys60 and Cys69, docking site for GapDH2), or all four Cys codons were changed towards serine codons, which gave rise to the complementation strains $\Delta cp12::cp12$ - Δ CysN, $\Delta cp12::cp12$ - Δ CysC, and $\Delta cp12::cp12$ - Δ CysNC, respectively.

First, we compared the growth of the *Synechocystis* WT with mutant $\Delta cp12$ under different CO₂ conditions in normal light and observed that both strains grew similarly (Suppl. Figure S8). However, metabolome analysis revealed distinct differences in the amounts of ribulose 1,5-bisphosphate (RuBP) and dihydroxyacetone phosphate (DHAP) (Figure 2). RuBP is the product of the CP12-regulated PRK reaction, while DHAP is in equilibrium *via* triose-phosphate isomerase with glyceraldehyde 3-phosphate (Gap), the product of CP12-regulated GapDH2 that is chemically unstable and difficult to quantify by LC-MS/MS. RuBP steady state contents were enhanced in mutant $\Delta cp12$ compared to WT when grown at ambient air (low CO₂ of 0.04%, LC), while DHAP was higher in mutant cells under high CO₂ supplementation (5% CO₂, HC). The differences became more pronounced under transient conditions. Much higher transient accumulations of RuBP and DHAP were observed in mutant $\Delta cp12$ than in WT 1 h after the shift from HC into LC conditions, while the RuBP contents were almost similar after 3 h HC to LC transfer (Figure 2). In contrast to the HC to LC shift, levels of RuBP and DHAP did not differ significantly between the two strains after the transfer of cells from LC into HC conditions. These data indicate that the absence of CP12 had marked influence on *in vivo* PRK and GapDH activities especially under non-steady state HC to LC shift conditions.

It has been previously shown that the mutant $\Delta cp12$ of *Synechococcus elongatus* showed slower growth under diurnal conditions (Tamoi et al., 2005), however, this was not the case with the *Synechocystis* mutant $\Delta cp12$ (Figure 3) as reported recently in an independent study (Blanc-Garin et al., 2022). This different phenotypes could be related to the different culture conditions or to the fact that the CP12 protein in *S. elongatus* is different, i.e. it misses the N-terminal Cys pair. *Synechocystis* is a cyanobacterium that can use external glucose for photomixotrophic growth (Rippka et al., 1979). In the light glucose enters the CBC *via* different glycolytic shunts and thereby enhances the flux through the cycle and CO₂ fixation (Schulze et al., 2022), which also has marked influence on the cellular redox state (e.g., Wang et al., 2022).

Our mutant $\Delta cp12$ could grow with glucose supplementation under continuous light (Suppl. Figure S9), however, glucose supplementation completely inhibited growth under diurnal conditions and in complete darkness compared to WT

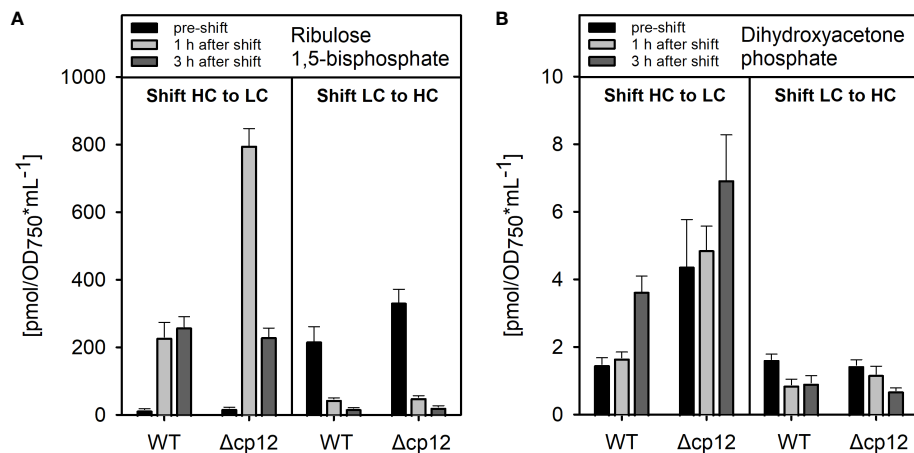


FIGURE 2

Metabolome analysis of products from the CP12-regulated enzymes PRK and GapDH2. The amounts of dihydroxyacetone phosphate (A) and ribulose 1,5-bisphosphate (B) were quantified by LC-MS/MS in cells of *Synechocystis* wild type (WT) or mutant $\Delta\text{cp}12$ pre-acclimated to high CO_2 conditions (5% CO_2 , HC) or ambient air with low CO_2 (0.04% CO_2 , LC) (black columns – pre-shift). Then, cells were shifted for one (light grey columns) or three hours (dark grey columns) from either HC into LC or LC into HC conditions. Metabolite levels are mean values \pm standard deviations from three biological replicates.

(Figure 3). The glucose sensitive phenotype of $\Delta\text{cp}12$ was completely reversed to WT-like growth after ectopic expression of native CP12 in the strain $\Delta\text{cp}12::\text{cp}12\text{-WT}$ (Figure 3). Furthermore, *Synechocystis* is capable of so-called photoheterotrophic growth, i.e. the strain can grow on glucose in the light when the photosynthetic electron transport is blocked by the photosystem II-specific inhibitor DCMU (3-(3,4-dichlorophenyl)-1,1-dimethylurea). As found before (Blanc-Garin et al., 2022), the addition of glucose in the light to DCMU-treated cells of mutant $\Delta\text{cp}12$ was toxic, whereas the strain could grow in the absence of DCMU on plates with glucose in continuous light (Suppl. Figure S9).

The CP12 protein is able to interact with two different CBC enzymes. The specific impact of GapDH2 or PRK binding on the

observed phenotypic alterations was analyzed in strains expressing CP12 variants either missing the N-terminal Cys pair for PRK association, the C-terminal Cys pair for GapDH2 association, or both. It has been shown that the site-specific mutation of these redox-sensitive Cys residues in CP12 specifically prevents the binding of GapDH2 or PRK (Moparthy et al., 2015). Like the complementation strain with native CP12 (Figure 3), the strain expressing the CP12- ΔCysN variant could grow in the presence of glucose in diurnal light/dark cycles almost like WT (Figure 4A). In contrast, the strain expressing the CP12- ΔCysC variant initiated slow growth only after the second day, while the lag phase in strain $\Delta\text{cp}12::\text{cp}12\text{-}\Delta\text{CysNC}$ was extended to three days (Figure 4A). These data indicate that binding and inactivation of GapDH2 activity *via*

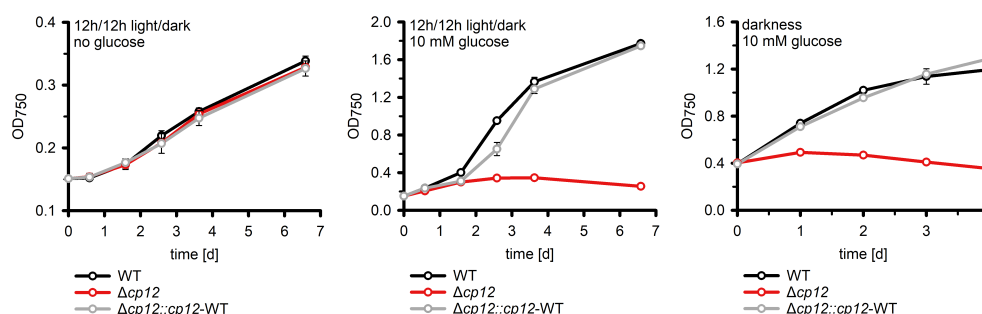


FIGURE 3

Growth of different strains in the absence and presence of glucose. The increase of optical density at 750 nm (OD_{750}) as proxy of biomass was compared in cultures of the *Synechocystis* wild type (WT), the mutant $\Delta\text{cp}12$, and the complementation strain $\Delta\text{cp}12::\text{cp}12\text{-WT}$. Shown are mean values and standard deviations from three independent cultivations.

CP12 has greater impact on glucose sensitivity than the absence of PRK association in strain $\Delta cp12::cp12-\Delta CysN$.

Analysis of glucose utilization in mutant $\Delta cp12$ and different complementation strains

To analyze why the mutant $\Delta cp12$ could not grow on glucose, the amount of glucose was quantified in the culture medium of different strains. WT cells (Figure 4B) and the complementation strain $\Delta cp12::cp12$ -WT (not shown) consumed all glucose from the medium during the first two days. In contrast, cultures of mutant $\Delta cp12$ showed only minor glucose consumption. To rule out that a secondary mutation might be responsible for the reduced glucose consumption of mutant $\Delta cp12$, the glucose transporter (Sll0771) and glucose-kinase (Sll0593) encoding genes were sequenced revealing that these genes had identical sequences in mutant as in WT (data not shown). Like mutant $\Delta cp12$, the strains with mutated C-terminal Cys pair $\Delta cp12::cp12-\Delta CysC$ and $\Delta cp12::cp12-\Delta CysNC$ were strongly affected in glucose consumption. The glucose consumption of strain $\Delta cp12::cp12-\Delta CysN$ was delayed compared

to WT but all glucose disappeared after four days, consistent with the ability of this strain to grow in the presence of glucose under diurnal conditions (Figures 4A, B).

Glucose addition not only has a marked impact on the redox state of *Synechocystis* cells, the excess organic carbon is also stored as glycogen. Glycogen pools increased in all strains to almost the same extent during the first day after glucose addition (Figure 4C). They remained almost stable during the further days in strains $\Delta cp12$, $\Delta cp12::cp12-\Delta CysC$ and $\Delta cp12::cp12-\Delta CysNC$ that are not able to grow properly in the presence of glucose in light/dark cycles. In contrast, WT and strain $\Delta cp12::cp12-\Delta CysN$ degraded internal glycogen at the end of the experiment, when the amount of glucose in the medium was consumed or strongly diminished (Figures 4B, C). The initial similar ability to accumulate glycogen in all strains indicates that glucose is entering the cells and is channeled into glycogen synthesis independently from CP12, however, the utilization of glucose and later glycogen reserves to promote growth is strongly affected in strains without CP12 or with CP12 variants unable to bind GapDH2.

Glucose as well as glycogen catabolism in *Synechocystis* mainly use the oxidative pentose phosphate pathway (OPPP) under dark conditions, which is initiated by the first enzyme glucose 6-

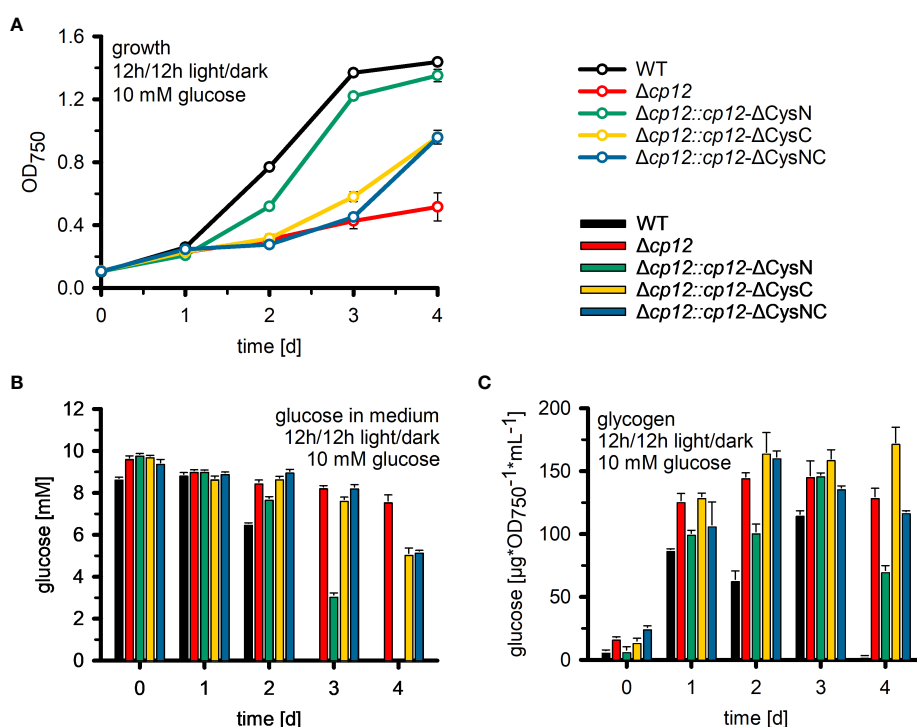


FIGURE 4

Utilization of glucose in mutant $\Delta cp12$ and strains expressing several CP12 variants. (A): The growth as an increase in the optical density at 750 nm (OD₇₅₀) of the *Synechocystis* sp. PCC 6803 wild type (WT) was compared to mutant strain $\Delta cp12$ with no CP12, and strains expressing CP12 variants with site-specific mutated Cys pairs, i.e. strains $\Delta cp12::cp12-\Delta CysN$, $\Delta cp12::cp12-\Delta CysC$, and $\Delta cp12::cp12-\Delta CysNC$, under diurnal conditions (12 h light/12 h dark) in the presence of 10 mM glucose. Glucose amounts in the medium (B) and cellular glycogen amounts (C) were quantified daily. Mean values \pm standard deviations from three biological replicates are shown.

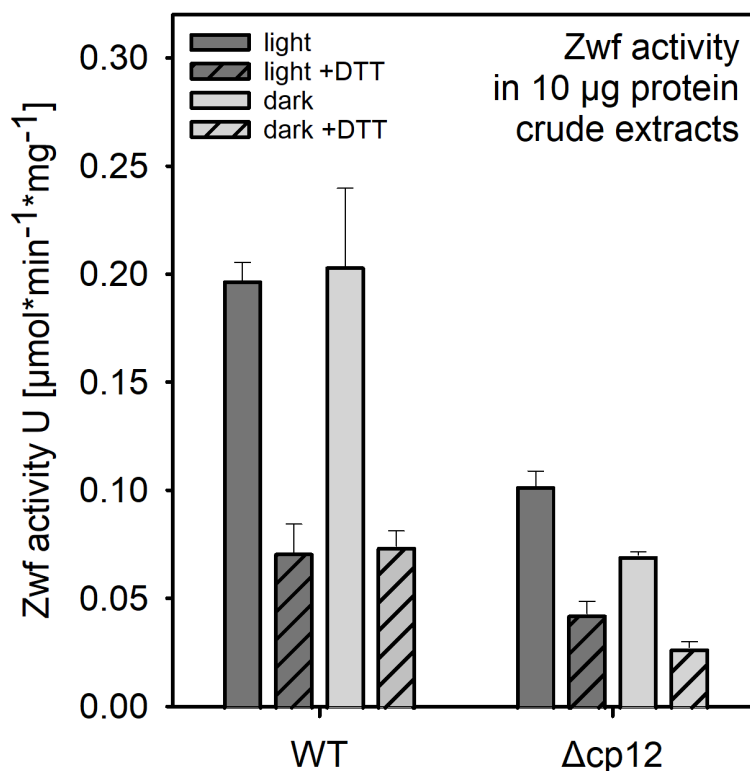


FIGURE 5

Glucose 6-phosphate dehydrogenase (Zwf) activities in the *Synechocystis* wild type (WT) and mutant $\Delta cp12$. Specific enzyme activities were measured in crude protein extracts from cells exposed to light or dark conditions in the presence of saturating glucose 6-phosphate amounts under oxidizing or reducing (+ 5 mM DTT). Data from one representative experiment are shown.

phosphate dehydrogenase (Zwf). The activity of Zwf was compared between WT able to use glucose for growth and mutant $\Delta cp12$ which was not able to do so. Protein extracts were obtained from cells either grown photoautotrophically in the light or from the dark phase. Three-times lower Zwf activities were found in mutant cells in protein extracts obtained from light- or dark-exposed cells (Figure 5). It is known that Zwf activity in *Synechocystis* and other cyanobacteria is redox-regulated using the regulator protein OpcA (Sundaram et al., 1998). The redox-regulation of Zwf occurred to almost the same extent in both strains, i.e. addition of DTT decreased the Zwf activity compared to oxidizing conditions to almost 50% (Figure 5).

Analysis of the redox state in mutant $\Delta cp12$ and different complementation strains

The action of CP12 on GapDH2 and PRK activities in light/dark cycles is redox-dependent. Moreover, the observed phenotype of mutant $\Delta cp12$ in the presence of glucose can also result from the inability of proper redox regulation. Redox

changes in WT, mutant $\Delta cp12$, and in strains expressing different CP12 variants were recorded by measuring NAD(P)H fluorescence changes in cells, which were pre-acclimated to different light intensities. Then, the NAD(P) pool was completely reduced by a saturating light pulse and the re-oxidation of the NAD(P)H was subsequently recorded in darkness. In WT cells, the NAD(P)H pool became re-oxidized to a new steady level within 2–12 s. This re-oxidation process was faster in cells pre-acclimated to stronger light intensities and was slower in cells incubated in darkness or weak light before the saturation pulse (Figure 6A). In contrast, the re-oxidation was much faster in cells of mutant $\Delta cp12$. Independent from the pre-illumination conditions, it was always completed within 2 s, similar to WT cells exposed to the highest light intensity (Figure 6B). This difference indicated that the entire GapDH pool is free in mutant $\Delta cp12$ and can take active part in the utilization of NAD(P)H, while in WT cells an increasing GapDH pool is bound to CP12 in darkness or under dim light decreasing the re-oxidation time of NAD(P)H. This interpretation is supported by the finding that the re-oxidation kinetics in the mutants with disturbed C-terminal Cys pair for GapDH2 binding, i.e. $\Delta cp12::cp12-\Delta CysC$ and $\Delta cp12::cp12-\Delta CysNC$

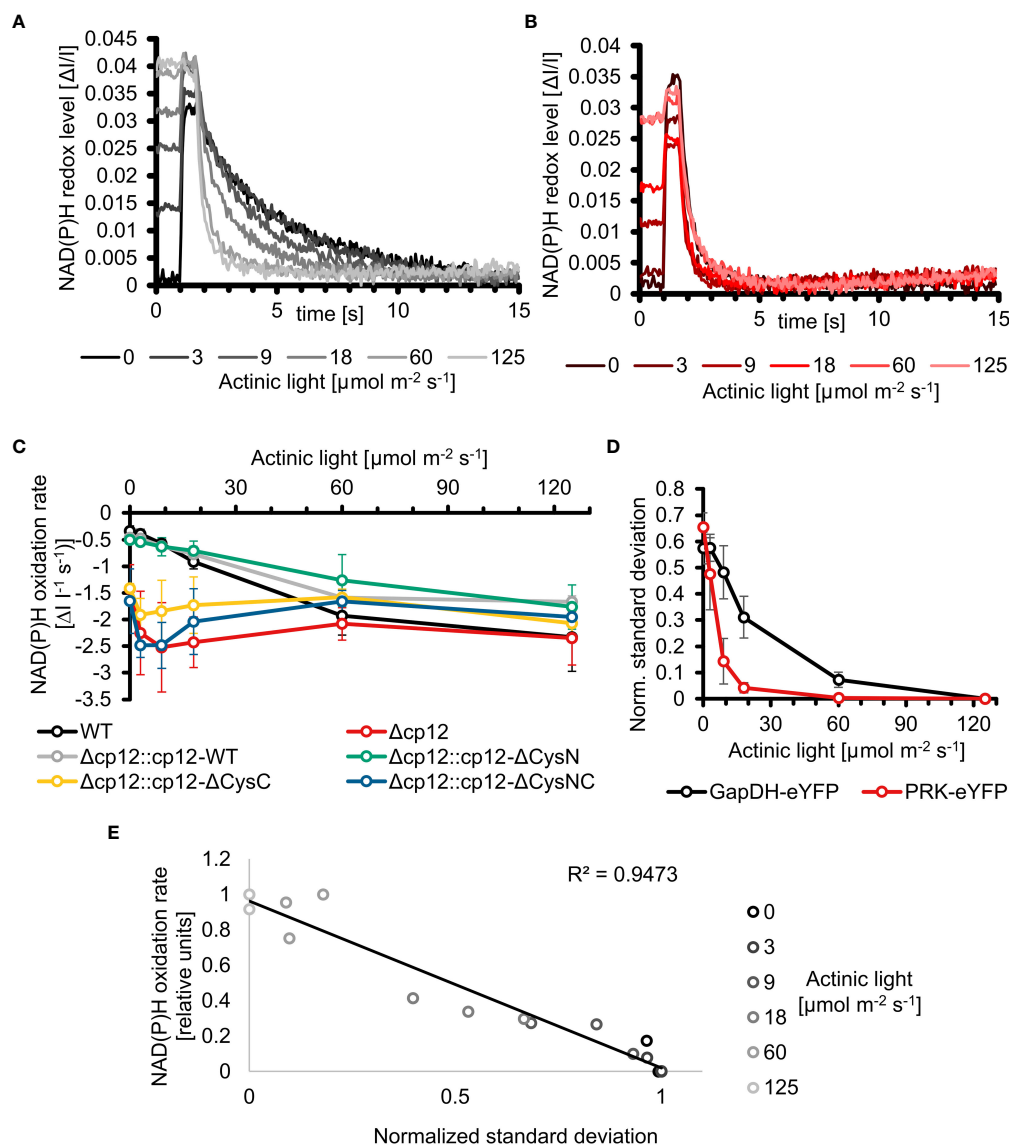


FIGURE 6

Redox changes in the *Synechocystis* wild type and mutant $\Delta\text{cp}12$ under different light conditions. (A, B) NAD(P)H redox changes measured *in vivo* via NAD(P)H fluorescence in wild-type (WT) (A) or mutant $\Delta\text{cp}12$ cells (B). The NAD(P)H pool was reduced to its maximum with a strong actinic light pulse (600 ms) and its re-oxidation in darkness was observed. The measured cells were pre-acclimated to the 5 different actinic light intensities or to darkness. (C) NAD(P)H oxidation rates of strains expressing different CP12 variants after pre-acclimation to different actinic light intensities. (D) Normalized standard deviations representing the heterogeneity of fluorescence signal distribution inside cells. The distribution of PRK-eYFP and GapDH-eYFP is measured under different actinic light conditions. (E) Scatterplot of the normalized standard deviation of GapDH-eYFP vs the NAD(P)H oxidation rate under different light intensities.

showed similarly fast NAD(P)H re-oxidation kinetics as mutant $\Delta\text{cp}12$. In contrast, the strains expressing native CP12 or the variant with mutated N-terminal Cys pair for PRK binding, i.e. $\Delta\text{cp}12::\text{cp}12\text{-WT}$ and $\Delta\text{cp}12::\text{cp}12\text{-}\Delta\text{CysN}$ are characterized by WT-like NAD(P)H re-oxidation kinetics (Figure 6C; Suppl. Figure S10). Moreover, the strains expressing eYFP-tagged GapDH2 or PRK in the WT background showed also similar NAD(P)H re-oxidation kinetics as WT (Suppl. Figure S11).

The different NAD(P)H re-oxidation kinetics in WT cells after pre-exposure to different light intensities also indicate that part of GapDH2 is already associated with CP12 under low light and less associated under high light, i.e. CP12 is not only mediating CBC activity in light/dark changes but also under different light intensities. This observation initiated attempts to measure the appearance of GapDH2-eYFP or PRK-eYFP complexes in cells exposed to different actinic light intensities

under the fluorescence microscope. These measurements show an exponential increase of PRK-eYFP and particularly of GapDH2-eYFP complex fluorescence with decreasing light intensities towards the maximum in complete darkness (Figure 6D). Plotting the oxidation rate of the NAD(P)H pool with the normalized standard deviations representing the heterogeneity of the fluorescence signal of GapDH2-eYFP resulted in a linear relation (Figure 6E).

Discussion

It is generally accepted that CP12 can bind GapDH and PRK under oxidative conditions, which occurs especially in darkened cells of oxygenic phototrophs to inactivate the CBC activity when light processes are not further working (reviewed in López-Calcano et al., 2014; Gurrieri et al., 2022). However, there is an increasing body of evidence that CP12-mediated regulation may extend over the light/dark regulation of CBC activity. To analyze the role of CP12 regulation in the model cyanobacterium *Synechocystis*, we first generated eYFP-tagged strains in *Synechocystis* to monitor for the first time CP12-GapDH2-PRK complex formation *in vivo*. Expressing eYFP-tagged PRK or GapDH2 variants in *Synechocystis* clearly showed the appearance of CP12-dependent complexes in darkness and their disappearance in the light. In the dark-shifted cells highly fluorescent spots appeared, which were not further visible in the mutant $\Delta cp12$. A clear correlation between spot appearance and the oxidation rate of the NAD(P)H pool was observed (see Figure 6), which indicated that their appearance is redox-dependent and resulted in inactivation of at least the GapDH2. The appearance of a distinct number of obvious large complexes was not expected and could indicate that CBC enzymes might be localized at specific parts of the cyanobacterial cell. One possible location would be near the carboxysome, which harbors all active RubisCO in the cyanobacterium. Usually one to five carboxysomes are visible in electron micrographs of *Synechocystis* (e.g. Hackenberg et al., 2012), which is similar to the number of CP12-GapDH2-PRK fluorescent spots, hence, these complexes might be associated to carboxysome(s) (see Figure 1). Instead of eYFP-tagging PRK or GapDH2, truncated versions of the CP12 protein were fused N-terminally with CFP and C-terminally with YFP to monitor thioredoxin-mediated redox-changes in *Anabaena* sp. PCC 7120 or in chloroplasts of *Arabidopsis* *in vivo* via FRET (Sugiura et al., 2019). These redox-sensing devices showed clear fluorescence increases of YFP under oxidizing conditions, i.e. when the internal disulfide bond was established after transfer into darkness, or decreased YFP fluorescence under reducing conditions, i.e. when the disulfide bond was released *via* reduced thioredoxin(s) after illumination. As found in our tagged strains (see Figures 1C, D), the reduction of CP12 *via* thioredoxins in the light occurred

faster than its oxidation after transfer into darkness (Sugiura et al., 2019).

Our fluorescent-tagged strains further allowed us to follow the different kinetics of GapDH2 and PRK binding to and release from CP12 in dark/light cycles. As expected from the structural model (McFarlane et al., 2019), GapDH-eYFP complexes appeared faster and disappeared more slowly than the PRK-eYFP complexes. Hence, the fluorescent-tagged *Synechocystis* strains also verified the predicted sequential order of CP12-complex formation *in vivo*. Moreover, the rate of complex formation was followed in darkened cells after their pre-incubation under different light intensities. The different kinetics clearly showed that *in vivo* at lower light, when the photosynthetic activity and hence the CBC flux is diminished, already a substantial part of GapDH2 is bound to CP12, whereas under high light conditions inducing high photosynthetic activities much less GapDH2 is CP12-associated (see Figure 6). These results provide clear evidence that CP12 is not only a device to switch on and off CBC activities in diurnal light/dark cycles, but it also fine-tunes CBC activities and light processes during the day under different light and accompanied redox conditions in the *Synechocystis* cell. Differences in the available light, especially high light incubations, have been shown also to induce intracellular fluctuations in the available CO₂, because many genes encoding proteins for acclimation to low CO₂ conditions were clearly induced in the transcriptome of *Synechocystis* exposed to high light conditions (Hihara et al., 2001). The observed changes in the amounts of RuBP and DHAP in $\Delta cp12$ cells under non-steady state conditions in cells switched from HC into LC conditions (see Figure 2) provide another indication that the enzymes GapDH2 and PRK are more active in the absence of CP12 compared to WT cells even under continuous light conditions.

The most severe phenotype in the $\Delta cp12$ cells was observed when the cells can consume added glucose in darkness as has been recently also reported by Blanc-Garin et al. (2022). These results indicate that in addition to CBC, the redox-dependent CP12-mediated regulation has a broader impact on carbohydrate metabolism than just regulating the CBC. Our results indicate that glucose uptake and glycogen metabolism is not primarily affected, but the glucose catabolism *via* the OPPP is strongly diminished. This hypothesis is supported by the reduced activity of Zwf in cells of $\Delta cp12$ (see Figure 5). The glucose-sensitive phenotype could be explained by the absence of proper GapDH2 and PRK regulation, initiation of futile cycles, and/or more enzymes of primary C-metabolism being regulated by CP12. The latter assumption is supported by the reported association of aldolase, which also plays an important role in sugar metabolism in oxygenic phototrophs, to the CP12-GapDH-PRK complex in *Chlamydomonas* (Erales et al., 2008). However, the main function of CP12-mediated inactivation of GapDH2 and PRK is usually related to the avoidance of futile

cycles between CBC and OPPP. The non-oxidative portion of the OPP overlaps to a large extent with the regenerative part of the CBC by the used enzymes but are involved in sugar catabolism and anabolism, respectively (reviewed in López-Calcano et al., 2014; Gurrieri et al., 2022). In this regard, the proper regulation of GapDH2 activity seems to be more important than PRK regulation, because expressing CP12 variants with mutated C-terminal Cys pairs necessary to bind GapDH2 show much fewer capabilities to complement the glucose-sensitive phenotype of $\Delta cp12$ (see Figure 4) or the observed redox imbalance (see Figure 6C). GapDH2 can use NADPH and is mainly involved in the conversion of glycerate 1,3-bisphosphate into Gap, while the GapDH1 that is supposed to be mostly active under dark conditions in WT cells (Koksharova et al., 1998) catalyzes the reverse reaction in WT cells. Hence, the dual activities of the two GapDH isoenzymes during the night could prevent proper glycolytic breakdown of glucose under dark conditions in $\Delta cp12$. Moreover, the utilization of NADPH by GapDH2 can likely also result in redox imbalance, because in WT cells NADPH is mostly produced in the dark *via* the OPPP, which is necessary to fuel important other enzymatic reactions of primary metabolism. Hence, redox imbalances especially in the presence of glucose could be another reason for the inability of $\Delta cp12$ to grow on glucose. However, in contrast to the independent study by Blanc-Garin et al. (2022) we could not detect glucose sensitivity at constant light. This deviation could be related to the different culture conditions in the two studies. In our experiments we grew cells at higher light intensities than in the experiments reported by Blanc-Garin et al. (2022). Our data in Figure 6 clearly indicate that at low light conditions part of CP12 is already associated with GapDH2, while this interaction is not detectable at higher light intensities.

Of course, mutation of CP12 could also impact the amount of its binding partners GapDH2 and PRK. Decreased PRK expression has indeed been reported in *cp12* mutants of Arabidopsis, whereas the amount of GapDH and many other CBC enzymes was not changed (López-Calcano et al., 2017). However, the GapDH2 and PRK activities remained unchanged in another $\Delta cp12$ mutant of *Synechocystis* (Blanc-Garin et al., 2022). As shown in the previous study and by us, expressing CP12 variants with N-terminal changed Cys pair involved in PRK-binding permits complementation of glucose utilization (see Figure 4) and results in WT-like redox changes (see Figure 6C). It has been shown that in addition to redox-dependent regulation of PRK *via* the CP12-GapDH complex, PRK activity in cyanobacteria and plants is directly redox-regulated by two internal Cys pairs, which can undergo redox-dependent disulfide bond formation thereby modulating PRK activity. Fukui et al. (2022) recently analyzed the contribution of this redox regulation and showed that especially the C-

terminally located Cys pair in PRK is subject to thioredoxin-mediated redox regulation. Oxidation of this Cys pair contributes to decreased PRK activity in the cyanobacterium *Anabaena* sp. PCC 7120, whereas its oxidation supports the binding of PRK into the CP12-GapDH complex in both, the cyanobacterium as well as Arabidopsis (Fukui et al., 2022). Hence, proper PRK regulation is achieved on more layers in cyanobacteria than just CP12, which seems to be the major regulatory measure to regulate GapDH2 and the photosynthetic CBC activity.

Collectively, our results indicate that CP12-dependent regulation of the entire carbon metabolism including the CBC and OPPP is crucial for metabolic adjustment under conditions leading to redox changes. In addition to diurnal conditions, we present evidence that redox changes due to glucose addition, different CO₂ or light conditions also depend on CP12-mediated metabolic fine-tuning in cyanobacteria. In this regard, the proper regulation of GapDH2 seems to be more important than PRK regulation, because the GapDH isoenzymes catalyze opposite reactions in carbon anabolism and catabolism and also use large amounts of NADPH or NADH, thereby significantly contributing to redox changes under the different growth conditions.

Data availability statement

The original contributions presented in the study are included in the article/supplementary material. Further inquiries can be directed to the corresponding author.

Author contributions

MH and KG conceived and planned the experiments. SL constructed mutant strains, performed physiological and biochemical characterization. SH generated fluorescence tagged strains. MT performed fluorescence microscopy and redox measurements. CM contributed to the establishment of fluorescence microscopy and its evaluation. SA processed and analyzed the LC-MS/MS data. MH wrote the manuscript with contributions of all authors. All authors approved the submitted version.

Funding

MH and KG acknowledge the funding from the German Research Foundation in the frame of the research consortium SCyCode (DFG, HA 2002/23-1, GU 1522/5-1, FOR2816) and from the Universities of Rostock and Kassel. SA was supported by The Max Planck Society.

Acknowledgments

The technical assistance of Klaudia Michl at the University of Rostock is acknowledged. We thank the Central Microscopy facility at the Department of Biology at the University of Kiel for assistance to establish microscopic analyses of eYFP-tagged strains.

Conflict of interest

The authors declare that the research was conducted in the absence of any commercial or financial relationships that could be construed as a potential conflict of interest.

References

- Appel, J., Hueren, V., Boehm, M., and Gutekunst, K. (2020). Cyanobacterial *in vivo* solar hydrogen production using a photosystem I-hydrogenase (PsaD-HoxYH) fusion complex. *Nat. Energy* 5, 458–467. doi: 10.1038/s41560-020-0609-6
- Arrivault, S., Guenther, M., Ivakov, A., Feil, R., Vosloh, D., Van Dongen, J. T., et al. (2009). Use of reverse-phase liquid chromatography, linked to tandem mass spectrometry, to profile the Calvin cycle and other metabolic intermediates in arabidopsis rosettes at different carbon dioxide concentrations. *Plant J.* 59, 824–839. doi: 10.1111/j.1365-3113.2009.03902.x
- Avilan, L., Gontero, B., Lebreton, S., and Ricard, J. (1997). Memory and imprinting effects in multienzyme complexes: i. isolation, dissociation, and reassociation of a phosphoribulokinase-glyceraldehyde-3-phosphate dehydrogenase complex from *Chlamydomonas reinhardtii* chloroplasts. *Eur. J. Biochem. FEBS* 246, 78–84. doi: 10.1111/j.1432-1033.1997.00078.x
- Berg, S., Kutra, D., Kroeger, T., Straehle, C. N., Kausler, B. X., Haubold, C., et al. (2019). Ilastik: interactive machine learning for (bio)image analysis. *Nat. Methods* 16, 1226–1232. doi: 10.1038/s41592-019-0582-9
- Blanc-Garin, V., Veaudor, T., Setif, P., Gontero, B., Lemaire, S., Chauvat, F., et al. (2022). First *in vivo* analysis of the regulatory protein CP12 of the model cyanobacterium *Synechocystis* PCC 6803: biotechnological implications. *Front. Plant Sci.* 13, 999672. doi: 10.3389/fpls.2022.999672
- Boehm, M., Alahuhta, M., Mulder, D. W., Peden, E. A., Long, H., Brunecky, R., et al. (2016). Crystal structure and biochemical characterization of chlamydomonas FDX2 reveal two residues that, when mutated, partially confer FDX2 the redox potential and catalytic properties of FDX1. *Photosynth. Res.* 128, 45–57. doi: 10.1007/s11220-015-0198-6
- Erales, J., Avilan, L., Lebreton, S., and Gontero, B. (2008). Exploring CP12 binding proteins revealed aldolase as a new partner for the phosphoribulokinase/glyceraldehyde 3-phosphate dehydrogenase/CP12 complex—purification and kinetic characterization of this enzyme from *Chlamydomonas reinhardtii*. *FEBS J.* 275, 1248–1259. doi: 10.1111/j.1742-4658.2008.06284.x
- Fukui, K., Yoshida, K., Yokochi, Y., Sekiguchi, T., Wakabayashi, K. I., Hisabori, T., et al. (2022). The importance of the c-terminal cys pair of phosphoribulokinase in phototrophs in thioredoxin-dependent regulation. *Plant Cell Physiol.* 63, 855–868. doi: 10.1093/pcp/pcac050
- Gründel, M., Scheunemann, R., Lockau, W., and Zilliges, Y. (2012). Impaired glycogen synthesis causes metabolic overflow reactions and affects stress responses in the cyanobacterium *Synechocystis* sp. PCC 6803. *Microbiology* 158, 3032–3043. doi: 10.1099/mic.0.062950-0
- Gurrieri, L., Fermani, S., Zaffagnini, M., Sparla, F., and Trost, P. (2022). Calvin-Benson Cycle regulation is getting complex. *Trends Plant Sci.* 26, 898–912. doi: 10.1016/j.tplants.2021.03.008
- Hackenberg, C., Hakanpaa, J., Cai, F., Antonyuk, S., Eigner, C., Meissner, S., et al. (2018). Structural and functional insights into the unique CBS-CP12 fusion protein family in cyanobacteria. *Proc. Natl. Acad. Sci. U.S.A.* 115, 7141–7146. doi: 10.1073/pnas.1806668115
- Hackenberg, C., Huege, J., Engelhardt, A., Wittink, F., Laue, M., Matthijs, H. C. P., et al. (2012). Low-carbon acclimation in carboxysome-less and photorespiratory mutants of the cyanobacterium *Synechocystis* sp. strain PCC 6803. *Microbiology* 158, 398–413. doi: 10.1099/mic.0.054544-0
- Hagemann, M., Song, S., and Brouwer, E. M. (2021). “Inorganic carbon assimilation in cyanobacteria: Mechanisms, regulation, and engineering,” in *Cyanobacteria biotechnology*. Eds. P. Hudson, S. Y. Lee and J. Nielsen (Weinheim, Germany, Wiley-Blackwell Biotechnology Series), 1–31. doi: 10.1002/9783527824908.ch1
- Hagemann, M., and Hess, W. R. (2018). Systems and synthetic biology for the biotechnological application of cyanobacteria. *Curr. Opin. Biotechnol.* 49, 94–99. doi: 10.1016/j.copbio.2017.07.008
- Hihara, Y., Kamei, A., Kanehisa, M., Kaplan, A., and Ikeuchi, M. (2001). DNA Microarray analysis of cyanobacterial gene expression during acclimation to high light. *Plant Cell* 13, 793–806. doi: 10.1105/tpc.13.4.793
- Hohmann-Marriott, M. F., and Blankenship, R. E. (2011). Evolution of photosynthesis. *Ann. Rev. Plant Biol.* 62, 515–548. doi: 10.1146/annurev-arplant-042110-103811
- Koksharova, O., Schubert, H., Shestakov, S., and Cerff, R. (1998). Genetic and biochemical evidence for distinct key functions of two highly divergent GAPDH genes in catabolic and anabolic carbon flow of the cyanobacterium *Synechocystis* sp. PCC 6803. *Plant Mol. Biol.* 36, 183–194. doi: 10.1023/a:1005925732743
- Liu, X., Xie, H., Roussou, S., and Lindblad, P. (2022). Current advances in engineering cyanobacteria and their applications for photosynthetic butanol production. *Curr. Opin. Biotechnol.* 73, 143–150. doi: 10.1016/j.copbio.2021.07.014
- López-Calcano, P. E., Abuzaid, A. O., Lawson, T., and Raines, C. A. (2017). Arabidopsis CP12 mutants have reduced levels of phosphoribulokinase and impaired function of the Calvin-Benson cycle. *J. Exp. Bot.* 68, 2285–2298. doi: 10.1093/jxb/erx084
- López-Calcano, P. E., Howard, T. P., and Raines, C. A. (2014). The CP12 protein family: a thioredoxin-mediated metabolic switch? *Front. Plant Sci.* 5. doi: 10.3389/fpls.2014.00009
- Lucius, S., Makowka, A., Michl, K., Gutekunst, K., and Hagemann, M. (2021). The entner-doudoroff pathway contributes to glycogen breakdown during high to low CO₂ shifts in the cyanobacterium *Synechocystis* sp. PCC 6803. *Front. Plant Sci.* 12. doi: 10.3389/fpls.2021.787943
- Mahbub, M., Hemm, L., Yang, Y., Kaur, R., Carmen, H., Engl, C., et al. (2020). mRNA localization, reaction centre biogenesis and thylakoid membrane targeting in cyanobacteria. *Nat. Plants* 6, 1179–1191. doi: 10.1038/s41477-020-00764-2
- McFarlane, C. R., Shah, N. R., Kabasakal, B. V., Echeverria, B., Cotton, C. A. R., Bubeck, D., et al. (2019). Structural basis of light-induced redox regulation in the Calvin-Benson cycle in cyanobacteria. *Proc. Natl. Acad. Sci. U.S.A.* 116, 20984–20990. doi: 10.1073/pnas.1906722116
- Moparthy, S. B., Thieulin-Pardo, G., de Torres, J., Ghenuche, P., Gontero, B., and Wenger, J. (2015). FRET analysis of CP12 structural interplay by GAPDH and PRK. *Biochem. Biophys. Res. Commun.* 458, 488–493. doi: 10.1016/j.bbrc.2015.01.135

Publisher's note

All claims expressed in this article are solely those of the authors and do not necessarily represent those of their affiliated organizations, or those of the publisher, the editors and the reviewers. Any product that may be evaluated in this article, or claim that may be made by its manufacturer, is not guaranteed or endorsed by the publisher.

Supplementary material

The Supplementary Material for this article can be found online at: <https://www.frontiersin.org/articles/10.3389/fpls.2022.1028794/full#supplementary-material>

- Oren, N., Timm, S., Frank, M., Mantovani, O., Murik, O., and Hagemann, M. (2021). Red/far-red light signals regulate the activity of the carbon-concentrating mechanism in cyanobacteria. *Sci. Adv.* 7, eabg0435. doi: 10.1126/sciadv.abg0435
- Rippka, R., Deruelles, J., Waterbury, J. B., Herdman, M., and Stanier, R. Y. (1979). Generic assignments, strain histories and properties of pure cultures of cyanobacteria. *J. Gen. Microbiol.* 111, 1–61. doi: 10.1099/00221287-111-1-1
- Schindelin, J., Arganda-Carreras, I., Frise, E., Kaynig, V., Longair, M., Pietzsch, T., et al. (2012). Fiji: an open-source platform for biological-image analysis. *Nat. Methods* 9, 676–682. doi: 10.1038/nmeth.2019
- Schulze, D., Kohlstedt, M., Becker, J., Cahoreau, E., Peyriga, L., Makowka, A., et al. (2022). GC/MS-based ¹³C metabolic flux analysis resolves the parallel and cyclic photomixotrophic metabolism of *Synechocystis* sp. PCC 6803 and selected deletion mutants including the entner-doudoroff and phosphoketolase pathways. *Microb. Cell Fact.* 21, 69. doi: 10.1186/s12934-022-01790-9
- Spät, P., Barske, T., Maček, B., and Hagemann, M. (2021). Alterations in the CO₂ availability induce alterations in the phospho-proteome of the cyanobacterium *Synechocystis* sp. PCC 6803. *New Phytol.* 231, 1123–1137. doi: 10.1111/nph.17423
- Stanley, D. N., Raines, C. A., and Kerfeld, C. A. (2012). Comparative analysis of 126 cyanobacterial genomes reveals evidence of functional diversity among homologs of the redox-regulated CP12 protein. *Plant Physiol.* 161, 824–835. doi: 10.1104/pp.112.210542
- Sugiura, K., Yokochi, Y., Fu, N., Fukaya, Y., Yoshida, K., Mihara, S., et al. (2019). The thioredoxin (Trx) redox state sensor protein can visualize trx activities in the light/dark response in chloroplasts. *J. Biol. Chem.* 294, 12091–12098. doi: 10.1074/jbc.RA119.007616
- Sundaram, S., Karakaya, H., Scanlan, D. J., and Mann, N. H. (1998). Multiple oligomeric forms of glucose-6-phosphate dehydrogenase in cyanobacteria and the role of OpcA in the assembly process. *Microbiology* 144, 1549–1556. doi: 10.1099/00221287-144-6-1549
- Tamoi, M., Miyazaki, T., Fukamizo, T., and Shigeoka, S. (2005). The Calvin cycle in cyanobacteria is regulated by CP12 via the NAD(H)/NADP(H) ratio under light/dark conditions. *Plant J.* 42, 504–513. doi: 10.1111/j.1365-313X.2005.02391.x
- Wang, Y., Chen, X., Spengler, K., Terberger, K., Boehm, M., Appel, J., et al. (2022). Pyruvate:ferredoxin oxidoreductase and low abundant ferredoxins support aerobic photomixotrophic growth in cyanobacteria. *Elife* 11, e71339. doi: 10.7554/eLife.71339
- Wang, H., Gau, B., Slade, W. O., Juergens, M., Li, P., and Hicks, L. M. (2014). The global phosphoproteome of *Chlamydomonas reinhardtii* reveals complex organellar phosphorylation in the flagella and thylakoid membrane. *Mol. Cell. Prot.* 13, 2337–2353. doi: 10.1074/mcp.M114.038281
- Wedel, N., and Soll, Jürgen (1998). Evolutionary conserved light regulation of Calvin cycle activity by NADPH-mediated reversible phosphoribulokinase/CP12/glyceraldehyde-3-phosphate dehydrogenase complex dissociation. *Proc. Natl. Acad. Sci. U.S.A.* 95, 9699–9704. doi: 10.1073/pnas.95.16.9699
- Yu, A., Xie, Y., Pan, X., Zhang, H., Cao, P., Su, X., et al. (2020). Photosynthetic phosphoribulokinase structures: Enzymatic mechanisms and the redox regulation of the Calvin-Benson-Bassham cycle. *Plant Cell* 32, 1556–1573. doi: 10.1105/tpc.19.00642
- Zinchenko, V. V., Piven, I. V., Melnik, V. A., and Shestakov, S. V. (1999). Vectors for the complementation analysis of cyanobacterial mutants. *Russ. J. Genet.* 35, 228–232.

Supplementary Data of the Frontiers in Plant Science manuscript

CP12 fine-tunes the Calvin-Benson cycle and carbohydrate metabolism in cyanobacteria

Running title: Role of CP12 in *Synechocystis*

Stefan Lucius¹, Marius Theune^{2,3}, Stéphanie Arrivault⁴, Sarah Hildebrandt³, Conrad W. Mullineaux⁵, Kirstin Gutekunst^{2,3}, Martin Hagemann^{1*}

1 - University Rostock, Department Plant Physiology, Albert-Einstein-Str. 3, 18059 Rostock, Germany

2 – University Kassel, Molecular Plant Physiology, Bioenergetics in Photoautotrophs, Heinrich-Plett-Str. 40, 34132 Kassel, Germany

3 - University Kiel, Botanical Institute, Am Botanischen Garten 5, 24118 Kiel, Germany

4 - Max Planck Institute of Molecular Plant Physiology, Am Mühlenberg 1, 14476 Potsdam-Golm, Germany

5 – School of Biological and Behavioural Sciences, Queen Mary University of London, London, United Kingdom

***Corresponding author:** Martin Hagemann, Institut für Biowissenschaften, Abteilung Pflanzenphysiologie, Universität Rostock, Albert-Einstein-Str. 3, Rostock D-18059, Germany; Tel: +49(0)3814986110; Fax: +49(0)3814986112; Email: martin.hagemann@uni-rostock.de

Table S1: List of strains investigated in the present study

Table S2: List of oligonucleotides used in the present study

Figure S1: Schematic view on CP12-mediated redox regulation of GapDH and PRK

Figure S2: Insert sequences for $\Delta cp12$ complementation constructs

Figure S3: Schematics of plasmids for creation of $\Delta cp12$ and complementation strains

Figure S4: Genotyping by PCR of $\Delta cp12$ and complementation strains

Figure S5: Genotyping by PCR of eYFP-tagged strains

Figure S6: Western blot analysis of eYFP tagged strains

Figure S7: Growth of eYFP-tagged strains

Figure S8: Growth of wild type and mutant $\Delta cp12$ under permissive conditions

Figure S9: Photoheterotrophic growth in the presence or absence of DCMU on plates

Figure S10: Ratio of photo-reducible NAD(P)H under different actinic light intensities

Figure S11: NAD(P)H oxidation kinetics in GapDH-eYFP and PRK-eYFP cells adapted to different light intensities

Supplementary Data 1: Metadata to obtain microscopic images

Supplementary Data 2: Video of PRK-eYFP-His and GapDH2-eYFP-His strains under light-dark and dark-light transition

Supplementary Table S1. List of strains investigated in the present study.

Strain name	Description
<i>Synechocystis</i> WT	<i>Synechocystis</i> sp. PCC 6803, glucose-tolerant wild type (WT)
$\Delta cp12$	WT with deleted native <i>cp12</i> gene <i>ss/3364</i> , replaced by Kan ^R gene <i>aphII</i>
$\Delta cp12::cp12$ -WT	$\Delta cp12$ with pVZ322 harboring native <i>cp12</i> gene and Spec ^R gene <i>aadA</i>
$\Delta cp12::cp12$ - Δ CysN	$\Delta cp12$ with pVZ322 harboring <i>cp12</i> gene with replaced cysteines C19S-C29S and Spec ^R gene <i>aadA</i>
$\Delta cp12::cp12$ - Δ CysC	$\Delta cp12$ with pVZ322 harboring <i>cp12</i> gene with replaced cysteines C60S-C69S and Spec ^R gene <i>aadA</i>
$\Delta cp12::cp12$ - Δ CysNC	$\Delta cp12$ with pVZ322 harboring <i>cp12</i> gene with replaced cysteines C19S-C29S-C60S-C69S and Spec ^R gene <i>aadA</i>
GapDH-eYFP	WT with c-terminal eYFP-tagged GapDH2 (<i>sl/1342</i>) and Gent ^R gene
PRK-eYFP	WT with c-terminal eYFP-tagged PRK (<i>sl/1525</i>) and Gent ^R gene
GapDH-eYFP:: $\Delta cp12$	GapDH-eYFP with deleted native <i>cp12</i> gene <i>ss/3364</i> replaced by Kan ^R gene <i>aphII</i>
PRK-eYFP:: $\Delta cp12$	PRK-eYFP with deleted native <i>cp12</i> gene <i>ss/3364</i> replaced by Kan ^R gene <i>aphII</i>

Supplementary Table S2. List of oligonucleotides used in the present study.

Primer name	Sequence 5'-3'	Application
cp12-fw	ATGAGCAATATTCAAGAAAAAATCGAAC	genotyping $\Delta cp12$ strains
cp12-rv	CTAGTCGTCGTAAATGCGGCAC	genotyping $\Delta cp12$ strains
cp12-flank-fw	GTACAAGGCCGCAATGGTGAG	genotyping of $\Delta cp12$, GapDH2-eYFP:: $\Delta cp12$ and PRK-eYFP:: $\Delta cp12$ and creation of $\Delta cp12$ strains
cp12-flank-rv	TAGGCGAATTAAGCCAACGTCTGTC	genotyping of $\Delta cp12$, GapDH2-eYFP:: $\Delta cp12$ and PRK-eYFP:: $\Delta cp12$ and creation of $\Delta cp12$ strains
cp12-fw-Sall	GTCGACATGAGCAATATTCAAGAAAAAATCGAAC	generation of $\Delta cp12$ strains
cp12-rv-NdeI	CATATGCTAGTCGTCGTAAATGCGGCAC	generation of $\Delta cp12$ strains
cp12-Fus-P2	TATTGCTCATGTCGACAAAGTTTAACCGCTACGATTG	generation of $\Delta cp12$ strains
cp12-Fus-P3	CGACGACTAGCATATGGGGCTGATGGGGCAAACCC	generation of $\Delta cp12$ strains
YFP-for	AGGGCGGCGCTAGCATGGTGAGCAAGGGCGAGGAGCTGTT	generation of pRSETA-Cr_eYFP-His
YFP-rev	GTGATGGTGATGGTGATGCCCGGGCTTGACAGCTCGTCCA	generation of pRSETA-Cr_eYFP-His
YFP-His-GENT-Fw	CACCATCACCATCACTAAGATGTCGACGGATGAAGGCACGAA	generation of pRSETA-Cr_eYFP-His_Gent
GENT-Rev	CAAGCTTCGAATTCCTAGATGTCGACCGAATTGTTAGGTGG	generation of pRSETA-Cr_eYFP-His_Gent
GapDH2-fw	TTAAAGGAGTGTTGGAATACACCGATTG	Genotyping of GapDH2-eYFP strain
GapDH2-rv	ATGGGGAAAGTTTCGCCGGG	Genotyping of GapDH2-eYFP strain
PRK-fw	TAGAGGAAATGGTTTATGTGGAAAACACC	Genotyping of PRK-eYFP strain
PRK-rev	GGCATCATTATCCTCCCCAGAAATAAGC	Genotyping of PRK-eYFP strain

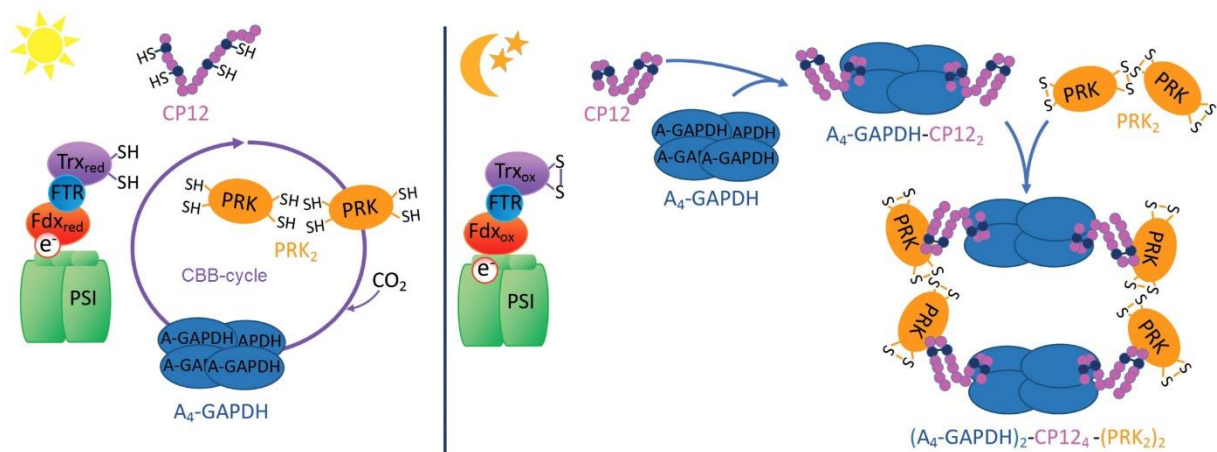


Figure S1: Schematic view on CP12-mediated redox regulation of GapDH and PRK.

Under reducing conditions, i.e. in the light, the CP12 is disordered due to the reduction of all four cysteine residues (depicted as dark dots) via thioredoxin (Trx). The two enzymes glyceraldehyde 3-phosphate dehydrogenase (GAPDH) and phosphoribulokinase (PRK) are active and participate in the CO₂-fixing Calvin-Benson-Bassham cycle (CBB cycle). Under oxidizing conditions, i.e. in the darkness, the CP12 is structured due to the disulfide bond formations at the N- or C-terminal cysteine residues, which then permitted to bind GAPDH and PRK thereby inactivation the CBB cycle.

A

```

a tta aac ttg gga atc ggt gta gtt gac ccc atg ctt tcc cgg agg aaa ctg ttg tga acc tgt gat cat
Leu Asn Leu Gly Ile Gly Val Val Asp Pro Met Leu Ser Arg Arg Lys Leu Leu --- Thr Cys Asp His

ttt cac aat tct tca tac tat ccc cgg tgg tgg ccc cca ggg ccg tat ggg gca agt tga ggt cag caa agt
Phe His Asn Ser Ser Tyr Tyr Pro Arg Trp Trp Pro Pro Gly Pro Tyr Gly Ala Ser --- Gly Gln Gln Ser

gag gaa aac cgc ata ttc ccg ttg tgg ttc ctt cta ccc aaa gcc aac caa att cgc taa cat gaa tga gcc
Glu Glu Asn Arg Ile Phe Pro Leu Trp Phe Leu Leu Pro Lys Ala Asn Gln Ile Arg --- His Glu --- Ala

1 tta ctc tct gta gac aat cgt agg cgg tta aac ttt atg agc aat att caa gaa aaa atc gaa cag gag cta
1 Leu Leu Ser Val Asp Asn Arg Arg Arg Leu Asn Phe Met Ser Asn Ile Gln Glu Lys Ile Glu Gln Glu Leu

37 gcc aac gct aga caa gtt tgc agt acc gat gaa gcc tct ccg gcg gag tgc gct gcg gcc tgg gat gcg gtg
13 Ala Asn Ala Arg Gln Val Cys Ser Thr Asp Glu Ala Ser Pro Ala Glu Cys Ala Ala Ala Trp Asp Ala Val

109 gaa gag cta gaa gcg gaa gcc gcc cac caa cgt caa caa cat ccc acc caa act acc ctg gaa aag ttc tgt
37 Glu Glu Leu Glu Ala Glu Ala Ala His Gln Arg Gln Gln His Pro Thr Gln Thr Thr Leu Glu Lys Phe Cys

181 gac gaa aac ccc gac gct gct gag tgc cgc att tac gac gac tag complementation insert cp12-WT
61 Asp Glu Asn Pro Asp Ala Ala Glu Cys Arg Ile Tyr Asp Asp ---

```

B

```

a tta aac ttg gga atc ggt gta gtt gac ccc atg ctt tcc cgg agg aaa ctg ttg tga acc tgt gat cat
Leu Asn Leu Gly Ile Gly Val Val Asp Pro Met Leu Ser Arg Arg Lys Leu Leu --- Thr Cys Asp His

ttt cac aat tct tca tac tat ccc cgg tgg tgg ccc cca ggg ccg tat ggg gca agt tga ggt cag caa agt
Phe His Asn Ser Ser Tyr Tyr Pro Arg Trp Trp Pro Pro Gly Pro Tyr Gly Ala Ser --- Gly Gln Gln Ser

gag gaa aac cgc ata ttc ccg ttg tgg ttc ctt cta ccc aaa gcc aac caa att cgc taa cat gaa tga gcc
Glu Glu Asn Arg Ile Phe Pro Leu Trp Phe Leu Leu Pro Lys Ala Asn Gln Ile Arg --- His Glu --- Ala

1 tta ctc tct gta gac aat cgt agg cgg tta aac ttt atg agc aat att caa gaa aaa atc gaa cag gag cta
1 Leu Leu Ser Val Asp Asn Arg Arg Arg Leu Asn Phe Met Ser Asn Ile Gln Glu Lys Ile Glu Gln Glu Leu

37 gcc aac gct aga caa gtt agc agt acc gat gaa gcc tct ccg gcg gag agc gct gcg gcc tgg gat gcg gtg
13 Ala Asn Ala Arg Gln Val Ser Ser Thr Asp Glu Ala Ser Pro Ala Glu Ser Ala Ala Ala Trp Asp Ala Val

109 gaa gag cta gaa gcg gaa gcc gcc cac caa cgt caa caa cat ccc acc caa act acc ctg gaa aag ttc tgt
37 Glu Glu Leu Glu Ala Glu Ala Ala His Gln Arg Gln Gln His Pro Thr Gln Thr Thr Leu Glu Lys Phe Cys

181 gac gaa aac ccc gac gct gct gag tgc cgc att tac gac gac tag complementation insert cp12-ΔCysN
61 Asp Glu Asn Pro Asp Ala Ala Glu Cys Arg Ile Tyr Asp Asp ---

```

C

```

a tta aac ttg gga atc ggt gta gtt gac ccc atg ctt tcc cgg agg aaa ctg ttg tga acc tgt gat cat
Leu Asn Leu Gly Ile Gly Val Val Asp Pro Met Leu Ser Arg Arg Lys Leu Leu --- Thr Cys Asp His

ttt cac aat tct tca tac tat ccc cgg tgg tgg ccc cca ggg ccg tat ggg gca agt tga ggt cag caa agt
Phe His Asn Ser Ser Tyr Tyr Pro Arg Trp Trp Pro Pro Gly Pro Tyr Gly Ala Ser --- Gly Gln Gln Ser

gag gaa aac cgc ata ttc ccg ttg tgg ttc ctt cta ccc aaa gcc aac caa att cgc taa cat gaa tga gcc
Glu Glu Asn Arg Ile Phe Pro Leu Trp Phe Leu Leu Pro Lys Ala Asn Gln Ile Arg --- His Glu --- Ala

1 tta ctc tct gta gac aat cgt agg cgg tta aac ttt atg agc aat att caa gaa aaa atc gaa cag gag cta
1 Leu Leu Ser Val Asp Asn Arg Arg Arg Leu Asn Phe Met Ser Asn Ile Gln Glu Lys Ile Glu Gln Glu Leu

37 gcc aac gct aga caa gtt tgc agt acc gat gaa gcc tct ccg gcg gag tgc gct gcg gcc tgg gat gcg gtg
13 Ala Asn Ala Arg Gln Val Cys Ser Thr Asp Glu Ala Ser Pro Ala Glu Cys Ala Ala Ala Trp Asp Ala Val

109 gaa gag cta gaa gcg gaa gcc gcc cac caa cgt caa caa cat ccc acc caa act acc ctg gaa aag ttc agc
37 Glu Glu Leu Glu Ala Glu Ala Ala His Gln Arg Gln Gln His Pro Thr Gln Thr Thr Leu Glu Lys Phe Ser

181 gac gaa aac ccc gac gct gct gag agc cgc att tac gac gac tag complementation insert cp12-ΔCysC
61 Asp Glu Asn Pro Asp Ala Ala Glu Ser Arg Ile Tyr Asp Asp ---

```

D

```

a tta aac ttg gga atc ggt gta gtt gac ccc atg ctt tcc cgg agg aaa ctg ttg tga acc tgt gat cat
Leu Asn Leu Gly Ile Gly Val Val Asp Pro Met Leu Ser Arg Arg Lys Leu Leu --- Thr Cys Asp His

ttt cac aat tct tca tac tat ccc cgg tgg tgg ccc cca ggg ccg tat ggg gca agt tga ggt cag caa agt
Phe His Asn Ser Ser Tyr Tyr Pro Arg Trp Trp Pro Pro Gly Pro Tyr Gly Ala Ser --- Gly Gln Gln Ser

gag gaa aac cgc ata ttc ccg ttg tgg ttc ctt cta ccc aaa gcc aac caa att cgc taa cat gaa tga gcc
Glu Glu Asn Arg Ile Phe Pro Leu Trp Phe Leu Leu Pro Lys Ala Asn Gln Ile Arg --- His Glu --- Ala

1 tta ctc tct gta gac aat cgt agg cgg tta aac ttt atg agc aat att caa gaa aaa atc gaa cag gag cta
1 Leu Leu Ser Val Asp Asn Arg Arg Arg Leu Asn Phe Met Ser Asn Ile Gln Glu Lys Ile Glu Gln Glu Leu

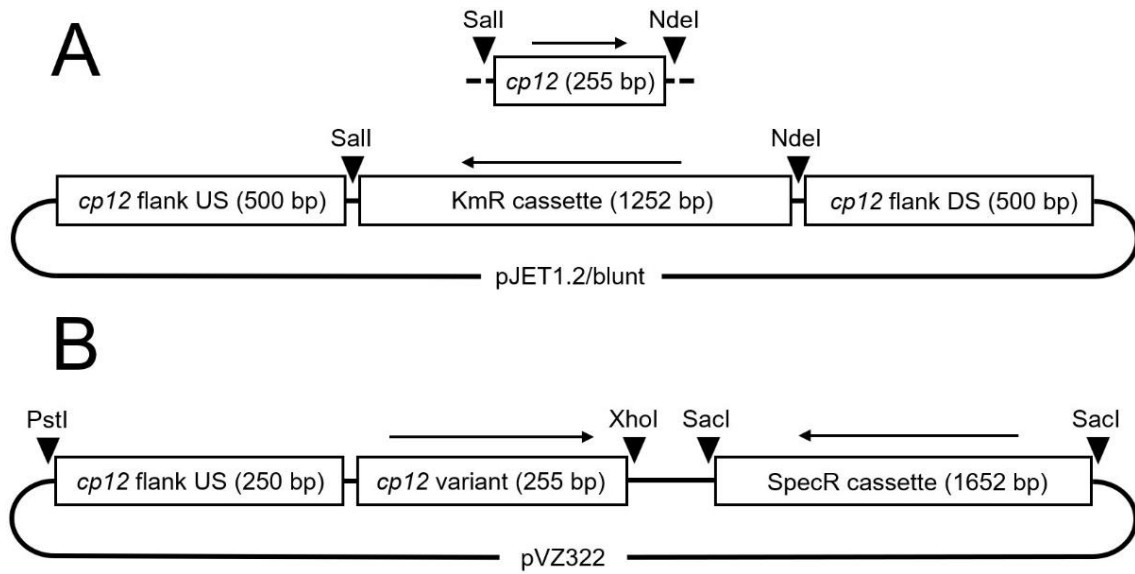
37 gcc aac gct aga caa gtt agc agt acc gat gaa gcc tct ccg gcg gag agc gct gcg gcc tgg gat gcg gtg
13 Ala Asn Ala Arg Gln Val Ser Ser Thr Asp Glu Ala Ser Pro Ala Glu Ser Ala Ala Ala Trp Asp Ala Val

109 gaa gag cta gaa gcg gaa gcc gcc cac caa cgt caa caa cat ccc acc caa act acc ctg gaa aag ttc agc
37 Glu Glu Leu Glu Ala Glu Ala Ala His Gln Arg Gln Gln His Pro Thr Gln Thr Thr Leu Glu Lys Phe Ser

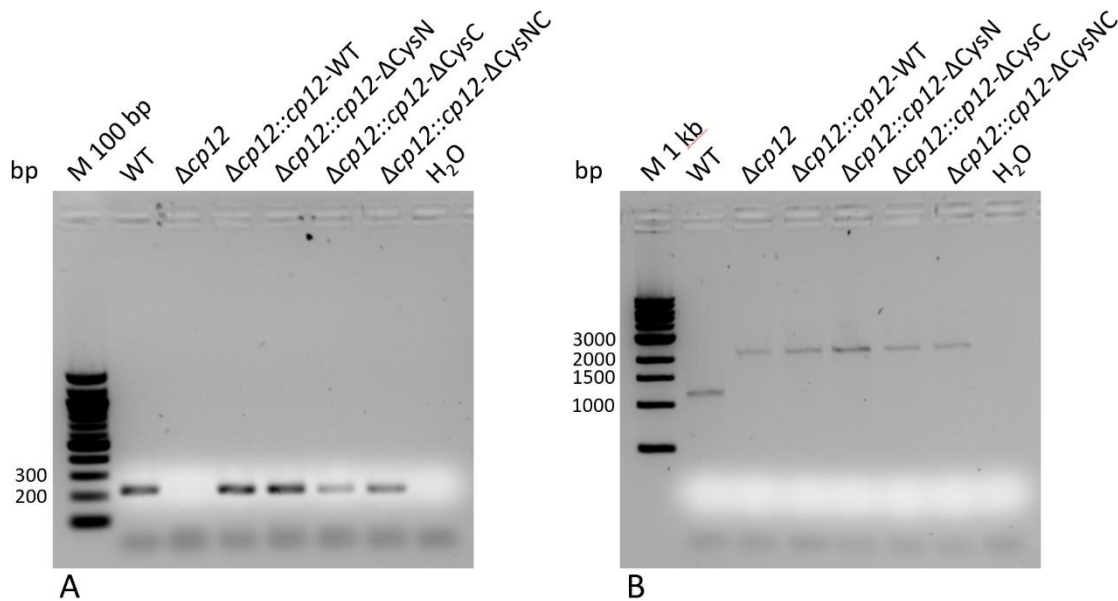
181 gac gaa aac ccc gac gct gct gag agc cgc att tac gac gac tag complementation insert cp12-ΔCysNC
61 Asp Glu Asn Pro Asp Ala Ala Glu Ser Arg Ile Tyr Asp Asp ---

```

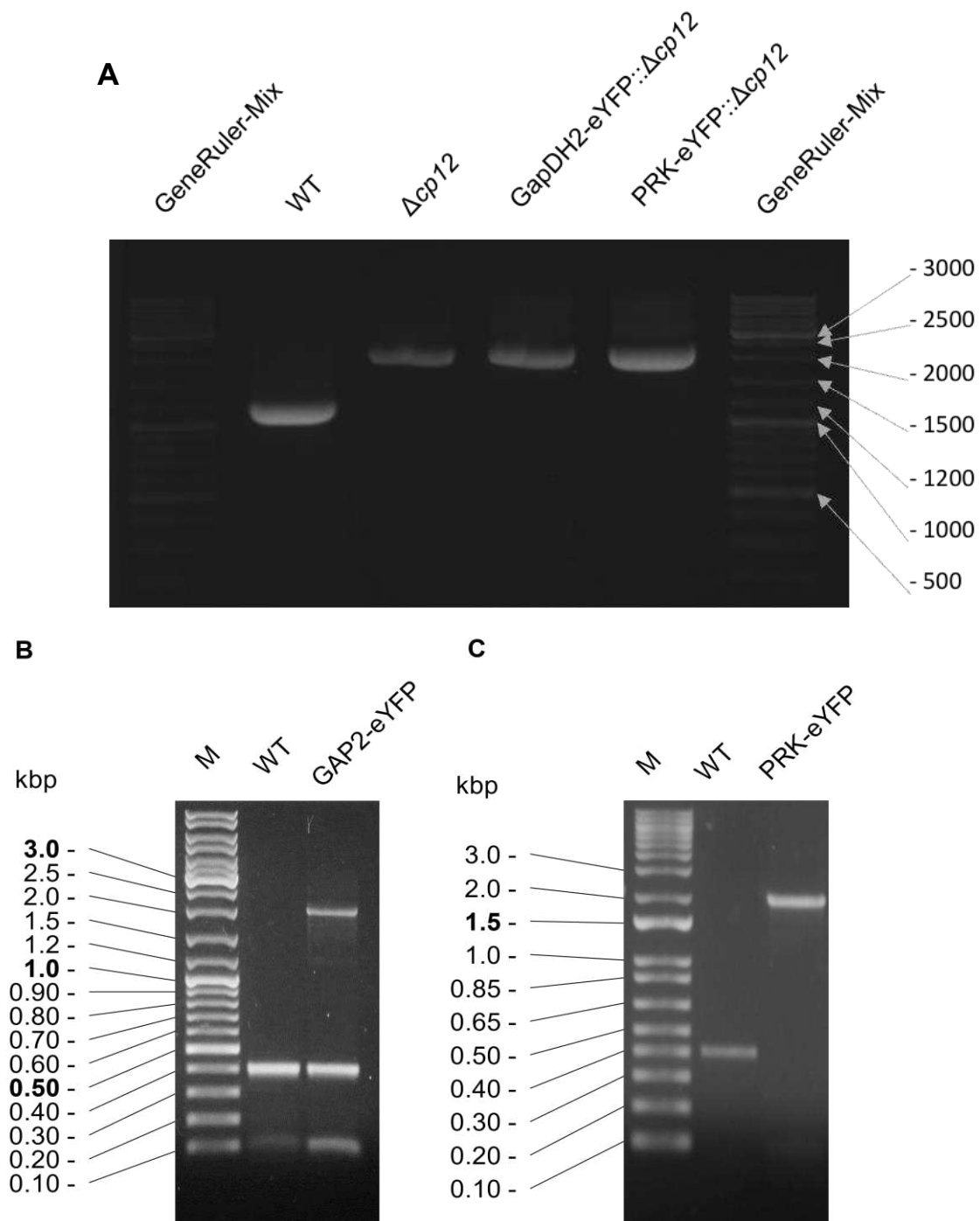
Supplementary Figure S2: Insert sequences for $\Delta cp12$ complementation constructs. Variants of *cp12* gene sequence have been synthesized and cloned into vector pVZ322. Black boxes indicate locations of cysteines or their replacement for serines, respectively. Black letters mark putative native promoter sequence of *cp12*. Red letters mark *cp12* gene sequence. **A** - native *cp12*. **B** - N-terminal cysteine pair replaced by serines. **C** - C-terminal cysteine pair replaced by serines. **D** - both cysteine pairs replaced by serines.



Supplementary Figure S3: Schematic drawings of plasmids for the generation of $\Delta cp12$ and complementation strains. A: *cp12* deletion mutant construct. **B:** example for generation of *cp12* complementation strains.

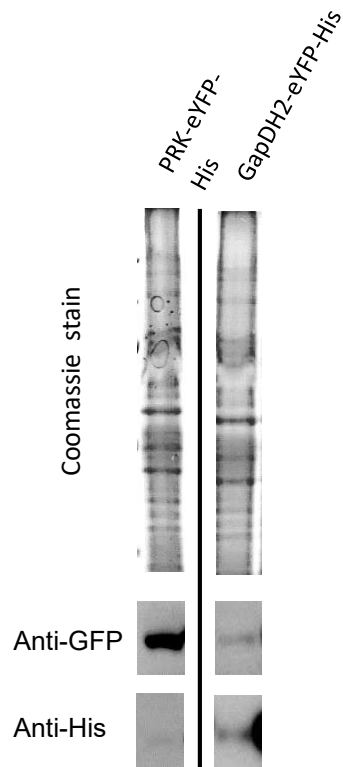


Supplementary Figure S4: Genotyping by PCR of $\Delta cp12$ and complementation strains. A - amplification with *cp12* gene specific primers *cp12-fw/cp12-rv*. **B** - amplification with *cp12* gene flanking primers *cp12-flank-fw/cp12-flank-rv* that bind 500 bp upstream or downstream of *cp12*. DNA from the different strains used for PCR is given for each lane. PCR results confirm complete segregation of all mutant strains.



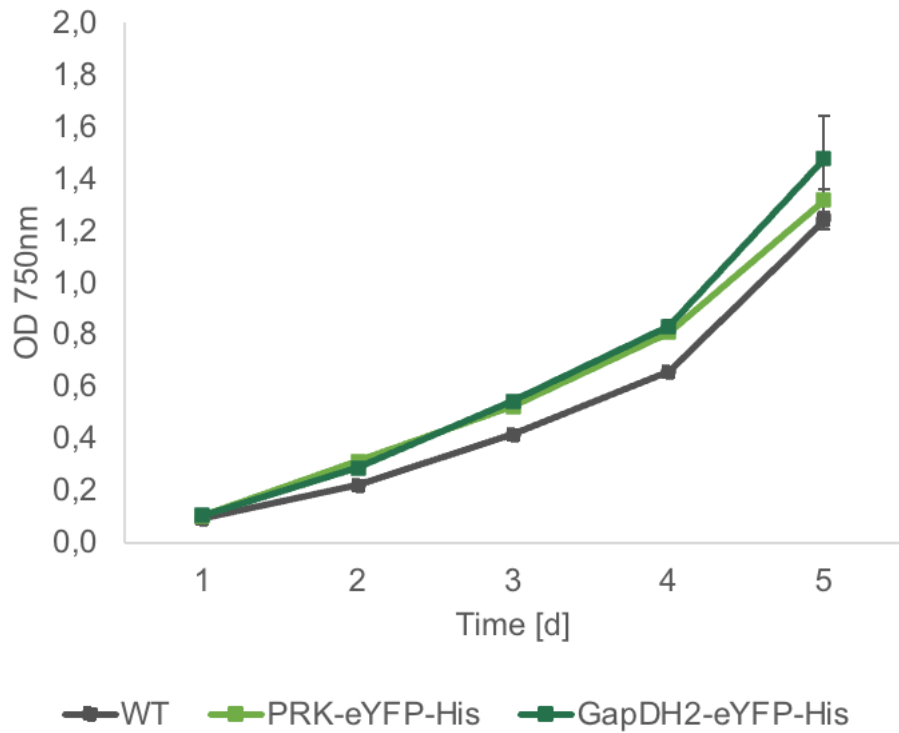
Supplementary Figure S5: Genotyping by PCR of eYFP-tagged strains.

A - Amplification of the *cp12* gene using primers cp12-flank-fw/cp12-flank-rv that bind 500 bp upstream or downstream of *cp12*. **B**- Amplification of the *gapDH2* gene using primers GapDH2-fw/GapDH2-rv that bind 250 bp upstream or downstream of the *gapDH2* gene. **C**- Amplification of the *prk* gene using primers PRK-fw/PRK-rv that bind 250 bp upstream or downstream of the *prk* gene. The template-DNAs were isolated from different strains as specified above each lane. PCR results confirm complete segregation of all mutant strains except GapDH2-eYFP.

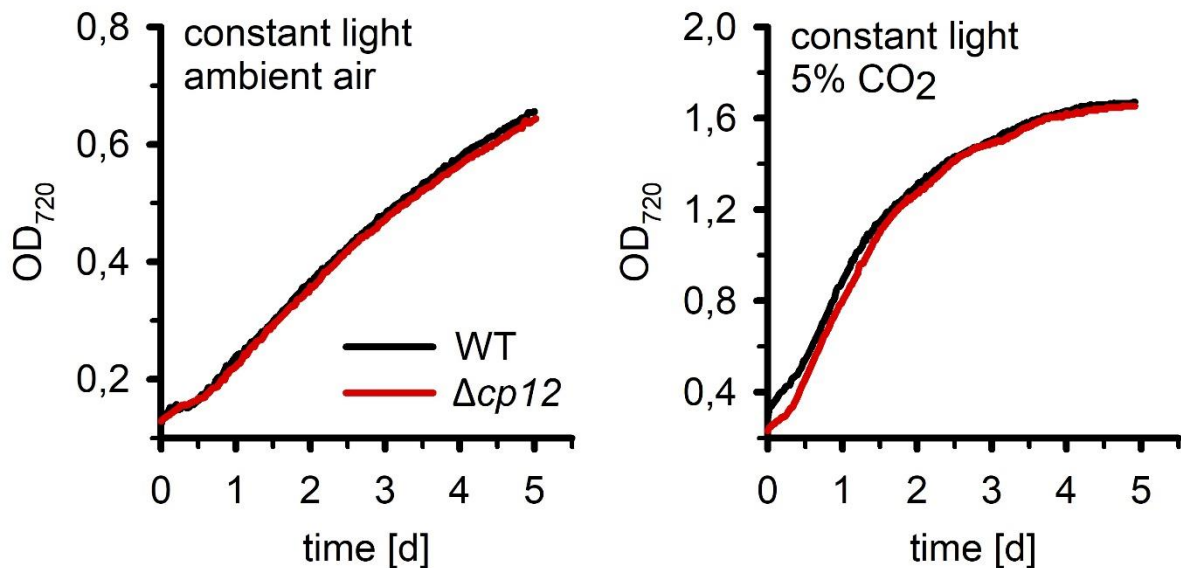


Supplementary Figure S6: Verification of the protein expression of the GapDH2-eYFP-His and PRK-eYFP-His by Western-blotting.

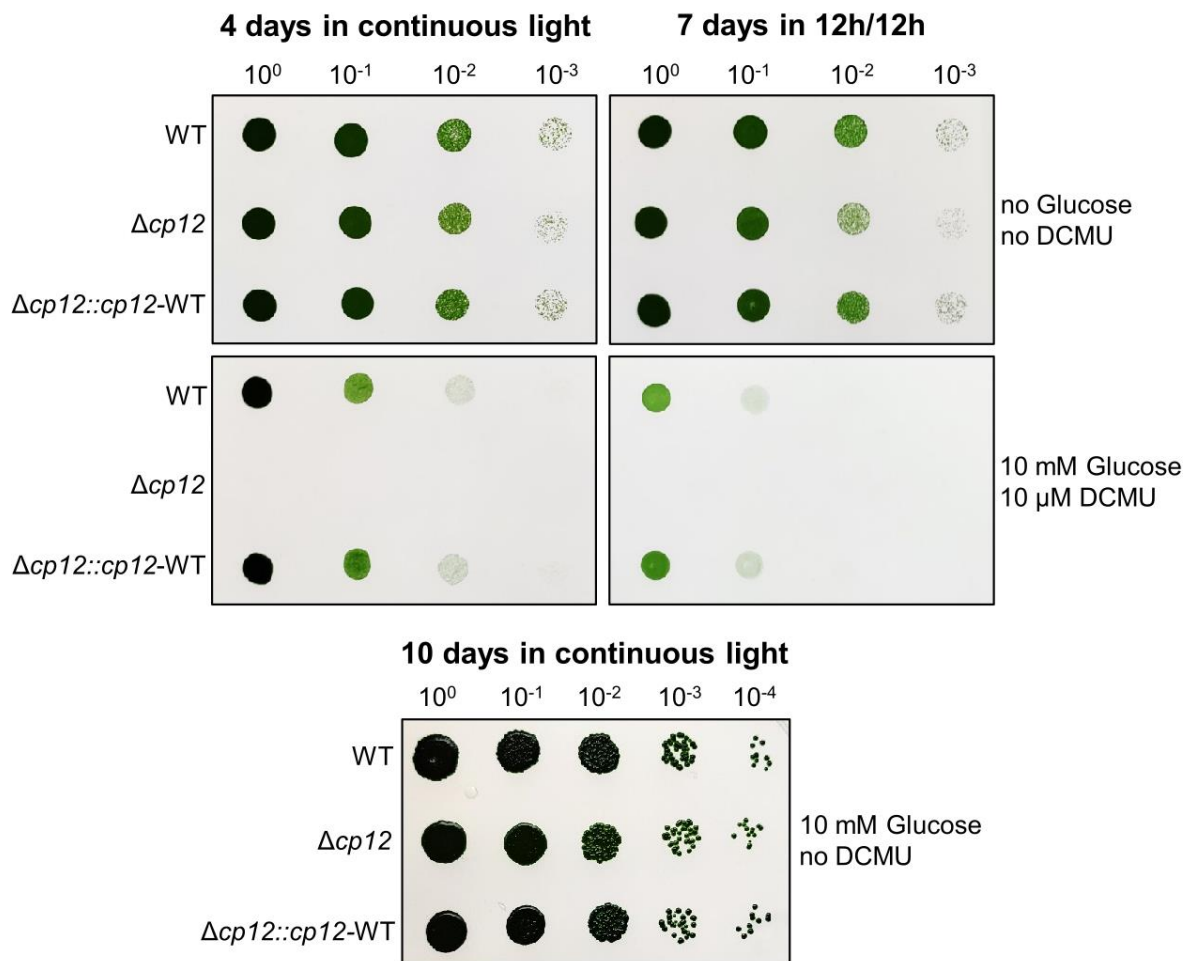
Cells were cultivated under photoautotrophic conditions in BG11. Whole-cell extracts were used to verify that the attached eYFP-His of the respective tagged proteins are expressed and that the fluorophores are bound to the protein of interest. The same amount of chlorophyll (0.15 μg) was loaded to each lane. Anti-GFP and anti_His antibodies showed a signal at the expected sizes: PRK-eYFP-His ~53 kDa; GapDH2-eYFP-His ~68kDa.



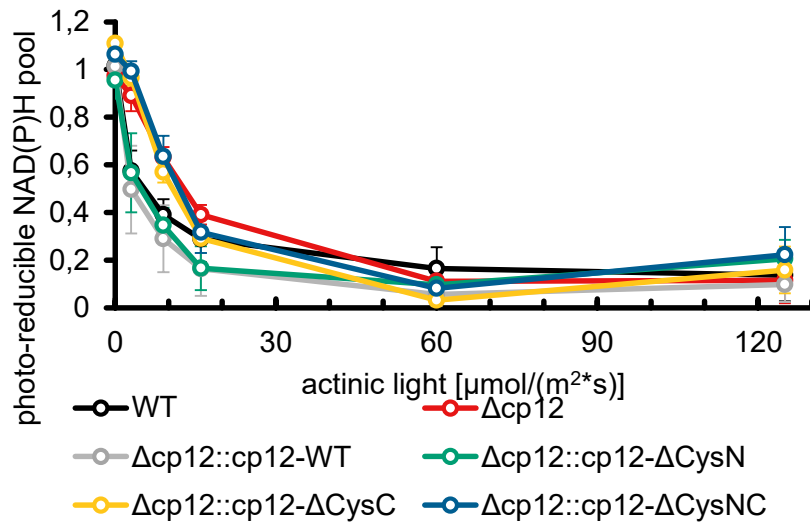
Supplementary Figure S7: Growth of eYFP-tagged strains under standard conditions. Growth of eYFP tagged strains was monitored under photoautotrophic conditions with bubbling by ambient air.



Supplementary Figure S8: Growth of wild type and mutant $\Delta cp12$ under permissive conditions. Cultures were grown at ambient air (0.04% CO₂, LC) and high CO₂ conditions (5% CO₂, HC). The increase of OD₇₂₀ is displayed compared as proxy of biomass.

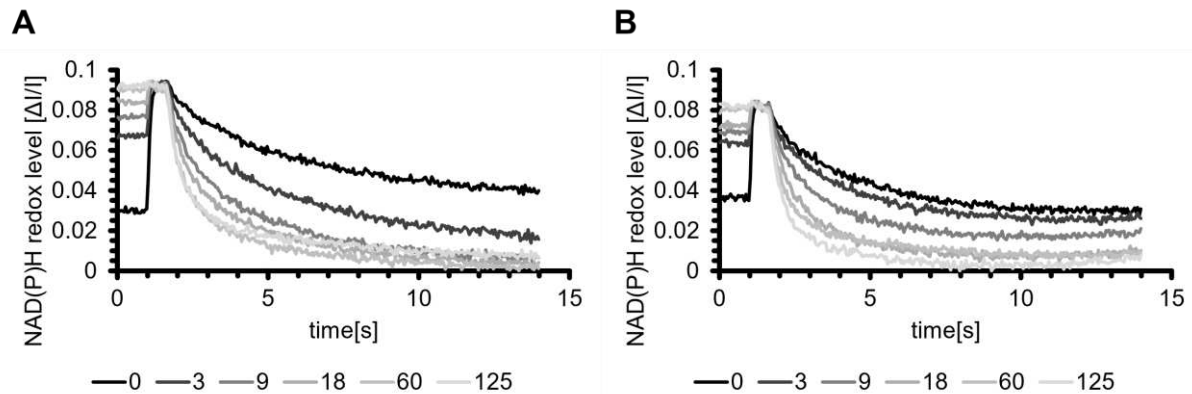


Supplementary Figure S9: Photoheterotrophic growth in the presence or absence of DCMU on plates. Liquid cultures were grown in shaking flasks under photoautotrophic conditions for three days. Samples of 1 ml culture were taken and their OD₇₅₀ was adjusted to 0.7 (dilution 10⁰) with fresh BG-11 for the drop dilution assays. A dilution series up to 10⁻⁴ was created for each strain and drops of 2 μ l culture were pipetted in a grid on 1.5% bacto agar BG-11 plates containing combinations of 10 mM glucose and 10 μ M DCMU or none of these additions. The plates were then incubated in either continuous light or diurnal conditions for the indicated time periods.



Supplementary Figure S10: Photo-reducible NAD(P)H level in different strains at increasing light conditions.

Cells of strains expressing different CP12 variants were acclimated to different actinic light conditions. Then, they were used for measurements in the NADPH-Modul (Walz, Germany) to determine the NAD(P)H reduction in darkness after a 600 ms long strong actinic light pulse.



Supplementary Figure S11: NAD(P)H oxidation kinetics in GapDH-eYFP and PRK-eYFP cells adapted to different light intensities

NAD(P)H redox changes measured *in vivo* via NAD(P)H fluorescence in GapDH-eYFP (A) or PRK-eYFP cells (B). The NAD(P)H pool was reduced to its maximum with a strong actinic light pulse (600 ms) and its re-oxidation in darkness was observed. The measured cells were pre-acclimated to the 5 different actinic light intensities or to darkness.

11.3 Publication III: The novel P_{II}-interactor PirC identifies phosphoglycerate mutase as key control point of carbon storage metabolism in cyanobacteria

Orthwein, T., Scholl, J., Spät, P., **Lucius, S.**, Koch, M., Macek, B., Hagemann, M., & Forchhammer, K. (2021). *Proceedings of the National Academy of Sciences*, (2021), 2019988118, 118(6).



The novel P_{II}-interactor PirC identifies phosphoglycerate mutase as key control point of carbon storage metabolism in cyanobacteria

Tim Orthwein^{a,1} , Jörg Scholl^{a,1} , Philipp Spät^{b,1} , Stefan Lucius^c, Moritz Koch^a , Boris Macek^b , Martin Hagemann^c , and Karl Forchhammer^{a,2}

^aInterfaculty Institute of Microbiology and Infection Medicine, University of Tübingen, 72076 Tübingen, Germany; ^bDepartment of Quantitative Proteomics, University of Tübingen, 72076 Tübingen, Germany; and ^cInstitute of Biological Sciences, Plant Physiology Department, University of Rostock, 18059 Rostock, Germany

Edited by Susan S. Golden, University of California San Diego, La Jolla, CA, and approved December 9, 2020 (received for review September 23, 2020)

Nitrogen limitation imposes a major transition in the lifestyle of nondiazotrophic cyanobacteria that is controlled by a complex interplay of regulatory factors involving the pervasive signal processor P_{II}. Immediately upon nitrogen limitation, newly fixed carbon is redirected toward glycogen synthesis. How the metabolic switch for diverting fixed carbon toward the synthesis of glycogen or of cellular building blocks is operated was so far poorly understood. Here, using the nondiazotrophic cyanobacterium *Synechocystis* sp. PCC 6803 as model system, we identified a novel P_{II} interactor, the product of the *slI0944* gene, which we named PirC. We show that PirC binds to and inhibits the activity of 2,3-phosphoglycerate-independent phosphoglycerate mutase (PGAM), the enzyme that deviates newly fixed CO₂ toward lower glycolysis. The binding of PirC to either P_{II} or PGAM is tuned by the metabolite 2-oxoglutarate (2-OG), which accumulates upon nitrogen starvation. In these conditions, the high levels of 2-OG dissociate the PirC–P_{II} complex to promote PirC binding to and inhibition of PGAM. Accordingly, a PirC-deficient mutant showed strongly reduced glycogen levels upon nitrogen deprivation, whereas polyhydroxybutyrate granules were overaccumulated compared to wild-type. Metabolome analysis revealed an imbalance in 3-phosphoglycerate to pyruvate levels in the *pirC* mutant, confirming that PirC controls the carbon flux in cyanobacteria via mutually exclusive interaction with either P_{II} or PGAM.

glycogen metabolism | polyhydroxybutyrate | cyanobacteria | nitrogen starvation | carbon flow

Cellular homeostasis relies on the capacity of living systems to adjust their metabolism in response to changes in the environment. Therefore, organisms must be able to sense the metabolic state and tune it in response to environmental fluctuations. It has been proposed that cyanobacteria do not extensively rely on direct environmental sensing but rather are primarily concerned about their internal metabolic state (1). This “introvert” lifestyle requires that they constantly and precisely monitor their intracellular milieu in order to detect imbalances caused by external perturbations. The maintenance of carbon/nitrogen (C/N) homeostasis is one of the most fundamental aspects of cellular physiology. For photoautotrophic organisms like cyanobacteria, it is essential to tightly interconnect CO₂ fixation and nitrogen assimilation. To fulfill this task, cyanobacteria use a sophisticated signaling network organized by the pervasive P_{II}-signaling protein. P_{II} proteins are fundamental for this task in most free-living prokaryotes and chloroplasts of green plants (2). They act as multitasking signal integrators, combining information on the metabolic C/N balance through interaction with the metabolite 2-oxoglutarate (2-OG) and on the cellular energy state by competitive adenosine triphosphate (ATP) or adenosine diphosphate (ADP) binding. 2-OG is ideally suited as a status reporter metabolite for C/N balance, as this tricarboxylic acid (TCA) cycle intermediate represents the precursor metabolite into which

ammonia is incorporated through the nitrogen assimilatory reactions catalyzed by the glutamine-synthetase–glutamate-synthase (GS/GOGAT) cycle (3).

The interaction of P_{II} proteins with various effector molecules, the conformational changes that ensue from these interactions, and their perception by the targets have been elaborated in great detail [recently reviewed (3–6)]. The three intersubunit clefts of the trimeric P_{II} proteins contain intercommunicating effector-molecule-binding sites; ADP and ATP compete for occupying these sites, and binding of ATP, but not ADP, creates a coordination sphere for the effector 2-OG through a bridging Mg²⁺ ion. Depending on the effector molecules bound, the large and flexible target-binding loops (termed T-loops), protruding from the effector binding sites, can adopt specific conformations, allowing signal receptor proteins to read out the metabolic information through protein–protein interactions (5). A variety of key metabolic enzymes, transcription factors, and transport proteins use this signaling path to tune their activity in response to the metabolic state. P_{II} in its different conformations can directly interact with various target proteins such as the N-acetyl-L-glutamate kinase, catalyzing the committed step in arginine

Significance

In this work, we identified the regulatory mechanism of the key control point of cyanobacterial carbon metabolism, the glycolytic phosphoglycerate mutase (PGAM) reaction, converting 3-PGA into 2-PGA and thereby exporting organic carbon from the photosynthetic Calvin cycle. We show that PGAM activity is controlled by a small modulator protein PirC (product of *slI0944*), which inhibits the enzyme through protein–protein interaction. The availability of PirC for PGAM inhibition is controlled by the pervasive carbon/nitrogen balance regulator P_{II}, which sequesters PirC at low 2-oxoglutarate levels and releases it at high 2-oxoglutarate levels. PirC-mediated inhibition of PGAM triggers glycogen accumulation, and disrupting this regulation allows the redirection of carbon flux, a decisive requirement for transforming cyanobacteria into green factories.

Author contributions: K.F. designed research; T.O., J.S., P.S., S.L., and M.K. performed research; B.M. contributed new reagents/analytic tools; T.O., J.S., P.S., B.M., M.H., and K.F. analyzed data; and K.F. wrote the paper.

The authors declare no competing interest.

This article is a PNAS Direct Submission.

This open access article is distributed under [Creative Commons Attribution-NonCommercial-NoDerivatives License 4.0 \(CC BY-NC-ND\)](https://creativecommons.org/licenses/by-nc-nd/4.0/).

¹T.O., J.S., and P.S. contributed equally to this work.

²To whom correspondence may be addressed. Email: karl.forchhammer@uni-tuebingen.de.

This article contains supporting information online at <https://www.pnas.org/lookup/suppl/doi:10.1073/pnas.2019988118/-DCSupplemental>.

Published February 1, 2021.

biosynthesis (7, 8); the acetyl-CoA carboxylase, catalyzing the rate-limiting step in fatty acid biosynthesis (9); the phosphoenolpyruvate carboxylase, which catalyzes an anaplerotic carbon fixation (10); or the glutamine-dependent nicotinamide adenine dinucleotide (NAD⁺) synthetase (11). Besides tuning the activity of enzymes, recent analyses revealed that, through direct protein–protein interaction, the abundant P_{II} proteins can also regulate transport activities, including an ensemble of nitrogen transporters such as the nitrate/nitrite transport system, the urea transport system, and the ammonium transporter (12).

A different mechanism underlies the ability of P_{II} proteins to modulate gene expression in response to different C/N ratios. In this case, the effect of P_{II} proteins is mediated through binding to a small signaling mediator protein called PipX (P_{II}-interacting protein X), which acts as a transcriptional coactivator of the global nitrogen control transcription factor NtcA. The latter controls a large regulon of about 80 genes (13). The mediator PipX swaps between P_{II}- and NtcA-bound states, thereby either tuning down or stimulating the activity of NtcA, respectively (6, 14). Partner swapping of PipX occurs in response to the effector molecule 2-OG and the ATP/ADP balance (14).

In a previous P_{II} protein interaction study, several putative P_{II} interactors of unknown function were identified (12). The most prominent hit was the product of the *slI0944* gene, a member of the NtcA regulon (11, 13). The *slI0944* gene product is annotated in Uniprot (<https://www.uniprot.org/uniprot/P77971>) as a protein of unknown function. Close homologs are widespread in the cyanobacterial phylum, pointing to an important function of this protein in the cyanobacterial metabolism. We previously observed that *slI0944* is up-regulated both at the transcriptional (15) and posttranscriptional (16) level during the response of the model cyanobacterium *Synechocystis* PCC 6803 (from now on termed *Synechocystis*) to nitrogen starvation. Following nitrogen depletion, the CO₂-fixation products are redirected toward glycogen synthesis, and, concomitantly, the phycobiliproteins and the entire photosynthetic machinery are proteolytically degraded, causing loss of pigments of the cells (referred as chlorosis) (15). Moreover, the carbon polymer polyhydroxybutyrate (PHB) slowly accumulates in granular structures, which are derived from glycogen turnover (17, 18). The metabolic activities decrease as the cells enter into a dormant-like state, in which they can survive for months. As soon as a combined nitrogen source becomes available again, chlorotic cells rapidly awake and resume metabolism (15, 18, 19). This is accompanied by a gradual decrease in the levels of *SlI0944* (19).

This study aimed to clarify the role of the *SlI0944* protein in *Synechocystis* and its involvement in P_{II} signaling. Our results indicate that *SlI0944* regulates the glycolytic carbon flux in a P_{II}-dependent manner through interaction with the 2,3-phosphoglycerate-independent phosphoglycerate mutase (PGAM) in response to the nitrogen status sensed via 2-OG. Specifically, we found that *SlI0944* swaps between P_{II} and PGAM in a 2-OG-dependent manner. This establishes PGAM as a key control point of cyanobacterial carbon flow, as predicted previously by kinetic modeling of the cyanobacterial low-carbon response (20, 21), and *SlI0944* as the key regulator of cyanobacterial carbon metabolism. We therefore named the *slI0944* product PirC (P_{II}-interacting regulator of carbon metabolism).

Results

In Silico Analysis Reveals High Conservation of *SlI0944* (PirC) among Cyanobacteria. According to the Uniprot database, the gene *slI0944* (from now on named PirC) of *Synechocystis* codes for a 164-amino-acid-long “uncharacterized protein” (<https://www.uniprot.org/uniprot/P77971>). A databank search for orthologues using the Basic Local Alignment Search Tool (BLAST) revealed that PirC is highly conserved among cyanobacteria. All the homologous proteins contain the Domain of Unknown Function 1830 (<http://pfam.xfam.org/family/PF08865>).

A conserved NtcA-binding site 5'-GTN₁₀AC-3', which is responsible for nitrogen-starvation-induced expression (22), is situated in front of the respective genes. These findings suggest that *pirC* and its orthologs might all be responsive to nitrogen starvation. Gene neighboring analysis in 53 cyanobacterial genomes revealed that in 67% of the cases, the *pirC* homologs are flanked by a gene encoding for a radical S-adenosyl methionine (SAM)-like protein, annotated as Elongator protein 3 (*SI Appendix, Fig. S1*), which was recently shown to be a non-canonical transfer RNA acetyltransferase (23). In *Synechocystis*, the *pirC* gene is upstream of *glgA1*, which encodes the major glycogen synthase that is required for acclimation to nitrogen deprivation (19).

Protein sequence alignments showed that the first 52 N-terminal amino acids of the annotated PirC sequence are not conserved in any of the other orthologs (*SI Appendix, Fig. S2*). Furthermore, the experimentally validated transcriptional start site from *Synechocystis* (24) suggests a shorter open reading frame (ORF) with Met-53 as putative translational start site for PirC. Our initial heterologous expression of the long and short *pirC* variant in *Escherichia coli* revealed that only the short variant can be expressed into a properly folded and soluble protein. This finding supports the notion that the 112-amino-acid-long version of PirC represents the physiologically relevant protein. Hence, this short variant was used in all subsequent work.

PirC Is a Strong P_{II}-Binding Partner. A first series of experiments were set out to verify the putative interaction between P_{II} and PirC (12). In vitro affinity purification experiments revealed that recombinant PirC coeluted with strep-tagged P_{II} in the presence of ATP or ADP, but not in the presence of ATP plus 2-OG (*SI Appendix, Fig. S3A*). As expected, in the control samples lacking strep-tagged P_{II}, the elution fractions did not contain any PirC. The observation that PirC is unable to interact with ATP- and 2-OG-bound P_{II} is common to many P_{II}-interacting partners and a sign of binding specificity (25). The influence of effector molecules on the interaction between PirC and P_{II} was further quantitatively analyzed by bio-layer interferometry (BLI). In this assay, binding of an analyte in solution to a ligand immobilized on a biosensor surface (or tip) produces a shift in wavelength, which serves as readout of analyte–ligand interaction. For our purposes, recombinant C-terminal His₈-tagged P_{II} was bound to the Ni-NTA biosensor surface, while strep-tagged PirC was added as analyte in solution. In the absence of effector molecules, we observed a weak interaction between P_{II} and PirC (Fig. 1*A* and *B*). In the presence of ATP or ADP, PirC binding to P_{II} strongly increased. Quantitative measurements revealed apparent *K_D* values of 37.3 ± 2.5 nM and 14.1 ± 0.7 nM for P_{II}–PirC complex formation in the presence of 2 mM ATP and ADP, respectively. Similar results were obtained using surface plasmon resonance (SPR) spectrometry. The maximum response after injection of PirC in presence of ATP over the P_{II}-loaded sensor was 270 response units (RUs) when the SPR sensor chip was loaded with 1,000 RUs of His-tagged P_{II} (*SI Appendix, Fig. S3B*). Given that in SPR spectrometry, the response signal in RUs is proportional to the mass change on the sensor, the mass increase of 270 RUs by PirC on 1,000 RUs of P_{II}-loaded sensor is close to one PirC monomer per P_{II} trimer bound. The inhibitory effect of 2-OG on P_{II}–PirC interaction was further quantified by BLI through titration with increasing 2-OG concentrations at a constant concentration of 2 mM ATP (Fig. 1*C*). A half maximal inhibitory concentration (IC₅₀) of 123.4 ± 1.1 μM for 2-OG was determined, a value close to the *K_D* of the third (lowest affinity) 2-OG-binding site of P_{II} (26). Therefore, it seems that occupation of all three effector binding sites in P_{II} with 2-OG is required to prevent complex formation with PirC.

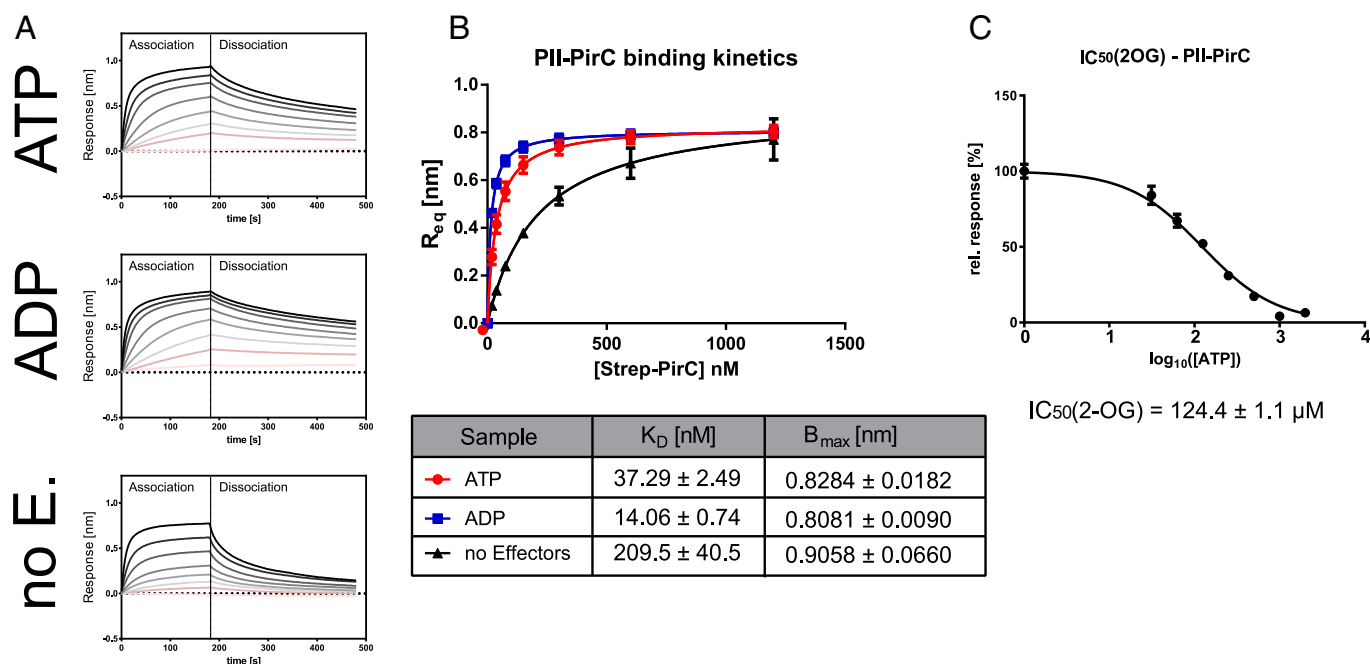


Fig. 1. Complex formation of P_{II} with PirC and modulation by effectors ADP, ATP, and 2-OG. (A) BLI binding assays. His-tagged P_{II} was immobilized on sensor tips and allowed to associate for 180 s with PirC in presence of either 2 mM ATP (Top), ADP (Middle), or without effectors (Bottom), followed by 300 s dissociation. The overlay of response curves with increasing concentrations of PirC (9.375 nM to 1,500 nM) is shown. (B) Plot of maximum binding responses from (A) for the calculation of binding constants (depicted below). (C) Plot of IC₅₀ determination for inhibition of PirC–P_{II} binding by increasing 2-OG concentrations at a constant 2 mM of ATP. All experiments were performed in triplicates, and corresponding SDs are shown in B and C.

Physiological Role of PirC in *Synechocystis*. The high conservation of *pirC* in the cyanobacterial phylum, including conservation of the NtcA-binding site, indicated an important function for PirC during acclimation to nitrogen depletion, a feature common to all the members of this phylum. To identify such a function, we generated a *pirC*-deficient mutant (ΔpirC) as well as strains complemented either with the native *pirC* gene ($\Delta\text{pirC}::\text{pirC}$) or with *pirC* variants encoding fluorescent proteins fused to PirC (SI Appendix, Fig. S4).

Acclimation of these strains to long-term nitrogen starvation was investigated under continuous light or in a day/night regime. Growth (as indicated by an increase in optical density) and degree of pigmentation as well as glycogen and PHB content were monitored over 1 mo. In the wild-type strain pigment degradation after removal of combined nitrogen required 21 d under day/night regimes but only 5 to 7 d in continuous light (SI Appendix, Fig. S5) (15). Pigment degradation was slightly retarded in the ΔpirC mutant compared to the wild-type and complemented strain. Moreover, the increase in optical density at 750 nm (OD₇₅₀) of the ΔpirC mutant was lower than that of the wild-type and complemented strains (Fig. 2A), which indicates that in the ΔpirC mutant, the final cell division upon nitrogen deprivation is delayed. In contrast to these rather modest effects, a striking phenotype for the ΔpirC strain was observed with respect to glycogen accumulation. After the removal of combined nitrogen sources, both the wild-type and complemented strain showed the typical rapid and steep increase in cellular glycogen levels, which were maintained throughout the entire period of nitrogen-starvation-induced chlorosis. By contrast, glycogen content in the ΔpirC mutant reached only 28% of the wild-type level and subsequently declined again. As opposed to glycogen, the ΔpirC mutant accumulated significantly more PHB (up to 49% of the cell dry mass) than the wild-type and the complemented strain (30% and 29% PHB per cell dry mass, respectively) (Fig. 2B). To confirm this result, PHB granules were visualized by fluorescence

microscopy after staining the cells with Nile Red or by transmission electron microscopy (TEM) (Fig. 2C). After 35 d of nitrogen depletion, a much higher PHB content was observed in the ΔpirC mutant than in the wild-type or complemented strain in both fluorescent and TEM micrographs, confirming the results of the chemical PHB quantification.

Identification of PirC-Controlled Processes. The altered glycogen and PHB accumulation patterns in nitrogen-deprived ΔpirC cells suggested a crucial role for PirC in carbon storage metabolism during nitrogen starvation. To elucidate the corresponding molecular mechanism, we aimed to identify additional molecular targets of PirC. To this end, coimmunoprecipitation (CoIP) experiments were conducted using crude extract of nitrogen-starved ΔpirC cells expressing a PirC–mCitrine fusion protein ($\Delta\text{pirC}::\text{pirC}$ –mCitrine). PirC–mCitrine in the crude extract of $\Delta\text{pirC}::\text{pirC}$ –mCitrine was precipitated using a GFP-trap consisting of an anti-GFP Nanobody/V_HH coupled to magnetic agarose beads (<http://www.chromotek.com>). Note that the anti-GFP nanobodies bind different variants of GFP, including mCitrine. Chromotek binding control magnetic agarose was used to determine the unspecific background binding. IPs were performed in the presence of Mg²⁺, ATP, and 2-OG or in the absence of additionally supplemented effectors. The eluates from independent experiments were analyzed after tryptic digestion by quantitative mass spectrometry to identify coimmunoprecipitating proteins. In the absence of 2-OG, immunoprecipitation of PirC–mCitrine only enriched for P_{II}, confirming that P_{II} is the major PirC-interaction partner in these conditions (SI Appendix, Fig. S6). The addition of 2-OG/ATP to the extract completely changed the pattern of coimmunoprecipitated proteins: instead of P_{II}, the enzyme 2,3-bisphosphoglycerate-independent PGAM, encoded by the gene *slr1945*, appeared as dominant PirC interactor (SI Appendix, Fig. S7). PGAM converts 3-phosphoglycerate (3-PGA) into 2-phosphoglycerate (2-PGA) at the beginning of

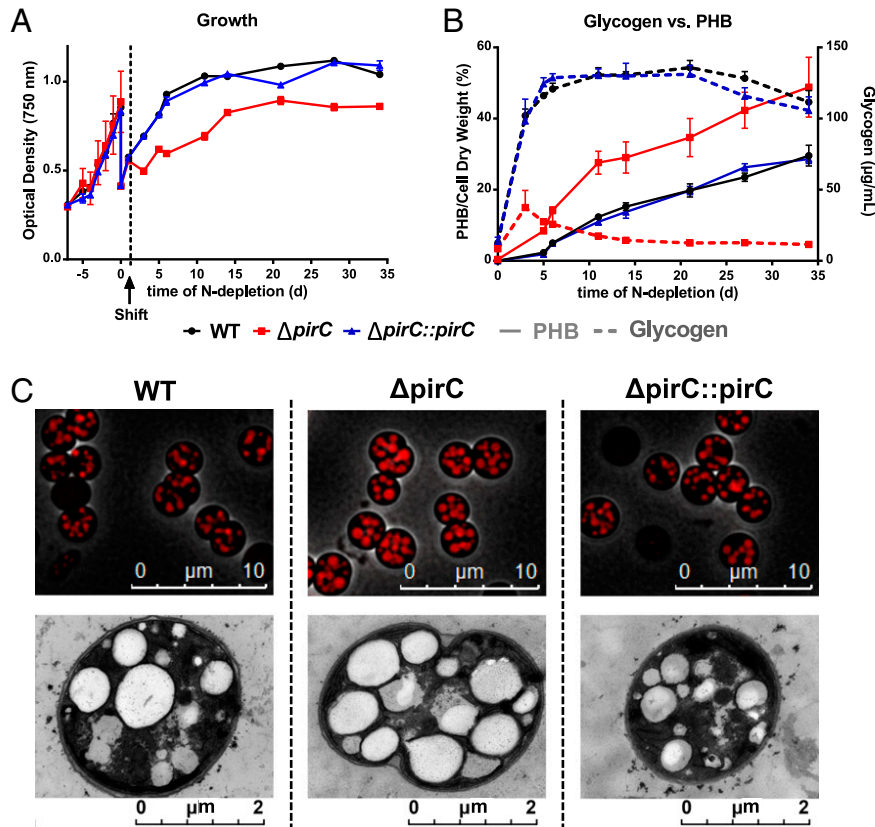


Fig. 2. Effect of PirC deletion on growth, carbon storage, and carbon polymer accumulation during chlorosis. The graphs represent the mean and SD from three biological replicates. (A) Growth curves of the wild-type (WT), the *pirC* null mutant ($\Delta pirC$), and the complemented ($\Delta pirC::pirC$) strain as measured by OD₇₅₀ starting 7 d before nitrogen depletion and during the 35 d of acclimation to nitrogen starvation, also known as chlorosis. (B) Glycogen and carbon polymer (PHB) content during chlorosis. PHB: plane lines; Glycogen: dashed lines. (C) Fluorescent and TEM micrographs of cells stained with Nile Red after 35 d of chlorosis. Top rows: three-dimensional (3D)-deconvoluted overlay pictures of phase contrast- and fluorescence microscopy images (1,000× magnification). Note that Nile Red stains the PHB granules within each cell. Bottom rows: TEM Pictures (5,000× magnification).

lower glycolysis. In addition to PGAM, an ortholog of the CcmP protein, encoded by the gene *slr0169*, was also found as a PirC-interacting protein, but with a lower enrichment factor compared to PGAM. CcmP has been identified as a minor shell protein in carboxysomes of *Synechococcus elongatus* PCC 7249. The trimeric shell protein has a central pore that can be opened and closed, most likely for the movement of metabolites such as the PGAM substrate 3-PGA (27, 28).

PirC Swaps from P_{II} to PGAM-Binding in a 2-OG-Dependent Manner, Thus Inhibiting PGAM Activity during Chlorosis. The observed interaction of PirC with PGAM suggested that PirC negatively regulates PGAM activity. This assumption is consistent with the decreased glycogen and increased PHB levels in the $\Delta pirC$ mutant because PGAM diverts newly fixed carbon from the Calvin cycle toward lower glycolysis, through which acetyl-CoA, the precursor metabolite of PHB, is produced. To validate the putative role of PirC in the regulation of PGAM, recombinant PGAM was purified via an N-terminal His₆-tag for biochemical characterization.

First, we tested the influence of PirC on PGAM catalytic activity using an enzymatic assay, in which the PGAM-catalyzed conversion of 3-PGA to 2-PGA is coupled with enolase, pyruvate kinase, and lactate dehydrogenase to the final oxidation of reduced nicotinamide adenine dinucleotide (NADH). The His-tag was removed from recombinant PGAM by thrombin cleavage to prevent interference with catalysis. Furthermore, we verified that PirC had no effect on the activities of the coupling enzymes (*SI Appendix, Fig. S8*). A clear PirC-dependent inhibition of PGAM

activity was observed when PirC was added at increasing concentrations to the reaction mix of the enzymatic assay. PirC inhibited PGAM in a competitive manner by increasing the K_M for the substrate 3-PGA rather than lowering the V_{max} . At nearly equimolar concentrations of PirC (200 nM) and PGAM (166 nM), the catalytic efficiency was reduced to one third. In the presence of an excess of PirC, the catalytic activity of PGAM could be reduced more than 10-fold as compared to the absence of PirC (Fig. 3A and Table 1).

Second, the interplay of P_{II} and PirC on PGAM activity was analyzed because we assumed that P_{II} might regulate the inhibitory interaction of PirC with PGAM, in analogy to the effect of P_{II} on PipX–NtcA interaction (14). To this end, we performed PGAM assays in the presence of PirC and P_{II} and supplemented the assays with ATP and different 2-OG concentrations, respectively (Fig. 3B). Addition of P_{II} in the absence of 2-OG abolished the inhibitory effect of PirC on PGAM activity. The K_M for 3-PGA returned to the value of noninhibited PGAM (Table 1). However, in the presence of 1 mM of 2-OG, a concentration corresponding to high C/N conditions in *Synechocystis* cells, PirC was again able to inhibit PGAM as in the absence of P_{II} . When 2-OG was added at a concentration of 0.123 mM (corresponding to the IC_{50,2-OG} value of P_{II} –PirC complex formation), the inhibition of PGAM was ~50% of the maximal inhibition with PirC in the absence of 2-OG. These results unambiguously indicate that in vitro, in presence of high 2-OG levels, binding of 2-OG to P_{II} disrupts P_{II} –PirC interaction and promotes binding of PirC to PGAM, thus inhibiting its activity.

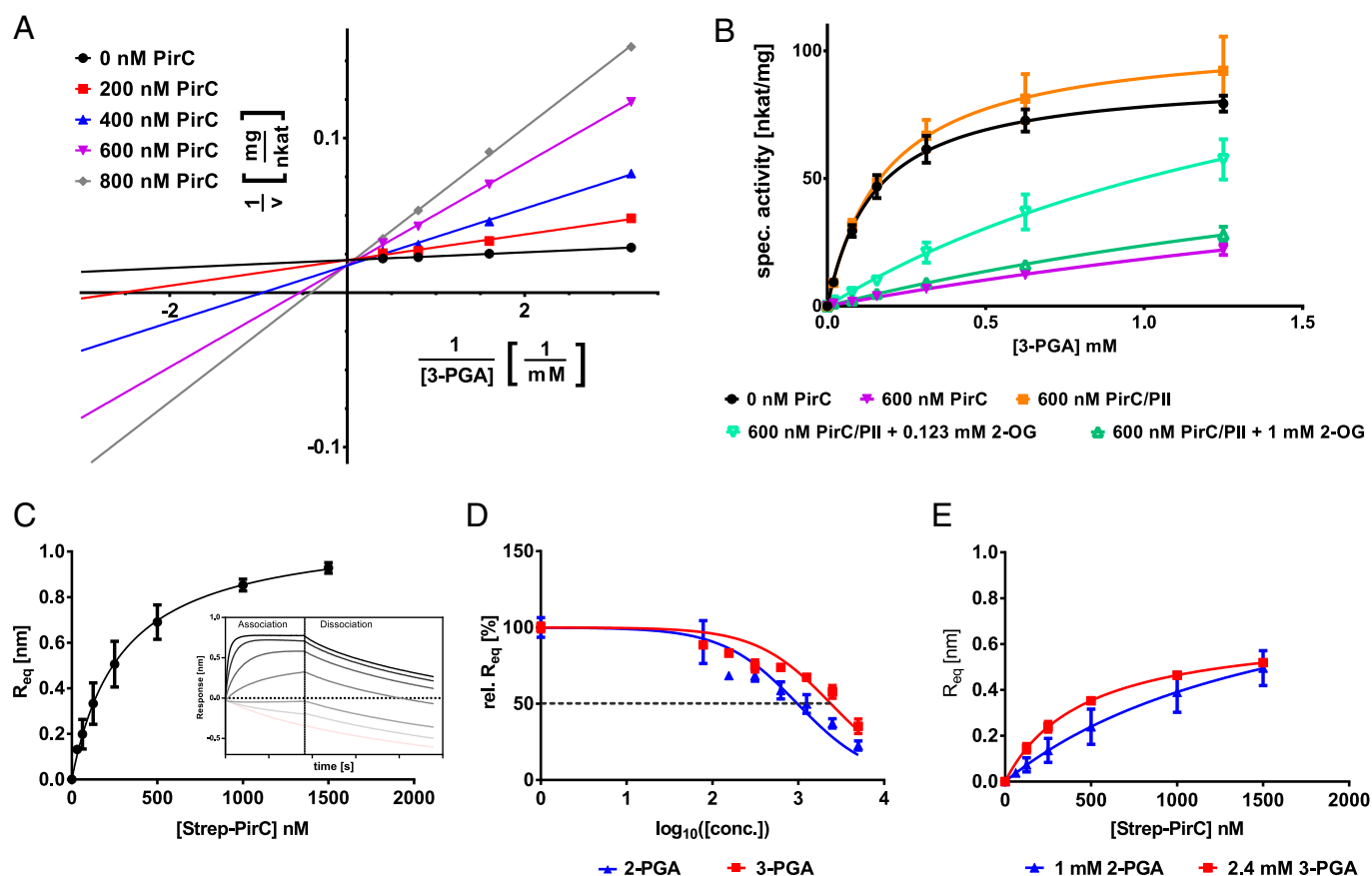


Fig. 3. Effect of PirC on PGAM enzyme activity and PGAM-PirC complex formation. (A) Inhibition of PGAM activity by increasing PirC concentrations represented as Lineweaver-Burk plot. The corresponding kinetic constants are shown in Table 1. PirC has no effect on coupling enzymes as shown in supplements (SI Appendix, Fig. S8). (B) Modulation of PGAM activity by PirC (600 nM) in presence or absence of P_{II} (600 nM trimer) and 0.4 mM ATP without or with 0.123 mM or 1 mM 2-OG. Each point represents the mean of triplicates. (C) Steady-state graph of PirC-PGAM binding assays using BLI. The mean of the R_{eq} value (three independent replicates) was plotted against the molar concentration of Strep-PirC. The inset shows the raw binding curves at different PirC concentrations. (D) Competitive inhibition of PirC-PGAM interaction by 2-PGA and 3-PGA. Plot shows determination of IC_{50} . (E) Steady-state graph of PirC-PGAM binding in presence of 2-PGA or 3-PGA at their IC_{50} concentrations.

The inhibitory effect of PirC binding on PGAM activity was further investigated using BLI assays. To this end, His₆-tagged PGAM was bound to the biosensor tip, and strep-tagged PirC protein was added in solution as analyte at varying concentrations (Fig. 3C). A stable PGAM-PirC complex formed in the absence of any effector molecules. The competitive inhibition mode (Fig. 3D) suggested that the substrates of PGAM could compete with PGAM-PirC interaction. Indeed, the addition of the PGAM substrates 3-PGA or 2-PGA (for the forward and backward reaction, respectively) had inhibitory effects on complex formation. Addition of 2-PGA inhibited complex formation 2.4 times stronger ($IC_{50} = 0.97$ mM) than 3-PGA ($IC_{50} = 2.4$ mM) (Fig. 3D). When the metabolites were added at their IC_{50} concentration, 2-PGA (1 mM) increased the K_D of PirC-PGAM interaction to 1,702 nM and 3-PGA (2.4 mM) to 459 nM, respectively (Fig. 3E and Table 1).

PirC Deletion Leads to Accumulation of the Metabolites of Lower Glycolysis. The above-described analysis of the PGAM-PirC-P_{II} triad demonstrated inhibition of PGAM activity by PirC, in response to the binding of the C/N-status reporter metabolite 2-OG to P_{II}. This suggests that in wild-type cells, during nitrogen starvation (i.e., when high 2-OG levels accumulate), the inhibition of PGAM by PirC supports the formation of high glycogen levels by diminishing carbon catabolism via lower glycolysis. In the absence of this inhibition (i.e., in the $\Delta pirC$ mutant), glycogen catabolism via glycolysis increases. To further verify this

hypothesis, we monitored over time the levels of metabolites in wild-type and $\Delta pirC$ mutant cells during the shift from nitrate-replete (NO₃) to nitrogen-depleted (-N) medium. Samples for metabolome analysis were withdrawn after 0, 6, 24, and 48 h from the shift. Nitrogen depletion had the expected effect on the total cellular steady-state metabolite pools (i.e., soluble amino acids were depleted to large extent, while organic acids accumulated), resulting in lowered N/C ratios under -N conditions (SI Appendix, Fig. S9). Most organic acids participating in the TCA cycle such as citrate, malate, and succinate accumulated in both strains in a similar manner when shifted to -N conditions (Fig. 4). Also, the products of ammonium assimilation via GS/GOGAT, glutamine (Gln), and glutamate (Glu) showed similar changes in the wild-type and $\Delta pirC$ strain with rapid decrease in Glu and slower decrease in Gln. Besides these general metabolic responses, in which the $\Delta pirC$ mutant showed no discernable differences, a few very specific and intriguing differences were recorded at decisive steps: the C/N-status reporter molecule 2-OG accumulated immediately after -N shift in both strains. In the wild-type, the 2-OG levels decreased gradually over the following 48 h, whereas they remained constantly elevated in $\Delta pirC$ cells, and they even slightly increased (Fig. 4). Moreover, the 3-PGA concentration increased in the wild-type over the course of nitrogen starvation, whereas it gradually declined in the $\Delta pirC$ mutant. The increasing 3-PGA levels, substrate of the PGAM, in the wild-type cells indicate in vivo inhibition of the PGAM reaction, whereas lack of PGAM inhibition by PirC

Table 1. Kinetic constants of PGAM under varying concentrations of PirC and changes of constants by addition of PirC-interacting molecules

Inhibition of PGAM by PirC at varying concentrations				
PirC, nM	K_M , mM	v_{max} , nkat · mg ⁻¹	k_{cat} , s ⁻¹	$k_{cat} · K_M^{-1}$, s ⁻¹ · M ⁻¹
0	0.1266 ± 0.0064	47.54 ± 0.52	2.776 ± 0.030	21959.0 ± 1104.7
200	0.3584 ± 0.0216	44.92 ± 0.75	2.623 ± 0.044	7329.8 ± 441.1
400	0.7056 ± 0.0499	46.56 ± 1.09	2.719 ± 0.063	3859.1 ± 273.0
600	1.376 ± 0.102	47.11 ± 1.39	2.751 ± 0.081	2002.2 ± 148.4
800	1.715 ± 0.145	43.27 ± 4.10	2.526 ± 0.239	1618.7 ± 369.4
Antagonistic effect of P _{II} and its modulation by 2-OG (0.4 mM ATP, 600 nM PirC, and 600 nM P _{II3})				
Modulators of PGAM	K_M , mM	v_{max} , nkat · mg ⁻¹	k_{cat} , s ⁻¹	$k_{cat} · K_M^{-1}$, s ⁻¹ · M ⁻¹
None	0.1499 ± 0.0121	89.76 ± 2.17	5.41 ± 0.13	36097.4 ± 2921.0
PirC	4.0220 ± 1.338	92.80 ± 24.78	5.59 ± 1.49	1390.9 ± 462.7
PirC/P _{II}	0.1855 ± 0.0247	105.90 ± 4.51	6.38 ± 0.27	34409.7 ± 4572.5
PirC/P _{II} + 0.123 mM 2-OG	1.8410 ± 0.5461	142.70 ± 28.47	5.56 ± 1.24	3021.7 ± 896.3
PirC/P _{II} + 1 mM 2-OG	2.887 ± 0.8542	92.28 ± 20.51	8.60 ± 1.72	2980.3 ± 881.8
Binding constants for PGAM–PirC binding and modulation by substrates				
Sample	K_D , nM	IC ₅₀ , mM		
No Effectors	2.89 ± 34.49	—		
2-PGA	1702 ± 744 (at IC ₅₀)	0.97 ± 0.001		
3-PGA	459.1 ± 32.0 (at IC ₅₀)	2.4 ± 0.001		

Binding constants of PGAM/PirC complex with or without the presence of the substrates.

explains the low 3-PGA levels in the $\Delta pirC$ mutant. 3-PGA is known as an allosteric activator of the glucose 1-phosphate-adenylyltransferase (GlgC) in bacteria, which catalyzes the initial step of glycogen synthesis (29). Downstream of the PGAM reaction, the levels of pyruvate responded inversely to 3-PGA, with decreasing levels in the wild-type but a strong increase in the $\Delta pirC$ mutant. The pyruvate level in the mutant was 14-fold higher than in the wild-type after 48 h of N starvation. Again, this observation is consistent with an increased flux through the PGAM reaction due to the missing inhibition by PirC, since the produced 2-PGA is further converted into pyruvate. The increased carbon flux toward pyruvate in the $\Delta pirC$ mutant lowers the carbon flux toward glycogen and increases the levels of PHB, which is derived from acetyl-CoA (i.e., the immediate reaction product from pyruvate).

Subcellular Localization of PirC. To determine the subcellular localization of PirC during different growth stages, when PirC presumably interacts preferentially with either P_{II} or PGAM, we analyzed cells expressing a PirC–GFP fusion protein ($\Delta pirC::pirC$ –eGFP) by fluorescence microscopy. The eGFP signal was centrally localized in the cytoplasm (SI Appendix, Fig. S10) in cells during exponential growth in nitrate-containing BG₁₁ medium, conditions that promote binding of PirC to P_{II}. Shifting the cells to nitrogen-depleted medium increased the 2-OG levels (see Fig. 4), which should promote dissociation of the P_{II}–PirC complexes and allow interaction of PirC with PGAM. Accordingly, the localization of PirC–eGFP changed after nitrogen downshift. The centrally localized eGFP signal slowly expanded to the peripheral region of the cytoplasm during the first 24 h after nitrogen starvation, where it then remained throughout chlorosis. This result corroborated the dynamics of PirC interactions and its response to nitrogen limitation.

Discussion

In this study, we identified a key control point of cyanobacterial carbon metabolism, the glycolytic PGAM reaction, converting 3-PGA into 2-PGA. In animal systems, where glycolysis supplies energy, it has been shown that glycolytic breakdown of glucose 6-phosphate is mainly regulated at the phosphofructokinase level according to the energy demand of the cells (30). By contrast, in photoautotrophic organisms, glycolytic steps are used in two directions, in the gluconeogenic direction toward glycogen

or starch synthesis and in the glucose catabolic direction, respectively, to produce precursors for multiple biosynthetic routes required for cell growth. The PGAM reaction is at the branch point of newly fixed CO₂. 3-PGA, the first stable reaction product from RubisCO-catalyzed CO₂ fixation, can be metabolized in two directions. Most of it is converted into 2,3-bisphosphoglycerate and further to glyceraldehyde-3-phosphate (GAP), from which the acceptor of RubisCO, ribulose 1,5-bisphosphate, is regenerated via the Calvin cycle reactions. Excess GAP is used via gluconeogenic reactions to synthesize glycogen (in plant starch). Alternatively, 3-PGA can be diverted from the Calvin cycle through its direct conversion to 2-PGA by PGAM. 2-PGA is further metabolized in lower glycolytic reactions, from where the majority of cellular amino acids and lipids are derived in photoautotrophs, with pyruvate, acetyl-CoA, and 2-OG representing key precursors.

The PGAM reaction was previously predicted as a key control point of carbon metabolism by kinetic modeling of the cyanobacterial low-carbon response (20, 21). It was shown that 2-PGA accumulates to high amounts (5 to 7 times) in cells shifted from high CO₂ (5%) to ambient air (0.04% CO₂) in *Synechocystis* (31) as well as in *Synechococcus elongatus* PCC 7942 (32). The high 2-PGA accumulation was taken as an indication that under carbon-limiting conditions, newly fixed organic carbon is directly deviated from the Calvin cycle into lower glycolysis by the PGAM reaction to sustain biosynthesis of amino acids and other cellular compounds. Here, we provide in vitro and in vivo evidence that the reaction catalyzed by the product of the *slr1945* gene, PGAM, represents a key control point for acclimation to nitrogen starvation. This control operates through a regulatory mechanism, in which the small regulatory protein PirC acts as a mediator of the signal from the pervasive P_{II} regulatory protein to tune the activity of PGAM, a control mechanism so far never described for enzymatic reactions. To further understand the competitive inhibition of PGAM by PirC, as demonstrated here through kinetic and binding studies, structural analysis of the enzyme complexes will be required.

According to our model depicted in Fig. 5, P_{II} binds to PirC under nitrogen-sufficient conditions, when 2-OG levels are low, thereby preventing the interaction with PGAM. Efficient conversion of 3-PGA to 2-PGA by highly active PGAM directs newly fixed carbon toward lower glycolysis to support the synthesis of amino acids and fatty acids. Only a minor fraction is converted into glycogen. When the cells experience nitrogen

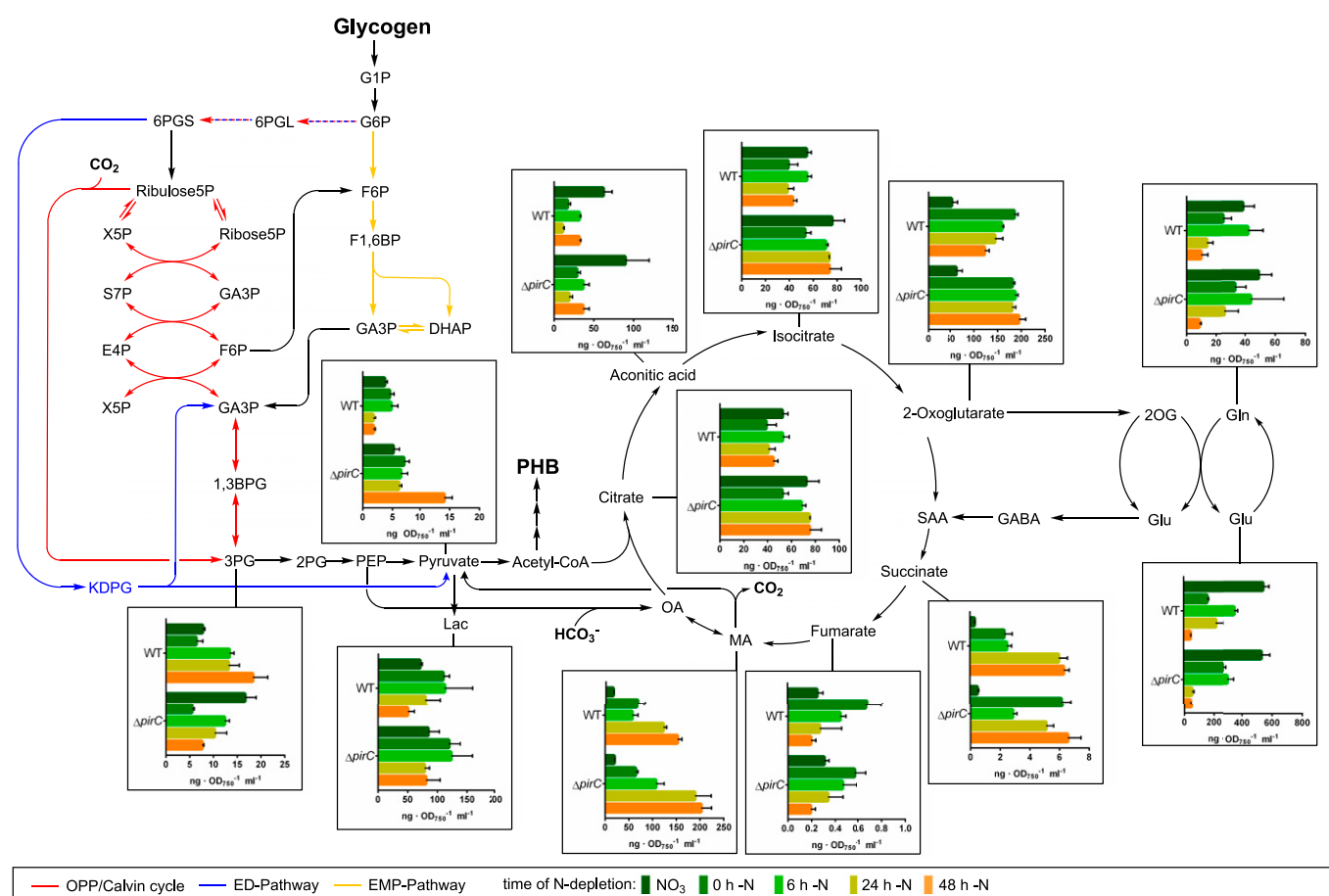


Fig. 4. Time course LC-MS analysis of steady-state levels of relevant metabolites during the short-term shift of wild-type (WT) and $\Delta pirC$ cells from NO_3 to $-N$ conditions depicted in a metabolic background. Totals of 0 h, 6 h, 24 h, and 48 h indicate the time from nitrogen depletion at which samples were withdrawn from the cultures for analysis. Each bar represents the metabolite level at a certain time point determined from two independent biological replicates each in technical duplicates. The error bars represent the SD of the combined data. The values are in ng per optical density at 750 nm per ml ($ng \cdot OD_{750}^{-1} \cdot ml^{-1}$). The result of the entire metabolite analysis is shown in *SI Appendix, Fig. S9*.

limitation, they accumulate the intracellular 2-OG levels. As a result of 2-OG binding to P_{II} , the P_{II} -PirC complex dissociates, and PirC interacts with PGAM, thereby inhibiting its enzymatic activity. This is accompanied by a relocalization of the PirC-eGFP signal from the central region of the cell to the periphery. The central localization of PirC-eGFP is indicative of the presence of PirC- P_{II} complexes as P_{II} was previously shown to localize in the central cytoplasm of cells grown in the presence of

nitrate (11). As a consequence of the PirC-PGAM interaction, conversion of 3-PGA to 2-PGA is blocked in nitrogen-starved cells, leading to increased 3-PGA levels, which are now redirected toward glycogen. Due to this metabolic switch, the flux toward amino acid synthesis is slowed down, thus adjusting cellular metabolism to the limited supply of nitrogen. Furthermore, 3-PGA is an allosteric activator of GlgC, which catalyzes the initial and regulated step of the glycogen synthesis (29). Hence,

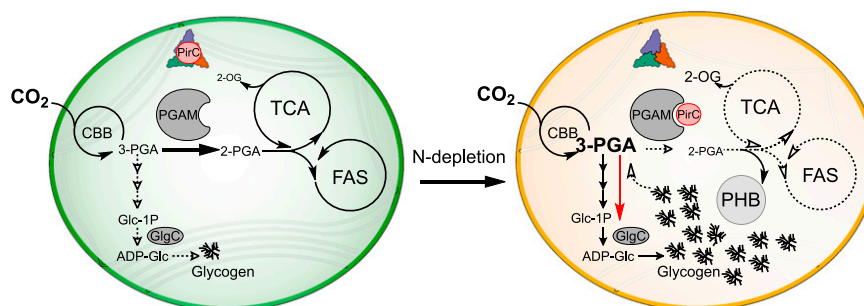


Fig. 5. Model of regulation of central carbon metabolism by PirC, P_{II} , and PGAM interactions. In vegetative cells, when 2-OG levels are low, P_{II} (depicted as trimer in blue, green, and red) binds to PirC and prevents the inhibition of PGAM. PGAM directs 3-PGA downstream to the biosynthesis of fatty acids (FAS) and amino acids mainly via the TCA cycle. When the cells are N depleted, 2-OG levels increase and promote release of PirC from P_{II} . PirC binds to and inhibits PGAM. This results in an elevation of the 3-PGA concentration. 3-PGA enhances the activity of GlgC and directs the carbon flux toward glycogen, resulting in enhanced glycogen accumulation. CBB: Calvin-Benson-Bassham cycle.

the PirC-mediated PGAM inhibition not only slows down lower glycolysis but also stimulates glycogen accumulation via the GlgC activation. The glycogen levels increase until the cells are densely packed with glycogen, which can amount up to 50% of the dry weight in chlorotic cells (15). Already after 24 h of nitrogen starvation, accumulation of glycogen reaches a maximum, and the levels remain high throughout chlorosis. Recent data indicate a constant turnover of glycogen until the cells enter complete dormancy (17). In *Synechocystis*, which expresses the PHB synthesis machinery, acetyl-CoA molecules arising from the residual glycolytic flux during chlorosis are directed toward PHB synthesis. Hence, the amount of PHB steadily increases during prolonged nitrogen starvation. In the Δ pirC mutant, PGAM cannot be appropriately inhibited. Therefore, increased flux toward 2-PGA and lower glycolysis leads to a massive accumulation of PHB. In agreement with this model, P_{II}-deficient *Synechocystis* mutants are unable to accumulate PHB during nitrogen-starvation-induced chlorosis (33). In the absence of P_{II}, PirC will constantly inhibit PGAM activity, resulting in decreased levels of metabolites downstream of 2-PGA (10) due to the limited supply of acetyl-CoA for PHB synthesis.

This glycolytic switch at the enzymatic level of PGAM via the small P_{II}-interacting regulatory protein PirC is reminiscent of the control of NtcA-dependent transcription by the small P_{II}-interacting protein PipX. The latter is either complexed to P_{II} under low 2-OG levels or bound to NtcA at elevated 2-OG levels (6). Hence, the two small P_{II}-mediator proteins, PirC as well as PipX, functionally interact to coherently reprogram metabolism and gene expression under low-nitrogen conditions. Through release of the P_{II}-PirC complex in response to increasing 2-OG levels, PirC tunes down PGAM activity. This response is further amplified by the concomitant dissociation of the P_{II}-PipX complex and association of PipX to NtcA, accompanied by NtcA-dependent expression of many low-nitrogen-induced genes, among which is the *pirC* gene. In chlorotic cells, *pirC* (*sl0944*) is among the most strongly up-regulated genes within the entire transcriptome (15), and, accordingly, PirC is one of the most highly enriched proteins during chlorosis (16). In an advanced stage of chlorosis, this strong accumulation of PirC ensures tight inhibition of glycolysis to maintain high glycogen levels, which are required for efficient exit from the dormant state of chlorosis (19).

Through engagement of such mediator proteins, P_{II} can largely expand its regulatory space. In principle, any cellular activity, which can be modulated through interaction with a peptide, could be tuned by P_{II} by engineering the peptide to bind P_{II}, thus providing a new toolbox for synthetic biology. It is also reasonable to speculate that disabling the regulation of PirC can be used for metabolic engineering in cyanobacteria, in particular, for the bioproduction of metabolites derived from lower glycolysis, such as succinate, malate, or lipids as well as fatty acids. Furthermore, cyanobacteria have the potential to synthesize isoprenoids or terpenes via the methylerythritol phosphate pathway whose precursors are pyruvate and GAP (34). In addition, genetically engineered cyanobacteria can be used for the synthesis of heterologous compounds such as l-butanol from acetyl-CoA (35). However, it should be kept in mind that the utility of the PirC mutation is especially beneficial for processes that are performed under nitrogen-limited conditions. As a proof of principle, we took advantage of the redirection of the carbon metabolism toward PHB synthesis in the PirC-deficient mutant to further increase the levels of PHB in the cell: we engineered the PirC-deficient mutant to express the high processive PHB biosynthetic enzymes from *Cupriavidus necator*, resulting in a strain that accumulates more than 80% PHB of cell dry mass under nitrogen-depleted conditions. This is by far the highest accumulation of PHB ever reported in a cyanobacterium (36). This result impressively demonstrates the impact and biotechnological potential of decoupling the regulation by PirC.

Materials and Methods

Full protocols are available in *SI Appendix, SI Materials and Methods*.

Strains and Cultivation. A list of all used strains for this study is provided in *SI Appendix, Table S1*. *Synechocystis* sp. PCC 6803 strains were cultivated in BG₁₁ medium according to Rippka (37) either at continuous illumination ($\sim 50 \mu\text{E m}^{-2} \cdot \text{s}^{-1}$) or light-dark conditions (12 h light and 12 h darkness) and 28 °C. For nitrogen depletion, cultures were cultivated in BG-11 media without 17.65 mM NaNO₃. Whenever necessary, appropriate antibiotics were added to the different strains to ensure the continuity of the mutation. Cultivation of *E. coli* cultures was performed with lysogeny broth (LB) medium and LB-agar.

Plasmids and Cloning. A list of all used primers, plasmids, and the cloning procedures is in *SI Appendix, Table S2* as well as in *SI Appendix, Fig. S4*.

Overexpression and Purification of Proteins. Recombinant proteins were overexpressed in *E. coli* Lemo21. His-tag proteins were purified on 1 mL Ni-NTA HisTrap columns (GE Healthcare) as described previously (10). For purification of strep-tagged proteins, 5 mL strep-tactin superflow columns were used as described previously (10). The His-tag of PGAM was removed by Thrombin cleavage using bovine thrombin of Sigma-Aldrich according to protocol (38).

ColP and Liquid Chromatography–Mass Spectrometry. For ColP experiments in presence of the P_{II} effector molecules, cells of *Synechocystis* Δ PirC::PirC-mCitrine cultures were harvested after 24 h N depletion and resuspended in 2 mL binding buffer (100 mM Tris [pH 7.5], 100 mM KCl, 1 mM MgCl₂, 1 mM DTT, 0.5 mM EDTA, 2 mM ATP, and 2-OG). After lysing the cells, the lysate was centrifuged, and from the supernatant, a volume containing 3 mg of protein was used for the immunoprecipitation using GFP-Trap Magnetic Agarose beads or control beads without antibodies according to the manufacturer's protocol (Chromotek, Planegg-Martinsried, Germany). Bound proteins were eluted by heating in sodium dodecyl sulfate (SDS) loading buffer, and the solution was subjected to short SDS-polyacrylamide gel electrophoresis (PAGE) runs on 12% Bis-Tris Gels (Invitrogen). After staining with Coomassie blue, protein regions were isolated and InGel digested with trypsin as described (39). After cleaning peptides with StageTips (40), liquid chromatography–mass spectrometry (LC-MS/MS) analysis was performed on a Q Exactive HF mass spectrometer (Thermo Fisher Scientific, Germany), using linear, segmented 60-min nano liquid chromatography (nanoLC) reversed phase (RP) gradients as described (16). From triplicate experiments, all raw data were processed using MaxQuant software suite (version 1.6.5.0) at default settings. Tandem mass spectrometry peak lists were searched against a target-decoy database of the *Synechocystis* proteome, including the sequence of PirC (Sl0944)-mCitrine. Label-free quantification (LFQ) was used to calculate LFQ intensities for each ColP sample as described in extended protocol in the supplement.

BLI Using the Octet K2 System. In vitro binding studies were done by BLI using Octet K2 system (FortéBio) as described previously (10). In the first step, P_{II}-His₆ (400 nM, trimeric) or PGAM-His₆ (500 nM) was immobilized on Ni-NTA sensors (FortéBio), followed by a 60-s baseline measurement. For the binding of PirC, the biosensors were dipped into the PirC solution for 180 s (association), with concentrations ranging between 9.375 nM to 1,500 nM. In P_{II}-binding studies, effector molecules ADP, ATP, or 2-OG were added to the binding buffer as indicated and in PGAM binding assays, 2PG or 3 PGA. Finally, the complexes were allowed to dissociate for 300 s. For each binding experiment, a negative control without an interaction partner was performed in parallel. The response in equilibrium (R_{eq}) was calculated using the data analysis software of the Octet System. To calculate the dissociation constant K_D , the concentration versus R_{eq} plots were made for each set of experiments.

Glycogen Measurement and PHB Quantification. Glycogen was quantified according to ref. 19. PHB was detected by high-performance LC as described previously (41).

PGAM Enzymatic Assay. The PGAM activity and the effect of PirC was determined by a coupled enzyme assay as described previous (42, 43) with 10 μg of purified PGAM used in a 1 mL reaction. The reaction mixture containing 20 mM Hepes-KOH (pH 8.0), 100 mM KCl, 5 mM MgSO₄, 0.4 mM MnCl₂, 50 $\mu\text{g} \cdot \text{mL}^{-1}$ BSA, 1 mM DTT, 0.4 mM ADP, 0.2 mM NADH, 0.5 U enolase (Sigma Aldrich), 2 U Pyruvate kinase (Sigma Aldrich), 2 U Lactate dehydrogenase

(Roche), and 10 μ g PGAM was prewarmed to 30 °C. The assay was started by adding the 3-PGA solutions. The resulted decrease of NADH over time was recorded with Specord50 (Jena Analytics) at 340 nm. As blank, an assay without 3-PGA was performed.

Fluorescence Microscopy and TEM. The visualization of PHB granules was done by phase contrast fluorescence microscopy using the Leica DM5500 B with the Leica CTR 5500 illuminator as described previously. Electron microscopic pictures of lead-citrate- and uranyl-acetate-stained microtome sections of glutaraldehyde and potassium-permanganate-fixed *Synechocystis* cells were prepared as described (44). The samples were then examined using a Philips Tecnai 10 electron microscope at 80 kHz.

Metabolome Analysis. For metabolome analysis by LC-MS, *Synechocystis* was cultivated in 200 mL under N depletion as described previously for 48 h under continuous lightning. The sampling was carried out 0, 6, 24, and 48 h after the shift. Samples of 5 mL liquid culture were quickly harvested onto nitrocellulose membrane filters and subjected to metabolome analytics as detailed in *SI Appendix*.

1. M. Y. Galperin, A census of membrane-bound and intracellular signal transduction proteins in bacteria: Bacterial IQ, extroverts and introverts. *BMC Microbiol.* **5**, 35 (2005).
2. K. A. Selim, E. Ermilova, K. Forchhammer, From cyanobacteria to archaeplastida: New evolutionary insights into P_{II} signalling in the plant kingdom. *New Phytol.* **227**, 722–731 (2020).
3. K. Forchhammer, K. A. Selim, Carbon/nitrogen homeostasis control in cyanobacteria. *FEMS Microbiol. Rev.* **44**, 33–53 (2020).
4. L. F. Huergo, R. Dixon, The emergence of 2-oxoglutarate as a master regulator metabolite. *Microbiol. Mol. Biol. Rev.* **79**, 419–435 (2015).
5. K. Forchhammer, J. Lüddecke, Sensory properties of the P_{II} signalling protein family. *FEBS J.* **283**, 425–437 (2016).
6. A. Forcada-Nadal, J. L. Llaser, A. Contreras, C. Marco-Marín, V. Rubio, The P_{II} -NAGK-PipX-NtcA regulatory axis of cyanobacteria: A tale of changing partners, allosteric effectors and non-covalent interactions. *Front. Mol. Biosci.* **5**, 91 (2018).
7. S. Burillo, I. Luque, I. Fuentes, A. Contreras, Interactions between the nitrogen signal transduction protein P_{II} and N-acetyl glutamate kinase in organisms that perform oxygenic photosynthesis. *J. Bacteriol.* **186**, 3346–3354 (2004).
8. A. Heinrich, M. Maheswaran, U. Ruppert, K. Forchhammer, The *Synechococcus elongatus* P signal transduction protein controls arginine synthesis by complex formation with N-acetyl-L-glutamate kinase. *Mol. Microbiol.* **52**, 1303–1314 (2004).
9. Y.-M. Zhang, S. W. White, C. O. Rock, Inhibiting bacterial fatty acid synthesis. *J. Biol. Chem.* **281**, 17541–17544 (2006).
10. J. Scholl, L. Dengler, L. Bader, K. Forchhammer, Phosphoenolpyruvate carboxylase from the cyanobacterium *Synechocystis* sp. PCC 6803 is under global metabolic control by P_{II} signaling. *Mol. Microbiol.* **114**, 292–307 (2020).
11. A. R. S. Santos et al., NAD⁺ biosynthesis in bacteria is controlled by global carbon/nitrogen levels via P_{II} signaling. *J. Biol. Chem.* **295**, 6165–6176 (2020).
12. B. Watzet et al., The signal transduction protein P_{II} controls ammonium, nitrate and urea uptake in cyanobacteria. *Front. Microbiol.* **10**, 1428 (2019).
13. J. Giner-Lamia et al., Identification of the direct regulon of NtcA during early acclimation to nitrogen starvation in the cyanobacterium *Synechocystis* sp. PCC 6803. *Nucleic Acids Res.* **45**, 11800–11820 (2017).
14. J. Espinosa, K. Forchhammer, S. Burillo, A. Contreras, Interaction network in cyanobacterial nitrogen regulation: PipX, a protein that interacts in a 2-oxoglutarate dependent manner with P_{II} and NtcA. *Mol. Microbiol.* **61**, 457–469 (2006).
15. A. Klotz et al., Awakening of a dormant cyanobacterium from nitrogen chlorosis reveals a genetically determined program. *Curr. Biol.* **26**, 2862–2872 (2016).
16. P. Spät, A. Klotz, S. Rexroth, B. Maček, K. Forchhammer, Chlorosis as a developmental program in cyanobacteria: The proteomic fundament for survival and awakening. *Mol. Cell. Proteomics* **17**, 1650–1669 (2018).
17. M. Koch, S. Doello, K. Gutekunst, K. Forchhammer, PHB is produced from glycogen turn-over during nitrogen starvation in *Synechocystis* sp. PCC 6803. *Int. J. Mol. Sci.* **20**, 20 (2019).
18. M. Koch, K. W. Berendzen, A. K. Forchhammer, On the role and production of polyhydroxybutyrate (PHB) in the cyanobacterium *Synechocystis* sp. PCC 6803. *Life (Basel)* **10**, 10 (2020).
19. S. Doello, A. Klotz, A. Makowka, K. Gutekunst, K. Forchhammer, A specific glycogen mobilization strategy enables rapid awakening of dormant cyanobacteria from chlorosis. *Plant Physiol.* **177**, 594–603 (2018).
20. J. Jablonsky, M. Hagemann, D. Schwarz, O. Wolkenhauer, Phosphoglycerate mutases function as reverse regulated isoenzymes in *Synechococcus elongatus* PCC 7942. *PLoS One* **8**, e58281 (2013).
21. J. Jablonsky, D. Schwarz, M. Hagemann, Multi-level kinetic model explaining diverse roles of isozymes in prokaryotes. *PLoS One* **9**, e105292 (2014).
22. M. F. Vázquez-Bermúdez, E. Flores, A. Herrero, Analysis of binding sites for the nitrogen-control transcription factor NtcA in the promoters of *Synechococcus* nitrogen-regulated genes. *Biochim. Biophys. Acta* **1578**, 95–98 (2002).
23. T.-Y. Lin et al., The Elongator subunit Elp3 is a non-canonical tRNA acetyltransferase. *Nat. Commun.* **10**, 625 (2019).
24. J. Mitschke et al., An experimentally anchored map of transcriptional start sites in the model cyanobacterium *Synechocystis* sp. PCC6803. *Proc. Natl. Acad. Sci. U.S.A.* **108**, 2124–2129 (2011).
25. K. Zeth, O. Fokina, K. Forchhammer, Structural basis and target-specific modulation of ADP sensing by the *Synechococcus elongatus* P_{II} signaling protein. *J. Biol. Chem.* **289**, 8960–8972 (2014).
26. O. Fokina, V.-R. Chellamuthu, K. Forchhammer, K. Zeth, Mechanism of 2-oxoglutarate signaling by the *Synechococcus elongatus* P_{II} signal transduction protein. *Proc. Natl. Acad. Sci. U.S.A.* **107**, 19760–19765 (2010).
27. F. Cai et al., The structure of CcmP, a tandem bacterial microcompartment domain protein from the β -carboxysome, forms a subcompartment within a microcompartment. *J. Biol. Chem.* **288**, 16055–16063 (2013).
28. A. M. Larsson, D. Hasse, K. Vålegård, I. Andersson, Crystal structures of β -carboxysome shell protein CcmP: Ligand binding correlates with the closed or open central pore. *J. Exp. Bot.* **68**, 3857–3867 (2017).
29. J. Preiss, Bacterial glycogen synthesis and its regulation. *Annu. Rev. Microbiol.* **38**, 419–458 (1984).
30. L. B. Tanner et al., Four key steps control glycolytic flux in mammalian cells. *Cell Syst.* **7**, 49–62.e8 (2018).
31. M. Eisenhut et al., Metabolome phenotyping of inorganic carbon limitation in cells of the wild type and photorespiratory mutants of the cyanobacterium *Synechocystis* sp. strain PCC 6803. *Plant Physiol.* **148**, 2109–2120 (2008).
32. D. Schwarz et al., Metabolic and transcriptomic phenotyping of inorganic carbon acclimation in the cyanobacterium *Synechococcus elongatus* PCC 7942. *Plant Physiol.* **155**, 1640–1655 (2011).
33. W. Hauf, "Regulation of carbon polymer accumulation in *Synechocystis* sp. PCC 6803," PhD thesis, University of Tübingen, Tübingen, Germany (2016).
34. B. Pattanaik, P. Lindberg, Terpenoids and their biosynthesis in cyanobacteria. *Life (Basel)* **5**, 269–293 (2015).
35. J. Anfelt et al., Genetic and nutrient modulation of acetyl-CoA levels in *Synechocystis* for n-butanol production. *Microb. Cell Fact.* **14**, 167 (2015).
36. M. Koch et al., Maximizing PHB content in *Synechocystis* sp. PCC 6803: Development of a new photosynthetic overproduction strain. *Microb. Cell Fact.* **19**, 231, <https://doi.org/10.1101/2020.10.22.350660> (2020).
37. R. Y. Stanier, J. Deruelles, R. Rippka, M. Herdman, J. B. Waterbury, Generic assignments, strain histories and properties of pure cultures of cyanobacteria. *Microbiology* **111**, 1–61 (1979).
38. K. L. Guan, J. E. Dixon, Eukaryotic proteins expressed in *Escherichia coli*: An improved thrombin cleavage and purification procedure of fusion proteins with glutathione S-transferase. *Anal. Biochem.* **192**, 262–267 (1991).
39. A. Shevchenko, H. Tomas, J. Havlis, J. V. Olsen, M. Mann, In-gel digestion for mass spectrometric characterization of proteins and proteomes. *Nat. Protoc.* **1**, 2856–2860 (2006).
40. J. Rappsilber, M. Mann, Y. Ishihama, Protocol for micro-purification, enrichment, pre-fractionation and storage of peptides for proteomics using StageTips. *Nat. Protoc.* **2**, 1896–1906 (2007).
41. M. Koch, T. Orthwein, J. T. Alford, K. Forchhammer, The Slr0058 protein from *Synechocystis* sp. PCC 6803 is a novel regulatory protein involved in PHB granule formation. *Front. Microbiol.* **11**, 809 (2020).
42. M. Chander, B. Setlow, P. Setlow, The enzymatic activity of phosphoglycerate mutase from gram-positive endospore-forming bacteria requires Mn²⁺ and is pH sensitive. *Can. J. Microbiol.* **44**, 759–767 (1998).
43. N. J. Kuhn, B. Setlow, P. Setlow, Manganese(II) activation of 3-phosphoglycerate mutase of *Bacillus megaterium*: pH-sensitive interconversion of active and inactive forms. *Arch. Biochem. Biophys.* **306**, 342–349 (1993).
44. G. Fiedler, M. Arnold, S. Hannus, I. Maldener, The DevBCA exporter is essential for envelope formation in heterocysts of the cyanobacterium *Anabaena* sp. strain PCC 7120. *Mol. Microbiol.* **27**, 1193–1202 (1998).
45. Y. Perez-Riverol et al., The PRIDE database and related tools and resources in 2019: Improving support for quantification data. *Nucleic Acids Res.* **47**, D442–D450 (2019).

Orthwein et al.

The novel P_{II} -interactor PirC identifies phosphoglycerate mutase as key control point of carbon storage metabolism in cyanobacteria

PNAS | 9 of 9
<https://doi.org/10.1073/pnas.2019881118>



Supplementary Information for

The Novel PII-Interacting Regulator PirC (SII0944) Identifies 3-Phosphoglycerate Mutase (PGAM) as Central Control Point of Carbon Storage Metabolism in Cyanobacteria

Tim Orthwein, Jörg Scholl, Philipp Spät, Stefan Lucius, Moritz Koch, Boris Macek, Martin Hagemann and Karl Forchhammer

Karl Forchhammer

Email: karl.forchhammer@uni-tuebingen.de

This PDF file includes:

SI Material and Methods

SI Figures and Tables

Fig. S1 to S10

Table S1 to S3

SI References

SI Material and Methods

Strains and cultivation

A list of all used strains for this study is provided in Table S1.

For preculturing and growth experiments, the *Synechocystis* sp. PCC 6803 (from now on *Synechocystis*) strains were cultivated in BG₁₁ medium according to Rippka (1). The cultivations were performed in Erlenmeyer flasks without baffles whereby 50 ml cultures were cultivated in 200 ml flask and 200 ml cultures in 500 ml flasks. Typical cultivation was performed either at continuous illumination ($\sim 50 \mu\text{E m}^{-2} \text{s}^{-1}$) or light-dark conditions (12 h light and 12 h darkness) and 28 °C while the cultures were shaken continuously at 125 rpm. For nitrogen depletion, cultures were cultivated in BG11 media without 17,65 mM NaNO₃. Whenever necessary, appropriate antibiotics were added to the different strains to ensure the continuity of the mutation.

For nitrogen deficiency experiments, pre-cultures of *Synechocystis* were cultivated for three days as described previous at an initial OD₇₅₀ of 0.1. Experimental cultures were then prepared in BG11 medium with a set starting OD₇₅₀ of 0.2 and grown for two days under identical conditions until they reached an OD₇₅₀ of 0.6-0.8. For the nitrogen shift experiments, cells from the cultures were harvested by centrifugation (4000 g, 10 min), washed with and resuspended in BG11₀ medium to create cultures with an initial OD₇₅₀ of 0.4.

Cultivation of *Escherichia coli* cultures was performed with LB medium and agar. Lennox broth: 5 g·l⁻¹ Yeast extract, 10 g·l⁻¹ Tryptone, NaCl 5 g·l⁻¹, solid: 15 g·l⁻¹ agar

Plasmids and cloning

A list of all used primer, plasmids and its cloning procedure are listed in Table S2 and Table S3 as well as in Figure S4.

Overexpression and Purification of Proteins

Escherichia coli Lemo21(DE3) were used for overexpression of the various kind of proteins. The expression of His-tagged proteins was performed as described in the manufactured expression protocol in 2-fold concentrated LB media. An overnight expression, induced by addition of 400 μM IPTG, in a 1 l culture was performed with 1 mM L-rhamnose at 25 °C during continuous shaking at 120 rpm. Additionally, dependent on the plasmid the appropriated amount of the antibiotic was added to the culture. The expression of Strep-tagged proteins based on pASK-lba5Plus expression plasmid was induced by addition of 200 $\mu\text{g}\cdot\text{l}^{-1}$ anhydrotetracycline without addition of L-rhamnose because of the T7 RNA polymerase independent expression.

The heterologous proteins containing His-tags were purified via 1 ml Ni-NTA HisTrap columns (GE Healthcare). The cells were lysed in 50 ml lysis buffer containing 50 mM Na-phosphate buffer pH 8, 300 mM NaCl, 1 mM DTT, 1 mM Benzamidine and 0,2 mM PMSF. The His-tagged proteins were loaded on the Ni-NTA column with Buffer A containing 50 mM Na-phosphate pH 8, 300 mM NaCl and eluted via a gradient of increasing imidazole (0-500 mM, Buffer B) using a ÄKTAPurifier™ System (GE Healthcare). After this first purification, the proteins were further purified via size exclusion chromatography using a Superdex™ 200 Increase 10/300 GL (GE Healthcare) with 50 mM Tris/HCl buffer containing 100 mM KCl and 0.5 mM EDTA.

For purification of Strep-tagged proteins, 5 ml Strep-tactin® superflow columns were used. Cells were lysed in lysis buffer containing 100 mM Tris/HCl pH 8, 150 mM NaCl, 1 mM EDTA and 1mM PMSF. The proteins were loaded on the column and eluted with buffer containing 5 mM Desthiobiotin. The buffer of each purified protein was exchanged via dialysis using dialysis buffer (50 mM Tris/HCl pH 7.8-8, 100 mM KCl, 5 mM MgCl₂, 0,5 mM EDTA, 40 % glycerol) and a 3 kDa cutoff dialysis tube. All purification steps were checked via SDS-PAGE according to previous studies (2).

The His-tag of PGAM was removed by Thrombin cleavage using Thrombin of bovine of Sigma Aldrich according to protocol (3).

In-batch Pulldown assay

Interactions between PirC and PII were first checked via an in-batch pulldown experiment. For this, His₆-PirC and Strep-PII were mixed in equimolar amounts and incubated for 20 min at room temperature in buffer containing 50 mM Tris/HCl, pH 7.8, 100 mM KCl, 0.5 mM EDTA, 10 mM MgCl₂ and additionally either 2 mM ATP, ADP or ATP and 2-OG. The mixtures were applied to Strep-Tactin XT coated magnetic beads. After 30 min of incubation the magnetic beads were removed via a strong magnet, followed by three times washing step with incubation buffer. For analysis of bound proteins via SDS-PAGE, the beads were boiled 10 min at 100 °C as described previously (2).

Co-Immunoprecipitation and Liquid chromatography-Mass spectrometry (LC-MS/MS)

To identify putative interaction partners of PirC, co-immunoprecipitation experiments were performed. For this, *Synechocystis* ΔPirC::PirC-mCitrine cultures were pre-cultivated in 100 ml BG11 medium to an OD₇₅₀ of ~0,8 and subsequently shifted to N-depleted medium. For Co-IP experiments in presence of the PII effector molecules, cells were harvested after 24 h N-depletion by centrifugation for 10 min at 4200 x g at 4 °C, followed by resuspension of the cell pellet in 2 ml binding buffer containing 100 mM TRIS (pH 7.5), 100 mM KCl, 1 mM MgCl₂, 1 mM DTT, 0.5 mM EDTA, 2 mM ATP and 2-OG. The cells were lysed with 150 µl glass beads in 1.5 ml screw cap tubes by harsh shaking in a high-speed homogenizer for 5 times 30 sec shaking at speed of 7 m · s⁻¹ with each 5 min break. The lysate was then centrifuged at 25,000 x g for 5 min at 4 °C and a supernatant volume corresponding to a protein yield of approx. 3 mg was used for the immunoprecipitation. Therefore, GFP-Trap Magnetic Agarose beads or control beads without antibodies were used according to the manufactured protocol (both Chromotek, Planegg-Martinsried, Germany). The loaded magnetic beads were heated for 10 min at 95 °C in SDS loading buffer for the dissociation of purified proteins. Protein solutions were subjected to short SDS-PAGE runs, in which proteins were allowed to migrate for 1.5 cm into 12% Bis-Tris Gels (Invitrogen) and then stained with Coomassie blue. Protein containing gel regions were isolated and subjected to InGel digestion with trypsin as described elsewhere (4). Three independent experiments, each including a PirC-mCitrine and a control CoIP were performed in total. Peptides were subjected to a clean-up step using StageTips (5) and subsequently analyzed by mass spectrometry. LC-MS/MS analysis was performed on a Q Exactive HF mass spectrometer (ThermoFisher, Germany), using linear, segmented 60 min nanoLC RP gradients as described elsewhere (16). All raw data was processed using MaxQuant software suite (version 1.6.5.0) at default settings. MS2 peak lists were searched against a target-decoy database of the *Synechocystis* sp. PCC 6803 proteome, including the sequence of PirC (SII0944)-mCitrine. Label free quantification was used to calculate LFQ intensities for each CoIP sample. Data from all experiments was analyzed via the Perseus software (version 1.6.5.0). For the identification of significantly enriched proteins in PirC-mCitrine CoIPs, a *t*-test was performed with the following requirements: each protein had to be detected in at least two replicates and an FDR of 0.01 at S0 = 0.1 was set.

Biolayer interferometry using the Octet K2 system

In vitro binding studies were done by Bio-layer interferometry (BLI) using Octet K2 system (FortéBio). The experiments were performed in HEPES buffer (20 mM HEPES-KOH pH 8.0, 5 mM MgCl₂, 0.005 % NP-40, For protein interactions of His₈-PII-strep-PirC 150 mM KCl and for the His₆-PGAM-strep-PirC interaction 10 mM MnCl₂ was added to the buffer. In the first step PII-His₈ (400 nM, trimeric) or PGAM-His₆ (500 nM) were immobilized on Ni-NTA sensors (FortéBio) followed by a 60 sec baseline measurement. For the binding of PirC, the biosensors were dipped into the PirC solution for 180 sec (Association), with concentrations ranged between 9.375 nM – 1500 nM.

Dependent on the experiment different effector molecules were added to the binding buffer, ADP, ATP and 2-OG in PII binding studies, and 2PG as well as 3 PGA in PGAM binding assays. The assay was terminated by a 300 sec dissociation step. To prevent false positive results in each experimental set one measurement without any interaction partner was performed. The biosensors were regenerated after each use with 10 mM glycine (pH 1.7) and 10 mM NiCl₂ as proposed in manufacturers recommendations. The recorded curves of a set were preprocessed by aligning to the average of the baseline step and to the dissociation step. The response in equilibrium (R_{eq}) was calculated using the Data Analysis Software of the Octet System. The Concentration versus R_{eq} plots were made for each set of experiments which were then used to calculate the Dissociation constant K_D .

Glycogen measurement

The determination of the glycogen content of *Synechocystis* cultures was performed according to previous studies (6, 7). The glycogen was isolated from cell pellets of 2 ml culture. The glycogen was hydrolyzed to glucose with 4,4 U · μ l⁻¹ amyloglucosidase from *Aspergillus niger* (Sigma Aldrich) for 2 h at 60 °C. The resulting glucose concentration was measured via o-toluidine assay (8). The samples were boiled in 1:6 dilution with a 6 % o-toluidine reagent (in glacial acetic acid) for 10 min, then cooled on ice and measured at 635 nm. The concentration of samples was calculated using a calibration curve of defined quantity of glucose (0, 10 μ g, 50 μ g, 100 μ g, 250 μ g, and 500 μ g).

PHB Quantification

Polyhydroxybutyrate was detected by high-performance liquid chromatography as described previously (9). Eleven ml of chlorotic cultures were centrifuged at 4200 x g for 10 min and the cell pellet was vacuum dried in pre-balanced 2 ml reaction tubes. To calculate the cell dry weight (CDW) the tube was cradled again. Then the pellet was boiled for 60 min in concentrated H₂SO₄ (18 mol · l⁻¹). Thereby, the cells were lysed and PHB converted to crotonic acid. Next, 110 μ l of this solution was diluted 1:10 with 14 mM sulfuric acid solution and centrifuged 5 min at 25,000 × g followed by another 1:2 dilution. After another centrifugation step 300 μ l of the clear supernatant was used for analytical HPLC. Reversed-phase HPLC was performed using the Chromatography system HP1090 M, equipped with a thermostated autosampler and diode-array-detector, HP Kayak XM 600 workstation. The crotonic acid was detected by measuring the absorbance at 210 nm. The crotonic acid concentration of the samples was calculated using a calibration curve of defined concentrations (0.5 mg·ml⁻¹, 0.25 mg·ml⁻¹, 0.125 mg·ml⁻¹ and 0.0625 mg·ml⁻¹)

PGAM enzymatic assay

The PGAM activity and the effect of PirC was determined by a coupled enzyme assay as described previous (10, 11). For that, 10 μ g of purified PGAM was used in a 1 ml reaction. The reaction mixture containing 20 mM HEPES-KOH (pH 8,0), 100 mM KCl, 5 mM MgSO₄, 0.4 mM MnCl₂, 50 μ g·ml⁻¹BSA, 1 mM DTT, 0.4 mM ADP, 0.2 mM NADH, 0.5 U enolase (Sigma Aldrich), 2 U Pyruvate kinase (Sigma Aldrich), 2 U Lactate dehydrogenase (Roche) and 10 μ g PGAM was pre-warmed to 30 °C. The Assay was started by adding the 3-PGA solutions. The resulted decrease of NADH over time was recorded with Specord50 (Jena Analytics) at 340 nm. A blank assay without 3-PGA was also performed, no decrease was detectable.

Phase contrast and fluorescence microscopy

The visualization of PHB granules was done by phase contrast fluorescence microscopy using the Leica DM5500 B with the Leica CTR 5500 illuminator. The integrated camera Leica DFC 360 FX was used for image acquisition. The settings were adjusted by the Leica Application Suite Advanced Fluorescence (LAS 4.0). The specimen was prepared by dropping 10 μ l of cell culture on an agarose coated microscope slide and observed using the Leica HCX PL FLUATAR (100 x

4

1,30 PH3) with immersion oil for a 1000-fold magnification. The visual detection of PHB via fluorescence was performed by staining the cells with 0,33 $\mu\text{g}\cdot\text{ml}^{-1}$ Nile Red. The fluorescence of Nile Red was excited with light between 542 – 568 nm (CYR3 channel) and of GFP like proteins with light between 455-495 nm (GFP channel). The images were processed by 3D deconvolution of all channels using LAS.

Transmission electron microscopy

For electron microscopic pictures, *Synechocystis* cells were fixed with glutaraldehyde and post-fixed with potassium permanganate, respectively. Afterwards, microtome sections were stained with lead citrate and uranyl acetate (12). The samples were then examined using a Philips Tecnai 10 electron microscope at 80 kV.

Metabolome analysis

For metabolome analysis by LC-MS *Synechocystis* was cultivated in 200 ml under N-depletion as described previously for 48 h under continuous lightning. The sampling was carried out 0, 6, 24 and 48 hours after the shift. Samples of 5 mL liquid culture were quickly harvested onto nitrocellulose membrane filters (\varnothing 25 mm, 0.45 μm pore size, Porafil NC, Macherey-Nagel) by vacuum filtration, put in 2 ml Eppendorf microtubes, and immediately frozen in liquid nitrogen. Cells on filters were stored at -80 °C until analysis.

Extraction was done using LC-MS grade chemicals. To every filter, 630 μL methanol and 1 μL carnitine as internal standard (1 $\text{mg}\cdot\text{ml}^{-1}$) were added. Cells were re-suspended by rough mixing and then incubating samples in a sonication bath for 10 min. Samples were shaken for 15 min prior to addition of 400 μL chloroform and incubation at 37 °C for 10 min. Next, 800 μL of ultrapure water were added. The extracts were shaken for 15 min and then incubated at -20 °C for at least 2 h. Cell debris and filters were removed by centrifugation (20000 g, 5 min, 4 °C). The upper polar phase was transferred completely into a new microtube and subsequently dried by vacuum concentration (Concentrator plus, Eppendorf). The dried extracts were re-suspended in 200 μL deionized water and filtrated (0.2 μm filters, Omnifix-F, Braun). The filtrates were then analysed via the high-performance liquid chromatograph mass spectrometer LCMS-8050 system (Shimadzu), as previously described by Selim et al., 2018 (13). LC-MS data analysis was done using the Lab solution software package (Shimadzu).

Heading

Subhead. Type or paste text here. You may break this section up into subheads as needed (e.g., one section on “Materials” and one on “Methods”).

SI Figures

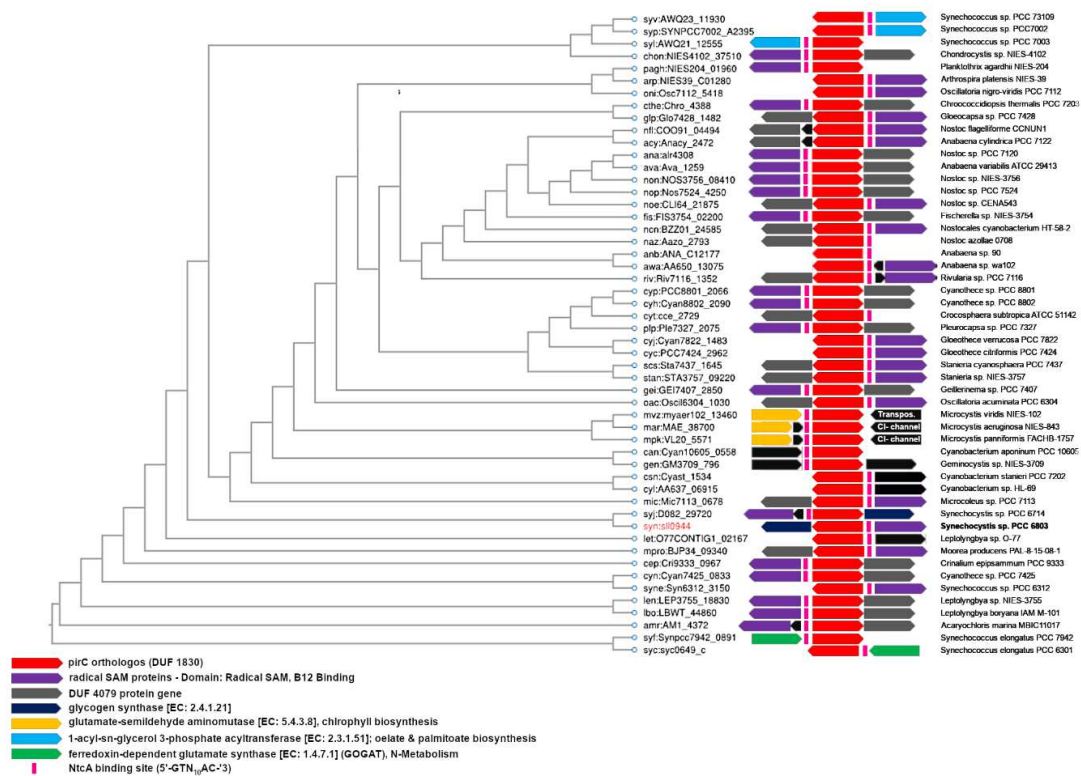


Fig. S1 - Cluster comparison of 53 different Cyanobacterial PirC orthologs. Detected by a Smith-Waterman (SW) algorithm based SSEARCH for bidirectional best hits of the KEGG SSDB (Sequence Similarity Database) with a SW-Score threshold of 100. Red arrows represents the pirC orthologous with direction. In front of each pirC gene a predicted NtcA binding site is present (5'-GTN10AC-3', pink bars). In 67 % of the cases the pirC are next to genes encoding radical SAM-like proteins (purple arrows).

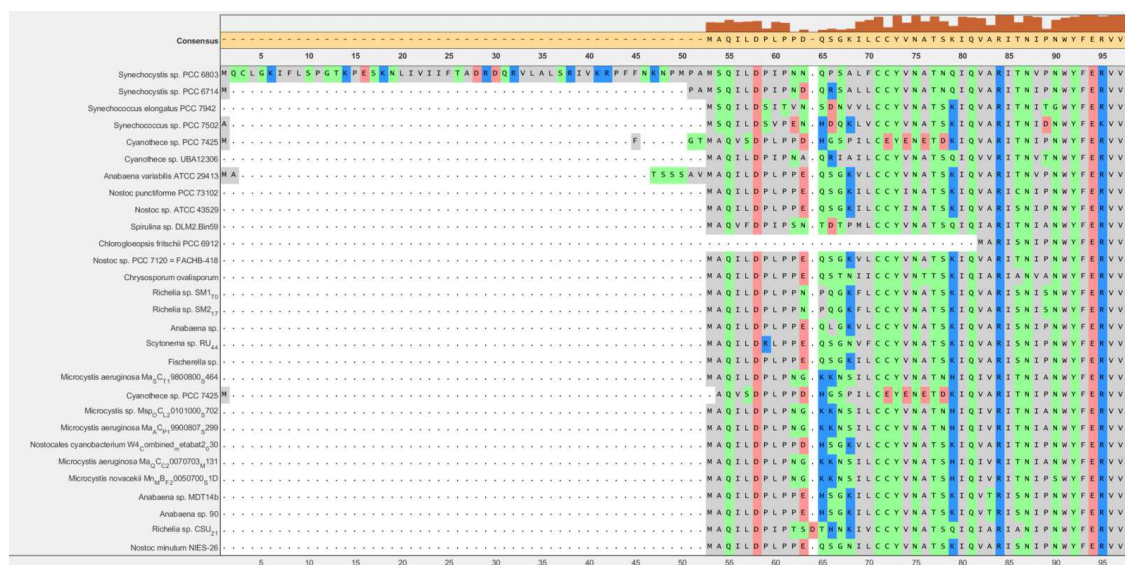


Fig. S2 – Multiple alignment of PirC orthologs of different cyanobacteria. It is shown that the first 52 AA are only present in *Synechocystis* sp. PCC 6803 PirC (first row). The picture shows extract of alignment of 29 different cyanobacterial orthologs of a multiple alignment of 74 different orthologs.

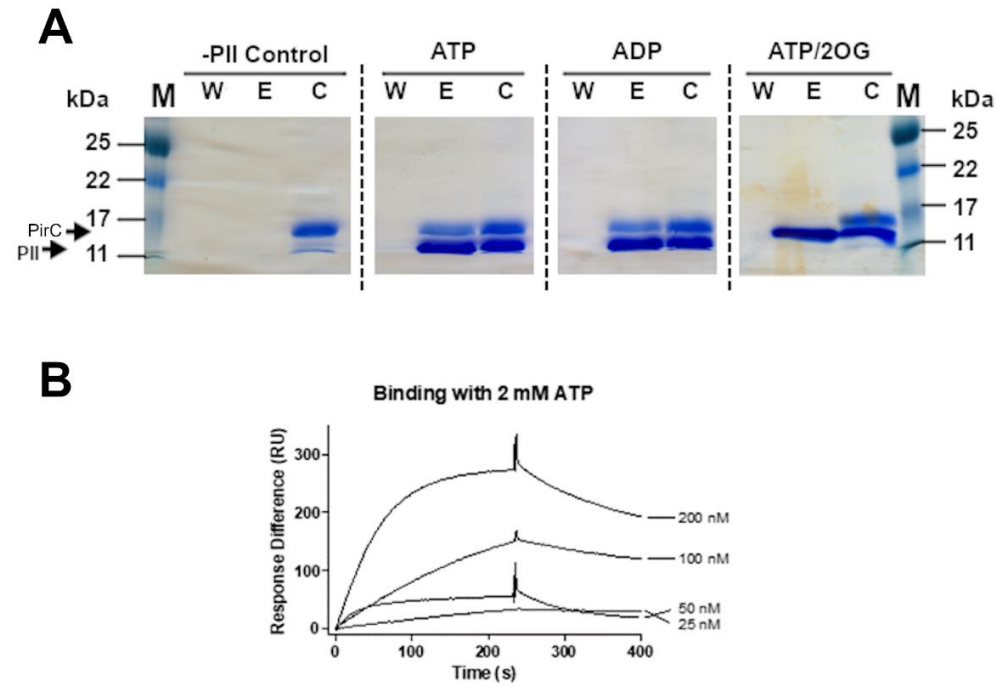


Fig. S3 - SDS-PAGE of in-batch pulldown assays in presence of 10 mM MgCl_2 and either 2 mM ATP, 2 mM ADP, or 2 mM ATP/2-OG. The first column represents the negative control without P_{11} . PirC was co-eluted with P_{11} attached to strep-tactin XT coated magnetic beads in presence of ATP and ADP, observable by two bands. However, there is no band in presence of ATP/2-OG. In the controls without P_{11} , no elution of PirC was observed. 1: Marker; W: washing fractions; E: elution fractions; C: control (reaction mix before the pulldown was performed).

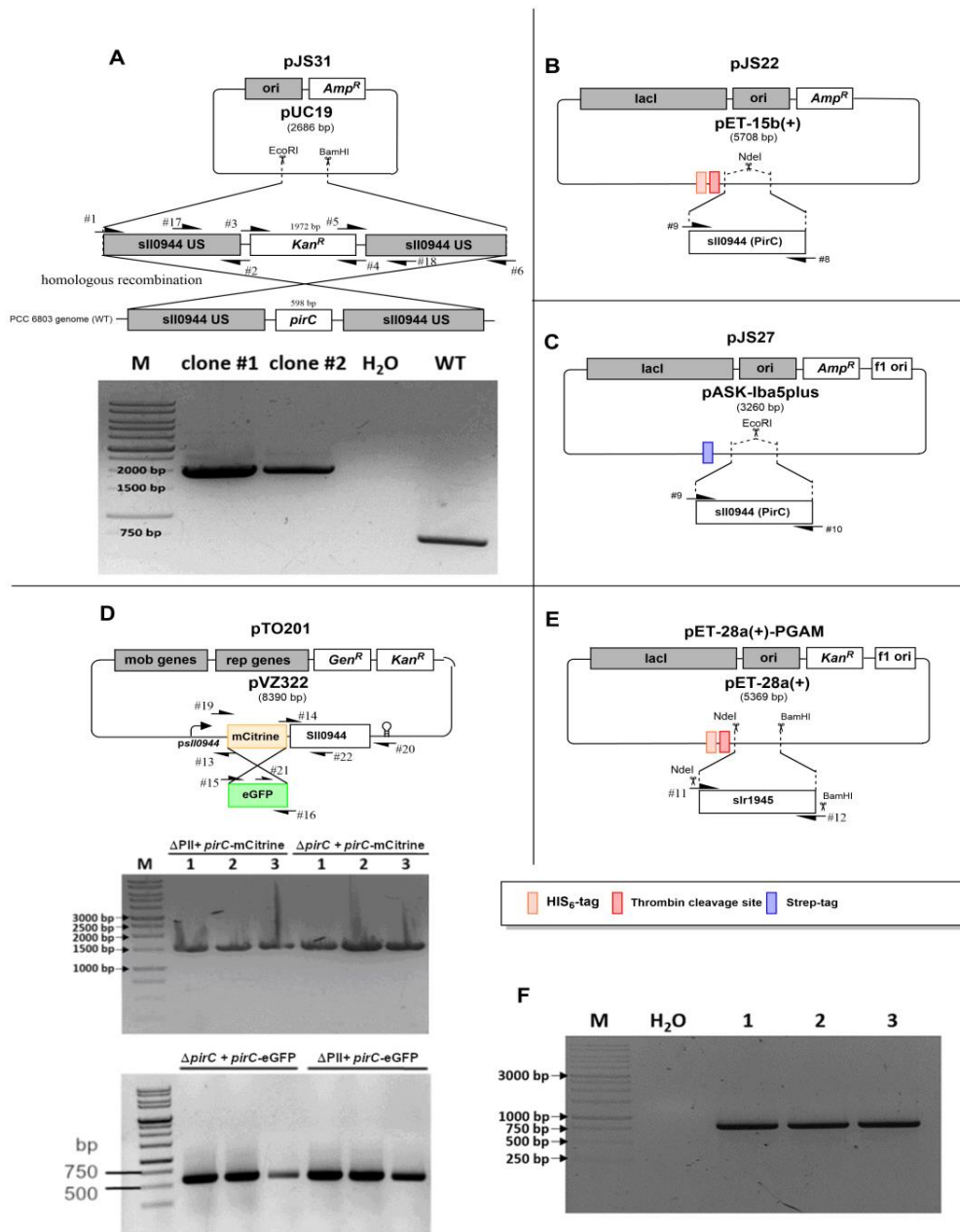


Fig. S4 - Plasmid Construction and mutant check in *Synechocystis* sp. PCC 6803. (A) Plasmid construction, gene deletion technique, manufactured by Gibson Assembly and colony PCR check of *Synechocystis* Δ *pirC* gene using primer pair #17/18 **(B)** Plasmid construction pJS22 for His₆-PirC expression in *E. coli*, manufactured by Gibson Assembly **(C)** Plasmid construction pJS27 for Strep-PirC expression in *E. coli*, manufactured by Gibson Assembly **(D)** Plasmid construction pTO201 for eGFP-PirC expression in *Synechocystis*, manufactured by Gibson Assembly as well as colony PCR of successful transformation of pVZ322-mCitrine-*pirC*-comp and pTO201. **(E)** Plasmid construction pET-28a(+)-PGAM for His₆-PirC expression in *E. coli*. Manufactured by Restriction/ligation method **(F)** colony PCR of successful transformation of pVZ322-*pirC*-comp.

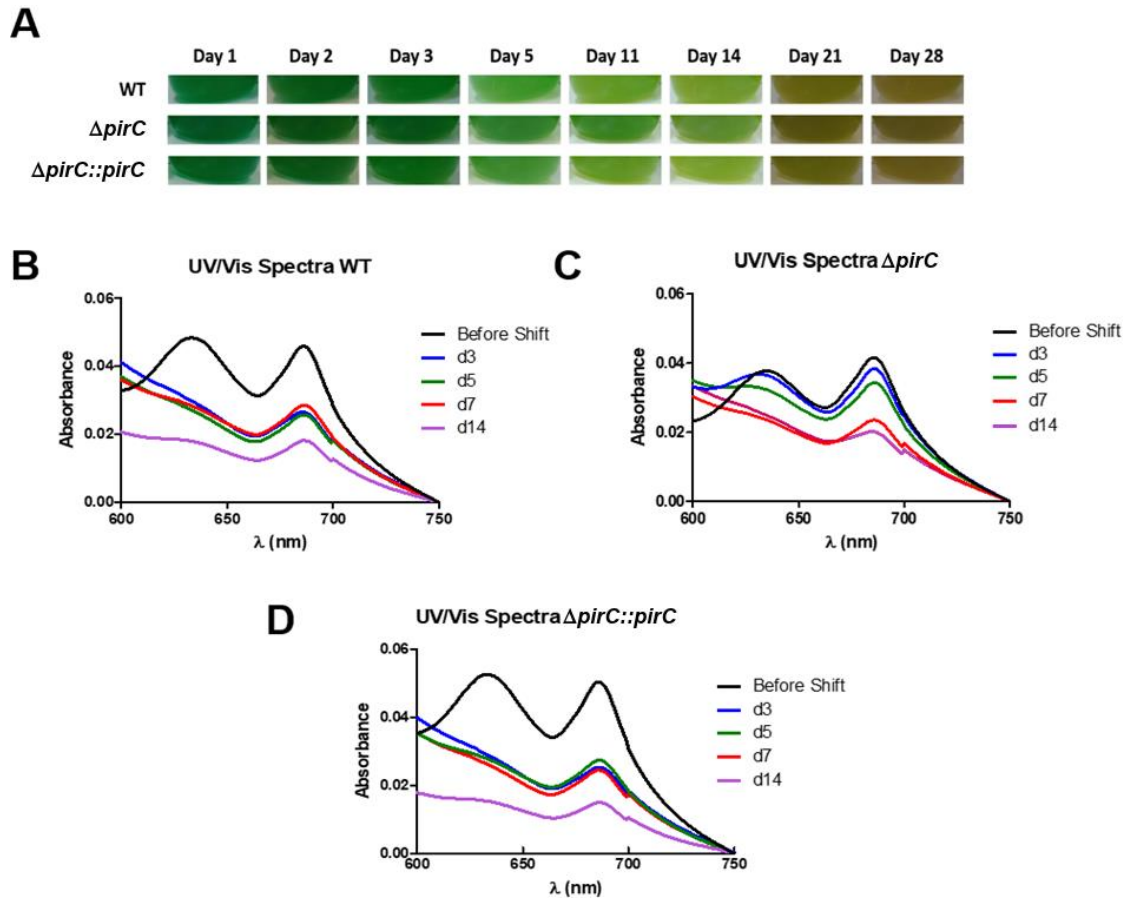


Fig. S5 - Chlorosis due to nitrogen depletion of *Synechocystis* wild type, $\Delta pirC$, and $\Delta pirC::pirC$ in the day/night cabinet. (A) Photographs showing depigmentation of representative cultures from the three replicates; **(B)** UV/Vis spectra (mean of three replicates) of the wild type; **(C)** UV/Vis spectra (mean of three replicates) of the $\Delta pirC$ mutant; **(D)** UV/Vis spectra (mean of three replicates) of the complemented mutant $\Delta pirC::pirC$.

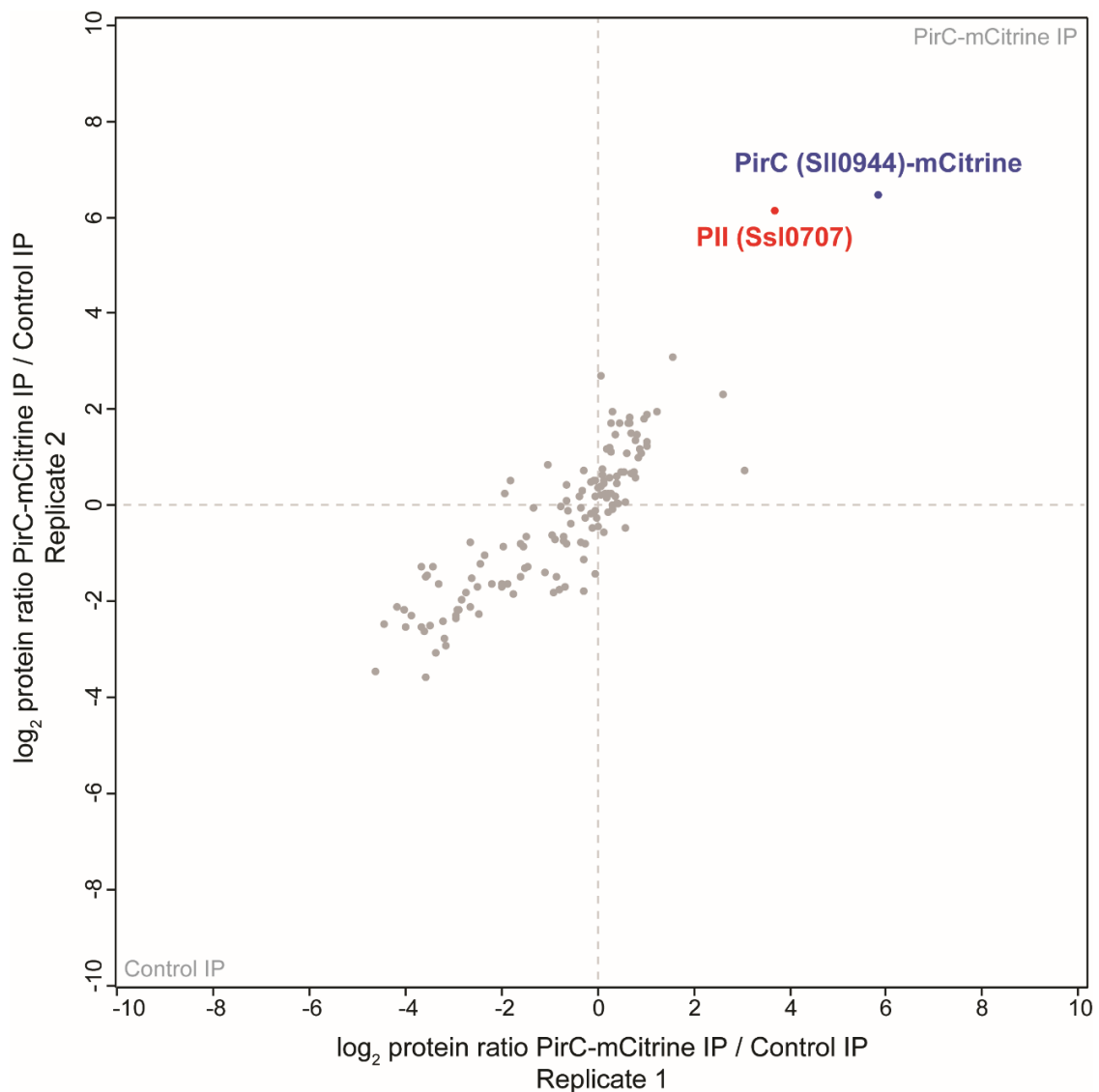


Fig. S6 - Validation of the interaction of the PirC-mCitrine construct with PII. The newly designed PirC-mCitrine fusion protein was tested in anti-GFP immunoprecipitation (IP) experiments for interaction with the PII protein at conditions of low ATP and 2-OG levels, as revealed in reverse IP experiments against a tagged PII construct (14). The scatterplot of two independent PirC-mCitrine IP experiments confirms a significant co-enrichment (p -value=0.01) of PirC and PII, indicated in blue and red, respectively. The IP was performed with crude cell extracts from nitrogen-starved cells of the $\Delta pirC::pirC-mCitrine$ strain, without addition of key metabolites. Extracts were either incubated with GFP-Trap coated magnetic agarose beads (PirC-mCitrine IP) or protein A/G agarose beads coated with an unrelated antibody (Control IP). IP eluates were differentially labeled by dimethylation labeling and analyzed by high accuracy LC-MS/MS. MS data was processed and analyzed as described elsewhere (14, 15).

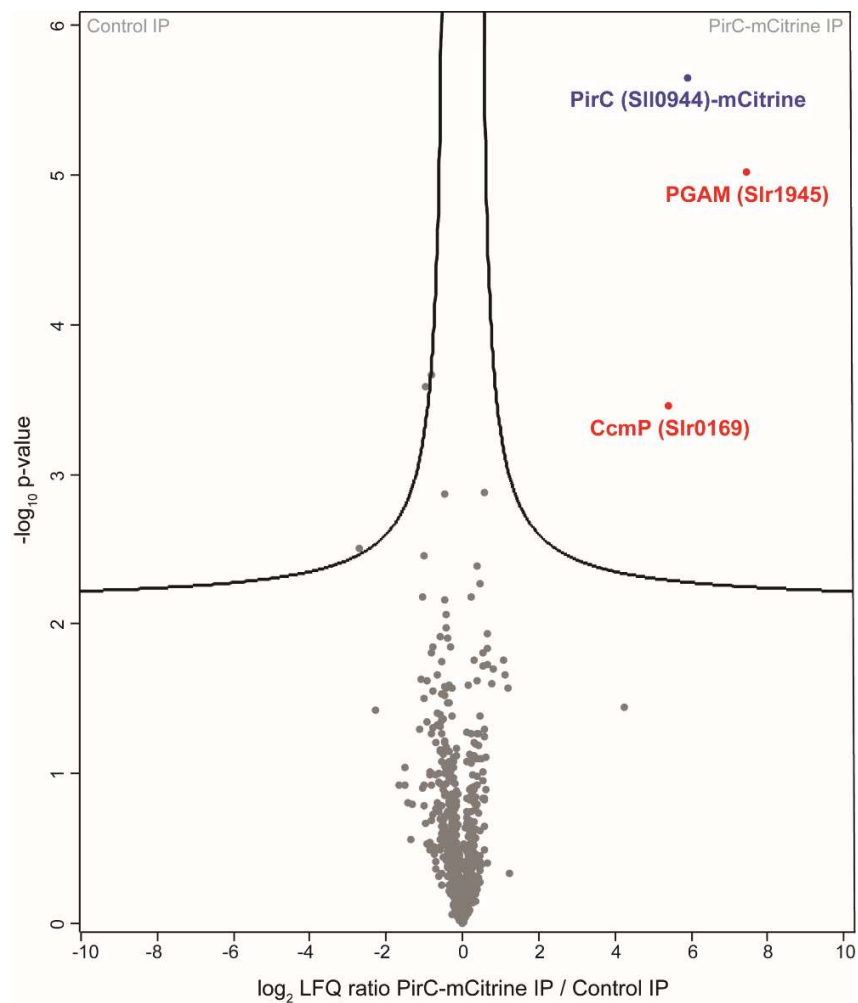


Fig. S7 - The PirC interactome at nitrogen starvation conditions. Volcanoplot of three independent PirC-mCitrine immunoprecipitation (IP) experiments displays co-enriched proteins. Crude cell extracts from the nitrogen-starved $\Delta pirC::pirC-mCitrine$ strain were incubated with either GFP-Trap coated magnetic agarose beads (PirC-mCitrine IP) or non-coated beads (Control IP) in presence of ATP, 2-OG and Mg^{2+} (each 2 mM). IP eluates were analyzed by high accuracy LC-MS/MS using label-free quantification to calculate protein enrichment ratios. Significantly enriched proteins were defined by *t*-test (FDR=0.01; S0=0.1) and are indicated in blue (PirC-mCitrine) or red (co-enriched proteins).

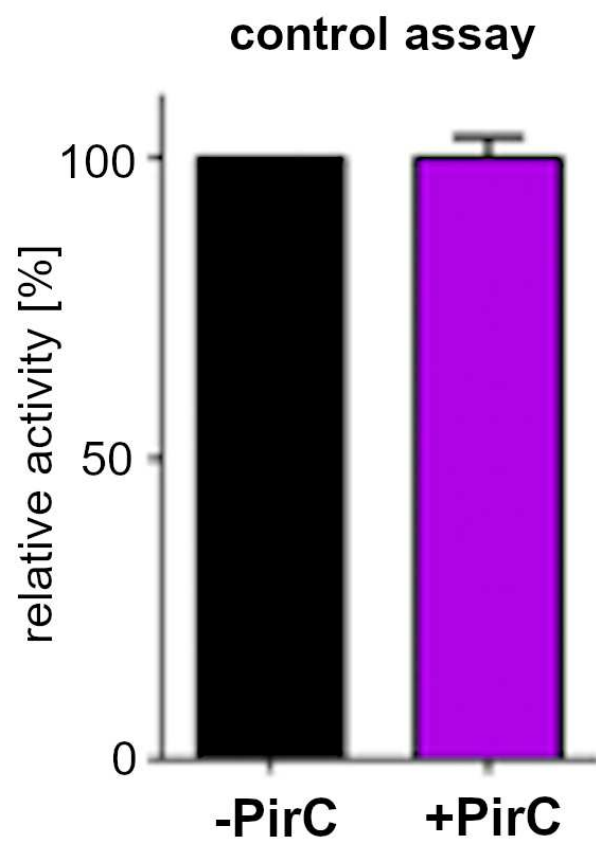


Fig. S8 – Control assay of coupled enzymes. Black bar represents the mean of triplicates with SD of control assay without PirC addition. Purple bar represents the mean of triplicates with SD of control assay with the addition of 600 nM PirC. In the assay 0.625 mM 2-PGA was added to the assay.

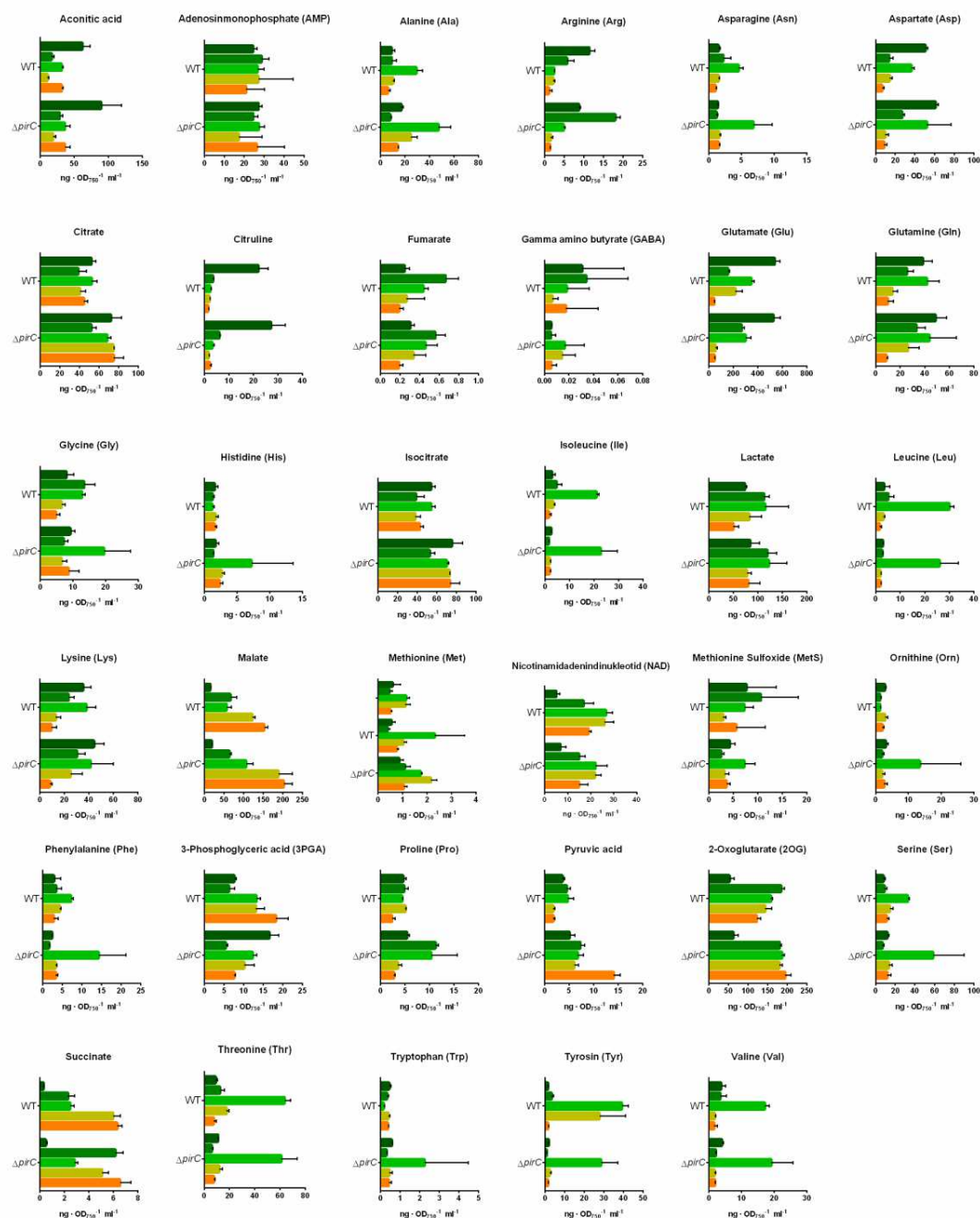


Fig. S9 – LC-MS analysis of the hole spectrum of measured compounds. On x-axis the concentration of the compounds is shown in $\text{ng} \cdot \text{OD}_{750}^{-1} \cdot \text{ml}^{-1}$. Each bar represents the mean of two technical replicates of two biological replicates. The Error bar represents the SD of the measurement.

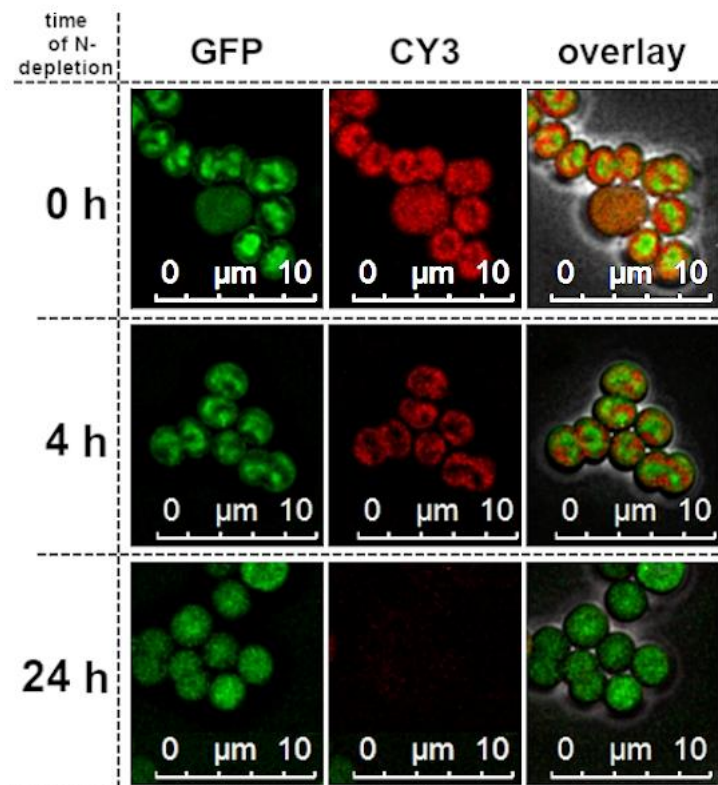


Figure S10 - Intracellular localization of the PirC-eGFP fusion protein in *Synechocystis* sp. PCC 6803. Change of the intracellular localization of the PirC-eGFP signal in *Synechocystis* after nitrogen depletion. Representative pictures of three biological replicates. Directly after the shift to nitrogen depleted conditions, the signal is localized centrally in the cytoplasm (0h) with no clear change after 4 h (4 h). However, the signal is more distributed throughout the cell after 24 h.

Table S1 - Used Organisms and strains in this study

Organism	Strain	Genotype	Purpose
<i>E. coli</i>	Top10	F- mcrA Δ (mrr-hsdRMS-mcrBC) Φ 80lacZ Δ M15 Δ lacX74 recA1 araD139 Δ (araleu)7697 galU galK rpsL (StrR) endA1 nupG	Molecular Cloning
<i>E. coli</i>	NEB10 β	Δ (ara-leu) 7697 araD139 fhuA Δ lacX74 galK16 galE15 e14- Φ 80dlacZ Δ M15 recA1 relA1 endA1 nupG rpsL (StrR) rph spoT1 Δ (mrr-hsdRMS-mcrBC)	Molecular Cloning
<i>E. coli</i>	Lemo21(DE3)	fhuA2 [lon] ompT gal (λ DE3) [dcm] Δ hsdS/ pLemo(CamR) λ DE3 = λ sBamHIo Δ EcoRI-B int::(lacI::PlacUV5::T7 gene1) i21 Δ nin5 pLemo = pACYC184-PrhaBAD-lysY	Protein Expression
<i>E. coli</i>	Lemo21(DE3) + pJS15	Lemo21(DE3) + pJS15	Expression of strep-Tagged PII protein
<i>E. coli</i>	Lemo21(DE3) + pJS22	Lemo21(DE3) + pJS22	Expression of His ₈ -Tagged PirC
<i>E. coli</i>	Lemo21(DE3) + pJS26	Lemo21(DE3) + pJS26	Expression of His ₈ -Tagged PirC
<i>E. coli</i>	Lemo21(DE3) + pJS27	Lemo21(DE3) + pJS27	Expression of strep-Tagged PirC
<i>E. coli</i>	Lemo21(DE3) + pET-28a(+)-PGAM	Lemo21(DE3) + pET-28a(+)-PGAM	Expression of His ₆ -Tagged PGAM
<i>Synechocystis</i> sp. PCC 6803	wild type glucose sensitive	WT	Background strain, control
<i>Synechocystis</i> sp. PCC 6803	Δ PII	ssl0707::Spec ^R	Control strain
<i>Synechocystis</i> sp. PCC 6803	Δ pirC	pirC::Kan ^R	Characterization of ssl0944 KO mutants
<i>Synechocystis</i> sp. PCC 6803	Δ pirC::pirC	pirC::Kan ^R pVZ322-pirC	Complementation of ssl0944 knock out
<i>Synechocystis</i> sp. PCC 6803	Δ pirC::pirC-mCitrine	Δ pirC pVZ322-pirC-mCitrine	Localization of PirC in Δ pirC and Co-immunoprecipitation
<i>Synechocystis</i> sp. PCC 6803	Δ pirC::pirC-eGFP	Δ pirC pVZ322-pirC- eGFP	Localization of PirC in Δ pirC and Co-immunoprecipitation

Table S2 - Used Primer in this study

#No	Primer	Sequence (5'-3')
#1	pUC19-pirCUS_fw	GTTTTCCCAGTCAGACGTTGTAACGACGGCCAGTGAATTGTCGGCTGAAATTCATC
#2	pirCUS-KanR_rev	GAATTGACATAAGCCTGTTCAATCAAATTTTTGACTCTG
#3	pirCUS-KanR_fw	CAGAGTCAAAAAATTTGATTCAACAGGCTTATGTCAATTC
#4	KanR-pirCDS_rev	CCAATTCATTAATTCAATTGGAGTTTGTAGAAACGCAAAAA
#5	KanR-pirCDS_fw	GCCATCCTGACGGATGGCCTTTTTGCGTTTCTACAACTCCAATGAATTAATGAATTGG
#6	pirCDS-pUC19_rev	CGCCAAGCTTGCATGCCTGCAGGTCGACTCTAGAGGATCTGGAACATGGCTTCCCCTTTC
#7	pET15b-pirC(correct)_fw	CATCATCATCACAGCAGCGGCTGGTGCCGCGCGGCAGCATGTGCGCAAATCTTGGACCC
#8	pirC-pET15b_rev	CCTTTCGGGCTTTGTTAGCAGCCGGATCCTCGAGCATACTATGCGACAAGAGATTGAC
#9	pASKIba5Plus-pirC_fw	CCACCCGCAGTTCGAAAAAGCGCGCGAGACCGCGGTCCCATGTGCGCAAATCTTGGACCC
#10	pASKIba5Plus-pirC_fw	GGTCGACCTCGAGGGATCCCCGGGTACCGAGCTCGAATTCTATGCGACAAGAGATTGAC
#11	Slr1945-NdeI-fw	CATATGATGGCAGAGGCACCGATCGCC
#12	Slr1945-BamHI-rv	GGATCCCTAACGGGAGAGATTGACCGG
#13	pVZmCit_pirC_fwd	CTGCAGGAGCAGAAGAGCATAC
#14	pVZmCit_pirC_rev	AGCCACTAAGGATTGGGAAG
#15	pTO201_eGfp_fwd	ACACGAGTCCGAGGATATGACTTCCCAATCCTTAGTGGCTATGAGTAAAGGAGAAGAAC
#16	pTO201_eGFP_rev	CTGGCTTTGCTTCCAGATGTATGCTCTTCTGCTCCTGCAGTTATTTGTATAGTTCATCCATGC
#17	6803 pirCKOcheck_fw	TGGCATGGCCTAAGTATTCC
#18	6803 pirCKOcheck_rev	GCGTTCTGCAGGGGATTACC
#19	pVZ322seq_fw	CCTGGCTTTGCTTCCAGATG
#20	pVZ322seq_rev	TGCCCCGATTACAGATCCTC
#21	seq_pTO201_fwd	CAATGCTTTGCGAGATACCC
#22	seq_pTO201_rev	AGCTCCATAGCCGCTTTC

Table S3 – Plasmids used in this study

Plasmid	Purpose	Source
pJS15	Expression of Strep-Tagged PII protein (Ssl0707) in E. coli	(16)
pJS22	Expression of His ₈ -Tagged PirC (Sll0944) in E. coli T7-strains	This study
pJS26	Expression of His ₈ -Tagged PII protein (Ssl0707) in E. coli T7-strains	(16)
pJS27	Expression of strep-Tagged PirC (Sll0944) in E. coli	This study
pJS31	Kan ^R deletion of the pirC gene in Synechocystis sp. PCC 6803	This study
pET-28a(+)-PGAM	Expression His ₈ -Tagged PGAM (Slr1945) in E. coli T7-strains	This study
pVZ322-pirC-comp	Complementation of pirC deletion	(17)
pVZ322-mCitrine-pirC-comp	Complementation of pirC deletion tagged to mCitrine protein	(17)
pTO201	Complementation of pirC deletion tagged to eGFP protein	This study

SI References

1. R. Y. Stanier, J. Deruelles, R. Rippka, M. Herdman, J. B. Waterbury, Generic Assignments, Strain Histories and Properties of Pure Cultures of Cyanobacteria. *Microbiology* **111**, 1–61 (1979).
2. U. K. Laemmli, Cleavage of structural proteins during the assembly of the head of bacteriophage T4. *Nature* **227**, 680–685 (1970).
3. K. Guan, J. E. Dixon, Eukaryotic proteins expressed in *Escherichia coli*: An improved thrombin cleavage and purification procedure of fusion proteins with glutathione S-transferase. *Analytical Biochemistry* **192**, 262–267 (1991).
4. A. Shevchenko, H. Tomas, J. Havlis, J. V. Olsen, M. Mann, In-gel digestion for mass spectrometric characterization of proteins and proteomes. *Nat Protoc* **1**, 2856–2860 (2006).
5. J. Rappsilber, M. Mann, Y. Ishihama, Protocol for micro-purification, enrichment, pre-fractionation and storage of peptides for proteomics using StageTips. *Nat Protoc* **2**, 1896–1906 (2007).
6. M. Gründel, R. Scheunemann, W. Lockau, Y. Zilliges, Impaired glycogen synthesis causes metabolic overflow reactions and affects stress responses in the cyanobacterium *Synechocystis* sp. PCC 6803. *Microbiology (Reading, England)* **158**, 3032–3043 (2012).
7. A. Klotz, J. Georg, L. Bučinská, S. Watanabe, V. Reimann, W. Januszewski, R. Sobotka, D. Jendrosseck, W. R. Hess, K. Forchhammer, Awakening of a Dormant Cyanobacterium from Nitrogen Chlorosis Reveals a Genetically Determined Program. *Current biology : CB* **26**, 2862–2872 (2016).
8. K. M. Dubowski, An o-Toluidine Method for Body-Fluid Glucose Determination. *Clinical Chemistry* **8**, 215–235 (1962).
9. M. Koch, T. Orthwein, J. T. Alford, K. Forchhammer, The Slr0058 Protein From *Synechocystis* sp. PCC 6803 Is a Novel Regulatory Protein Involved in PHB Granule Formation. *Frontiers in microbiology* **11**, 809 (2020).
10. M. Chander, B. Setlow, P. Setlow, The enzymatic activity of phosphoglycerate mutase from gram-positive endospore-forming bacteria requires Mn²⁺ and is pH sensitive. *Canadian journal of microbiology* **44**, 759–767 (1998).

11. N. J. Kuhn, B. Setlow, P. Setlow, Manganese(II) activation of 3-phosphoglycerate mutase of *Bacillus megaterium*: pH-sensitive interconversion of active and inactive forms. *Archives of biochemistry and biophysics* **306**, 342–349 (1993).
12. G. Fiedler, M. Arnold, S. Hannus, I. Maldener, The DevBCA exporter is essential for envelope formation in heterocysts of the cyanobacterium *Anabaena* sp. strain PCC 7120. *Molecular microbiology* **27**, 1193–1202 (1998).
13. K. A. Selim, F. Haase, M. D. Hartmann, M. Hagemann, K. Forchhammer, PII-like signaling protein SbtB links cAMP sensing with cyanobacterial inorganic carbon response. *Proceedings of the National Academy of Sciences of the United States of America* **115**, E4861–E4869 (2018).
14. B. Watzer, P. Spät, N. Neumann, M. Koch, R. Sobotka, B. Macek, O. Hennrich, K. Forchhammer, The Signal Transduction Protein PII Controls Ammonium, Nitrate and Urea Uptake in Cyanobacteria. *Frontiers in microbiology* **10**, 1428 (2019).
15. P. J. Boersema, R. Raijmakers, S. Lemeer, S. Mohammed, A. J. R. Heck, Multiplex peptide stable isotope dimethyl labeling for quantitative proteomics. *Nat Protoc* **4**, 484–494 (2009).
16. J. Scholl, L. Dengler, L. Bader, K. Forchhammer, Phosphoenolpyruvate carboxylase from the cyanobacterium *Synechocystis* sp. PCC 6803 is under global metabolic control by PII signaling. *Molecular microbiology*. 10.1111/mmi.14512 (2020).
17. A. Klotz, *Awakening of dormant cyanobacteria: Nitrogen starvation-induced chlorosis and resuscitation of Synechocystis sp. PCC6803* (2017).

12 Appendix

12.1 Contribution to manuscripts

Lucius, S., Makowka, A., Michl, K., Gutekunst, K., & Hagemann, M. (2021). The Entner-Doudoroff Pathway Contributes to Glycogen Breakdown During High to Low CO₂ Shifts in the Cyanobacterium *Synechocystis* sp. PCC 6803.

Frontiers in Plant Science, 12:787943.

- Planning and performance of CO₂ shift experiments
- Sampling and extraction of metabolites from experimental cultures for LC-MS measurement, analysis of metabolomic data and data interpretation
- Principal component analysis and heat map illustration
- Sampling and extraction of glycogen from experimental cultures, glycogen analysis and data interpretation
- Overall contribution to manuscript writing

Lucius, S., Theune, M., Arrivault, S., Hildebrandt, S., Mullineaux, C. W., Gutekunst, K., & Hagemann, M. (2022). Cp12 fine-tunes the Calvin-Benson cycle and carbohydrate metabolism in cyanobacteria.

Frontiers in Plant Science, 13.:1028794.

- Vector design and cloning of Cp12 deletion construct, native complementation construct and cysteine variant constructs
- Generation of *Synechocystis* strains $\Delta cp12$, $\Delta cp12::cp12-\Delta CysN$, $\Delta cp12::cp12-\Delta CysC$, and $\Delta cp12::cp12-\Delta CysNC$
- Physiological analysis and growth experiments on $\Delta cp12$ strains with and without glucose in different light regimes
- Sampling and extraction of glycogen from experimental cultures, glycogen analysis and data interpretation
- Planning and performance of CO₂ shift experiments
- Sampling and extraction of metabolites from experimental cultures for LC-MS measurement, analysis of metabolomic data and data interpretation
- Execution of redox measurement experiments together with Marius Theune during research stay with Gutekunst group in Kassel
- Overall contribution to manuscript writing

Orthwein, T., Scholl, J., Spät, P., **Lucius, S.**, Koch, M., Macek, B., Hagemann, M., & Forchhammer, K. (2021). The novel P_{II}-interactor PirC identifies phosphoglycerate mutase as key control point of carbon storage metabolism in cyanobacteria.

Proceedings of the National Academy of Sciences, (2021), 2019988118, 118(6).

- Planning and performance of nitrogen depletion experiment
- Sampling and extraction of metabolites from experimental cultures for LC-MS measurement, analysis of metabolomic data and data interpretation
- Vector design and cloning of *slr1945* overexpression construct for recombinant expression experiments
- Respective methods part written for manuscript, review and approval of manuscript

12.2 Wissenschaftlicher Lebenslauf

Persönliche Daten

Name: Stefan Lucius
Geburtsdatum: 02.03.1995 in Köthen (Anhalt)

Akademische Berufserfahrung

11/2018 – 12/2022 Promotionsstudent, Universität Rostock
Institut für Biowissenschaften, AG Pflanzenphysiologie
Betreut durch: Prof. Dr. Martin Hagemann

01/2018 – 03/2018 Wissenschaftliche Hilfskraft, Universität Rostock
Institut für Biowissenschaften, AG Pflanzenphysiologie

10/2016 – 12/2016 Studentische Hilfskraft, Universität Rostock
Institut für Biowissenschaften, AG Pflanzengenetik

Akademische Ausbildung

2016 – 2018 Master of Science – Studiengang Funktionelle Pflanzenwissenschaften
Universität Rostock, Mathematisch-Naturwissenschaftliche Fakultät

2013 – 2016 Bachelor of Science – Studiengang Biowissenschaften
Universität Rostock, Mathematisch-Naturwissenschaftliche Fakultät

Auslandsaufenthalt

03/2019 – 04/2019 Gastwissenschaftler, University of Tsukuba, Japan
Institute of Life and Environmental Sciences
Betreut durch: Prof. Dr. Iwane Suzuki

Abschlussarbeiten

MSc: „Charakterisierung von *Arabidopsis* Antisense-PGPase-Pflanzen nach Expression cyanobakterieller PGPasen“
Universität Rostock, Institut für Biowissenschaften, AG Pflanzenphysiologie
Betreut durch: Prof. Dr. Martin Hagemann

BSc: „Charakterisierung der Triebhaltung bei *Vitis vinifera* und *Arabidopsis thaliana*“
Universität Rostock, Institut für Biowissenschaften, AG Pflanzengenetik
Betreut durch: Prof. Dr. Renate Horn

Erschienenene wissenschaftliche Publikationen

- 2022 **Lucius, S.**, Theune, M., Arrivault, S., Hildebrandt, S., Mullineaux, C. W., Gutekunst, K., & Hagemann, M. (2022). CP12 fine-tunes the Calvin-Benson cycle and carbohydrate metabolism in cyanobacteria. *Frontiers in Plant Science*, 13.
- 2021 **Lucius, S.**, Makowka, A., Michl, K., Gutekunst, K., & Hagemann, M. (2021). The Entner-Doudoroff Pathway Contributes to Glycogen Breakdown During High to Low CO₂ Shifts in the Cyanobacterium *Synechocystis* sp. PCC 6803. *Frontiers in Plant Science*, 12.
- Orthwein, T., Scholl, J., Spät, P., **Lucius, S.**, Koch, M., Macek, B., Hagemann, M., & Forchhammer, K. (2021). The novel P_{II}-interactor PirC identifies phosphoglycerate mutase as key control point of carbon storage metabolism in cyanobacteria. *Proceedings of the National Academy of Sciences*, 118(6), 2019988118.
- 2020 de Alvarenga, L. V., **Lucius, S.**, Vaz, M. G. M. V., Araújo, W. L., & Hagemann, M. (2020). The novel strain *Desmonostoc salinum* CCM-UFV059 shows higher salt and desiccation resistance compared to the model strain *Nostoc* sp. PCC 7120. *Journal of Phycology*, 56(2), 496–506.
- 2018 Rai, S., **Lucius, S.**, Kern, R., Bauwe, H., Kaplan, A., Kopka, J., & Hagemann, M. (2018). The *Synechocystis* sp. PCC 6803 Genome Encodes Up to Four 2-Phosphoglycolate Phosphatases. *Frontiers in Plant Science*, 9.

Wissenschaftliche Publikationen auf Preprint-Servern

- 2022 Treves, H., **Lucius, S.**, Feil, R., Stitt, M., Hagemann, M., & Arrivault, S. (2022). Operation of Carbon-Concentrating Mechanisms in Cyanobacteria and Algae requires altered poising of the Calvin-Benson cycle. *BioRxiv*, 2022.08.23.504937.

Fachvorträge und Posterpräsentationen

SCyCode FOR2816 Symposium, Leipzig, 2022

Vortrag: "The role of Cp12 in carbon regulation of *Synechocystis* sp. PCC 6803." **Lucius, S.**, Theune, M., Gutekunst, K., Hagemann, M.

German-Japanese Meeting on Green Aquatic Biology, Potsdam, 2022

Poster: "The role of Cp12 in inorganic carbon acclimation of *Synechocystis* sp. PCC 6803". **Lucius, S.**, Hagemann, M.

SCyCode FOR2816 Symposium, Leipzig, 2020

Vortrag: "Metabolic regulation of isoenzymes in the triosephosphate hub of *Synechocystis* sp. PCC 6803." **Lucius, S.**, Hagemann, M.

72. Jahrestagung der DGHM & Jahrestagung der VAAM, Leipzig, 2020

Poster: "Metabolic regulation of isoenzymes in the triosephosphate hub of *Synechocystis* sp. PCC 6803." **Lucius, S.**, Hagemann, M.

4th Early Career Researcher Symposium on Cyanobacteria, Tübingen, 2019

Poster: "Metabolic regulation of carbon allocation and CO₂ acclimation in *Synechocystis* sp. PCC 6803." **Lucius, S.**, Hagemann, M.

Botanik-Tagung der Deutschen Botanischen Gesellschaft, Rostock, 2019

Poster: "Metabolic regulation of carbon allocation and CO₂ acclimation in *Synechocystis* sp. PCC 6803." **Lucius, S.**, Hagemann, M.

12.3 Selbständigkeitserklärung

Ich versichere hiermit an Eides statt, dass ich die vorliegende Arbeit selbstständig angefertigt und ohne fremde Hilfe verfasst habe. Dazu habe ich keine außer den von mir angegebenen Hilfsmitteln und Quellen verwendet und die den benutzten Werken inhaltlich und wörtlich entnommenen Stellen habe ich als solche kenntlich gemacht.

Ort, Datum

Stefan Lucius

12.4 Acknowledgements

My sincerest thanks go out to my supervisor Prof. Martin Hagemann. Thank you for showing me what it means to progress in scientific research, for always being available to immediately discuss potentially promising results, and for continuous motivation to stay on track with this project. I surely learned a lot from you. Thank you for your trust to give me the opportunity of a research stay far away in Japan.

Further, my thanks go out to all the PUR team members who helped me on this project and who made these four years in the lab an enjoyable experience. Especially thanks to Klaudia for teaching me how to handle *Synechocystis*, and for support and assistance in crucial experiments. Thank you Thomas for being my project partner and pulling through all SCyCode meetings, talks and conferences together.

I would like to thank Prof. Kirstin Gutekunst and Marius Theune for making our successful collaborations possible, and for your great company and supervision during my research stay in your lab in Kassel.

Thanks to all my friends and family who kept motivating me during this time. Especially to my parents and my sister for continuous support and curiosity even though it will always remain difficult for me to explain to you what I was actually working on.

Thank you Luna, for your encouragement, friendship and love that inspired me to start and finish this PhD journey.